IDENTIFICATION OF MINIMUM UNIT OF ANALYSIS FOR SEISMIC PERFORMANCE ASSESSMENT OF MASONRY BUILDINGS IN AGGREGATE

Dissertation

submitted to and approved by the

Faculty of Architecture, Civil Engineering and Environmental Sciences

University of Braunschweig – Institute of Technology

and the

Department of Civil and Environmental Engineering

University of Florence

in candidacy for the degree of a

Doktor-Ingenieurin (Dr.-Ing.) /

Dottore di Ricerca in Civil and Environmental Engineering*)

by

Chiara Bernardini

born 12/01/1986

from Sinalunga, Italy

Submitted on	11 February, 2019
Oral examination on	06 May, 2019
Professorial advisors	Prof. Martin Empelmann
	Prof. Andrea Vignoli

2019

*) Either the German or the Italian form of the title may be used.

«IDENTIFICATION OF MINIMUM UNIT OF ANALYSIS
FOR SEISMIC PERFORMANCE ASSESSMENT
OF MASONRY BUILDINGS IN AGGREGATE»

To my dear uncle Vezio

Acknowledgements

I would like to thank my supervisors Professor Vignoli and Professor Empelmann for their valuable guidance and kind support during these three years.

A special thanks to Ing. Sonia Boschi, Ing. Andrea Borghini and Ing. Alberto Ciavattone for their constant availability and their contributions of time and ideas.

Thanks to Professor Vicente for the opportunity to share research and opinions, allowing to improve my work.

Thanks to the group of PhD students with whom I have shared this experience, especially to Chiara and Silvia for the laughter and the anxiety.

Thanks to my family, who always supports me, and to my little nephews, Tommaso, Giovanni and Zeno, because they make everything better.

Thanks to my friends, Federica and Lucia, who are always there, rain or shine.

Thanks to Alessio, for the unconditional love, support and patience. I owe this goal to him.

Abstract

Italy is characterized by high seismicity and the recent earthquakes (L'Aquila 2009, Emilia Romagna 2012, Centre of Italy, 2016) have highlighted the high vulnerability of the Italian real estate, mainly composed of historical and old masonry buildings. The greatest damages mostly occurred in the historical centres, where masonry buildings in aggregate are the prevalent structural typology.

This circumstance has renewed the need of procedures for the seismic risk assessment and the unitary planning of strengthening interventions, according to a specific methodology appropriate for the masonry aggregates, in order to achieve safety standards and reduce the losses. Indeed, in the seismic vulnerability assessment, the identification of a determined building (i.e., structural unit, S.U.) as an independent structure can become difficult, since it is often in adjacency to others and the same boundary walls are shared. Moreover, as the masonry aggregates result from continued urban growth phenomena, they usually comprise different structural typologies and a wide range of construction materials. Consequently, it is known that these systems do not have an independent structural behaviour, given the reciprocal interactions with adjacent structures during a seismic event (namely, the "aggregate effect"), and their analysis is naturally affected by several sources of uncertainties. With reference to the analysis of the global seismic behaviour (in-plane mechanisms of failure), several studies have been performed in recent years to address this issue; however, it is not yet clear how these interactions can be represented in numerical models even if in a simplified form, without modelling the entire aggregate or simply the isolated structure.

Hence, this research project aims at understanding how the "aggregate effect" should be modelled for a more accurate assessment of the global seismic performance of the masonry buildings in aggregate, reducing the uncertainties related to too extensive knowledge process and providing tools for the definition of new guidelines for the masonry aggregates.

To this end, a new procedure, referred to as *"target structural unit approach"*, is proposed, aiming at identifying the optimal portion of the aggregate that best represents the "aggregate effect" for the investigated building, i.e. the Minimum Unit of Analysis (M.U.A.). This procedure is based on a multi-level analysis of the seismic response of the target structural unit, investigating different modelling configurations in addition to the complete aggregate or the isolated building. The evaluation is preliminarily performed at global– and wall– level; then, the structural unit– level is introduced as additional verification level, with the aim to understand the variability of the seismic response of the case study building in function of different boundary conditions.

A preliminary step of this study is a sensitivity analysis on prototype aggregates, necessary to evaluate the influence of the main interaction factors on their global seismic performance. Then, the new procedure for M.U.A. definition is defined and applied on the prototypes, for providing general schemes in function of

the analysed case. Finally, the procedure is validated on two real masonry aggregates: an L aggregate in Faro (Portugal) and a row aggregate in Castelnuovo (L'Aquila).

Zusammenfassung

Italien ist gekennzeichnet durch eine hohe Seismizität, und die jüngsten Erdbeben (L'Aquila 2009, Emilia Romagna 2012, Mittelitalien, 2016) haben die starke Anfälligkeit des italienischen Immobilienvermögens, das hauptsächlich aus historischen und alten Gebäuden aus Mauerwerk besteht, deutlich gemacht. Die größten Schäden entstanden in erster Linie in den historischen Zentren, in denen Gebäudekomplexe aus Mauerwerk die vorherrschende Konstruktionsform darstellen.

Dieser Umstand hat die Notwendigkeit von Verfahren für die Bewertung des seismischen Risikos sowie zur einheitlichen Planung von Konsolidierungs- und Verbesserungsmaßnahmen entsprechend einer spezifischen, für Komplexe aus Mauerwerk geeigneten Methodologie bekräftigt, um Sicherheitsstandards zu erzielen und Verluste zu reduzieren. Tatsächlich kann bei der Beurteilung der seismischen Anfälligkeit die Identifizierung eines bestimmten Gebäudes (d. h. einer Gebäudeeinheit, ital. S.U.) als eigenständiges Gebäude schwierig sein, da es häufig an andere grenzt und sie gemeinsame Trennwände besitzen. Weil die Gebäudekomplexe aus Mauerwerk zudem das Ergebnis einer kontinuierlichen städtischen Entwicklung sind, umfassen sie in der Regel verschiedene Konstruktionstypologien sowie eine Vielzahl an Baumaterialien. Folglich weiß man, dass diese Systeme aufgrund der Wechselwirkungen mit den angrenzenden Gebäuden während eines seismischen Ereignisses (ital. „Effetto Aggregato"; Gebäudekomplex-Effekt) kein unabhängiges strukturelles Verhalten aufweisen und ihre Analyse zwangsläufig durch verschiedene Unsicherheitsfaktoren beeinflusst wird. Im Hinblick auf die Analyse des seismischen Gesamtverhaltens (Bruchmechanismen in der Ebene) wurden in den vergangenen Jahren zahlreiche Studien durchgeführt, um dieses Problem anzugehen; dennoch ist weiterhin nicht klar, wie diese Interaktionen, wenn auch in vereinfachter Form, in numerischen Modellen dargestellt werden können, ohne den gesamten Gebäudekomplex oder nur das isolierte Gebäude zu modellieren.

Ziel dieses Forschungsprojektes ist somit, zu verstehen, wie der „Effetto Aggregato" (Gebäudekomplex-Effekt) für eine genauere Beurteilung der seismischen Gesamtleistungen der Gebäudekomplexe aus Mauerwerk modelliert werden sollte, um die Unsicherheiten im Zusammenhang mit einem zu umfangreichen Erkenntnisprozess zu reduzieren und Instrumente für die Definition neuer Richtlinien für Gebäudekomplexe aus Mauerwerk bereitzustellen.

Zu diesem Zweck wird ein neues Verfahren vorgeschlagen, das als „approccio unità strutturale target" (Ansatz der Target-Gebäudeeinheit) bezeichnet wird, um den optimalen Abschnitt des Gebäudekomplexes zu identifizieren, der den „Effetto Aggregato" (Gebäudekomplex-Effekt) für das untersuchte Gebäude, d. h. die kleinste Analyseeinheit (ital. M.U.A.), am besten darstellt. Dieses Verfahren basiert auf einer mehrstufigen Analyse der seismischen Reaktion einer Target-Gebäudeeinheit, wobei ergänzend zu den Konfigurationen des vollständigen Gebäudekomplexes oder des isolierten Gebäudes verschiedene Modellierungskonfigurationen untersucht werden. Die Bewertung erfolgt zunächst auf der Gesamt- und Wandebene; daraufhin wird die Ebene der Gebäudeeinheiten als zusätzliche Überprüfungsebene eingeführt,

um die Variabilität der seismischen Reaktion des untersuchten Gebäudes, bezogen auf die unterschiedlichen Rahmenbedingungen, zu verstehen.
Eine Vorbereitungsphase dieser Studie ist eine Sensitivitätsanalyse an Prototyp-Komplexen, welche zur Beurteilung des Einflusses der wichtigsten Interaktionsfaktoren auf ihre seismische Gesamtleistung erforderlich ist. Dann wird das neue Verfahren an den Prototypen definiert und angewendet, um allgemeine Muster abhängig vom analysierten Fall zu erhalten. Schließlich wird das Verfahren an zwei realen Mauerwerk-Komplexen validiert: Einem L-förmigen Komplex in Faro (Portugal) und einem in Reihe angeordneten Komplex in Castelnuovo (L'Aquila).

Sommario

L'Italia è un'area totalmente sismica e i recenti terremoti (L'Aquila 2009, Emilia Romagna 2012, Centro Italia, 2016) hanno messo in luce l'elevata vulnerabilità del patrimonio immobiliare italiano, composto principalmente da edifici storici e antichi in muratura. I maggiori danni si sono verificati soprattutto nei centri storici, dove gli edifici in muratura in aggregato sono la tipologia strutturale prevalente.

Questa circostanza ha rinnovato la necessità di procedure per la valutazione del rischio sismico e la pianificazione unitaria di interventi di consolidamento e miglioramento, secondo una metodologia specifica appropriata per gli aggregati in muratura, al fine di raggiungere standard di sicurezza e ridurre le perdite. Infatti, nella valutazione della vulnerabilità sismica, l'identificazione di un determinato edificio (cioè unità strutturale, S.U.) come struttura indipendente può diventare difficile, poiché spesso è adiacente ad altri e le pareti di confine sono condivise. Inoltre, poiché gli aggregati in muratura derivano da continui fenomeni di crescita urbana, di solito comprendono diverse tipologie strutturali e una vasta gamma di materiali da costruzione. Di conseguenza, è noto che questi sistemi non hanno un comportamento strutturale indipendente, date le reciproche interazioni con le strutture adiacenti durante un evento sismico (ovvero l'"effetto aggregato"), e la loro analisi è naturalmente influenzata da diverse fonti di incertezza. Relativamente all'analisi del comportamento sismico globale (meccanismi di rottura nel piano), negli ultimi anni sono stati condotti numerosi studi per affrontare questo problema; tuttavia, non è ancora chiaro come queste interazioni possano essere rappresentate in modelli numerici anche se in una forma semplificata, senza modellare l'intero aggregato o unicamente la struttura isolata.

Pertanto, questo progetto di ricerca mira a comprendere come l'"effetto aggregato" debba essere modellato per una valutazione più accurata delle prestazioni sismiche globali degli edifici in muratura in aggregato, riducendo le incertezze legate a un processo di conoscenza troppo esteso e fornendo strumenti per la definizione di nuove linee guida per gli aggregati murari.

A tal fine, viene proposta una nuova procedura, definita *"approccio unità strutturale target"*, per identificare la porzione ottimale dell'aggregato che meglio rappresenta l'"effetto aggregato" per l'edificio indagato, ovvero l'Unità Minima di Analisi (M.U.A.). Questa procedura si basa su un'analisi multilivello della risposta sismica dell'unità strutturale target, studiando diverse configurazioni di modellazione, in aggiunta alle configurazioni di completo aggregato o di edificio isolato. La valutazione viene eseguita preliminarmente a livello globale e di parete; quindi, il livello di unità strutturale viene introdotto come ulteriore livello di verifica, con l'obiettivo di comprendere la variabilità della risposta sismica dell'edificio investigato in funzione delle diverse condizioni al contorno.

Una fase preliminare di questo studio è un'analisi di sensibilità su aggregati prototipo, necessaria per valutare l'influenza dei principali fattori di interazione sulle loro prestazioni sismiche globali. Quindi, la nuova procedura è definita e applicata sui prototipi, per fornire schemi generali in funzione del caso

analizzato. Infine, la procedura viene convalidata su due aggregati di muratura reali: un aggregato a L a Faro (Portogallo) e un aggregato a riga a Castelnuovo (L'Aquila).

Contents

List of Figures

List of Tables

List of Abbreviations

α_d	Capacity-to-demand displacement ratio
α_{PGA}	Capacity-to-demand acceleration ratio
μ_D	Mean Damage grade
η	Viscous damping coefficient
a_g	Seismic acceleration in A ground type and T1 topography category
C	Conventional strength
C_U	Use coefficient
CF_{KL}	Confidence factor related to a knowledge level
DPM	Damage Probability Matrix
F_0	Maximum amplification factor of the spectrum in acceleration
H	Seismic exposure
I	Macroseismic Intensity
IS	Safety (or risk) Index
I_V	Vulnerability Index
k*	Equivalent stiffness
KL	Knowledge Level
LS	Limit State
MDOF	Multi Degree Of Freedom
M.I.U.	Minimum Intervention Unit
M_L	Local Magnitude
M.U.A.	Minimum Unit of Analysis
PGA	Peak Ground Acceleration
PL	Performance Levels
P_{VR}	Probability of exceedance in the reference period
q	Behaviour factor
R	Seismic risk
S	Ground factor (S_T*S_S); S_T: topographic coefficient; S_S: soil coefficient
SDOF	Single Degree of Freedom
SPI	Seismic Performance Indicator
S.U.	Structural Unit
S.U.s	Structural Units
T_C*	Upper limit of the period of the constant spectral acceleration range
T_B	Period corresponding to the beginning of the constant acceleration range of the spectrum TB=TC/3;
T_D	Period corresponding to the beginning of the constant displacement range: TD = 4.0*a_g/g+1.6
T_R	Return period of the seismic action
V	Seismic Vulnerability
V_{bu}	Maximum normalized base shear
V_N	Nominal life
V_R	Reference period

Chapter 1.
Introduction

In this chapter, the research topic and motivations are presented. The outline of the thesis is given.

Contents

1.1 RESEARCH TOPIC AND MOTIVATIONS

Italy is a totally seismic area and the earthquakes occurred in this Century produced huge damages and losses; the recent seismic events in L'Aquila (2009), Emilia Romagna (2012) and Centre of Italy (2016) are an example.

(a)

(b)

Figure 1-1: Castelnuovo (L'Aquila) - 06/04/2009 (a), Amatrice (Rieti) - 24/08/2016 (b).

These events have highlighted the high vulnerability of the Italian real estate, mainly composed of historical and old masonry buildings; the greatest damages mostly occurred in the historical centres, where masonry buildings in aggregate are the prevalent structural typology. This circumstance has renewed the necessity of procedures for the assessment of the seismic risk and the unitary planning of strengthening and improvement interventions, according to a specific methodology appropriate for these structures, in order to achieve safety standards and reduce the losses. However, some specific strategies have been introduced in Italy only recently, with the aim to provide a systematic framework of the methodology and operational tools for the survey, the diagnostics, the choice of the interventions and the final design (O.P.C.M. n. 3431 del 03/05/2005; ReLUIS, 2010).

A ***masonry aggregate*** can be defined as a not homogeneous group of ***structural units*** (hereinafter referred as S.U.s), which are characterized by a common manufacturing process and that naturally interact under seismic action because connected in plan and in height by structural links (NTC 2008). As they result from a continued urban growth phenomenon, the aggregates usually comprise different structural typologies and a wide range of construction materials. Consequently, an adequate preliminary knowledge is fundamental to perform a reliable seismic safety assessment. In addition, it is known that their behaviour differs from that of the isolated buildings, due to an "aggregate effect" that influences the overall seismic response.

Figure 1-2: Example of a masonry aggregate and identification of a S.U.

Even though local mechanisms are usual failures in masonry aggregates, the in-plane mechanisms are equally notable and still less examined; indeed, there is a research gap in defining numerical models able to translate the "aggregate effect". In this context, this research project focuses the attention on the global seismic performance of masonry buildings in aggregate.

Figure 1-3: M.I.U in a row aggregate.

With reference to the global seismic assessment of a S.U., it appears clear the necessity and the difficulty to identify the ***Minimum Unit of Analysis*** **(M.U.A.)** (ReLUIS, 2010), defined as the optimal portion of the aggregate to be considered in the modelling, in order to take account of the reciprocal interactions between different S.U.s. For this reason, the M.U.A. should include the **Minimum Intervention Unit (M.I.U.)**, i.e. the structure on which we are going to intervene, and some of the adjacent S.U.s.

However, despite the importance of this topic, in the scientific literature there are no indications on how the M.U.A. should be defined. For this reason, this research project aims to deepen the "aggregate effect" and to provide a procedure for M.U.A. definition, improving the methodology of analysis of these structures. This would allow providing tools for the definition of guidelines for masonry buildings in aggregate, supporting retrofitting strategies and evaluating their efficiency.

1.2 Outline of the work

The present thesis is organized in 7 Chapters, that can be grouped into three parts, as resumed in the following scheme.

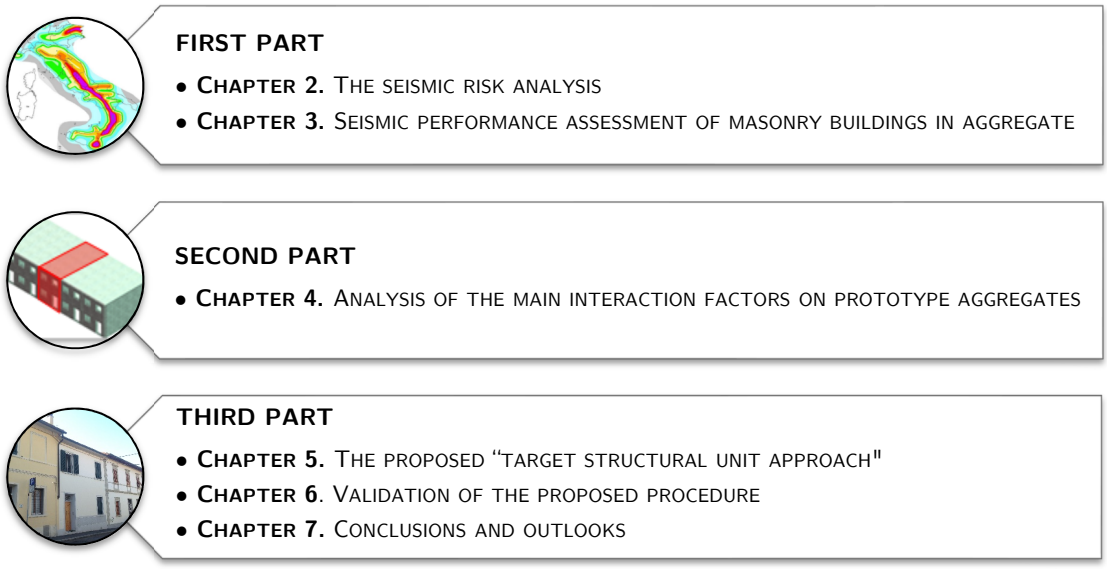

Figure 1-4: Scheme of the thesis.

The **FIRST PART** (Chapter 2 and 3) contains a general overview of the seismic risk analysis and deepens the seismic performance assessment of masonry buildings in aggregates.

In detail, **Chapter 2** introduces the seismic risk concept and focuses on seismic hazard, exposure and vulnerability. Moreover, the main structural vulnerability methods are reviewed.

Chapter 3 contains an overview of the typical mechanisms of failure of existing masonry structures and of the analytical methods for evaluating the seismic capacity. Then, the seismic performance of masonry buildings in aggregate is reviewed, deepening the "aggregate effect" concept. Finally, the assumptions of this work and the adopted analysis methods are illustrated.

The **SECOND PART** (Chapter 4) deepens the analysis of the interaction effects among adjacent buildings.

In **Chapter 4**, the results of a sensitivity analysis performed on prototype aggregates are presented, in order to evaluate the influence of the main interaction factors, as the aggregate typology, the number of S.U.s, the floors typology, the presence of material heterogeneities and of differences in height.

The **THIRD PART** (Chapter 6, 7 and 8) presents a new procedure, referred to as *"target structural unit approach"*, for the definition of the Minimum Units of Analysis (M.U.A.) for masonry buildings in aggregate.

In **Chapter 5**, the procedure is defined and applied on prototype aggregates, and general indications for identifying the M.U.A are provided as function of the different characteristics.

In **Chapter 6**, the proposed procedure is validated on two case studies: the first is an L aggregate located in Faro (Portugal), the second is a row aggregate located in Castelnuovo (L'Aquila).

Finally, in **Chapter 7** conclusions and outlooks of this work are illustrated.

The results obtained for all the analysed prototype aggregates are resumed in **Annex A**, while for the real masonry aggregates in **Annex B**.

Chapter 2.

The seismic risk analysis

This chapter provides a general overview of the main concepts of the seismic risk analysis, focusing on the determination of the seismic hazard and providing a review of the state of art for the main vulnerability assessment methods.

Contents

2.1 SEISMIC RISK

Seismic risk is the extent of the expected damage in a given time interval, depending on the type of seismicity, the constructions strength and the human settlement (http://www.protezionecivile.gov.it/jcms/it/descrizione_sismico.wp). It is classically expressed as a mathematical relationship of three different aspects, as reported in the following equation:

$$R_{ie}|T = |(H_i) \otimes (V_e) \otimes E|_T \qquad (1)$$

where:

- R is the seismic risk, defined as the probability of exceedance of a certain level of loss in a certain period (T) of a certain exposed element (E) for a seismic event of fixed I intensity;
- H is the seismic hazard, that is the probability of occurrence of an earthquake of I intensity in a given site and in a certain time period (T);
- E is the exposure and it measures the value of the elements exposed to the seismic risk. It mainly depends on location, accessibility, level and type of employment, function of the building and the presence of economic goods and historic/cultural services (www.protezionecivile.gov.it and Zuccaro, 2004);
- V is the vulnerability and it is the propensity of a structure to suffer damage when an earthquake of I intensity occurs.

These aspects are deepened in the following paragraphs.

2.2 SEISMIC HAZARD

Seismic hazard of a territory is the probability that, in a given area and in a certain time period, an earthquake of a given intensity occurs.

The intensity of an earthquake can be measured through instrumental measurements (earthquake magnitude, §2.2.1; peak ground acceleration, §2.2.3) or in function of the type and amount of damages that it produces (macroseismic intensity, §2.2.2).

Italian Code defines the seismicity of an area in terms of the peak ground acceleration parameter (PGA), whose distribution on Italian territory is accessible through interactive maps edited by the National Institute of Geophysics and Volcanology (Figure 2-1, http://esse1-gis.mi.ingv.it).

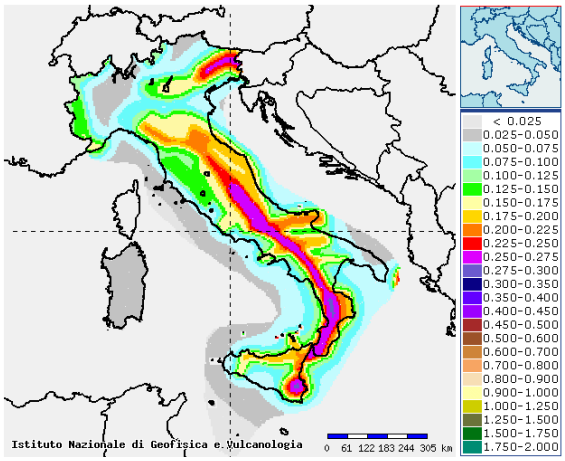

Figure 2-1: Map of seismic hazard for a P_{VR} of 10% in 50 years.

2.2.1 Earthquake magnitude

The earthquake magnitude is an indirect measure of the mechanical energy released by an earthquake in the hypocentre and it is calculated from the amplitude of the seismic waves recorded by a seismograph compared to a sample magnitude.

The most famous magnitude scale is the Richter Local Magnitude M_L (Richter, 1935), for which the logarithm (base 10) of the measure of the maximum trace amplitude of a seismograph is compared to the trace amplitude of a conventional reference earthquake (1 micrometer recorded on a Wood-Anderson seismograph at a distance of 100 km from the epicentre, considered as the representative displacement for an event with zero magnitude). Each level of M_L corresponds to an energy increase of about 30 times.

2.2.2 Macroseismic intensity

The macroseismic intensity scales are related to a qualitative description of the earthquake effects, depending on local conditions (presence and type of construction, distance from the epicentre, etc.) and on the earthquake characteristics. They are recognized as indicators, immediately after an earthquake event, of the overall earthquake damages.

In 1873 De Rossi – Forel proposed the first modern macroseismic scale, composed of 10 degrees. It was modified by Mercalli (10 degrees) in 1902. The Mercalli Scale was further modified by Cancani – Sieberg in 1904 and then in 1912 (Mercalli – Cancani – Sieberg, 1912, MCS, IMCS). The MCS scale is composed of 12 levels, from the first "very light event", with almost no perception of the earthquake, up to the twelfth "heavy catastrophic event", with the collapses of structural elements.

In 1956, Richter introduced in the Mercalli scale 4 different classifications for masonry buildings depending on the seismic resistance (Modified Mercalli, 1956, MM).

The Sponheuer – Medvedev – Karnik Scale (1964, MSK) is similar to the MM and it classifies all non-seismic designed buildings into 3 categories, classifying the percentage quantities and degrees of damage. While the MCS scale considers the total damage regardless the presence of different type of structures, the MSK scale presents 5 classes of damage for 3 classes of buildings (Margottini, Molin, & Serva, 1992).

In 1988, the European Seismological Commission, starting from the MSK scale, defined a new scale called European Macroseismic Scale (EMS), called in the following EMS-98 (Grünthal, 1998). The EMS-98 shows a vulnerability classification of structures depending on different materials (masonry, reinforced concrete, steel and timber) and on geometrical and structural parameters (ERD: Earthquake Resistant Design); it proposes 7 classes (from “A” to “F”) at decreasing vulnerability.

As shown in Figure 2-2 (a), the Vulnerability Table gives the most likely vulnerability class and the probable variation range for each type of structure. The vulnerability classes are assigned to the buildings according to the greater frequency of damage they showed after past seismic events; in Figure 2-2 (b) classification of damage to masonry buildings is shown.

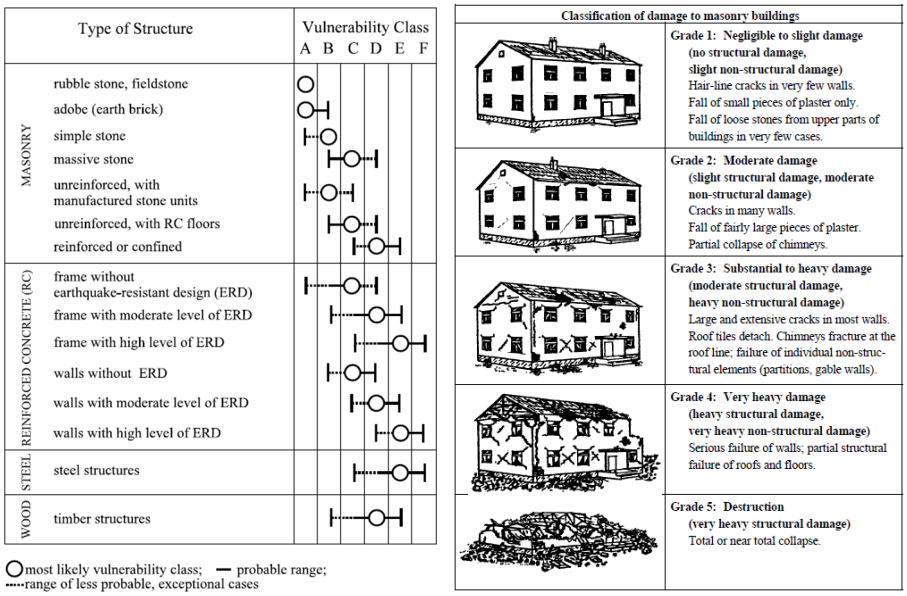

Figure 2-2: Vulnerability Table (a) and damage levels in EMS-98 (b) (Grünthal, 1998).

In Figure 2-3 an example of a correlation between the MCS and MSK scales is shown (Margottini, Molin, & Serva, 1992).

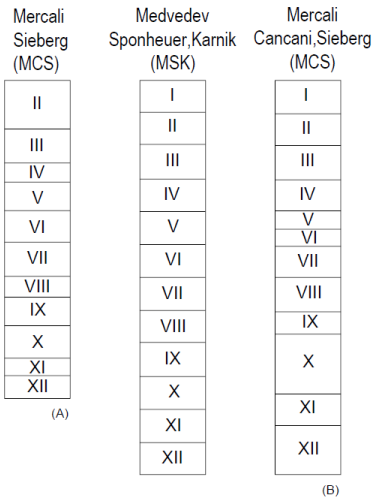

Figure 2-3: Comparison between the MCS and MSK scales as proposed by Murphy et al., 1977 (a), and Levret and Mohammadioun, 1984 (b) (Margottini et al., 1992).

2.2.3 Peak ground acceleration and response spectra by NTC 2008

The peak ground acceleration (PGA) is the largest value of horizontal acceleration obtained from the accelerogram of a component of an earthquake in a specific area.

The response spectrum describes the maximum response of a Single Degree Of Freedom (SDOF) system to an input motion as a function of its natural period and damping ratio (usually 5.0%) (NTC 2008). The SDOF response may be expressed in terms of acceleration, velocity or displacement. PGA is the value of the acceleration response spectrum for the natural period equal to zero.

NTC 2008 divides Italian territory into 5x5 kilometres grid; for each point of the grid line, seismic hazard is identified through the following parameters:

- a_g [g]: peak ground acceleration for A category of soil (rock) and T1 topography category;

- T_c^* [s]: upper limit of the period of the constant spectral acceleration range;
- F_0: maximum amplification factor of the spectrum in acceleration.

The seismic action related to each limit state is defined from the reference period V_R of the construction and the related probability of exceedance (P_{VR}), illustrated below.

2.2.3.1 Nominal life and reference period

The period of reference V_R is the product of the nominal life of the structure V_N and the use coefficient C_U:

$$V_R = V_N \cdot C_U \quad (2)$$

The nominal life V_N (Table 2-1) is the number of years in which the structure must be able to be used for the purpose it was built and it depends on the type of structure.

The use coefficient C_U (Table 2-2) depends on the use class that is assigned to the structure:

- Class I: buildings characterized by occasional presence of people, agricultural buildings;
- Class II: buildings characterized by normal crowding, no content dangerous to the environment and without essential public and social functions;
- Class III: buildings characterized by significant crowding;
- Class IV: buildings with public functions or strategic importance, also with reference to the management of civil protection in the event of disasters.

Table 2-1: Nominal life for different type of buildings (Table 2.4.I of NTC 2008).

Construction type		V_N [years]
1	Provisional building – structure in construction phase	≤ 10
2	Ordinary building, bridges, infrastructural buildings, dams of small dimension	≥ 50
3	Big buildings of big dimensions or strategic relevance	≥ 100

Table 2-2: Coefficient C_U (Table 2.4.II of NTC 2008).

Use class	I	II	III	IV
C_U	0.7	1.0	1.5	2.0

The probability of exceedance in the reference period P_{VR} varies in function of the considered limit state (Table 2-3). Starting from the probability of exceedance P_{VR} and the nominal life V_N, the return period of the seismic action T_R is defined as in the following:

$$T_R = -\frac{V_R}{\ln(1 - P_{VR})} = -\frac{C_U \cdot V_N}{\ln(1 - P_{VR})} \quad (3)$$

For an ordinary building with normal crowding ($C_U = 1.00$, $V_N = 50$ years), the return periods of each LS are shown in Table 2-3.

Table 2-3. Probability of exceedance (P_{VR}) and return periods (T_R) for an ordinary building in function of the LS (Table 3.2.I of NTC 2008).

Limit State			P_{VR}	T_R
Damage limitation state	Operational	SLO	81%	30
	Damage	SLD	63%	50
Ultimate limit state	Life Safety	SLV	10%	475
	Collapse	SLC	6%	975

Once defined these parameters, the seismic hazard is known, and the response spectrum can be calculated as described in the following.

2.2.3.2 Response spectra

The elastic response spectrum in acceleration is defined by the following expressions (Eq. 3.2.4. NTC 2008):

$$0 \le T < T_B \qquad S_e(T) = a_g \cdot S \cdot \eta \cdot F_0 \cdot \left[\frac{T}{T_B} + \frac{1}{\eta \cdot F_0}\left(1 - \frac{T}{T_B}\right)\right] \qquad (4)$$

$$T_B \le T < T_C \qquad S_e(T) = a_g \cdot S \cdot \eta \cdot F_0 \qquad (5)$$

$$T_C \le T < T_D \qquad S_e(T) = a_g \cdot S \cdot \eta \cdot F_0 \cdot \left(\frac{T_C}{T}\right) \qquad (6)$$

$$T_D \le T \qquad S_e(T) = a_g \cdot S \cdot \eta \cdot F_0 \cdot \left(\frac{T_C \cdot T_D}{T^2}\right) \qquad (7)$$

in which:

- T is the vibration period;
- $S_e(T)$ is the horizontal acceleration spectral coordinate;
- $S = S_S \cdot S_T$ is the coefficient that considers the ground type and topographical condition. S_S is identified in Table 2-4 for different ground types and S_T is defined in Table 2-5;
- η is a coefficient depending on the viscous damping (it is 1 for damping coefficient equal to 5%);
- F_0 is the maximum amplification factor of the spectrum in acceleration;
- T_C is the period corresponding to the beginning of the constant velocity range in the spectrum: $T_C = C_C \cdot {T_C}^*$. C_C is defined in Table 2-4;
- T_B is the period corresponding to the beginning of the constant acceleration range of the spectrum: $T_B = T_C/3$;
- T_D is the period corresponding to the beginning of the constant displacement range: $T_D = 4{,}0 \cdot \frac{a_g}{g} + 1{,}6$.

The ground effect is considered by means of the coefficients S and C_C, defined below.

Ground types and topographic categories

NTC 2008 classifies soils into 4 categories from "A" (*rock*) to "E" (*deposits of loose-to-medium cohesionless soil*), in function of the average value of the shear wave velocity, $V_{s,30}$, if available, otherwise the value of N_{SPT} should be used (Standard Penetration Test) (Table 3.2.II NTC 2008).
For each soil category, the coefficients S_S and C_C are provided (Table 2-4).

Table 2-4: Coefficients S_S and C_C for different soil type (Table 3.2.V NTC 2008).

Ground-type	S_S	C_C
A	1.00	1.00
B	$1.00 \le 1.40 - 0.40 \cdot F_0 \cdot \frac{a_g}{g} \le 1.20$	$1.10\ (T^*_C)^{-0.20}$
C	$1.00 \le 1.70 - 0.60 \cdot F_0 \cdot \frac{a_g}{g} \le 1.50$	$1.05\ (T^*_C)^{-0.33}$
D	$0.90 \le 2.40 - 1.50 \cdot F_0 \cdot \frac{a_g}{g} \le 1.80$	$1.25\ (T^*_C)^{-0.50}$
E	$1.00 \le 2.00 - 1.10 \cdot F_0 \cdot \frac{a_g}{g} \le 1.60$	$1.15\ (T^*_C)^{-0.40}$

For surface configurations, the classification of Table 3.2.IV of NTC 2008 can be adopted and, consequently, the values of the coefficient S_T are provided in Table 3.2.VI of NTC 2008 (Table 2-5).

Table 2-5: Topographic categories (Table 3.2.IV-VI NTC 2008).

Category	Surface configuration	S_T
T1	Level ground, slopes and isolated hills with an average inclination i ≤ 15°	1
T2	Slopes with an average inclination i > 15°	1.2
T3	Elevations with a much smaller crest width than at the base and average inclination 15° ≤ i ≤ 30°	1.2
T4	Elevations with a much smaller crest width than at the base and average inclination i > 30°	1.4

In order to consider the ductility of the structure, the design response spectra can be defined.

Design response spectrum

The response spectrum in terms of acceleration can be divided for q, defined as a structure coefficient that considers the dissipation capacity of the structure, its over strength, the increase of the period as a result of plasticization.
As defined in EC8 (1998), the behaviour factor q approximates the ratio of the seismic forces (that the structure would experience if its response was completely elastic with 5% viscous damping) to the minimum seismic forces that may be used in design - with a conventional elastic analysis model - still ensuring a satisfactory response of the structure. When performing a non-linear static analysis (pushover analysis), the demand spectrum in term of acceleration is considered assuming q equal to 1, since the non-linearity of the structure is already considered by the type of analysis.

In addition to the response spectrum in terms of acceleration, the one in terms of displacement is also defined.

Displacement response spectrum

The elastic displacement response spectrum $S_{De}(T)$ is obtained by direct transformation of the elastic acceleration response spectrum $S_e(T)$, using the following expression:

$$S_e(T^*) = S_{De}(T^*) \cdot \omega^2 = S_{De}(T^*) \cdot (2\pi/T^*)^2 \quad (8)$$

T* is the period of the structure.

ADRS format

The response spectrum can be represented in an Acceleration Displacement Response Spectra (ADRS) format, which requires representation in a spectral acceleration format, Sa, versus displacement Spectral, Sd (Chopra & Goel, 1999). This format is necessary to apply the Capacity Spectrum Method (§2.6.2.1)

Figure 2-4 shows elastic response spectra in terms of acceleration (a), displacement (b) and in ADRS format (c), obtained for different ground types for Florence.

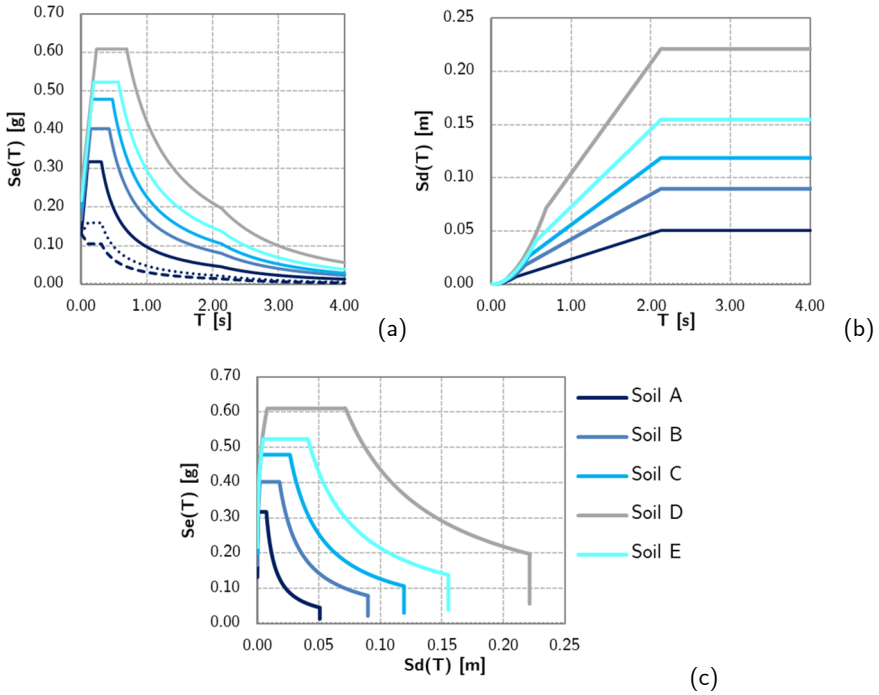

Figure 2-4: Response spectra in acceleration (a), in displacement (b) and ADRS format (c).

2.3 SEISMIC EXPOSURE

The seismic exposure is a measure of the importance of the object exposed to risk in relation to the main characteristics of the built environment. It consists of the value of the elements that compose the territory: settlement system, population, economic activities, monuments, social services (http://www.regione.toscana.it/speciali/rischio-sismico/fattori-di-rischio). The definition of exposure is a very difficult and time-consuming aspect of a seismic risk study (Rota, Penna, Strobbia, & Magenes, 2011). An example is the Exposure Indicator (I_e) introduced by Tuscany Region for the seismic risk assessment at territorial scale: this is obtained from the weighted average of population and housing for each municipality, by processing the data deriving from ISTAT census; four exposure classes are defined based on the I_e values. Through the combination of exposure, vulnerability and hazard classes, it has been possible to assign a risk class to each municipality (Regione Toscana - Settore Sismica, 2016).

2.4 SEISMIC VULNERABILITY AND GENERAL CLASSIFICATION OF THE VULNERABILITY ASSESSMENT METHODS

The seismic vulnerability of a structure is related to its structural features and it expresses its trend to be damaged when an earthquake occurs. It may be observed that vulnerability is a behavioural aspect which describes a cause-effect relation between the earthquake and the damage (Sandi, 1986).
As is common knowledge, for an existing building the mitigation of the seismic risk is closely related to the reduction of its seismic vulnerability.
Three main levels of vulnerability affecting buildings can be identified:

- **Structural vulnerability**: is associated with the susceptibility of the elements composing the resistant system to suffer a certain degree of damage. The nature of the damage can be described quantitatively, using observations of post-earthquake structural damage, or qualitatively, using parameters that define the structural response and determining a damage index.
- **Non-structural vulnerability**: is associated with the susceptibility of architectural elements (interior walls, doors, windows, balconies, panels, decorative elements, etc.) and building components (pipes, installations and other equipment).
- **Functional vulnerability**: is defined as the potential for disruption to the operation of an installation as a result of the increased demand on the services provided. It is about assessing the post-earthquake response capacity of buildings considered essential (hospitals, fire stations, police stations, etc.) and on which maintenance of functions is required.

The seismic vulnerability can be essentially quantified in several ways, which allow estimating damage directly or indirectly:

- **Indexes or classes of vulnerability**: allow estimating, in a relative way, the propensity of a structure to suffer damage.
- **Damage probability matrices, vulnerability curves and fragility curves**: indicate an explicit relation (vulnerability function), which allows estimating directly the structural damage to different levels of seismic action.

In detail, the *vulnerability function* of an element represents the probability that its response to seismic loads exceeds its performance LS, defined considering physical and socio-economic considerations (Milutinovic & Trendafiloski, 2003). This is a relationship which defines the expected damage for a building or a class of buildings as a function of the ground motion (Figure 2-5). It can be derived from a numerical adjustment to a set of damage data observed for different constructive typologies (observed vulnerability) or can be generated through a numerical simulation process using mechanical models (calculated vulnerability). In order to estimate the damage, the capacity of the building must be compared with the seismic demand (Lang, 2002).

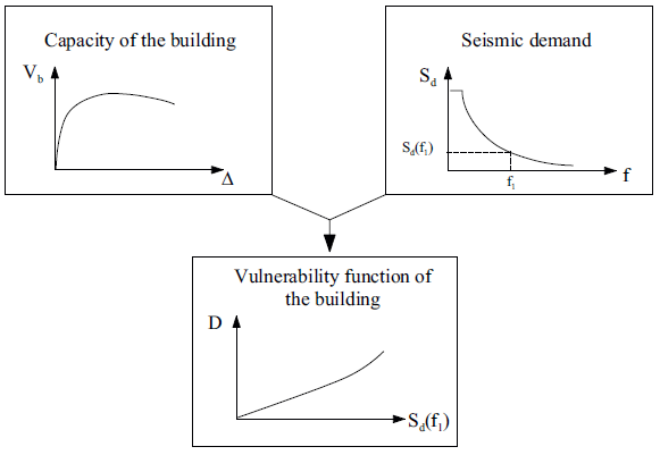

Figure 2-5: Principle of a vulnerability function (Lang, 2002).

Table 2-6: Vulnerability assessment methods for buildings (Lang, 2002).

Expenditure	Increasing computation effort →				
Application	Building stock		Individual building		
Methods	Observed vulnerability	Expert opinions	Simple analytical models	Score assignment	Detailed analysis procedures
	1° level of approach		**2° level of approach**		**3° level of approach**

Table 2-7: Classifications of vulnerability assessment methods.

			LEVEL OF DETAIL		
			1° level of approach	**2° level of approach**	**3° level of approach**
INTENDED RESULTS	**Direct**	**Typological**	DPM		
		Mechanical		Simple mechanical models	**Numerical detailed models**
	Indirect	**Typological**	Vulnerability index methods		
	Hybrid	**Typological**		Macroseismic method	

USED TOOLS & QUALITY OF INFORMATION
Empirical
Analytical
Hybrid

Many vulnerability assessment methods have been developed in the last years (Calvi, et al., 2006). They differ in expenditure and precision and their choice depends on the objective of the assessment and on the availability of data. As shown in Table 2-7, it is possible to classify the vulnerability assessment methods on the following aspects:

- level of detail,
- intended results,
- quality of the source of information and used tools.

A first classification of the vulnerability assessment method considers the **level of detail** (Table 2-7). In detail:

- First level approaches use a considerable amount of qualitative information; they are suitable for a large-scale assessment, by using a limited level of information detail.
- Second level approaches are based on mechanical models, supported by better quality information, with respect to constructive aspects, characterization of materials and accurate geometric information.
- Third level approaches involve the use of numerical modelling techniques that require a complete and rigorous survey of individual buildings.

A second classification, proposed by Corsanego & Petrini (1990), refers to the ***intended results of the methods***, depending on the number of steps involved in the definition of the risk evaluation (Figure 2-6).

- **Direct techniques** directly estimate the damage caused to a structure by an earthquake; two types of methods can be employed: typological and mechanical.
  Typological methods consider the structure belonging to a typological class and the evaluation of the probability of a group or type of buildings, suffering a certain level of damage, is based on the observed and recorded damages in post-earthquake surveys.
  Mechanical methods require a reduced number of parameters with which it is possible to evaluate the seismic behaviour of the constructions.
- **Indirect techniques** determine a vulnerability index, establishing relationships between the degree of damage and the seismic intensity and defining curves or functions of vulnerability, supported by statistical studies of post-earthquake available damage data.
  The first Vulnerability Form was developed in Italy in the '80s (GNDT, 1993) and it is widely used in Italy since then.
- **Conventional techniques** introduce a vulnerability index for the prediction of the level of damage, giving a relative measure of vulnerability due to the difference between the evaluated aspects, which are characteristic of a certain constructive typology. There are two types of approaches: the first one qualifies the different physical characteristics of structures empirically and the second one is based on the criteria defined in seismic design standards for structures, evaluating the capacity-demand relationship of buildings. An example of the first type is ATC-13, which defines damage probability matrices for 78 classes of structure, 40 of which refer to buildings.
- **Hybrid techniques** combine features of the methods described previously. An example is the macroseismic method developed by Lagomarsino and Giovinazzi (2006), which combines a typological method with an indirect technique; indeed this methodology is based on the vulnerability classes defined in the EMS-98 scale (Grünthal, 1998), which is improved through an indirect methodology that introduces a more rigorous characterization of vulnerability.

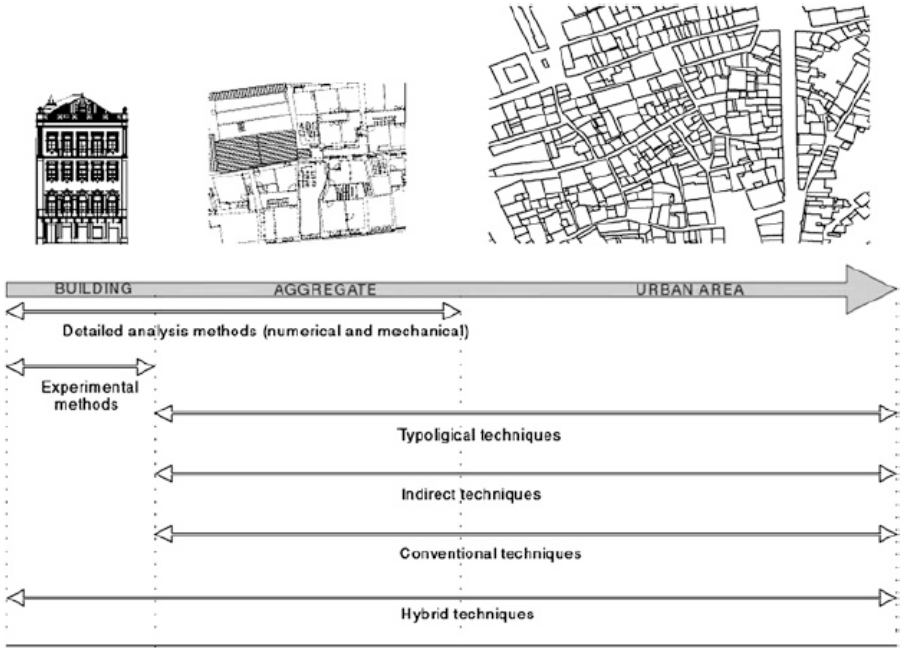

Figure 2-6: Analytical techniques used at different evaluation scales (Vicente, et al., 2014).

A third classification is function of the ***quality of the source of information and used tools*** in the project. There are:

- **Empirical methods** (§2.5), used for a large-scale assessment and based on qualitative evaluations, considering that certain classes of structures that share common structural and loading patterns tend to experience similar types of damage.
- **Analytical-theoretical methods** (§2.6), based on mechanical or numerical procedures to assign seismic vulnerability on buildings either through detailed time-history analysis or through simplified methods.
- **Hybrid methods** (§2.7), based on simplified quantitative evaluations that combine empirical and analytical methods and generally used for the territorial approach.

These methods are explained in detail in the next paragraphs.

As illustrated in Chapter 3, analytical methods are used in this work (as highlighted in red in Table 2-7) by performing nonlinear static analyses.

2.5 EMPIRICAL METHODS

The empirical methods are mainly based on qualitative evaluations, as expert's opinions and/or observations of the damage after seismic events. They are used for a large-scale assessment (first level of approach) when the detailed analysis of each structure can be prohibitively expensive to be performed, and the obtained results are qualitative and representative for a building class: for each one, a series of standard vulnerability functions can be developed.

2.5.1 Vulnerability Index methods

The Vulnerability Index Methods consist in assigning to each building a Vulnerability Index (I_V), by filling out a vulnerability form after a visual inspection necessary to identify the building structural system and its seismic deficiencies.

The form includes several parameters related to the building seismic response, which should be evaluated considering 4 vulnerability classes of growing vulnerability (A: best conditions, B, C and D: worst conditions), to which a score is assigned. Different weights are attributed to the parameters and the vulnerability index Iv is obtained combining, by a weighted average, the different scores and the relative weights.

In the following, the different available forms are briefly illustrated.

2.5.1.1 GNDT II Level Form – 11 Parameters Form

The method of the Vulnerability Index was developed by Benedetti & Petrini (1984) and GNDT (1993); it was successfully applied in Italy and calibrated on a large sample of data in recent years.

The form allows assessing the vulnerability of a structure according to 11 parameters representative of the building's propensity to suffer damage as a result of a seismic event. Each parameter is associated with a class (A - optimal, B, C and D - unfavourable); to each class, a score is attributed. Moreover, each parameter has a weight coefficient, to take account of the different importance that the various elements assume in seismic behaviour.

The vulnerability index I_V is calculated as the weighted sum of the scores of the individual parameters, as shown in the following equation:

$$I_V = \sum_{i=1}^{n} V_i P_i \qquad (9)$$

where:

- n is the number of the parameters,
- V_i is the attributed score to a class,
- P_i is the weight coefficient.

I_V belongs to [0, 382.5] range: it is 0 when the parameters are all in "A" class and 382.5 when they are all in "D" class. It is usually normalized in a 0-100% range, dividing the calculated I_V by the maximum values it can reach (382.5).

In Table 2-8 each parameter, the associated scores and their weights are shown.

Table 2-8: GNDT II Level Form.

GNDT II LEVEL FORM - 11 PARAMETERS – MASONRY BUILDINGS					
Parameters	**Scores**				**Weight**
	A	**B**	**C**	**D**	
P1 - Type and organisation of resistant system	0	5	20	45	1.00
P2 - Quality of resistant system	0	5	25	45	0.25
P3 - Conventional strength	0	5	25	45	1.50
P4 - Building position and type of foundation	0	5	25	45	0.75
P5 - Horizontal elements (floors)	0	5	15	45	var.
P6 - Planimetric configuration	0	5	25	45	0.25
P7 - Configuration in elevation	0	5	25	45	var.
P8 - Maximum distance among the walls	0	5	25	45	0.25
P9 - Coverage/roof	0	15	25	45	var.
P10 - Non-structural elements	0	5	25	45	0.25
P11 - Actual state (conservation status)	0	5	25	45	1.00

Particular attention should be paid to the parameter **P3 - Conventional strength**, that will be used in this work to provide general indications for the M.U.A. definition (§5.3).
This parameter allows estimating the horizontal conventional strength of the building, under the hypothesis of a global box-behaviour. By means of an expedited calculation, the structure resistance to the horizontal action is quantified for the two horizontal directions. For each storey, it is necessary to individuate:

- N: number of floors (from the ground floor).
- At: average covered area over the section that identifies the verification plan.
- A_X, A_Y: total cross-sections of resistance elements in the two orthogonal directions. The length of the resistant elements is measured between the inter-axis of the orthogonal walls. The area of the inclined elements (angle α) must be multiplied by $\cos 2\alpha$.
- A: minimum value of A_X, A_Y.
- B: maximum value of A_X, A_Y.
- $A_0 = A/A_t$ and $\gamma = B/A$.

The horizontal minimum acceleration capacity is given by:

$$C = \frac{A_0 \tau_k}{qN} \sqrt{1 + \frac{qN}{1.5 A_0 \tau_k (1+\gamma)}} \qquad (10)$$

in which τ_k is the shear resistance (in absence of normal load) associated to the diagonal cracking and it can be estimated considering the Italian Code, as reported in paragraph 3.4 (C.M. 617/2009). q is the average weight per unit of covered area and it is calculated as:

$$q = \frac{(A+B)h}{A_t} P_m + P_s \qquad (11)$$

where P_m is the weight of the masonry and P_s is the average weight per unit area of the floor.

The GNDT II Level Form is suitable for isolated masonry buildings. From it, new vulnerability forms were recently created for masonry structures in aggregate, as for example the "Formisano Form" and

"Aveiro Form", which both refer to the vulnerability assessment of a S.U. within the aggregate. There is also the "Aggregate Form", that concerns the study of the vulnerability of a complete aggregate. For all these Forms, the calculation method of the Vulnerability Index (I_V) is the same mentioned above (13).

2.5.1.2 "Formisano" Form – 15 Parameters Form

The methodology by Benedetti & Petrini developed for isolated masonry buildings was integrated by Formisano et al. (2015). The "Formisano Form" allows estimating the vulnerability of a S.U. within an aggregate, including 5 more additional parameters, representative of the interaction among buildings, and deleting the P3 (§2.5.1.1):

- P11: presence of adjacent buildings with different height;
- P12: position of the building within the aggregate;
- P13: number of staggered floors;
- P14: structural or typological heterogeneity among adjacent S.U.s;
- P15: percentage difference of opening areas among adjacent façades.

Scores and weights assigned to the 5 additional parameters were numerically calibrated by implementing static nonlinear analyses to some case studies; therefore, the out-of-plane mechanisms were not considered. Differently from the original form, also negative scores are used, considering the beneficial effects deriving from the aggregate condition on the seismic behaviour of a masonry building.
The new survey form is shown in Table 2-9, where the new 5 parameters are highlighted in grey.

Table 2-9: "Formisano" Form (15 parameters).

FORMISANO FORM - 15 PARAMETERS – MASONRY BUILDINGS SU					
Parameters	**Scores**				**Weight**
	A	**B**	**C**	**D**	
P1 - Vertical elements organization	0	5	20	45	1.00
P2 - Type and quality of vertical elements	0	5	25	45	0.25
P3 - Building position and type of foundation	0	5	25	45	0.75
P4 - Plan distribution of structural elements	0	5	25	45	1.50
P5 - Regularity in plan	0	5	25	45	0.50
P6 - Regularity in elevation	0	5	25	45	0.50 - 1.00
P7 - Floors	0	5	15	45	0.75 - 1.00
P8 - Roof	0	15	25	45	0.75
P9 - Details (non-structural elements)	0	0	25	45	0.25
P10 - Actual state (conservation status)	0	5	25	45	1.00
P11 - Presence of adjacent buildings with different height	-20	0	15	45	1.00
P12 - Position of the building within the aggregate	-45	-25	-15	0	1.50
P13 - Number of staggered floors	0	15	25	45	0.50
P14 - Structural or typological heterogeneity among adjacent S.U.s	-15	-10	0	45	1.20
P15 - Percentage difference of opening areas among adjacent façades	-20	0	25	45	1.00

2.5.1.3 "Aveiro" Form – 14 Parameters Form

The "Aveiro" Form was developed by Vicente (2008) and it adds 3 parameters to the GNDT II level form. This form is specifically calibrated for masonry S.U. within the aggregate and it is composed of 14 parameters, which can be divided into 4 macro-classes to emphasise their differences and relative importance.

Table 2-10: "Aveiro" Form (14 parameters).

AVEIRO FORM - 14 PARAMETERS – MASONRY BUILDINGS SU					
Parameters	**Scores**				**Weight**
	A	**B**	**C**	**D**	
a) Structural building system					
P1 - Type of resisting system	0	5	20	50	0.75
P2 - Quality of resisting system	0	5	20	50	1.00
P3 - Conventional strength	0	5	20	50	1.50
P4 - Maximum distance between walls	0	5	20	50	0.50
P5 - Number of floors	0	5	20	50	1.50
P6 - Location and soil conditions	0	5	20	50	0.75
b) Irregularities and interactions					
P7 - Aggregate position and interaction	0	5	20	50	1.50
P8 - Plan configuration	0	5	20	50	0.75
P9 - Height regularity	0	5	20	50	0.75
c) Floor slabs and roofs					
P10 - Wall façade openings and alignments	0	5	20	50	0.50
P11 - Horizontal diaphragms	0	5	20	50	1.00
P12 - Roofing system	0	5	20	50	1.00
d) Conservation status and other elements					
P13 - Fragilities and conservation status	0	5	20	50	1.00
P14 - Non-structural elements	0	5	20	50	0.50

The first group includes parameters characterising the building resisting system, the type and quality of masonry, material, masonry fabric, arrangement and quality of connections between walls. The second group considers building irregularities and the interaction between S.U.s. The third group evaluates the horizontal structural systems. Finally, the fourth group evaluates structural fragilities and the conservation state. The added parameters are:

- P5: number of floors;
- P7: aggregate position and interaction;
- P10: wall façade openings and alignments.

The new survey form is shown in Table 2-10, where the new 3 parameters are highlighted in grey.

2.5.1.4 Aggregate Form – 5 Parameters Form

This Form (Ferreira, Vicente, & Varum, 2012) was developed for the evaluation of the aggregate in its entirety and it is composed of 5 parameters. The evaluated parameters are almost qualitative, suitable for preliminary screening of the buildings in case of large-scale assessment.

Table 2-11: Aggregate Form (5 parameters).

AGGREGATE FORM - 5 PARAMETERS					
Parameters	**Scores**				**Weight**
	A	**B**	**C**	**D**	
P1 - Quality of the masonry fabric	0	5	20	50	1.50
P2 - Misalignment of openings	0	5	20	50	0.50
P3 - Irregularities in height	0	5	20	50	0.75
P4 - Plan geometry	0	5	20	50	0.75
P5 - Location and soil quality	0	5	20	50	0.75

2.5.2 Damage Probability Matrix (DPM)

The method of Damage Probability Matrix (DPM) was first developed by Whitman (1973) and it provides the use of probabilistic matrices of damage for the prediction of the damage caused by seismic events. The DPM represents the probability of occurrence of a certain damage state for a level of macroseismic intensity in a specific building typology. Figure 2-7 shows the general format of DPM. Damage to buildings is described by 8 levels, while the intensity of the earthquake is described by the modified Mercalli intensity scale (MMI). Each level of damage is identified by two different aspects: a description of the physical damage (structural and non-structural) and an objective ratio among the reparation cost of the considered damage and the reconstruction cost of the whole building. In the columns of the levels of intensity, each number is the probability that a certain damage state will occur, since a level of earthquake intensity is experienced; the sum of the probabilities in each column is 100%.

DAMAGE	STRUCTURAL	NON-STRUCTURAL	DAMAGE	INTENSITY OF EARTHQUAKE				
STATE	DAMAGE	DAMAGE	RATIO (%)	V	VI	VII	VIII	IX
0	NONE	NONE	0-0.05	95	79	33	6	0
1	NONE	MINOR	0.05-0.3	5	18	34	19	2
2	NONE	LOCALIZED	0.3-1.25	0	3	20	44	18
3	NOT NOTICEABLE	WIDESPREAD	1.25-3.5	0	0	10	13	30
4	MINOR	SUBSTANTIAL	3.5-7.5	0	0	3	6	20
5	SUBSTANTIAL	EXTENSIVE	7.5.20	0	0	0	12	10
6	MAJOR	NEARLY TOTAL	20-65	0	0	0	0	7
7	BUILDING CONDEMNED		100	0	0	0	0	8
8	COLLAPSE		100	0	0	0	0	5

Figure 2-7: Format for Damage Probability Matrix (Whitman, 1973).

Whitman completed the matrix for different structural typologies, considering the data collected after the 1971 San Fernando earthquake (California, 6.6 magnitude - Richter Scale). Each damaged building of the sample (over 1600 buildings) was classified in function of the level of damage (buildings in areas where the intensity exceeded VIII were excluded), the material of construction, the age of the building and the number of storeys. All the collected data allowed the creation of matrices of probability of damage.

In the following, the DPM for the area hit by VII level of MM scale of San Fernando earthquake is proposed.

DAMAGE PROBABILITIES (%) AND MEAN DAMAGE RATIOS (%) FOR INTENSITY VII ZONE OF SAN FERNANDO EARTHQUAKE

Date Const.	Pre-1933				Post-1947					
No. Stories	5-7		8-13		5-7		8-13		14-18	19+
Type of Const.	Co	St	Co	St	Co	St	Co	St	St	St
Damage State										
0	16	18	16	6	21	24	27	44	43	21
1	16	9	12	13	26	28	33	31	43	54
2	26	46	28	53	16	38	32	6	0	25
3	21	27	14	16	26	5	8	16	14	0
4	11	0	21	0	11	5	0	3	0	0
5	0	0	7	9	0	0	0	0	0	0
6	10	0	2	3	0	0	0	0	0	0
7	0	0	0	0	0	0	0	0	0	0
MDR - %	4.4	1.1	2.7	2.5	1.1	.66	.43	.52	.43	.24
No. Bldgs.	19	11	43	32	19	21	37	32	14	24

Figure 2-8: DPM for the area hit by VII level of MM scale of San Fernando earthquake (Whitman, 1973).

2.5.2.1 EMS-98 DPM

The EMS-98 scale (§2.2.2) contains a definition of the structural typologies and of the damage distribution correlated to each degree of intensity; consequently, it can be considered as a vulnerability model able to provide, for a given intensity, the probable damage distribution. Indeed, recalling that a damage matrix contains the probability for the buildings belonging to a certain vulnerability class to suffer a certain damage level for a given intensity, the damage pattern related to each intensity degree may be reported in terms of a DPM for each vulnerability class (Figure 2-9). However, as observed by Giovinazzi (2005) and Bernardini et al. (2007 B), the provided model is vague and incomplete, since the damage level is characterized through the quantitative terms "Few", "Many" and "Most", represented by the scale as three narrowly overlapping percentage ranges (Figure 2-10); moreover, the distribution of damage is incomplete as the Macroseismic Scale considers only the most common and easily observable situations.

Dk/I	*0*	*1*	*2*	*3*	*4*	*5*
V		Few A or B				
VI		Many A or B, Few C	Few A or B			
VII			Many B, Few C	Many A, Few B	Few A	
VIII			Many C, Few D	Many B, Few C	Many A, Few B	Few A
IX			Many D, Few E	Many C, Few D	Many B, Few C	Many A, Few B
X			Many E, Few F	Many D, Few E	Many C, Few D	Most A, Many B, Few C
XI			Many F	Many E, Few F	Most C Many D, Few E	Most B, Many C, Few D
XII						All A or B, Nearly All C, Most D or E or F

Figure 2-9: Damage distributions for different vulnerability classes and different intensity degrees according to EMS-98 macroseismic scale (Bernardini et al., 2007 B).

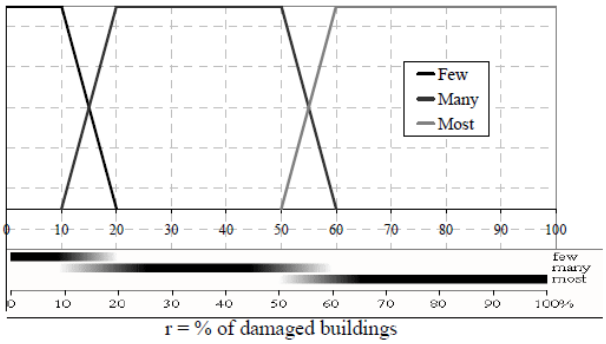

Figure 2-10: Narrowly overlapping percentage ranges corresponding to the linguistic terms Few, Many, Most (Giovinazzi, 2005).

2.5.3 Vulnerability curves

Vulnerability curves are one of the main variants of vulnerability functions (§2.4), expressed in terms of the vulnerability index. They correlate the mean damage grade for different vulnerability classes with the macroseismic intensity and the vulnerability index.

Guagenti & Petrini (1989) started the first studies on vulnerability-damage correlations, relying on observations of damage data on masonry buildings hit by earthquakes. In order to quantify the seismic vulnerability of a building, they defined a correlation between the variable y (ground acceleration) defined in the range (y_i, y_c) where y_i corresponds to the starting point of the damage and y_c refers to collapse, and the variable d (damage level), defined in the range (0, 1). As shown in Figure 2-11, for each level of acceleration y, it is possible to find infinite levels of damage d, each of them is characterized by a probability density conditioned function P{d|y}. The values of y_i and y_c are aleatory variables too.

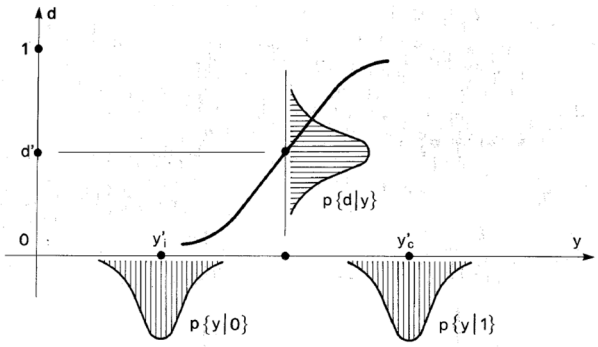

Figure 2-11: Ground acceleration – damage probabilistic law (GNDT, 1993).

The DPM (§2.5.2) are the discretisation of the probabilistic approach of this problem: for each finite number of couple (d_h,y_k) a DPM, whose generic point is P{d_h|y_k}, is defined.

Considering the high level of uncertainties that the probabilistic approach can bring to the analysis, generally a deterministic approach is preferred; in this case, the function y_k-d_h may be expressed through a trilinear law, as shown in Figure 2-12:

$$\begin{aligned} d &= 0 && when\ y_k < y_i \\ d &= \frac{y-y_i}{y_c-y_i} && when\ y_i < y_k < y_c \\ d &= 1 && when\ y_k > y_c \end{aligned} \qquad (12)$$

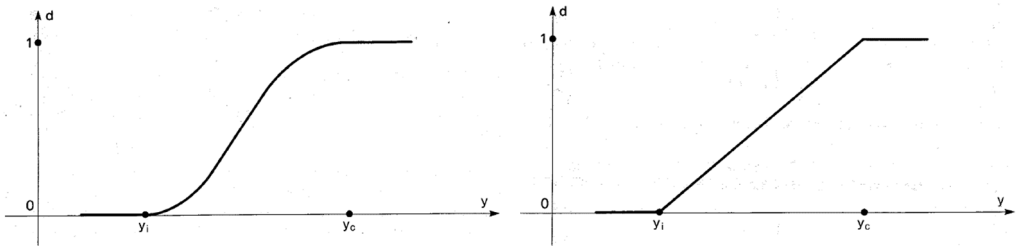

Figure 2-12: Ground acceleration – damage deterministic law (a) and trilinear approximation function (GNDT, 1993).

Guagenti & Petrini (1989) studied a consistent sample of damaged masonry buildings, belonging the to the historical city centres of the villages of Venzone (Udine, intensity IX MCS of May 1976 earthquake), Tarcento and San Daniele (Udine, intensity VIII MCS of May 1976 earthquake); some other buildings were added from the 1984 Parco d'Abruzzo earthquake (intensity VII MCS). The level of damage of each building was considered, as well as the level of the ground acceleration, estimated by the equation (10). By using the trilinear law, the accelerations y_i and y_c was defined through the following formulas:

$$y_i = \alpha_i \cdot exp\,(-\beta_i \cdot I_V) \qquad y_c = (\alpha_c + \beta_c \cdot {I_V}^{\gamma})^{-1} \tag{13}$$

where:

- $\alpha_i = 0.08,\ \beta_i = 0.01950$
- $\alpha_c = 1.00,\ \beta_c = 0.00191\ ,\ \gamma = 1.80$

This model allows calculating the accelerations y_i and y_c, in correspondence of the structural first damage and collapse, considering all the possible values of the Vulnerability Index I_V related to the filling out of the GNDT II Form (§2.5.1.1).

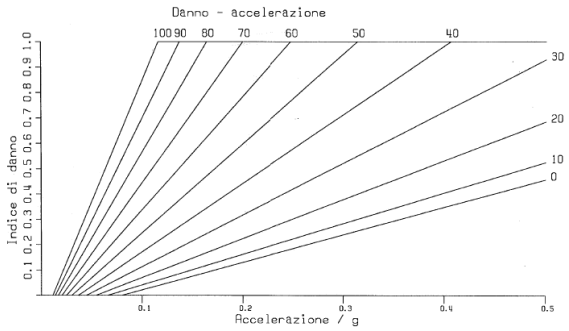

Figure 2-13: Relation among damage, acceleration and I_V (Guagenti & Petrini, 1989).

In the formulation by Guagenti & Petrini, the seismic hazard is defined in term of PGA (derived from the MCS macroseismic intensities) and the damage is expressed in terms of an economic damage index (d_e, in a [0-1] range). Another formulation of vulnerability curves derives from the macroseismic method (§2.5.4), based on the definition of mean damage grade for vulnerability classes according to the EMS-98 scale.

2.5.4 Macroseismic method

In order to overcome the problem of the incompleteness and vagueness of DPM derived from EMS-98, Giovinazzi proposed a Macroseismic Method (Giovinazzi, 2005), in which the distribution of damage is completed introducing a beta probability distribution of damage grade and the uncertain quantitative definition of the level of damage through the terms "Few", "Many" and "Most" is resolved through a fuzzy

set theory, translating the linguistic terms into a precise probability value and modelling them as bounded probability ranges. A conventional vulnerability index V, assuming values from 0 to 1, is introduced and it represents the belonging of a building to a vulnerability class. In compliance with the fuzzy set theory, vulnerability index membership functions have a plausible range (χ=1) and linear possible ranges, representative of the transition between two adjacent classes.

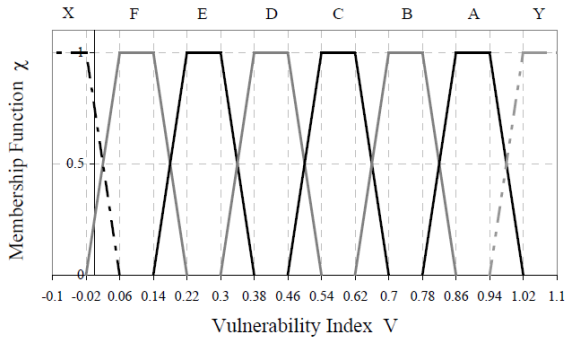

Figure 2-14: Vulnerability index membership functions for EMS 98 vulnerability classes (Giovinazzi, 2005).

An analytical continuous expression to describe the vulnerability curves is proposed; it provides the mean damage grade μ_D as a function of the macroseismic intensity I, only depending from the vulnerability index V and the ductility index Q (Eq. 19):

$$\mu_D = 2.5[1 + \tanh\left(\frac{I+6.25V-13.1}{Q}\right)] \qquad 0 \leq \mu_D \leq 5 \qquad (14)$$

The vulnerability index V value determines the position of the curve; an increase of V equal to ΔV=0.16 means that the same damage grade is produced by a one degree less earthquake. The ductility index Q determines the rate of increase in the damage with intensity. The curves derived from EMS-98 scale are characterized by Q=2.3.

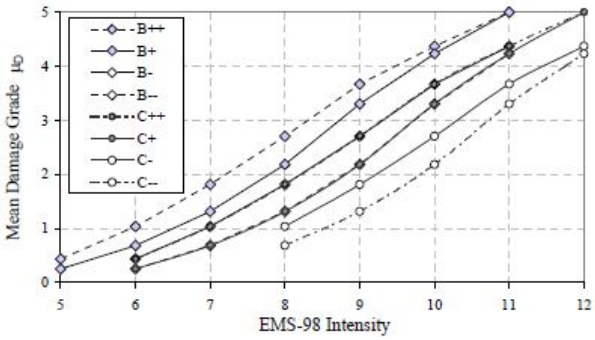

Figure 2-15: Example of vulnerability curves (Giovinazzi, 2005).

With reference to the macroseismic methods, Bernardini et al. (2007) proposed a modified analytical expression of the vulnerability curves. The DPM were parameterized with respect to a single parameter V ∈ [0, 1], independent from the intensity of the earthquake and measured by a fuzzy set associated to each vulnerability class ("A"-"F", in EMS-98). Fixed V and the intensity I, the mean value of a DPM is determined through a well-defined analytical function and, multiplying it by a function $f(V,I)$ depending on the intensity I and the vulnerability index V, the expression of the relationship of the vulnerability curves is obtained as shown in the following expression:

$$\mu_D = [2.5 + 3 \cdot \tanh\left(\frac{I+6.25 \cdot V-12.7}{3}\right)] \cdot f(V,I), \quad 0 \leq \mu_D \leq 5$$
$$f(V,I) = \begin{cases} e^{\frac{V}{2}(I-7)} & if\ I \leq 7 \\ 1 & if\ I > 7 \end{cases} \tag{15}$$
$$V = 0.56 + 0.0064 \cdot I_V$$

2.6 ANALYTICAL METHODS

The analytical methods use mechanical or numerical procedures to assign seismic vulnerability on buildings, by using detailed numerical models. Therefore, they require a large amount of information in terms of geometry, constructive technology and materials; for this reason, they are usually suitable for a small sample of buildings.

These methods allow the calculation of the level of vulnerability of the analysed structures through the *safety index* (IS), that is the ratio of the seismic capacity of the structure (in terms of peak ground acceleration, $a_{g,C}$, or reference period, $T_{R,C}$) that produces on the structure the achievement of the chosen limit state, and the seismic demand of the site in which the structure is collocated, associated the same limit state. Since the safety index involves the seismic demand (hazard) and the structural vulnerability, it is usually considered as an *index of seismic risk*; in terms of peak ground acceleration, it is equal to:

$$IS = \frac{a_{g,C}}{a_{g,D}} \tag{16}$$

The most used analysis procedures for this group of methods are (ASCE/SEI 41-13; FEMA 273; FEMA 440; EN1998-1:2004; NTC 2008):

- Linear static analysis: seismic action is modelled by a distribution of equivalent static lateral forces related to the 1st modal shape of the structure in the considered direction. The nonlinear behaviour is considered through the adoption of a behaviour factor, which numerically reduces the demand (design spectrum). This type of analysis is suitable for the study of regular buildings, where the 1st vibration mode is predominant in determining the response.
- Linear dynamic analysis: it is based on spectral modal analysis, assuming that the dynamic response of a structure can be determined by independently considering the response of each natural mode of vibration using an elastic response spectrum; the effects of each mode are combined in a statistical way. Materials have linear elastic behaviour and the non-linear behaviour is considered by the adoption of the behaviour factor.
- **Nonlinear static analysis**: it considers the nonlinear behaviour of the structure and it is based on the determination of the capacity curve (pushover curve), which is proportional to the relationship between the total base shear and the displacement at the top of the structure, when subjected to constant gravity loads and increasing lateral forces or monotonic displacements. This method is suitable for regular buildings, where the 1st vibration mode is preponderant in the response of the structure; it is also the main analysis adopted for existing masonry structures. For this reason, it is the adopted method in this work; it is deepened in §3.1.2.1.
- Nonlinear dynamic analysis (time-history): material nonlinearity is considered, and seismic action is modelled by temporal movement histograms (real or artificially generated accelerograms); the structure response is determined on the basis of step-by-step integration procedures.

2.6.1 Mechanisms methods

These methods allow the analysis of a large number of buildings with a reduced calculation effort, by using few parameters to evaluate the seismic behaviour of the constructions.

An example of these methods is FaMIVE (Failure Mechanisms Identification and Vulnerability Evaluation) methodology (D'Ayala & Speranza, 2002), based on the prior identification of the most probable mechanisms of collapse (Figure 2-16, §3.1.1). By filling of an interactive electronic form with geometrical features, loads, restraints and boundary condition, a static limit analysis is performed, and the lower failure loads factor/multiplier is determined. Each type of collapse is associated with an expected degree of damage, according to the EMS-98.

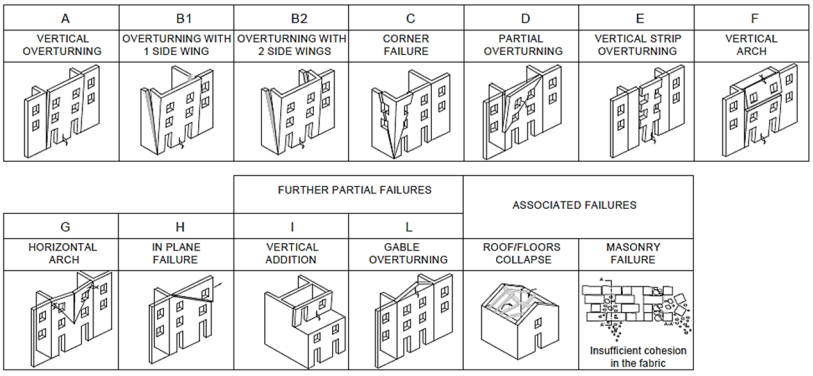

Figure 2-16: Considered out-of-plane mechanisms (D'Ayala & Speranza, 2002).

2.6.2 Capacity Spectrum based methods

Capacity spectrum methods constitute evaluation procedures of the structural performance and they require the definition of the capacity curve and the response spectrum characterizing the seismic action. The capacity curve can be estimated by using detailed analyses, such as a nonlinear analysis (§2.6.2.1, §2.6.2.2), or mechanical simplified models (§2.6.2.3, §2.6.2.4).

In the following, the keynotes of these methods are described.

2.6.2.1 Capacity Spectrum Method

The *Capacity Spectrum Method (CSM)*, developed by Freeman (1998), is a procedure that compares the capacity of the structure, in the form of a pushover curve (§3.1.2.1), with the demand on the structure.

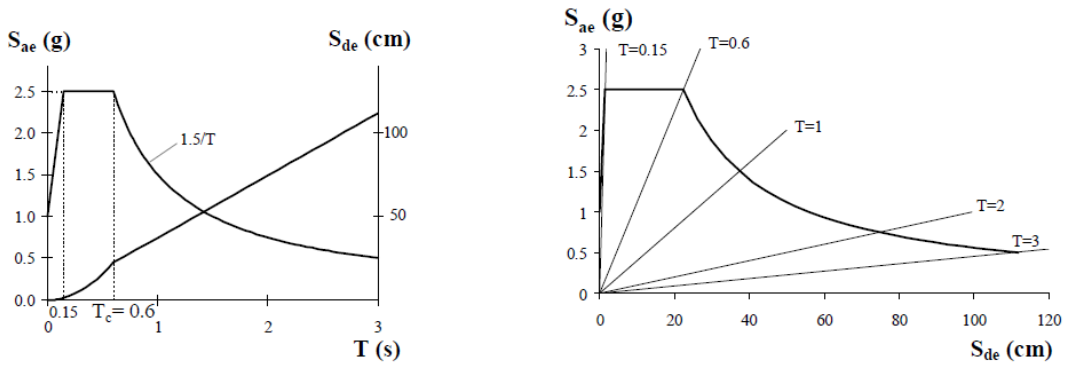

Figure 2-17: Typical elastic acceleration (S_{ae}) and displacement spectrum (S_{de}) for 5% damping normalized to 1.0 g PGA. (a) Traditional format, (b) AD format. (Fajfar, 2000).

The seismic action is characterized by an elastic response spectrum (§2.2.3), defined for a given damping level, which accounts for the energy dissipation of a structure resulting from hysteresis mechanisms (Figure 2-17). As previously introduced, in order to apply the Capacity Spectrum Method, the response spectrum must be represented in the ADRS format (Chopra & Goel, 1999).

As shown in Figure 2-18, the graphical intersection of the two curves approximates the response of the structure, indicated as performance point, and it allows a direct understanding of the level of structural safety.

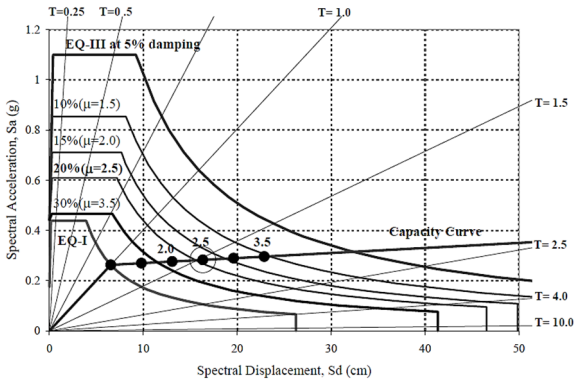

Figure 2-18: Capacity spectrum method (CSM) (Freeman, 1998).

2.6.2.2 N2 Method

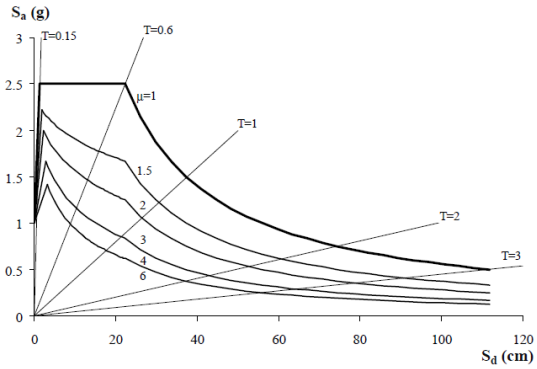

Figure 2-19: Demand spectra for constant ductilities in AD format normalized to 1.0 g PGA (Fajfar, 2000).

The N2 Method, modified CSM formulation (Fajfar, 2000), is based on an inelastic response spectrum defined, for an inelastic S.D.O.F. system and for constant ductility, by applying a reduction factor R_μ due to ductility, based on the expressions of Vidic et al. (1994), as shown in Figure 2-19:

$$S_a = \frac{S_e}{R_\mu}$$
$$S_d = \mu \frac{S_{De}}{R_\mu} = \frac{\mu}{R_\mu} \frac{T^2}{4\pi^2} S_{ae} = \mu \frac{T^2}{4\pi^2} S_a \quad (17)$$

Where: μ is the ductility factor defined as the ratio between the maximum displacement and the yield displacement; R_μ is the reduction factor due to dissipation hysteretic energy of ductile structures.

In Figure 2-20 both the demand spectra and the capacity diagram are plotted. The intersection of the radial line corresponding to the elastic period of the idealized bilinear system T* with the elastic demand spectrum S_{ae} defines the acceleration demand required for the elastic behaviour and the corresponding

elastic displacement demand. The yield acceleration S_{ay} represents both the acceleration demand and the capacity of the inelastic system.

R_μ can be determined as the ratio between the acceleration of the elastic system $S_{ae}(T^*)$, calculating in correspondence of the elastic period T*, and the acceleration of the inelastic system S_{ay}:

$$R_\mu = \frac{S_{ae}(T^*)}{S_{ay}} \tag{18}$$

R_μ can be expressed by the following formula:

$$R_\mu = \begin{cases} (\mu - 1)\dfrac{T}{T_C} + 1 & T < T_C \\ \mu & T \geq T_C \end{cases} \tag{19}$$

where T_c is the characteristic period of the ground motion (§0).

As shown in Figure 2-20, if $T^* \geq T_C$, the inelastic displacement demand S_d is equal to the elastic displacement demand S_{de}. If $T^* < T_C$, the displacement demand can be determined either from the definition of ductility or from equations (22) and (24). In both cases ($T^* < T_C$ and $T^* \geq T_C$), the inelastic demand corresponds to the intersection point of the capacity diagram with the demand spectrum corresponding to the ductility demand μ.

$$S_d = \begin{cases} \mu D_y^* = \dfrac{S_{de}}{R_\mu}\left(1 + (R_\mu - 1)\dfrac{T_C}{T^*}\right) & T^* < T_C \\ S_{de}(T^*) & T^* \geq T_C \end{cases} \tag{20}$$

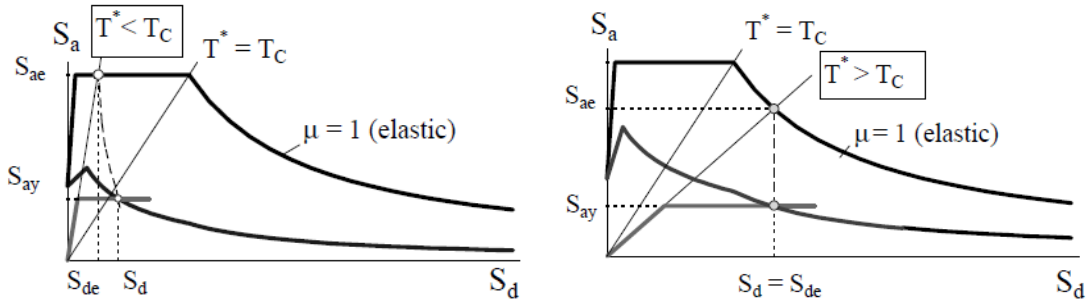

Figure 2-20: Elastic and inelastic demand spectra versus capacity diagram (Fajfar, 2000).

2.6.2.3 The displacement-based approach by Calvi

The method developed by Calvi (1999) is based on the evaluation of displacement capacity of different building types, computed for a set of performance levels, to be compared with displacement demand, evaluated by considering appropriate displacement spectra with an equivalent period of vibration. The different building types are defined considering few parameters (i.e. age of construction, number of floors and type of material). Four limit states are determined depending on the level of damage, in order to discretise the expected building response:

- LS1: no damage, either structural and non-structural;
- LS2: minor structural damage and/or moderate non-structural damage;
- LS3: significant structural damage and extensive non-structural damage;
- LS4: collapse.

The results are presented in terms of probability of occurrence of each specific damage limit state for a given earthquake motion, represented through an appropriate displacement response spectrum for each building. For each structural type and for each damage state, a structural equivalent model is defined

(Figure 2-21) in terms of secant stiffness, corresponding to the maximum displacement (drift) allowed by the limit state LS, and of viscous damping equivalent to the energy dissipated by the structure, again in correspondence of the LS. From it, the following quantities are determined:

- minimum and maximum expected displacement capacity;
- minimum and maximum expected vibration period, corresponding to the secant stiffness to the displacement capacity;
- displacement demand reduction factor as a function of the expected energy dissipation level.

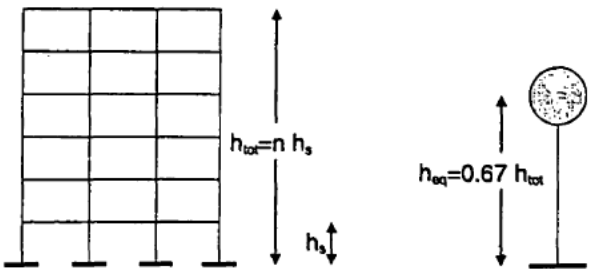

Figure 2-21: Representation of an equivalent SDOF model (Calvi, 1999).

In the plane of the displacement spectrum, a series of rectangles are defined by the determined values of displacement and period (minimum and maximum) and they may be intersected by the spectral curve defining the input motion. The probability of occurrence of a given damage state is reached by integrating a probability density function (assumed constant over the rectangles) in the area below the displacement spectrum. The computed probability can be interpreted as the probability that a building, defined by the rectangle, attains the corresponding limit state, for the ground motion defined by the spectral line; alternatively, it can be interpreted as the percentage of the total number of similar buildings, represented by the rectangle, attain the corresponding limit state.

Considering the reduced number of data, the definition of damage intervals rather than deterministic values, its adaptability to various structural typologies, this methodology is not reliable, and it should not be used to assess the response of single buildings.

2.6.2.4 The mechanical simplified method by Cattari et al. (2004)

Cattari et al. (2004) propose a simplified model focused on masonry buildings, in which capacity curves are identified as perfectly elastic-plastic bilinear defined by three typological quantities: 1. T, the period of vibration; 2. Ay, the horizontal yield acceleration characterizing the structural strength; 3. the last displacement of the structure du (Figure 2-22).

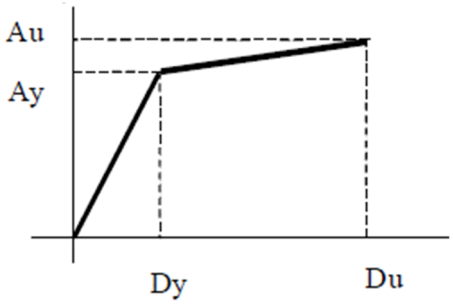

Figure 2-22: Capacity curve (Cattari, et al., 2004).

In accordance with (Calvi, 1999), 4 limit states are defined; in this method, the identification of the limit damage is correlated to points defined on the bilinear in terms of displacements (Figure 2-23):

$S_{d,1} = 0.7D_y$

$S_{d,2} = 1.5D_y$

$S_{d,1} = 0.5(D_y + D_u)$

$S_{d,4} = D_u$

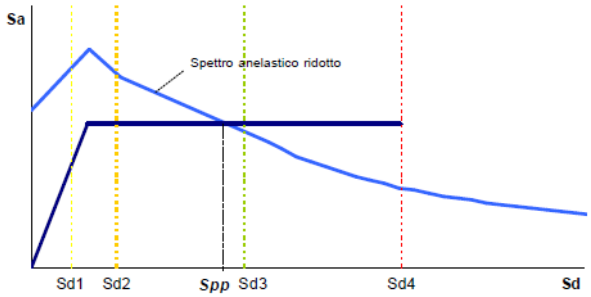

Figure 2-23: Limit states associated with the displacement of the structure (Cattari, et al., 2004).

The evaluation of the expected performance level for the system is deterministic; introducing it as the average standard deviation, the fragility curves can be defined (Figure 2-24).

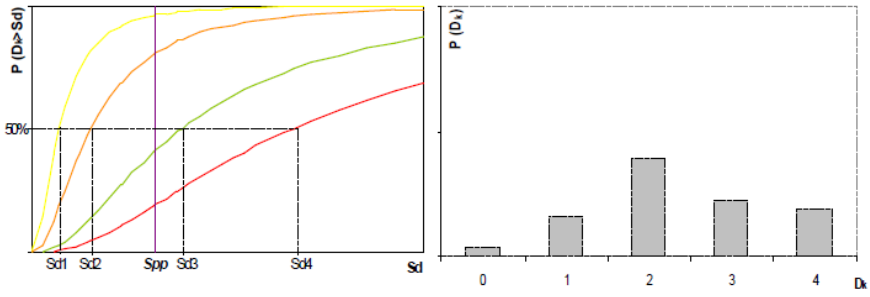

Figure 2-24: Fragility curves for the damage limit states (a) and relative probability of occurrence for the displacement in correspondence with the performance point (b) (Cattari, et al., 2004).

2.6.3 Fragility curves

For a given set of buildings, the fragility curves provide the conditional probability of being in $P[D = ds]$ or exceeding $P[D > ds]$ a given damage state ds, as a function of the demanded spectral displacement (to be considered as an estimation of the mean value), obtained with the performance point. Like vulnerability curves, fragility curves represent action-damage relationships for different types of buildings. However, the fragility curves describe in a continuous way the probability of exceedance of the damage limit states, conventionally adopted between 0 and 5 (Sd1 to Sd5).

A building fragility model (Figure 2-25) consists of a suite of fragility curves, each of them is characterized by the median value and the lognormal standard deviation (β) of seismic hazard parameter (i.e., the spectral displacement S_d):

$$P[ds|S_d] = \Phi[\frac{1}{\beta_{ds}} \ln\left(\frac{S_d}{\bar{S}_{d,ds}}\right)] \quad (21)$$

where:

– S_d is the spectral displacement (seismic hazard parameter);

- $\bar{S}_{d,ds}$ is the median value of spectral displacement at which the building reaches a certain threshold of the damage state ds;
- β_{ds} is the standard deviation of the natural logarithm of spectral displacement of damage state ds;
- Φ is the standard normal cumulative distribution function.

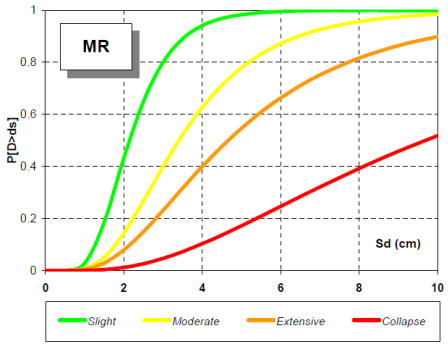

Figure 2-25: Example of a fragility model (Milutinovic & Trendafiloski, 2003).

2.7 HYBRID METHODS

The hybrid methods represent a combination of empirical and analytical methods and they are based on simplified quantitative evaluations. They generally are used for a territorial approach, in order to have a first estimation of the seismic vulnerability through the evaluation on the risk index, as a ratio among the seismic capacity and the seismic demand.

An example of hybrid method is the SAVE project ("*Strumenti Aggiornati per la Vulnerabilità sismica del patrimonio Edilizio e dei sistemi urbani, INGV/GNDT Research Group*" , Dolce & Moroni, 2004), developed for public heritage of Italy, such as schools, hospitals, etc., which allows to calculate the capacity of the structure under the hypothesis of the global box behaviour.

§

In the following Chapter 3, the analytical methods related to the analysis of existing masonry buildings are described, focusing on that used in this work.

Chapter 3.
Seismic performance assessment of masonry buildings in aggregate

In this chapter, the seismic performance assessment of masonry buildings in aggregate is deepened. First, the typical behaviours (local and global) of existing masonry structures are presented, together with the related analytical methods for evaluating the seismic capacity. Then, the problem of the seismic vulnerability assessment for the masonry aggregates is reviewed. Finally, the hypotheses of this work and the adopted analysis methods are illustrated.

It should be remembered that the main topic of this study is the seismic performance of masonry buildings in aggregate related to a ***global box behaviour*** *since this is not sufficiently deepened in literature. Therefore, the following results and considerations are reliable for buildings characterized by a masonry quality able to avoid collapse for walls disintegration and in which the local mechanisms are inhibited. The* ***nonlinear static analysis*** *is the analytical method adopted for evaluating the seismic capacity.*

Contents

3.1 SEISMIC BEHAVIOUR OF MASONRY BUILDINGS

It is common knowledge that the seismic response of masonry buildings may occur through two categories of collapse mechanisms: 1st failure modes (out-of-plane mechanisms) and the 2nd failure modes (in-plane mechanisms) (Giuffrè, 1993). The activation of such mechanisms depends on several factors, related to the building characteristics, especially to the age and the state of conservation and to the action direction; in particular, they must be characterized by a masonry quality able to avoid collapse for walls disintegration (Borri et al., 2015).
In the case of out-of-plane mechanisms, the wall is stressed along its weakest direction, while in the case of in-plane mechanisms the seismic force acts along its most resistant direction (Figure 3-1).

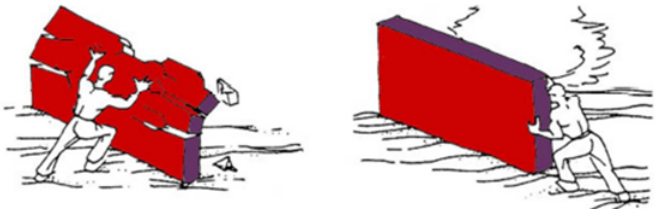

Figure 3-1: Out-of-plane (left) and in-plane behaviour (right).

The 1st failure modes (§3.1.1) occur when each wall is not well connected with the other parts of the structure (orthogonal walls and floors); in this case, the seismic action can cause simple or composed overturning of the wall, horizontal or vertical bending, overturning of the corner, etc. (Figure 3-2). Since these failure modes consist in a local behaviour of a part of the structure, independently from the remaining, they are called *local mechanisms.*

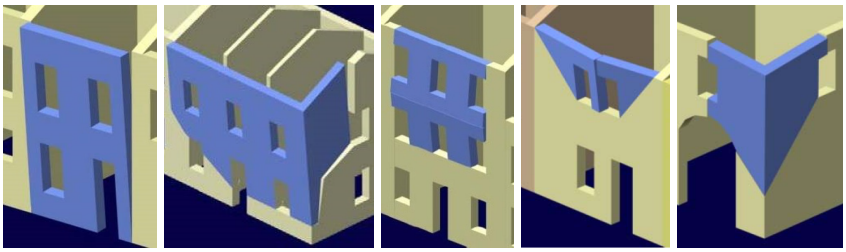

Figure 3-2: Typologies of out-of-plane mechanisms (www.reluis.it).

The 2nd failure modes (§3.1.2) can occur when a structure presents a "global box behaviour" (Figure 3-3), depending on the presence of connection among orthogonal walls and between horizontal and vertical elements, able to guarantee the horizontal distribution of shear forces. In this case, the walls collapse after reaching the maximum in-plane shear resistance, following different ways of failure in function of geometry, restraint conditions and material properties of the masonry.

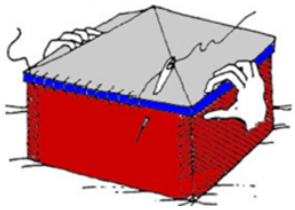

Figure 3-3: Global box behaviour.

Although both typologies of failure should be investigated in the seismic assessment of masonry structures, this work focuses the attention on the **global box behaviour** of masonry buildings in aggregate,

since there is still a clear research gap about this topic. On the contrary, the analysis of the local mechanisms for this kind of structures is widely deepened in the literature; some examples are the works by Giuffrè (1993), Giuffrè & Carocci (1999), Valluzzi et al. (2007) and Boschi (2015).
Therefore, as previously mentioned, the following results are reliable for buildings presenting connections among orthogonal walls and between horizontal and vertical elements, able to explicate a global behaviour, in which the local mechanisms are inhibited.

In the following, both out-of-plane (§3.1.1) and in-plane (§3.1.2) mechanisms of failure are illustrated. Moreover, the nonlinear static analysis is deepened (§3.1.2.1), since is the adopted method for evaluating the seismic capacity in this work.

3.1.1 Out-of-plane mechanisms of failure

Out-of-plane mechanisms are characterized by the collapse of portions of the structure (usually the façades) for loss of equilibrium (De Felice & Giannini, 2001; D'Ayala & Paganoni, 2011; Cattari et al., 2012; Ferreira et al., 2015). They can be grouped into three main sets:

- Overturnings,
- Vertical bendings,
- Horizontal bendings.

Additional subgroups can be identified in relation to the geometry and the portion of the wall involved in the mechanism (AA.VV. Dirett. scientifico Borri, 2011).
The analysis of these mechanisms requires the identification of macroelements, by considering the geometry, the diachronic process of building up and the presence of weakest portions.
The method is based on the limit analysis of a rigid body, with the calculation of the minimum multiplier of horizontal loads (α_0) by applying the second theorem of the limit analysis (kinematic theorem). The method is based on equilibrium equations by writing the equation of the Principle of Virtual Work (Eq. 27):

$$\alpha_0 \left(\sum_{i=1}^{n} P_i \delta_{X,i} + \sum_{j=n+1}^{n+m} P_j \delta_{X,j} \right) - \sum_{i=1}^{n} P_i \delta_{y,i} - \sum_{h=1}^{o} F_h \delta_h = L_{fi} \qquad (22)$$

where:

- n is the number of blocks which characterizes the mechanisms;
- m is the number of the weight forces not applied to the elements of kinematic chain elements but whom masses, with the effect of seismic actions, are able to generate horizontal forces on the kinematic chains;
- o is the number of external forces, assumed independent from the seismic action, applied to the different blocks;
- P_i is the resultant of the weights-forces applied to the k-th block;
- P_j is the resultant of the weight-force not directly applied to the k-th block, but whose mass determines on it a horizontal seismic action, since it is not efficaciously transmitted to another part of the structure;
- F_h is the generic external force applied to one of the blocks;
- $\delta_{x,i}$ is the virtual horizontal displacement of the application point of the i-th weight P_i, assumed as positive if directed as the seismic force that triggered the mechanism;

- $\delta_{x,j}$ is the virtual horizontal displacement of the application point of the j-th weight P_i, assumed as positive if directed as the seismic force that triggered the mechanism;
- $\delta_{y,i}$ is the virtual vertical displacement of the application point of the P_i, assumed as positive if upwards directed;
- δ_h is the virtual displacement of the application point of the external force F_h, projected in its direction;
- L_{fi} is the total work of the possible internal forces (tie-rod extension, friction sliding in presence of good connection of the slabs; in this case, the phenomena are not contemplated in the work).

Figure 3-4 shows an example of a simple overturning of a monolithic two-storey wall; the macroelements are subjected to:

- W_i: self-weights of the panels;
- N_{Vi}: permanent weight carried by the walls (roofs, floors...), applied with a certain eccentricity e_i;
- αW_i, αN_{Vi}: system of horizontal forces proportional to the vertical one;
- N_{Hi}: horizontal external forces.

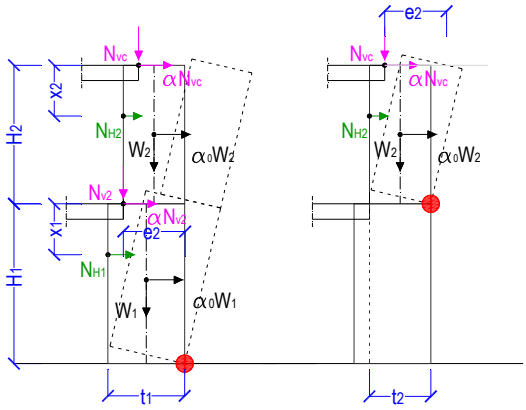

Figure 3-4: Overturning of a monolithic wall: calculation scheme (from Boschi, 2015).

NTC 2008 provides two procedures for the evaluation of safety verification for the out-of-plane mechanisms: linear and non-linear analysis.

In the following, the methodology of the kinematic linear analysis is briefly illustrated.

3.1.1.1 Linear kinematic analysis

In the linear kinematic analysis, the assessment of the capacity is performed by applying Eq. 27, considering the initial configuration of the macroelement (with infinitesimal rotation θ). It corresponds to the formulation of the limit equilibrium of rotation around the hinge configuration; with this simplification, α_0 can be calculated as the ratio of stabilizing moment and overturning moment. Then, the participating mass M^* is evaluated considering the virtual displacement of the application points forces associated to the kinematic movement:

$$M^* = \frac{\left(\sum_{i=1}^{n+m} P_i \delta_{X,i}\right)^2}{g \sum_{i=1}^{n+m} P_i \delta_{x,i}^2} \qquad (23)$$

where:

- $n+m$ is the number of weight forces considered as horizontal seismic force;
- $\delta_{x,i}$ is the horizontal virtual displacement of the application point of P_i.

The seismic capacity acceleration is the product between the coefficient α_0 and the g gravity, divided for the participating mass M^* (C.M. 617/2009):

$$a_0^* = \frac{\alpha_0 \sum_{i=1}^{m+n} P_i}{M^* FC} = \frac{\alpha_0 g}{e^* FC} \quad (24)$$

where:

- g is the gravity acceleration;
- $e^* = \frac{gM^*}{\sum_{i=1}^{n+m} P_i}$ is the participation mass factor;
- FC is the confident factor (C.M. 617/2009), equal to 1.35.

Safety verification

Referring to the linear kinematic analysis, the verification of the Safety Limit State (SLV) of local mechanisms can be carried out with refers to two conditions.
In presence of an element clamped to the ground, the following condition should be satisfied:

$$a_0^* \geq \frac{a_g(P_{VR})S}{q} \quad (25)$$

in which q is the behaviour factor equal to 2.
If the analysed macroelement is placed at a certain altitude, the demand acceleration is typically amplified compared to those at the ground level. An approximation acceptable consists in verifying, in addition to the ground level verification (previous equation), also the following condition:

$$a_0^* \geq \frac{S_e(T_1)\gamma\psi(Z)}{q} \quad (26)$$

3.1.2 In-plane mechanisms of failure

Three are the main typologies of in-plain mechanisms of failure (Figure 3-5):

- shear due to bending collapse,
- diagonal cracking shear,
- sliding shear.

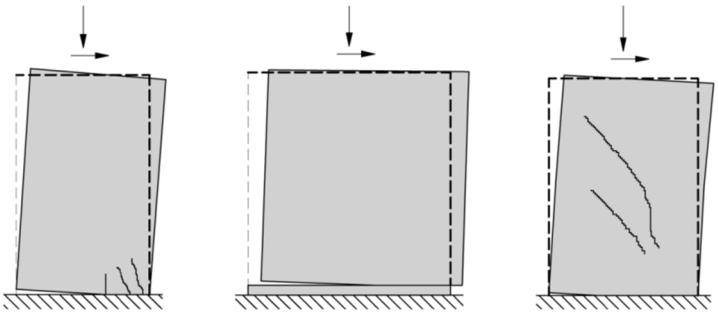

Figure 3-5: In-plane collapse of masonry walls: bending (a), sliding (b) and diagonal cracking (c).

While the first two are typical of existing masonry buildings, for which a perfect sliding surface is not easily detectable, the third is characteristic of more recent typologies of masonry (such as brick masonry). For each mechanism, NTC 2008 provides the ultimate shear value, $V_{R,BC}$, $V_{R,DC}$, $V_{R,S}$, respectively; the minimum value among them represents the maximum shear force that the panel can achieve during an earthquake.

Bending collapse

This mechanism occurs in the form of crushing by compression of the plasticized fibres of the resistant cross-section, which have reached their last deformation, and the collapse is similar to an overturning. In presence of a low value of the compression strength (N), the compressed area partially covers the section and a horizontal cracking arise in the tense side, due to the horizontal thrust. The value of the resistant moment is given by the following formula (NTC 2008):

$$M_{BC} = \frac{\sigma_0 t l^2}{2}\left(1 - \frac{\sigma_0}{k f_d}\right) \quad (27)$$

where:

- σ_0 is the compressive stress in the wall centre,
- t is the wall's thickness,
- l is the wall's length,
- f_d is the compression resistance of masonry,
- k is a coefficient in the range 0.85-1.

For cantilever scheme, $V_{R,BC} = M_{BC}/h$, while for fixed scheme, $V_{R,BC} = 2M_{BC}/h$; h is the wall height.

Diagonal cracking shear

For this mechanism, the collapse occurs when the shear stress achieves a limit tensile value and the damage is represented by diagonal cracks. The formulation of the limit strength follows the Turnšek e Cačovic formulation (Turnšek & Cačovic, 1971; C.M. 617/2009):

$$V_{R,DC} = lt\frac{1.5\tau_{0d}}{b}\sqrt{1 + \frac{\sigma_0}{1.5\tau_{0d}}} \quad (28)$$

where:

- τ_{0d} is the shear resistance in absence of normal strength,
- b is a correcting coefficient related to the strength distribution in the section, depending on the wall slenderness.

Sliding shear

This mechanism appears when a part of the wall translates along a lesion that generally develops along the mortar joints. It follows the Mohr-Coulomb theory, represented by the formula $\tau=c+\mu\sigma$, and the shear resistance can be expressed as (EN1996-1-1:2005, NTC 2008):

$$f_{v,k} = f_{vk0} + \mu_m \sigma_m < f_{vk,lim} \quad (29)$$

where:

- f_{vk0} is the sliding shear resistance,
- σ_m is the normal compression,
- $\mu_m = 0.4$ is the friction ratio.

Consequently, the limit shear strength is calculated as:

$$V_{R,S} = l' t f_{vd} \quad (30)$$

where:

- $f_{vd} = \frac{f_{vk}}{\gamma_M}$ is the design sliding shear resistance,
- $l't$ is the compressed section.

The **nonlinear static analysis** is widely adopted in international standards (FEMA 273, 1997; ASCE/SEI 41-13, 2014; FEMA 440, 2005; EN1998-1:2004; NTC 2008) for existing masonry buildings, since it allows to consider the nonlinear behaviour of masonry even for low seismic actions, in addition to an inferior computational effort. The procedure is illustrated below.

3.1.2.1 Nonlinear static analysis

The procedure consists of several steps:

1. Pushover analysis execution;
2. Identification of displacements related to different Performance Levels (PL) or Limit States (LS);
3. Derivation of the capacity or pushover curve of an equivalent nonlinear SDOF system, that represents the inelastic capacity of the structure;
4. Evaluation of the displacement demand for the seismic input motion to be considered for each PL; it may be evaluated by different formulations, as for example the CSM (Freeman, 1998) and the N2 method (Fajfar, 2000), previously deepened in paragraphs 2.6.2.1. and 2.6.2.2;
5. Comparison between displacement and capacity demand.

Pushover curve

The pushover curve (Figure 3-6) expresses the relation between the global base shear force and the displacement at the top of the structure (control node). It is determined by applying to the structure distribution of lateral forces (or displacements) monotonically increasing, up to the ultimate capacity of the structure. Its shape depends on the capacity in terms of strength and deformation of each element.

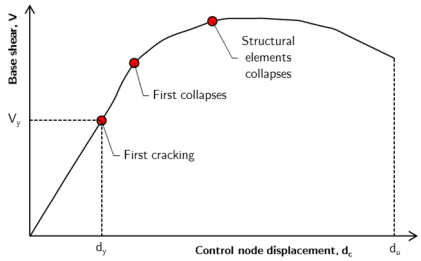

Figure 3-6: Pushover curve.

To correctly represent the distribution of the inertial forces produced by the seismic oscillation, in the analysis, two different types of lateral load pattern distributions should be considered (Figure 3-7):

- a triangular distribution (T), proportional to the 1st modal shape, since initially the structure behaves as an elastic system;
- a uniform distribution (U), proportional to the masses of each storey, since as the damage increases, the dynamic behaviour of the structure changes, until the limit condition where the structure acts mainly considering the distribution of the masses.

The choice of the load pattern distribution to apply can be a critical step; indeed, for example, in presence of irregular masonry buildings, the applying of a triangular distribution can be unreliable, since the influence of higher modes of vibration can be more significant.

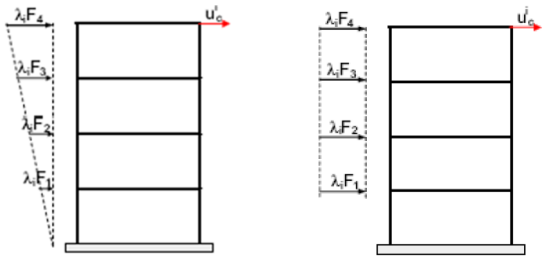

Figure 3-7: Lateral loads: triangular (a) and uniform (b) distribution.

In the initial part of the curve, most of the elements react elastically; then, some of them achieve their plastic phase, characterized by a stiffness decrease. As the lateral loads increase, more and more elements reach their ultimate displacement, leading to a global stiffness decrease. In detail, an elastoplastic bilinear constitutive law is adopted for the panels. The maximum shear strength corresponds to the limit shear value as a function of the examined failure mechanisms, while the ultimate displacement is a percentage of the total deformable height of the panel: $0.4\%h$ for shear collapse and $0.6\%h$ for flexural collapse, respectively (NTC 2008).

When the stiffness reduction exceeds the 20%, the analysis stops; this value has been conventionally adopted as the reduction threshold of the shear resistance, in agreement with the indications of NTC 2008 and EN1998-1:2004.

Bilinear capacity curve

In order to define a capacity spectrum to be compared with the design demand spectrum (§2.2.3.2), an equivalent SDOF system with an equivalent mass, m^*, and rigidity, k^*, is assumed. The MDOF (multi degree of freedom) pushover curve is converted by using the modal participation factor:

$$\Gamma = \varphi^t M\tau / \varphi^t M\varphi \qquad (31)$$

where: φ is the eigenvector, M the matrix of masses, τ the drag vector which indicates the masses involved in the analysed direction.

The equivalent mass, m^*, of the SDOF system is defined as:

$$m^* = \varphi^t M\tau \qquad (32)$$

The capacity spectrum is completely defined by the identification of the elastic fundamental period, T^*, the yield capacity, V_y, and by ductility μ_D. The assessment of these quantities requests the determination of the equivalent bilinear curve of the SDOF curve (Figure 3-8).

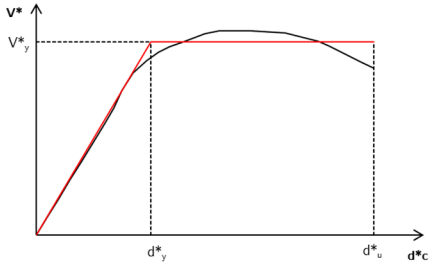

Figure 3-8: Bilinear capacity curve.

The stiffness of the bilinear system is calculated imposing the passage of the elastic part at the 70% of the maximum base shear:

$$k^* = F^*_{70\%} / d^*_{70\%} \qquad (33)$$

The maximum value of the elastic part is calculated with an energetic balance, assuming the same area below the SDOF curve and the bilinear one. By a 2nd order equation, it is possible to find:

$$F_y^* = \left(d_u^* - \sqrt{{d_u^*}^2 - \frac{2Area^*}{k^*}} \right) k^* \quad (34)$$

where $Area$ is the surface below the SDOF curve, while d_u^* is the ultimate displacement and represents the threshold after which the structure is no longer safe for the occupants.

It is then possible to assess the period and the displacement corresponding to the yielding point of the SDOF system through the following equations:

$$T^* = 2\pi\sqrt{m^*/k^*} \quad (35)$$

$$d_y^* = F_y^*/k^* \quad (36)$$

Hardening and softening phenomena are not considered in this definition; hence the yield capacity and ultimate capacity are considered equal.

The available ductility of the SDOF system is defined as:

$$\mu_D = d_u^*/d_y^* \quad (37)$$

This parameter represents the ability of a structure to undergo large-amplitude deformations in the inelastic range, without suffering a substantial reduction in strength. The higher the value of μ_D, the greater the safety level, since ductile structures can dissipate relevant quantities of energy during the deformation by attrition and hysteresis phenomena.

Safety verification

Safety verification consists of checking if the structure withstands the seismic demand and it requires the calculation of the demand displacement, d_{max}, by means of the displacement spectrum of the considered construction site and of the equivalent period, T^*, adopting the seismic performance-based assessment procedure recommended both by EN1998-3:2004 and the NTC 2008.

The equivalence between the bilinear system and an elastic one allows to calculate the acceleration that produces a certain displacement, related for example to a Limit State; this equivalence permits to use the elastic spectrum in terms of displacement and acceleration.

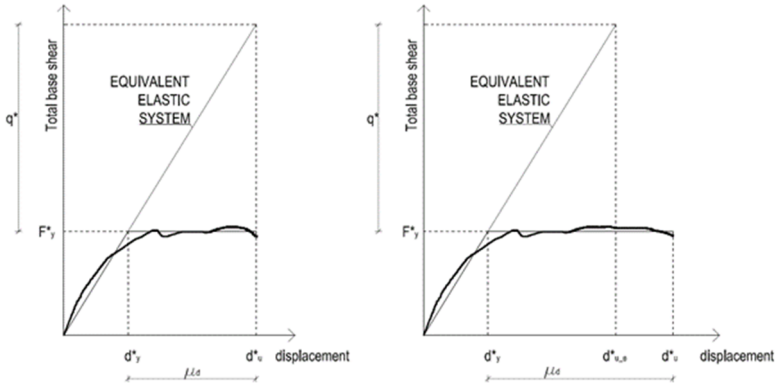

Figure 3-9: Equivalent elastic system for flexible systems, ($T^* > T_C$, left) and rigid systems ($T^* \leq T_C$, right).

The procedure depends on the stiffness of the structure. In order to define if a structure is rigid or flexible, the equivalent period, T^*, should be compared with a reference one. In accordance with NTC 2008, the comparison can be made with the period T_C, corresponding to the end of the plateau in the acceleration spectrum. In particular:

- if $T^* > T_C$, the structure is considered as flexible;
- if $T^* \leq T_C$, the structure is considered as rigid.

As shown in Figure 3-9, when a system is flexible, its deformations are equal to that of an elastic system of same stiffness; on the contrary, when a system is rigid, can sustain greater deformations.

The analytical procedure for calculating displacements and accelerations requires the definition of the ductility demand, μ_D, and of the behaviour factor, q^*.

In presence of flexible structures, q^* coincides with the ductility demand, while for rigid structures μ_D assumes greater values. The relations among these quantities are:

$$\mu_D = q^* \qquad \text{if } T^* > T_C \tag{38}$$

$$\mu_D = 1 + (q^* - 1)\frac{T_C}{T^*} \qquad \text{if } T^* \leq T_C \tag{39}$$

The behaviour factor, q^*, represents the ratio between maximum elastic force and yielding force:

$$q^* = m^* S_e(T^*)/F^*{}_y \tag{40}$$

The demand displacement, d^*_{max}, can be evaluated by using the following Eq.

$$d^*_{max} = d^*_{e,max} = S_{De}(T^*) \qquad \text{if } T^* > T_C \tag{41}$$

$$d^*_{max} = \frac{d^*_{e,max}}{q^*}\mu_D = \frac{S_{De}(T^*)}{q^*}\mu_D \qquad \text{if } T^* \leq T_C \tag{42}$$

Excessive levels of dissipation can cause an overestimation of the structure ductility and they indicate unreliable analyses; consequently, NTC 2008 defines a threshold limit for this parameter: $q^* < 3$.

If this value is exceeded, the value of the capacity acceleration should be limited.

In order to evaluate the capacity acceleration $S_e(T^*)$, q^* can be evaluated by using Eq. 43 and 44:

$$q^* = \mu_D \qquad \text{if } T^* > T_C \tag{43}$$

$$q^* = 1 + (\mu_D - 1)\frac{T^*}{T_C} \qquad \text{if } T^* \leq T_C \tag{44}$$

It is important to remind that these evaluations are referred to the structure capacity; therefore, in Eq. 48 and 49, μ_D is the available ductility of the SDOF system, as defined in Eq. 42.

Four different cases for the calculation of the capacity acceleration in relation to the ultimate displacement can be summarized (Table 3-1).

Table 3-1: Possible cases for the evaluation of capacity acceleration.

		$\boldsymbol{d^*_u}$	$\boldsymbol{S_e(T^*)}$
Flexible structures $\boldsymbol{T^* > T_C}$	$\boldsymbol{q^* < 3}$	$d^*_u = d^*_{u,e} = S_{De}(T^*)$	$S_e(T^*) = S_{D_e}(T^*) \cdot \omega^2 = = S_{D_e}(T^*) \cdot (2\pi/T^*)^2$
	$\boldsymbol{q^* > 3}$	$d^*_u = d(q*)$	$q^* = S_e(T^*) \cdot m^*/F^*_y \leq 3 \rightarrow S_e(T^*) = 3 \cdot F^*_y/m^*$
Rigid structures $\boldsymbol{T^* \leq T_C}$	$\boldsymbol{q^* < 3}$	$d^*_u = \left(d^*_{u,e}/q^*\right) \cdot \mu_D = = \left(d^*_{u,e}/q^*\right) \cdot [1 + (q^* - 1)\, T_C/T^*] > d^*_{u,e}$ $d^*_{u_e} = (d^*_u \cdot q^*)/[1 + (q^* - 1)\, T_C/T^*]$	$d^*_{u,e} = S_{D_e}(T^*)$ $S_e(T^*) = S_{D_e}(T^*) \cdot \omega^2 = = S_{D_e}(T^*) \cdot (2\pi/T^*)^2$
	$\boldsymbol{q^* > 3}$	$d^*_u = d(q*)$	$q^* = S_e(T^*) \cdot m^*/F^*_y \leq 3 \rightarrow S_e(T^*) = 3 \cdot F^*_y/m^*$

However, since the spectral accelerations of Table 3-1 are associated with different dynamic systems (in terms of mass and stiffness), the capacity PGA_C associated to the capacity spectral acceleration of the considered structure must be calculated, in order to compare the results from different structures.

As previously mentioned in 2.2.3, the PGA is the value of the acceleration response spectrum for the natural period equal to zero. The PGA_C can be calculated by defining a spectrum which, for the period T^* of the equivalent SDOF system, gives the same spectral acceleration $S_e(T^*)$ calculated in the capacity

analysis. The *fixed shape spectrum* method, schematized in Figure 3-10, can be applied: the level of PGA is increased up to the same spectral acceleration.

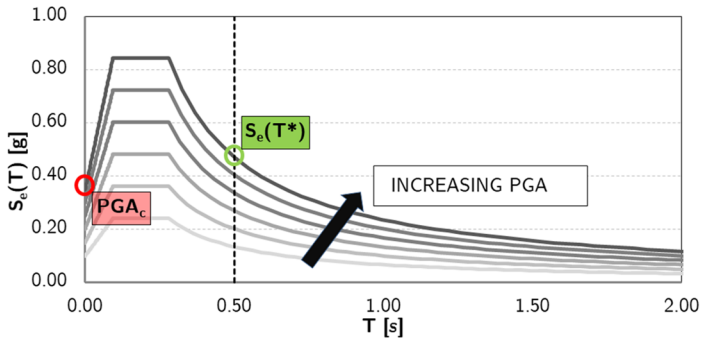

Figure 3-10: Assessment of the PGA_C.

In this work, the safety verifications refer to the Life Safety limit state (SLV, Table 2-3), for which an elastic response spectrum with a return period, TR, of 475 years is considered. The seismic risk indicators are the capacity-to-demand displacement and acceleration ratios:

$$\alpha_d = d_u/d_{max} \quad (45)$$

$$\alpha_{PGA} = PGA_C/PGA_D \quad (46)$$

Safety is verified when both ratios are higher than 1.

§

In order to highlight the differences between isolated and in-aggregate structures, the seismic vulnerability assessment for the masonry buildings in aggregate is reviewed in the following paragraph. In particular, the "aggregate effect" refers to the effects of interactions between adjacent buildings during a seismic event.

3.2 The "aggregate effect"

Over the centuries, the diachronic process of building up, in adjacency and in continuity with the existing built environment, has led to the complete occupation of free spaces and to the creation of complex structural systems (i.e., masonry aggregates), in which structures may differ in geometry, materials, construction techniques and state of preservation (Giuffrè & Carocci, 1999; Carocci, 2001).

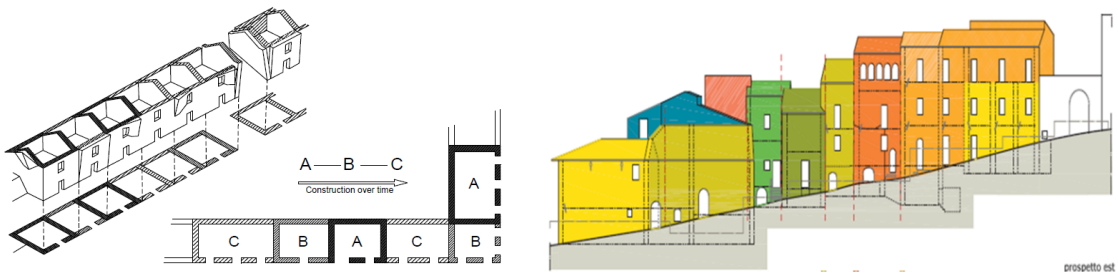

Figure 3-11: Diachronic construction process and building interaction (Giuffrè, 1990, and Indelicato, 2010).

The S.U.s present in-height structural continuity and a unique dynamic behaviour; they are characterized by a common manufacturing process or by vertical and horizontal homogeneous elements that contribute to the uniform distribution of vertical and horizontal loads (Borghini at al., 2011). They are bordered by

open spaces, structural joints or buildings structurally contiguous but typologically different. In historical centres, the aggregate coincides with the block, when there are no joints or other disconnections between the different buildings, and it is therefore limited by streets and squares.

The seismic vulnerability assessment of the masonry buildings in aggregate differs from that of the isolated buildings because of more complex geometrical configurations, that are often influenced by the site characteristics (Carocci, 2006). As already seen in Caniggia & Maffei (1979), the most widespread typologies in Italian historical centres are the row aggregate, composed of several S.U.s organized in line, and the L aggregate, characterized by a two-dimensional development starting from the corner building. Moreover, these structures are characterized by evolutionary processes difficult to analyse, due to uncertainties related to the knowledge level of construction techniques, mechanical properties of materials and effective structural organisation. For this reason, Carocci & Tocci (2007) highlighted the importance of performing a preliminary "critical reading" of the constructive techniques and of the diachronic construction process of the aggregate as a fundamental step that should precede the assessment phase.

At the current state-of-the-art, it is commonly accepted that some additional aspects could influence the seismic behaviour of a S.U.; for example, the following features should be considered in the analysis.

- **Material heterogeneities**: in presence of a more rigid building in the centre of the aggregate, the side buildings can withstand a higher level of excitation, probably because the whole aggregate is reinforced (Ulrich, Negulescu, & Ducellier, 2015).
- **Difference among opening areas**, that may influence the distribution of horizontal actions between the façades.
- **Position of the S.U. within the aggregate**: an internal S.U. is constrained by the others in comparison to a corner or a header building.
- **Differences in height**: for example, a building in adjacency with taller buildings may suffer minor damage compared to one in adjacency with buildings significantly lower, even if the lower construction may be subject to a vulnerability induced by the possible collapse of the higher ones.
- **Presence of staggered floors**, that can generate local thrusting forces on common walls as well as effects of pounding.

These aspects are representative of the interactions among buildings and they are considered in the vulnerability index method forms recently implemented for the evaluation of the vulnerability assessment of historical city centres at large scale (§2.5.1; Formisano et al., 2015; Ferreira et al., 2012).

In the past few years several studies were developed aiming at identifying the main particularities inherent to buildings enclosed in aggregate (the main examples are the work by Giuffrè and Carocci) and at evaluating their influence over the asset global seismic behaviour; in fact, even though local mechanisms are usual in aggregates, the in-plane mechanisms are equally notable.

Athanassiadou et al. (1994), for example, studied the seismic behaviour of adjacent buildings in a row, subjected to seismic excitation in the direction of their common axis, modelling them as SDOF structures in series (Figure 3-12). They observed that the effect of pounding in a row is more pronounced for the end structures and it increases as the number of structures increase; moreover it is smaller when the adjacent structures have similar dynamic characteristics. In the case of adjacent S.U.s with different natural periods, the most affected are the rigid ones, despite their relative position in the row. The most adverse case is when the rigid buildings are placed at the end of the row.

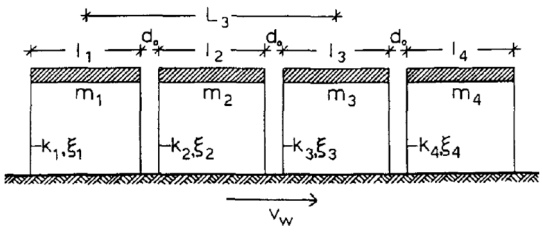

Figure 3-12: Analytical model for adjacent structures (Athanassiadou, Penelis, & Kappos, 1994).

Also Amadio et al. (2011) deepened the seismic response of extended and regular row aggregates, composed of S.U.s characterized by constant stiffness, noticing that is uniform and translational for transverse earthquake (Figure 3-13a); it is, therefore, possible to study separately each S.U., but considering the portion of mass deriving from the adjacent units, that weighs on the common walls. On the contrary, in presence of a longitudinal earthquake, each S.U. is influenced by the presence of the adjacent ones; indeed, a resistant arch mechanism could be generated, producing a significant capacity increase of all S.U.s, with the exception of the external ones (Figure 3-13b). For these, the study of the single S.U. is therefore generally in favour of safety. When the aggregate is characterized by plan irregularity or by S.U.s with different stiffness, its seismic response is more complex, because it could be influenced by translational and torsional effects.

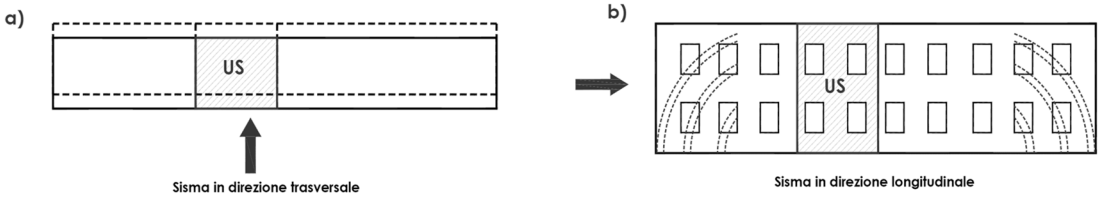

Figure 3-13. Seismic response of a row aggregate in presence of transversal (a) and longitudinal (b) earthquake (adapted from Amadio et al., 2011).

Moreover, Senaldi et al. (2010) investigated the effects of the length of the row aggregates and of the presence of flexible floors, by applying nonlinear dynamic analyses on idealised configurations. In relation to the transversal response, the external units show a higher deformation compared to the internal ones.
The importance to contemplate the historical evolution of masonry buildings was highlighted in Betti et al. (2011), where the seismic assessment of the museum of Casa Vasari in Arezzo (Italy) was evaluated by considering different structural configurations, according to the effectiveness of the connections between the structural elements.
Boschi et al. (2013) proposed a methodology for both pre- and post-earthquake assessment of existing masonry buildings, which was applied to a building aggregate located in Castelnuovo (Italy) hit by the April 2009 L'Aquila earthquake. This fact allowed the comparison between observed and expected damage, in terms of both in-plane and out-of-plane seismic response.
Moreover, Lagomarsino et al. (2014) deepened the performance-based assessment of complex monumental buildings in aggregate, stressing out the necessity to define numerical models able to guarantee a reliable assessment, taking into account the interaction effects, but with a reasonable computational effort.

Although the importance of considering the interactions between adjacent buildings is nowadays a consensual fact in literature, there is still a clear research gap concerning how the "aggregate effect" should be accounted for in the assessment phase in relation to a global box behaviour.

NTC 2008 recommends considering the effects of interaction by modelling the analysed S.U. with loads or forces deriving from the adjacent structures. Moreover, it proposes a simplified method for the global analysis, that allows in presence of rigid floors the distinct analysis of each inter-storey through nonlinear static analysis. In presence of flexible floors, instead, each wall can be analysed as an independent structure subject to vertical loads and to the parallel seismic action.

Similarly, in ReLUIS (2010), a mechanical model based on the linear static analysis is introduced.

Moreover, a common method for seismic assessment of a building within an aggregate consists in comparing its global capacity by considering two distinct conditions: the isolated building and the entire aggregate.

Based on this approach, Pujades et al. (2012) and Ferrito et al. (2016) noticed that, along the direction of aggregate, the "aggregate effect" does not improve significantly the seismic response of the isolated buildings, while along the transversal direction the confinement produces a small reduction of their seismic vulnerability. Moreover, as confirmed in Amadio et al. (2011) and Ulrich et al. (2015), row-end buildings proved to be more vulnerable, since they are not efficiently braced to the adjacent buildings. Fagundes et al. (2017), instead, stressed out the importance of accounting for the presence of staggered floors and in-height irregularities in numerical models for a more accurate estimation of the seismic response of buildings enclosed in aggregate.

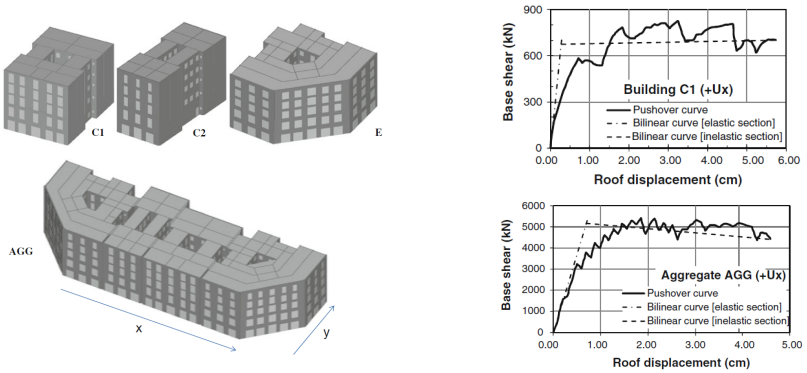

Figure 3-14: Example of the common approach of analysis of buildings in aggregate (from Pujades et al., 2012).

Nevertheless, if on one hand, the analysis of the case study building in the isolated condition is an extreme approximation since the contribution of the adjacent S.U.s is lost, on the other hand, the study of the entire aggregate requires a too onerous investigation and can lead to unreliable results.

Valotto et al. (2016) proposed the implementation of simplified models for representing the boundary conditions of the investigated S.U., by adopting linear springs, pillars or simplified representations for the boundary buildings. However, they noticed that springs or pillars are not representative of the stiffness of the walls in continuity to those of the analysed S.U.; indeed, the linear elastic springs operate only in elastic phase, while pillars are not sufficient. Moreover, if considering simplified models for the adjacent S.U.s, all of them have to be always modelled.

Based on these considerations, the seismic safety assessment of buildings enclosed in aggregate should be conducted by identifying the optimal portion of the aggregate in order to represent the "aggregate effect", on the basis of the surrounding conditions. As previously introduced, this was addressed in ReLUIS (2010), with the introduction of the ***Minimum Unit of Analysis*** **(M.U.A.)** concept, which is defined as the portion of the aggregate in which the analysed ***Minimum Intervention Unit*** **(M.I.U.)**

and the adjacent S.U.s are enclosed. The M.I.U. represents the minimum operative scale that a repair or reconstruction project, designed for one or more homogeneous S.U.s, should refer to.

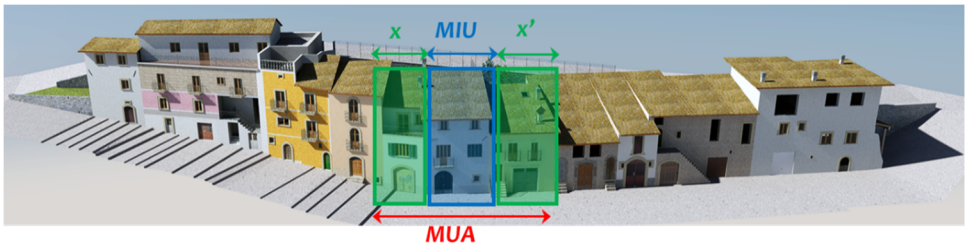

Figure 3-15: Identification of M.I.U. and M.U.A. (ReLUIS, 2010).

However, in literature, there are no indications on how to identify the M.U.A., mainly due to the great variety of existing cases.

Starting from this, the study herein presented aims at deepening the "aggregate effect", by analysing the most influential factors in the global seismic response of masonry aggregates, and at providing general schemes and a procedure *("target structural unit approach")* to define the M.U.A.
In the following, the hypothesis and the methodology of this work are described.

3.3 HYPOTHESIS AND METHODOLOGY OF THE WORK

As previously stated, the proposed *"target structural unit approach"* is suitable for structures able to explicate a global box behaviour, allowing the performing of the pushover analysis. The three-dimensional models are developed by using a Frame by Macro Elements model approach, implemented in the commercial release of 3Muri software code (STADATA, 2017) and illustrated in §3.3.2.
The procedure of the nonlinear static analysis (pushover) is illustrated in §3.1.2.1. The load pattern distributions considered in this work are listed above (Table 3-2). The presented results usually refer to the uniform load pattern distributions, considered as the most representative especially for irregular masonry buildings (as already mentioned in §3.1.2.1).

Table 3-2: Load pattern distributions considered in this work.

N.	Direction	Load pattern distribution	Eccentricity
1	+X	uniform	0%
2	+X	triangular	0%
3	-X	uniform	0%
4	-X	triangular	0%
5	+Y	uniform	0%
6	+Y	triangular	0%
7	-Y	uniform	0%
8	-Y	triangular	0%

In the following chapters, the results are generally shown in terms of:

- pushover curves,
- Seismic Performance Indicators (SPI): such as the equivalent stiffness k^*, the maximum normalized base shear V_{bu} and the α_{PGA}.

As previously introduced, the SPI refer to the Life Safety limit state (SLV, T_R = 475 years). It should be noticed that the variability of the seismic performance of the target S.U. to the changing of its boundary

conditions is evaluated in terms of seismic capacity; for this reason, the equivalent stiffness k^* and the maximum base shear V_{bu} are chosen as SPI, also because they can be evaluated directly from the pushover curve.

The main features of this work and the modelling assumptions are described in the following.

3.3.1 Main features

The application of the proposed procedure is based on the following aspects.

a) Identification of the complete aggregate condition

The most reliable seismic response of the target S.U. is considered to be in the complete aggregate condition (§5.1.3), assuming an accurate modelling of the structural features; therefore, S.U.s that are separated by disconnections from the rest of compound, or that do not ensure the structural continuity, should be excluded. Consequently, the knowledge process of the aggregate is a crucial step to perform a correct seismic assessment, since it allows a reliable definition of the aggregate and of its S.U.s. It consists in the analysis of the masonry types and quality, the analysis of building typologies and constructions details, and the analysis of the cracking pattern, where possible.

However, it should be considered that, as the number of S.U.s increases, often some parts of the aggregate may be inaccessible, or the collected information may be insufficient. Hence, the complete aggregate condition could be affected by uncertainties and the reference condition for the investigated S.U. would be undefined. In this case, the proposed procedure would allow identifying the variation range of the M.U.A. (§5.1.3.1).

b) Definition of several modelling configurations

Once that the aggregate is determined, the primary idea for identifying the M.U.A. of the target S.U. consists in considering several modelling configurations, in addition to the complete aggregate configuration; this allows evaluating the variability of the seismic behaviour for different boundary conditions.

c) Multi-level analysis

The main assumption introduced in this study is to believe that the "aggregate effect" is not adequately captured by only evaluating the global response of the above-mentioned modelling configurations, but an evaluation at both target S.U.– and wall– level should be also carried out, to better understand the variability in terms of seismic capacity of the case study building.

As illustrated in Figure 3-16, the capacity curves at S.U.– and wall– level are reproduced by considering, for the nodes belonging to the walls of interest, average displacements and sum of the base shear forces, extracted by the results of the analyses performed on the global models. Once obtained the pushover curves, the equivalent stiffness k^* and the maximum base shear V_{bu} are directly evaluated.

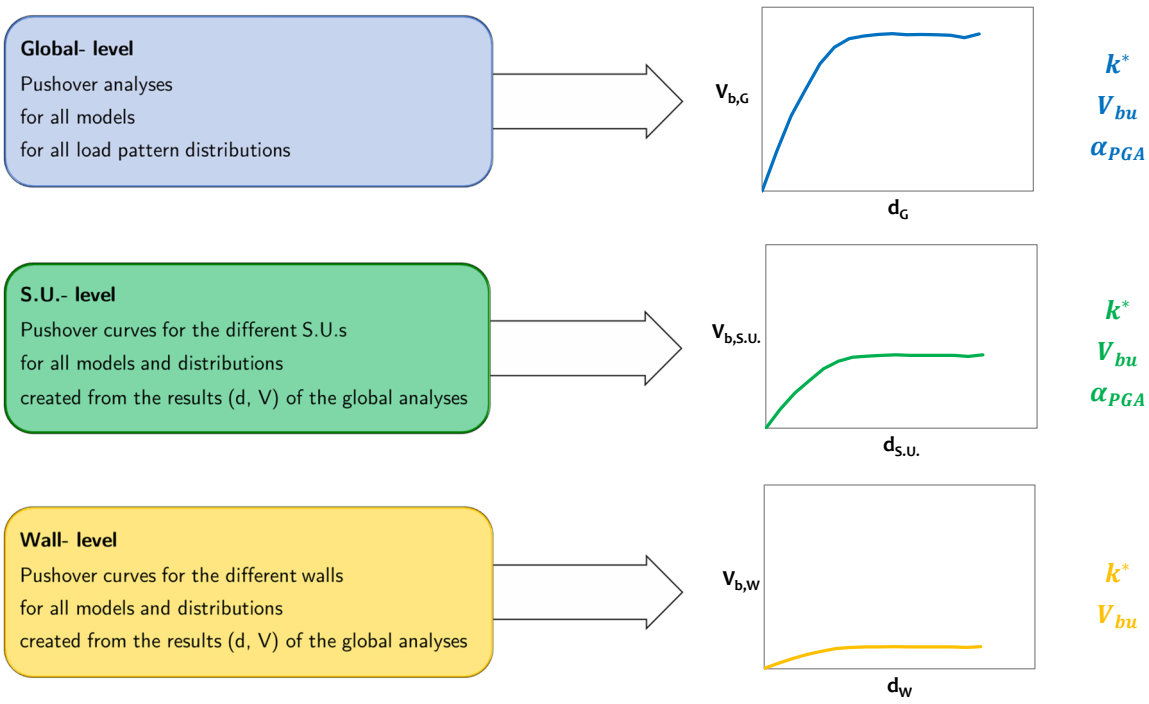

Figure 3-16: Framework of the multi-level analysis.

3.3.2 Modelling assumptions

The Frame by Macro Elements model approach follows the assumption that the in-plane response of masonry walls with openings can be discretised by a set of one-dimensional piers and spandrels macro-elements, as shown in Figure 3-17 (Lagomarsino et al, 2013; Penna et al., 2014).

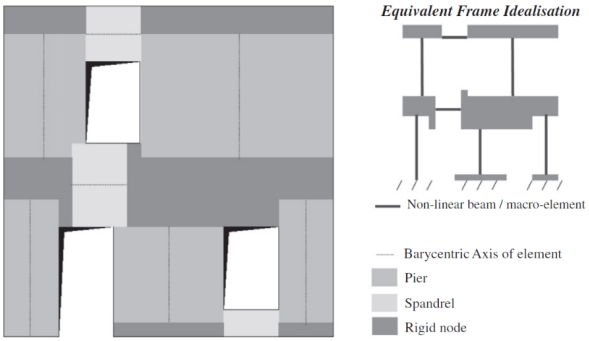

Figure 3-17: Example of equivalent frame idealization (from Lagomarsino et al., 2013).

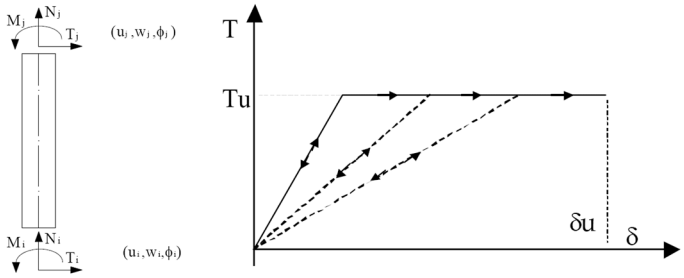

Figure 3-18: Bilinear elastic-perfectly plastic behaviour.

As deepened in Lagomarsino et al. (2013), each macro element is assumed as a nonlinear beam element with bilinear elastic perfectly plastic behaviour (Figure 3-18). Its response is directly faced in terms of global stiffness, strength and ultimate displacement capacity by assuming a proper force-displacement relationship and appropriate drift limits, as previously explained in paragraph 3.1.2.1.

The floors are modelled as orthotropic membrane finite elements of equivalent thickness, s; their stiffness is a parameter that strongly influences the global response of the model. As illustrated in Figure 3-19, in case of rigid floors (as concrete slabs), the horizontal forces are homogeneously redistributed among the walls, allowing complete cooperation, while in presence of flexible floors (as wooden floors) the walls are differently stressed.

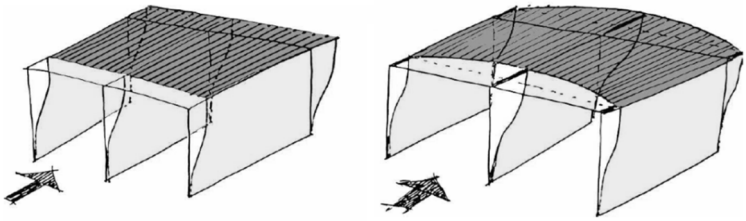

Figure 3-19: Example of rigid (left) and flexible (right) floors.

Few assumptions are considered in the modelling: the heterogeneity inherent to stone masonry is disregarded; arched windows are considered rectangular; horizontal diaphragms are assumed sufficiently connected to masonry walls to ensure the box-behaviour; timber roofs are modelled as horizontal diaphragms; internal timber staircases are not modelled, and the foundations are modelled as rigid.

In order to have comparable results, the same control node is selected for all the models and analyses, chosen in a barycentric position at the top of the target S.U. Since in many cases (both in the prototypes and in the real case studies) both rigid and flexible diaphragms are present, the use of mass-weighted average displacements at the referred control node is believed to be the most adequate option to draw the pushover curve.

Moreover, the pushover curves are normalised. In particular, the displacements at the control node (d) are normalized by its height (h_{cn}), while the total base shear strength (V_b) is divided by the weight of the considered structure, producing the normalized displacement d/h_{cn} and the normalized base shear V_b/W:

- W_{Mi} of global model Mi,
- W_{M*i} of target S.U. M^*_i,
- W_w of the boundary wall.

With reference to the mechanical properties of materials, a knowledge level KL1 is assumed for all cases; consequently, minimum values of strength parameters and average values of stiffness are considered (NTC 2008). Moreover, a confidence factor, CF_{KL1}, equal to 1.35, is applied to strength parameters (compressive and shear strength, respectively f_m and τ_0). Additionally, a cracked stiffness condition is applied to the stiffness parameters, meaning that the values of the Elastic (E) and Shear modulus (G) are halved.

Chapter 4.

Analysis of the main interaction factors on prototype aggregates

In this chapter, the results of a sensitivity analysis performed on prototype aggregates are shown and discussed. The ideal aggregates are generated from the combination of basic S.U.s of defined characteristics. The sensitivity analysis is performed through nonlinear analysis and by considering different modelling configurations, to assess the influence of some structural factors on their seismic global behaviour: the aggregate typology, the number of S.U.s, the floors typology, the presence of material heterogeneities and of differences in height. The results are shown in terms of sensitivity indexes, percentage changes of maximum normalized base shear (V_{bu}) and equivalent stiffness (k^*), pushover curves at both global- and S.U.- level, base shear trend on each S.U., base shear distribution among the walls.

Contents

4.1 Main characteristics of the prototype aggregates

The prototype aggregates are based on the features of the typical aggregates of the suburbs of Florence (Figure 4-1), considered because of their recurring characteristics and their spread in Italian territory. These structures were built at the beginning of the XX century and are composed of 2-3 storeys buildings. Each building is adjacent to the neighbour one and, consequently, the boundary walls are in common. Each structure is usually characterized by a width of 4 - 6 m and a depth of 8 - 12 m, for a plan dimension ratio of ½. The geometry of the openings is quite regular.

Figure 4-1: Typical aggregates in the suburbs of Florence.

The prototypes are generated starting from a **basic S.U.**, characterised by plan dimensions of 4.80 x 9.60 m and 2 storeys of 3 m. It has 2 rooms per storey and there are 3 alignments in X direction (x1, x2, x3) and 2 alignments in Y direction (y1, y2). The openings in X direction are regular and aligned; in Y direction there are no openings. The walls have a thickness of 40 cm and are composed of stone masonry, to which the 1st category from the classification of Tab. C8A.2.1 of C.M. 617/2009 is assigned.

With the aim to assess the sensitivity to the differences in height, also a three-storey basic S.U. is considered. Moreover, to evaluate the sensitivity to the material heterogeneities, a basic S.U. in hollow brick masonry is defined, to which the 8th category from the classification of Tab. C8A.2.1 is assigned. This type of masonry is chosen since, in comparison to the stone masonry, it presents stiffness parameters (E and G) 5 times greater and shear strength (τ_0) 15 times greater.

The mechanical characteristics of the masonry typologies are resumed Table 4-1. As introduced in 3.3.2, a knowledge level KL1 is assumed.

Table 4-1. Mechanical properties assigned to masonry panels (Tab. C8A.2.1 of MIT 2009).

Masonry typology	w [kN/m^3]	E [N/mm^2]	G [N/mm^2]	f_m [N/cm^2]	τ_0 [N/cm^2]
Stone masonry	19	435	145	74.07	1.48
Hollow brick masonry	12	2250	675	296.30	22.20

The floors are organized in parallel to the main front and the applied loads are constant (Table 4-2). They are modelled as orthotropic membrane finite elements of equivalent thickness. Rigid floors (R) are characterized by an infinite stiffness, while flexible floors (F) are modelled as timber elements characterized by an equivalent modulus of elasticity $E_{1,eq}$= 68750 MPa in the warping direction. In the sensitivity analysis, each S.U. is characterized by the same floor type at both the 2 storeys.
The foundations are modelled as fully restrained.

Table 4-2. Loads on floors.

Loads		**Value [kN/m^2]**
Permanent	G1	2.50
Non-permanent	G2	2.50
Variable	Q	2.00

The main 3 typologies of basic S.U. are shown in the following Figure 4-2.
The analysed aggregates are generated starting from the basic S.U. Different modelling configurations are considered by interchanging the above-mentioned basic S.U.s, in order to evaluate the sensitivity to the structural features described in the next paragraph.

Figure 4-2: Type of basic S.U.: plan (a), front and back façades (b) and internal wall (c).

Two main aggregate typologies are considered since they are the most common typology in Italian territory:

- **row aggregate:** characterized by a longitudinal development;
- **"L" aggregate**: composed of S.U.s organized both in the X and Y direction; the corner S.U. is composed of 2 basic S.U.s.

4.2 INVESTIGATED FACTORS

The uncertainties considered in this work are related to different factors, listed in the following, from which different models are generated. Each factor is analysed separately, in order to evaluate its influence independently; moreover, the defined combinations are those that maximize the effects.

a) Aggregate typology

As previously indicated, the aggregate typologies considered in this study are the **row** and **"L"** aggregate. The following Figure 4-3 shows the configurations composed of 5 S.U.s, whose behaviour will be deepened in the following paragraphs, as explained in paragraph 4.4.2.

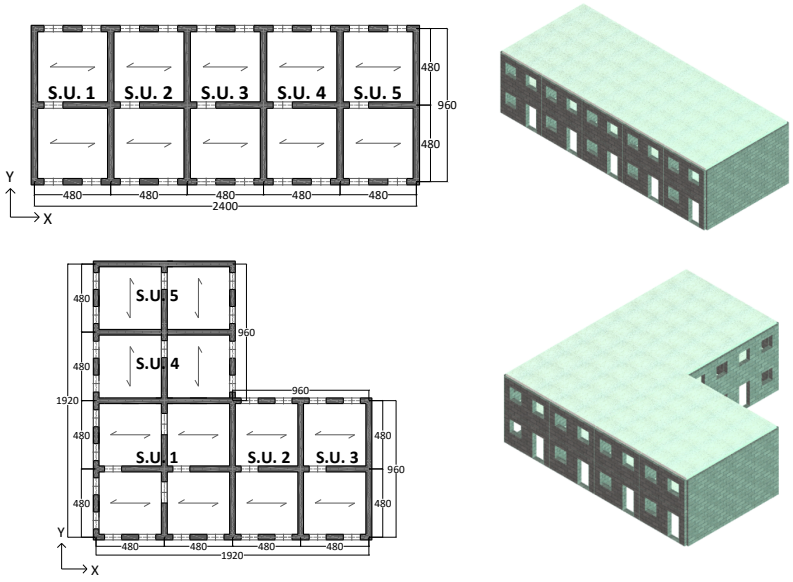

Figure 4-3: Plan and 3D view of the main typology of row (upper row) and L aggregate (bottom row).

b) Number of S.U.s

The prototype aggregates are composed of **2**, **3**, **4** or **5** S.U.s, as shown in the following Figure 4-4.

This choice depends on the fact that the aggregates in historical centres are often of small-scale or the knowledge process allows to identify joints or disconnections, excluding some portions from the analysed configuration (Figure 4-5, as abovementioned in §3.3.1). Moreover, detailed models for the global analysis are suitable for aggregates not too extended, for which the effort related to the knowledge process is acceptable. However, even in the presence of wide-large aggregates, the influence of the n° of S.U. decreases with distance, as shown in the following paragraph 5.5.

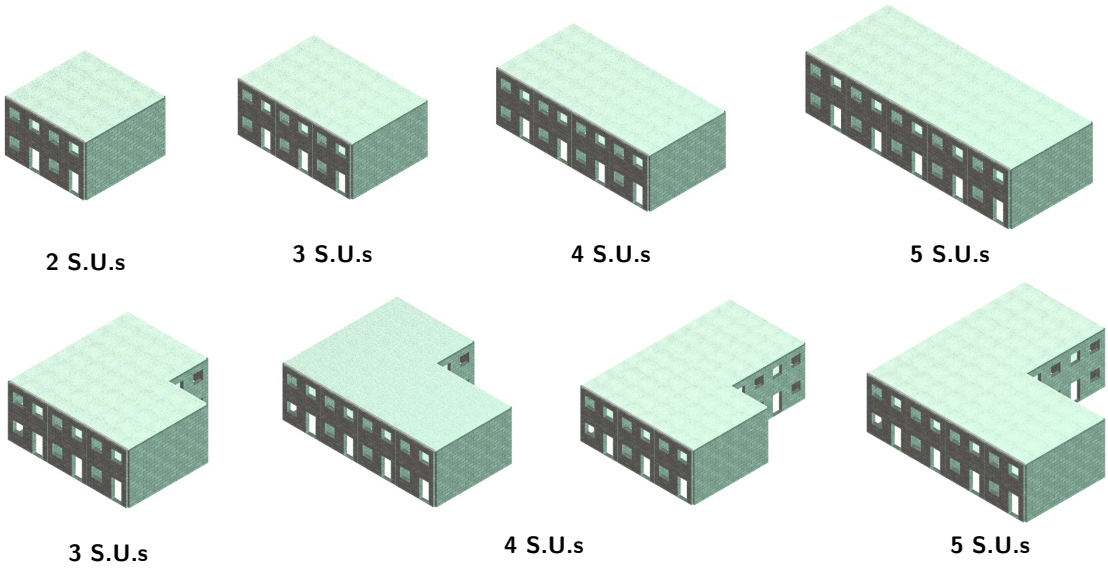

Figure 4-4: Row (upper row) and L (bottom row) aggregate typologies in function of the number of S.U.s.

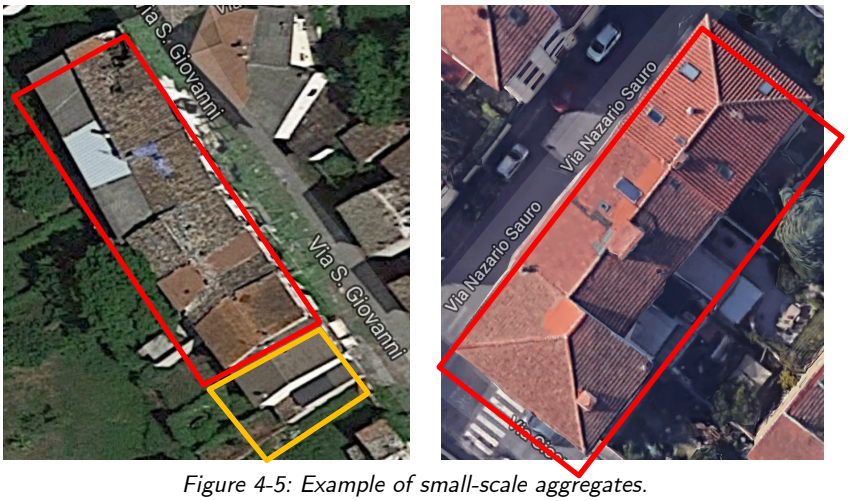

Figure 4-5: Example of small-scale aggregates.

c) Floors typology

Floors are considered as rigid or flexible since they represent two extreme conditions that often coexist in these structures. Indeed, in existing buildings floors are usually flexible (as for example, timber floors without continuous concrete slabs); however, they also can be rigid, often because of strengthening interventions that often were realized just in some portions/S.U.s of the aggregate (Figure 4-6).

Rigid floors are modelled as slabs that allow the distribution of both vertical and horizontal loads to the vertical structures, guaranteeing a global response of the building. Flexible floors are characterized by in-plane flexible elements that only share vertical loads to the walls; in this case, these are mainly stressed out of their plain.

Different configurations are considered, by combining the basic S.U.s with rigid (R) or flexible (F) floors in different layouts. Table 4-3 summarizes all the cases considered in the modelling; they are also represented in Figure 4-7, where the rigid floors are highlighted in grey, while the flexible ones are in brown.

Figure 4-6: Example of rigid (left) and flexible (right) floors.

Table 4-3: Modelling configurations of the prototype aggregates in function of the floors typologies.

Basic S.U.	
Model	**Floor-type**
	1° S.U.
R	Rigid
F	Flexible

Row aggregate					
Model	**Floor-type**				
	1° S.U.	**2° S.U.**	**3° S.U.**	**4° S.U.**	**5° S.U.**
R	Rigid	Rigid	Rigid	Rigid	Rigid
F	Flexible	Flexible	Flexible	Flexible	Flexible
RRFFF	Rigid	Rigid	Flexible	Flexible	Flexible
FFRFF	Flexible	Flexible	Rigid	Flexible	Flexible
FRRRF	Flexible	Rigid	Rigid	Rigid	Flexible

L aggregate					
Model	**Floor-type**				
	Corner S.U.	**2° X-S.U.**	**3° X-S.U.**	**2° Y-S.U.**	**5° Y-S.U.**
R	Rigid	Rigid	Rigid	Rigid	Rigid
F	Flexible	Flexible	Flexible	Flexible	Flexible
RFF	Rigid	Flexible	Flexible	Flexible	Flexible
FRR	Flexible	Rigid	Rigid	Rigid	Rigid

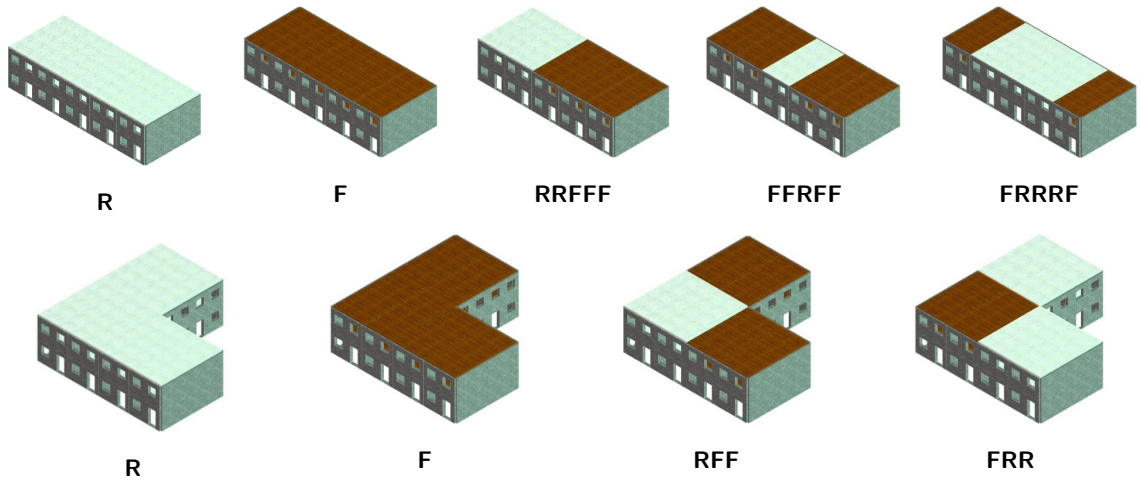

Figure 4-7: Row (upper row) and L (bottom row) aggregate typologies in function of the floors typologies.

d) Material heterogeneities

The coexistence of different masonry types is common in the aggregates, since buildings were built in different time periods or because some portions could be reinforced by strengthening interventions.

The basic S.U. is characterized by stone masonry 40 cm - thick walls (**murA**); moreover, additional cases are considered, as shown in Figure 4-8:

- **murA**: all the S.U.s are in stone masonry.
- **murB**: the internal/corner S.U.s are in hollow brick masonry (i.e., are more resistant and rigid);
- **murC**: the external S.U.s are in hollow brick masonry (i.e., are more resistant and rigid).

For murB and murC cases, only rigid (R) and flexible (F) floors are modelled. The stone masonry is highlighted in grey, while the hollow brick masonry is in red.

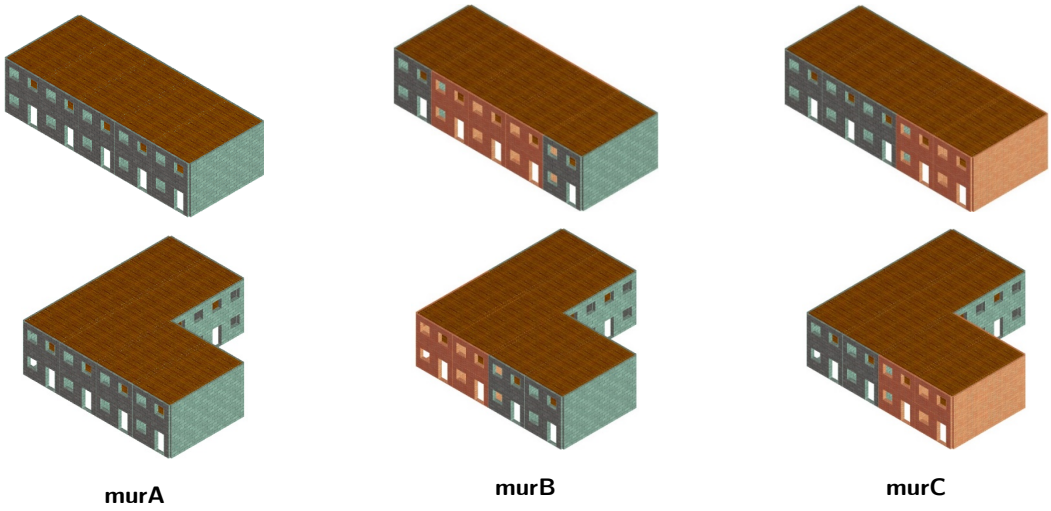

Figure 4-8: Row (upper row) and L (bottom row) aggregate typologies in function of the material heterogeneities.

e) Differences in height

The aggregate typology considered in this study is usually composed of 2-3 storeys buildings and the differences in height generally consist of 1 storey, as shown in the following Figure 4-9.

Figure 4-9: Example of differences in height.

The basic S.U. has 2 storeys; in order to evaluate the influence of the differences in height, the configurations illustrated in Figure 4-10 are considered:

- **hA**: all the S.U.s have 2 storeys;

- **hB**: the internal/corner S.U.s have 3 storeys,
- **hC**: the external S.U.s has 3 storeys.

Also for this factor, only rigid (R) and flexible (F) floors are modelled.

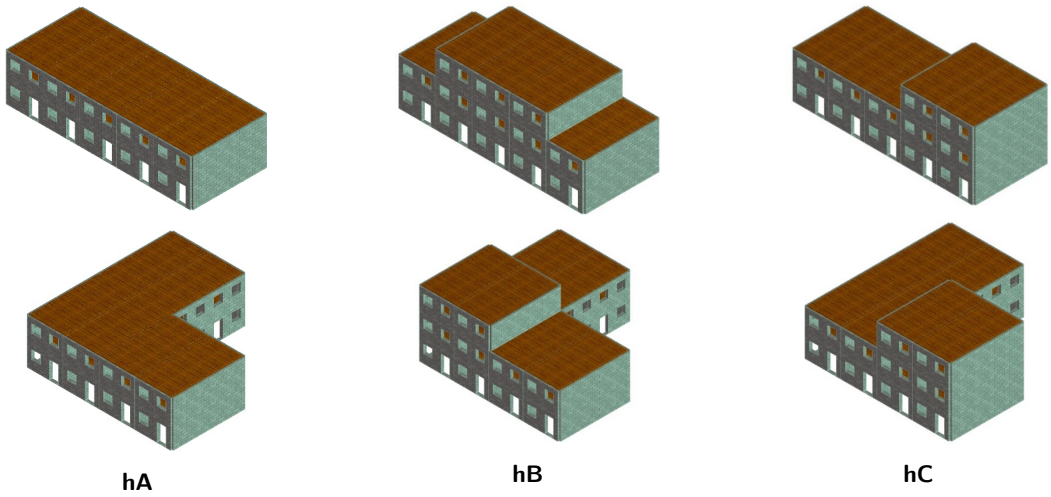

Figure 4-10: Row (upper row) and L (bottom row) aggregate typologies in function of differences in height.

All the investigated factors are resumed in the following Table 4-4.

Table 4-4. Resume of the investigated structural factors and of the modelling configurations.

Factors		Configurations
Y1	**Aggregate typology**	Row
		L
Y2	**Number of S.U.**	1
		2
		3
		4
		5
Y3	**Floors stiffness**	R
		F
		RRFFF / RFF
		FFRFF
		FRRRF / FRR
Y4	**Material heterogeneities**	murA
		murB
		murC
Y5	**Differences in height**	hA
		hB
		hC

Some preliminary results of the sensitivity analysis are illustrated in Bernardini et al. (2017).

4.3 THE SENSITIVITY ANALYSIS PROCEDURE

The sensitivity analysis is an essential tool for the seismic assessment of existing buildings since it allows to identify the most influential factors affecting the structural response.

The procedure, described in the following, is deepened in Cattari et al. (2015).

As it is known, the uncertainties can be classified as aleatory or epistemic.

- **Aleatory uncertainties**: are related to the knowledge of some parameters that can be expressed by means of probability distributions, as for example mechanical characteristics of materials. They can be associated with variables X_k $(k = 1{:}N)$, where N is the total numbers of parameters.
- **Epistemic uncertainties**: refer to constructive or modelling factors (as for example structural details), that are not quantifiable through a parameter, but requires the logic-tree approach.

They can be related to factors Y_j $(k = 1{:}M)$. Each factor Y_j could require two or more possible models $(q = 1{:}m_j)$ and the number of alternatives may differ for each factor. The final models are obtained by the factorial combination of all possible configurations; for example, if two alternatives $(m_j = 2,\ \forall\, j = 1{:}M)$ are considered for each factor, 2^M models have to be considered.

The sensitivity is assessed with respect to a SPI: for example, the maximum Intensity Measure compatible with the fulfilment of performance levels (IM_{PLi}) can be used.

The procedure requires the performing of 2N+1 analyses for each mth model:

- a first one by adopting as reference for all the parameters the plausible mean value $\bar{x}_k$;
- a set of $2N$ analyses in which each parameter is changed one by one according to the lower $\bar{x}_{k,low}$ or higher $\bar{x}_{k,up}$ bound of the rational range.

The sensitivity to variables X_k is assessed through the variable $\Delta_{PLi,Xk}$ computed as (Figure 4-11):

$$\Delta_{PLi,Xk} = 2\frac{IM_{PLi,k-max} - IM_{PLi,k-min}}{IM_{PLi,k-max} + IM_{PLi,k-min}} \tag{47}$$

where:

$$IM_{PLi,k-min} = min\,(IM_{PLi,k-low}, IM_{PLi,k-mean}, IM_{PLi,k-up}) \tag{48}$$

$$IM_{PLi,k-max} = max\,(IM_{PLi,k-low}, IM_{PLi,k-mean}, IM_{PLi,k-up}) \tag{49}$$

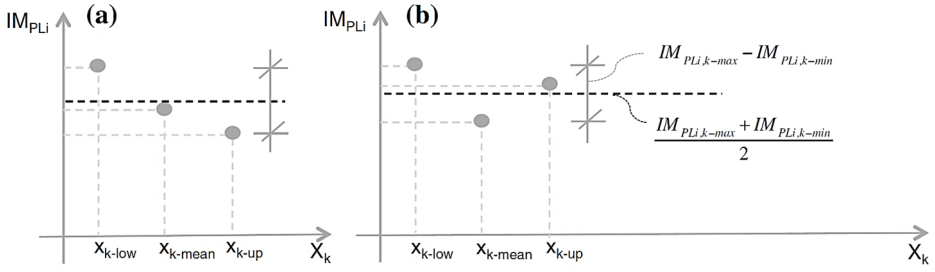

Figure 4-11: Computation of the $\Delta_{PLi,Xk}$ sensitivity associated to aleatory uncertainties.

The **sensitivity to epistemic uncertainties** is measured through the $\Delta_{PLi,Yj}$ parameter, which in case of M factors, for the jth epistemic uncertainty is given by (Figure 4-12):

$$\Delta_{PLi,Yj} = 2\frac{max\,(\mu_{j,IMPLi,mean,q}) - min\,(\mu_{j,IMPLi,mean,q})}{max(\mu_{j,IMPLi,mean,q}) + min\,(\mu_{j,IMPLi,mean,q})} \tag{50}$$

where $\mu_{j,IMPLi,mean,q}$ is the mean of the IM_{PLi} values (computed by assuming the mean value for all random variables) resulting from the branches of the logic tree associated to the qth option for the factor Y_j.

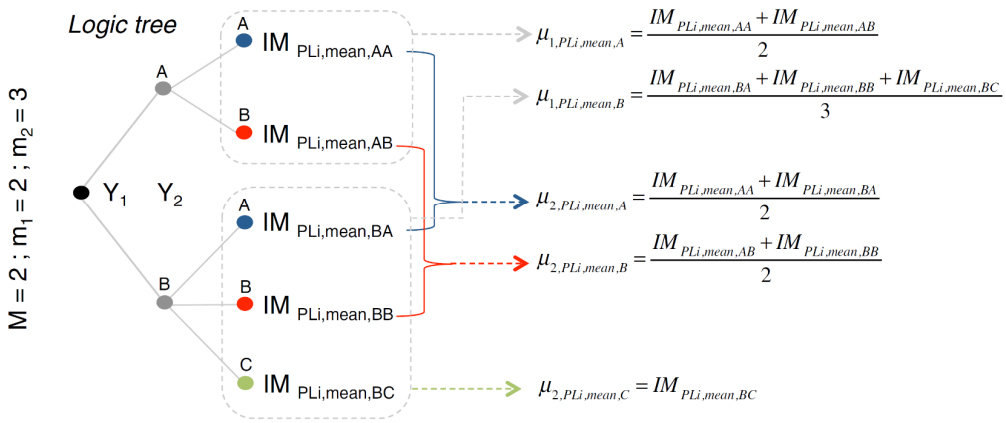

Figure 4-12: Computation of the $\Delta_{PLi,Yj}$ sensitivity associated to epistemic uncertainties.

In this work, the **logic tree approach** is applied, since the investigated factors are considered as epistemic uncertainties (listed in Table 4-4). The sensitivity of the seismic response of the prototype aggregates to the different factors is expressed through the sensitivity index $\Delta_{PLi,Yj}$, evaluated as shown in Figure 4-12 by means of the Eq. 54. The normalized maximum base shear, V_{bu}, and the stiffness, k^*, referring to the Life Safety limit state (SLV, Table 2-3), are chosen as IM_{PLi} (also referred to as SPI). The applied methodology and the considered results are illustrated in the following Figure 4-13; it is based on the assumptions introduced in paragraph 3.3 and on the framework illustrated in Figure 3-16. In detail, the pushover curves and the SPI are obtained for all models and load pattern distributions (Table 3-2), considering the 3 levels of analysis. The pushover curves at S.U.- and wall- levels are created from the results of the global analyses (average displacements, d, and sum of base shear forces, V) of the nodes belonging to the walls of interest.

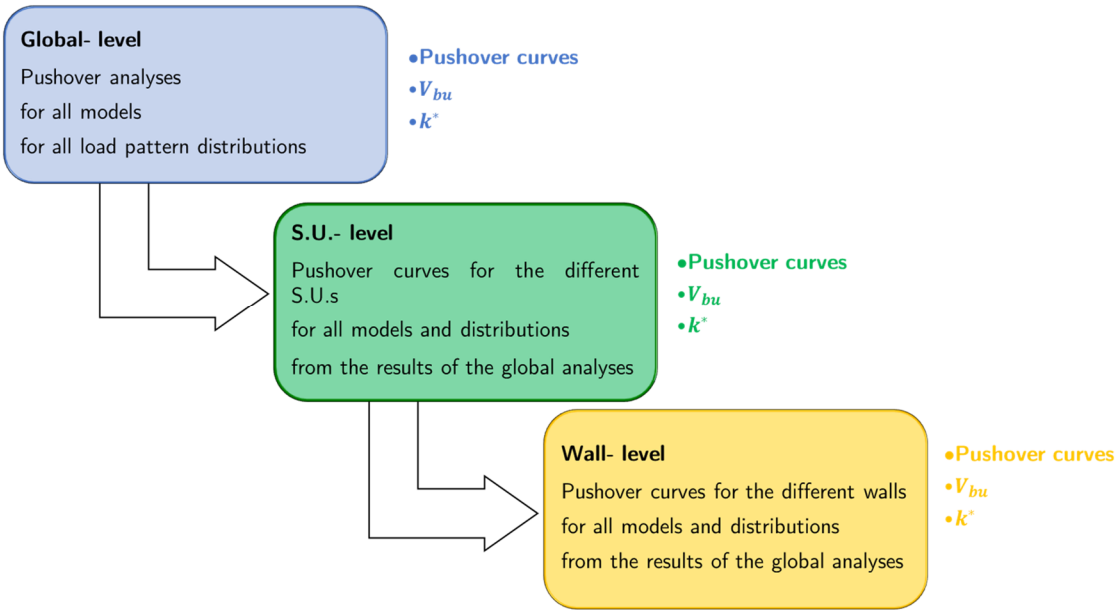

Figure 4-13: Multi-level methodology for the sensitivity analysis.

Once that the SPI are obtained for the 3 levels of analysis, the sensitivity indexes $\Delta_{SLV,Yj}$ are calculated for all the investigated factors Y_j.

As an example, Figure 4-14 shows the framework for the calculation of the sensitivity index $\Delta_{SLV,Y1}$, referring to the aggregate typology Y_1, considering the results at global- level.

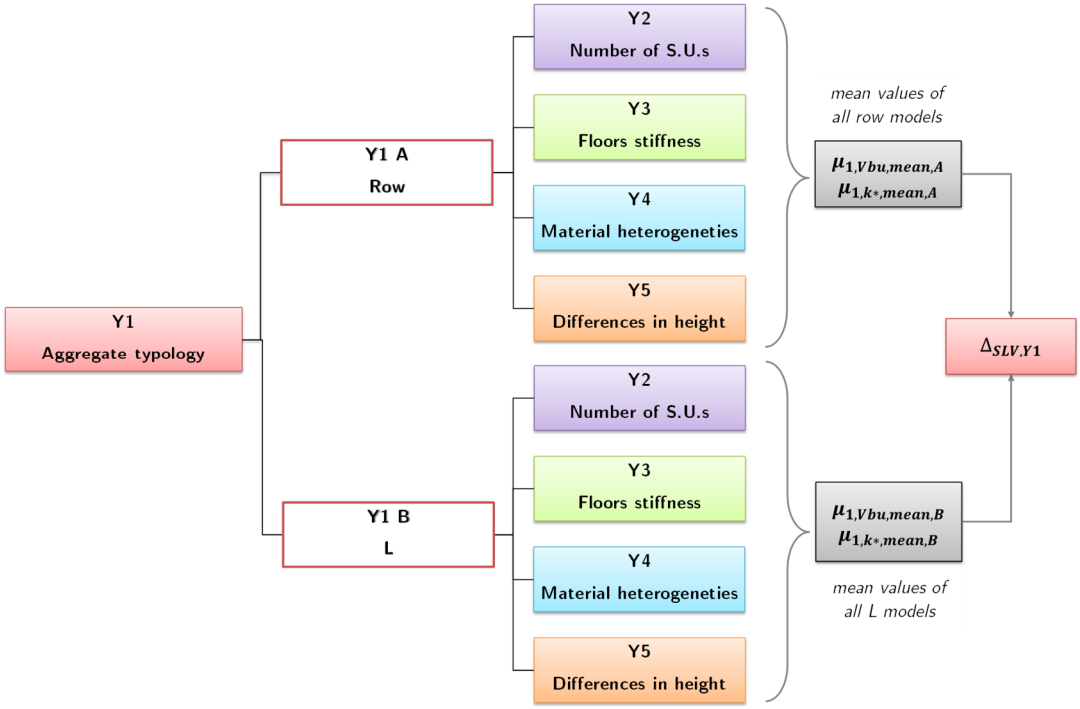

Figure 4-14: Example of calculation of the sensitivity index $\Delta_{PLi,Y1}$ for the aggregate typology.

In the following paragraph 4.4, the results are shown in terms of sensitivity indexes $\Delta_{SLV,Yj}$ at global- and S.U.- level. Then, the sensitivity to floors stiffness (§4.6), material heterogeneities (§4.7) and differences in height (§4.8) is deepened for the row and L aggregates composed of 5 S.U.s; this choice is explained in paragraph 4.5, where the influence of the number of S.U.s in the aggregate is studied. The results are in terms of percentage changes and pushover curves, at both global- and S.U.- level, trend of the maximum normalized base shear V_{bu} on each S.U. and base shear distribution among the walls.

4.4 GENERAL RESULTS

In this paragraph, the sensitivity indexes $\Delta_{SLV,Yj}$, related to the normalized maximum base shear ($\Delta\%\ V_{bu}$) and the stiffness ($\Delta\%\ k^*$), are presented in terms of the average values for direction of analysis (X and Y) and general mean value (referred to as "global"), by considering both global- level (§4.4.1) and S.U.- level. (§4.4.2).

4.4.1 Global- level

The general sensitivity at global- level is shown in Figure 4-15, by comparing the sensitivity indexes $\Delta_{SLV,Yj}$ ($\Delta\%\ V_{bu}$ and $\Delta\%\ k^*$) obtained for all the factors Y_j.

The most influential factor in the seismic behaviour of masonry aggregates at global- level is the number of S.U.s. This factor produces a general variation of 68% in terms of V_{bu} and more than 100% in terms of k^*; its influence in Y direction doubles that in X direction.

The presence of material heterogeneities and of differences in height have both a relevant influence, producing global variations of V_{bu} greater than 50% and of k^* in the order of 90%, regardless of the directions of analysis.

The aggregate typology influences the seismic behaviour especially in Y direction, with a sensitivity in this direction of 49% for V_{bu} and 87% for k^*.

Finally, the floors stiffness results to be the least influential factor, with a global sensitivity of 29% in terms of V_{bu} and 42% in terms of k^*. This parameter, unlike the previous ones, is more deciding in X direction, because this is the direction in which the floors are organized.

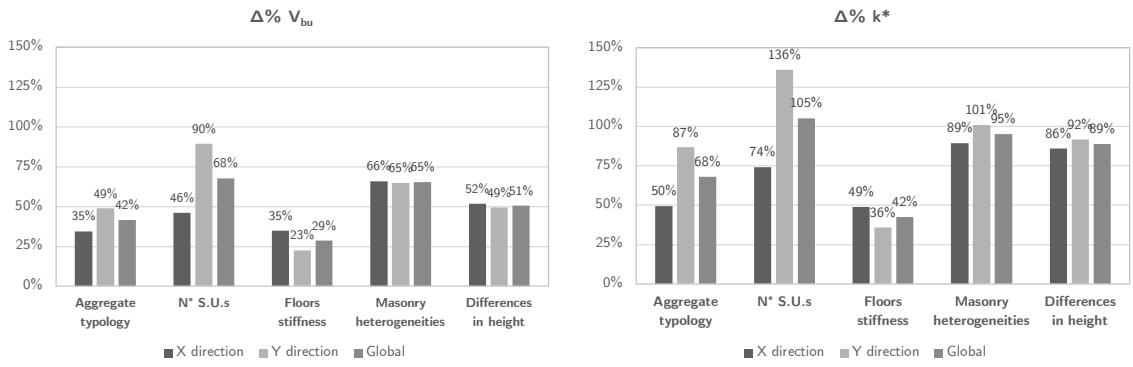

Figure 4-15: Global- level: general sensitivity in terms of V_{bu} and k^*.

In the following, the influence of each investigated factor is compared by aggregate typology.

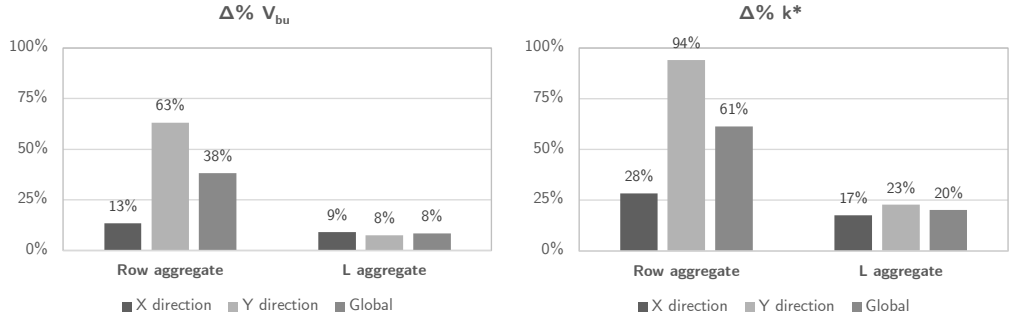

Figure 4-16: Global- level: sensitivity to n° S.U.s in terms of V_{bu} and k^*.

The sensitivity to the n° S.U.s is compared in Figure 4-16 by aggregate typology.
It can be noticed that the variation of the n° S.U.s is more relevant for the row aggregate, especially in terms of k^* in Y direction, with a change equal to 94%, while for the L aggregate it doesn't exceed 25%.

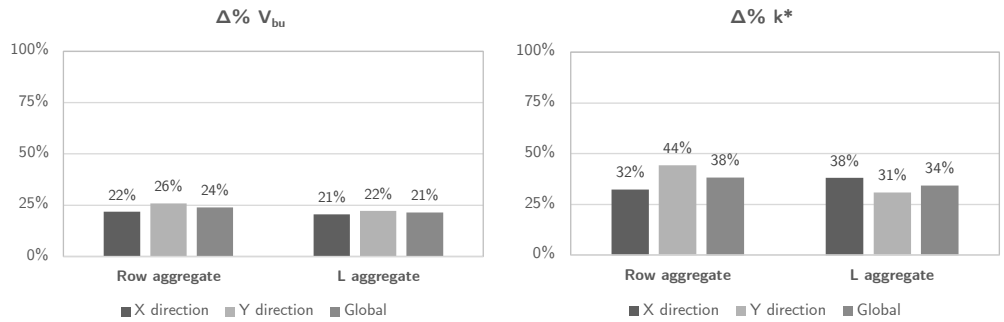

Figure 4-17: Global- level: sensitivity to floors stiffness in terms of V_{bu} and k^*.

Furthermore, the influence of the stiffness of the floors over the two aggregate typologies can be observed in Figure 4-17. This parameter influences both in a similar way, with a general variation in terms of V_{bu} in the order of 20% and in terms of k^* in the order of 35%.

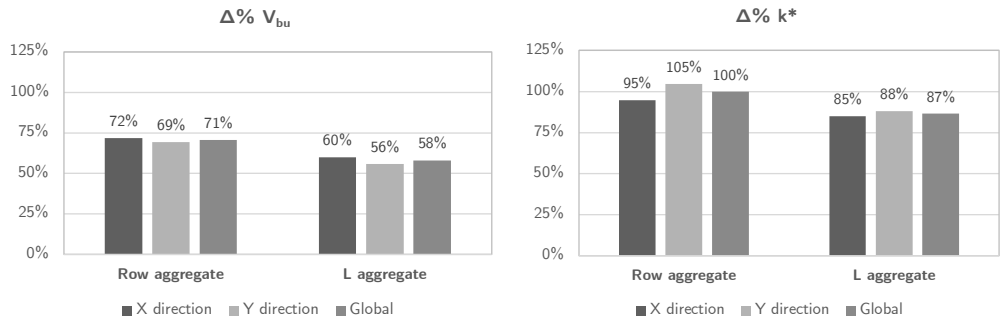

Figure 4-18: Global- level: sensitivity to material heterogeneities in terms of V_{bu} and k^*.

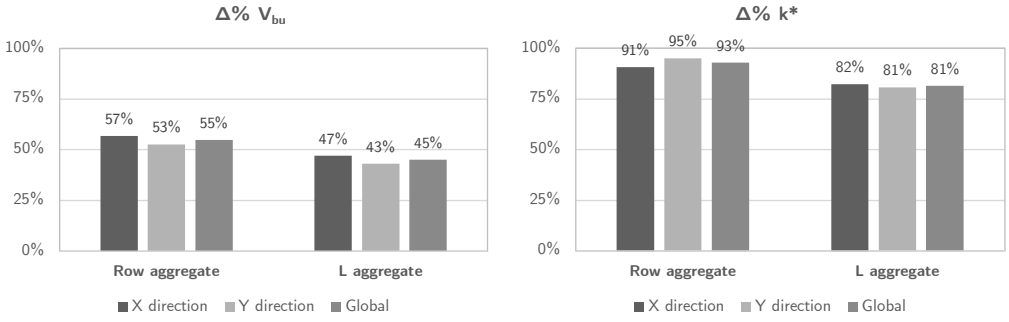

Figure 4-19: Global- level: sensitivity to differences in height in terms of V_{bu} and k^*.

As previously noticed, the material heterogeneities and the differences in height produce greater variations in the seismic behaviour, regardless of the directions of analysis. A comparison of the sensitivity to these factors between the row and the L aggregate is shown in Figure 4-18 and Figure 4-19, respectively. The row aggregate is, in general, more sensitive to these factors than the L aggregate.
Considering k^*, the change is in the order of 100% for the row aggregate, while for the L aggregate is almost 85%. With regards to V_{bu}, this is more influenced by the material heterogeneities for both aggregate typologies.

4.4.2 S.U.- level

The sensitivity to the different parameters is evaluated also at S.U- level, considering 3 main conditions, schematized in Figure 4-20:

- External S.U.
- Internal S.U.
- Corner S.U.

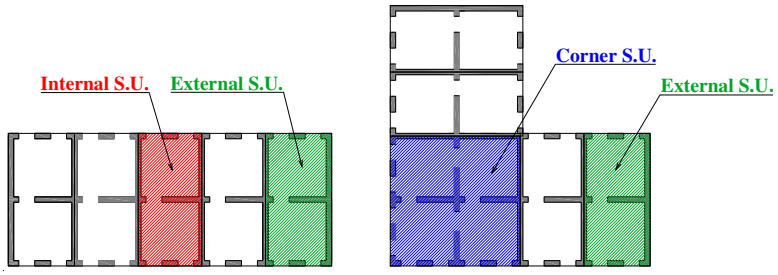

Figure 4-20: Scheme of the S.U. conditions.

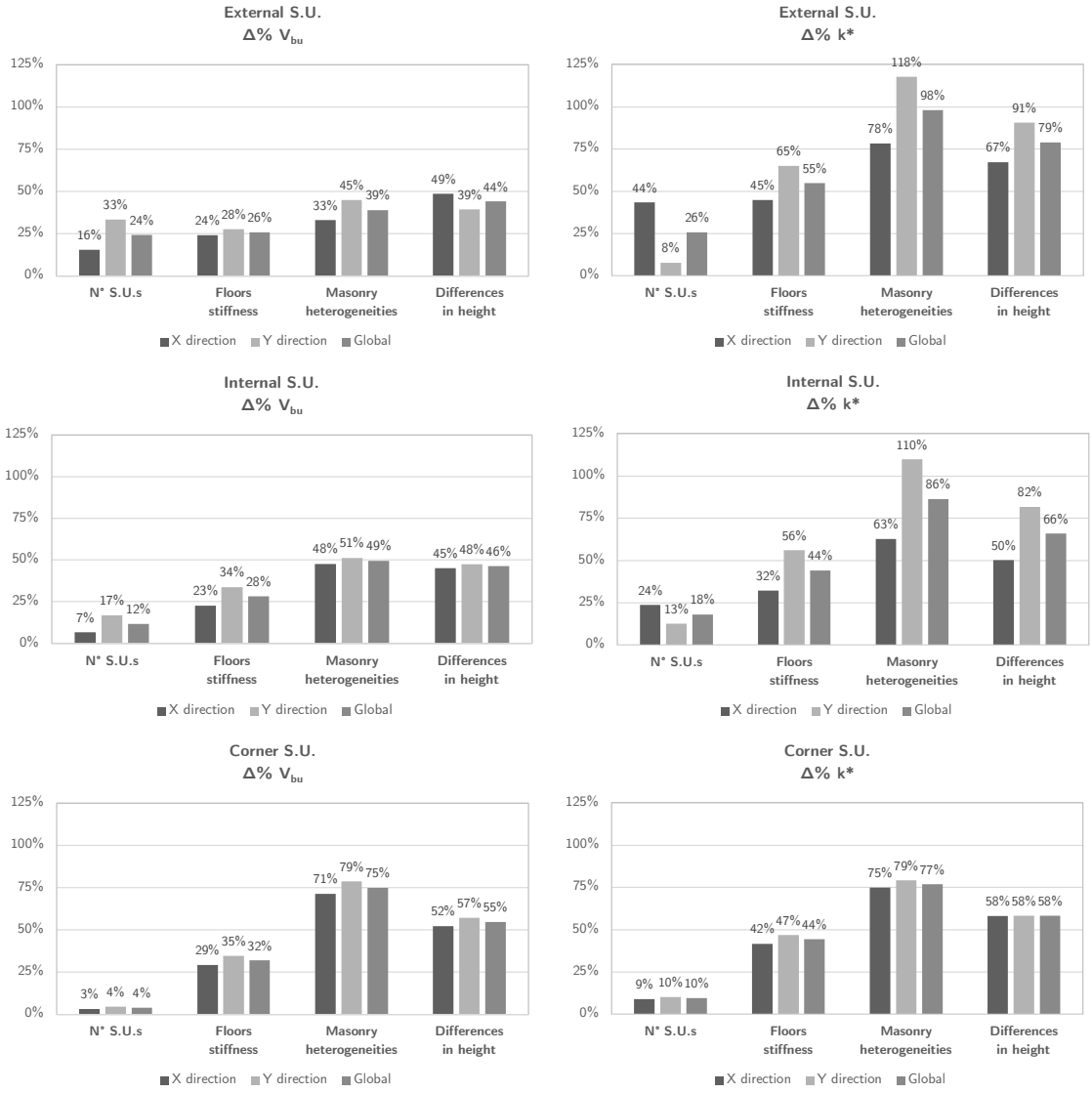

Figure 4-21: S.U.- level: general sensitivity for an eternal S.U. (upper row), an internal S.U. (middle row) and a corner S.U. (bottom row), in terms of V_{bu} and k^*.

The obtained sensitivity indexes $\Delta_{SLV,Yj}$, in terms of the normalized maximum base shear and the stiffness ($\Delta\%\,V_{bu}$ and $\Delta\%\,k^*$), are compared in Figure 4-21.

Firstly, the condition of external S.U. is the most sensitive, especially in terms of k^* and in Y direction, while the corner position is the least influenced.

The presence of material heterogeneities results to be the most influential factor, producing a variation in terms of k^* of about 100% for the external S.U., of 86% for the internal S.U. and, finally, of 77% for the corner S.U. The same trend, but with lower values, can be observed in presence of differences in height; the external condition is characterized by a k^* variation of almost 80%, while the corner position of 58%.

The variation of the stiffness of the floors produces global changes between 45% and 55% in terms of k^* and of about 30% in terms of V_{bu}, for all the S.U. conditions.

Finally, the variation of the n° S.U.s does not significantly influence the response, regardless of the S.U. condition, with deviations that don't exceed 20%. This aspect is deepened in the following paragraph 4.5, where the pushover curves at S.U.- level obtained for aggregates composed of 5, 7 and 9 S.U.s are compared.

4.5 Influence of the number of S.U.s within the aggregate

In the next paragraphs, the sensitivity to the floors stiffness, material heterogeneities and differences in height are deepened for the row and L aggregates composed of 5 S.U.s, shown in Figure 4-22.

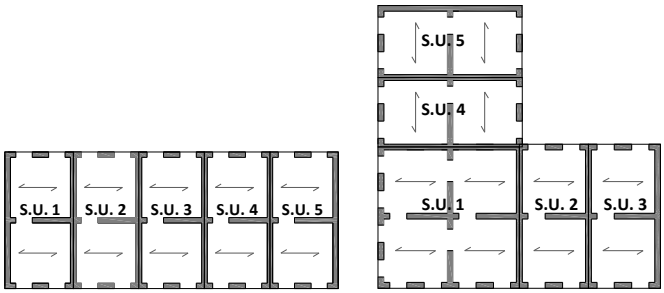

Figure 4-22: Scheme of the investigated aggregates of 5 S.U.s: row (left) and L (left) typology.

This choice is in accordance with the previous results, from which the number of S.U.s results to be the least influential factor at S.U.- level. In fact, the influence of the other buildings on the target S.U. decreases with the distance, as shown below.

With reference to an internal S.U. of a row aggregate, in Figure 4-23 it is possible to observe that the pushover curves at S.U.- level (considering both positive directions of analysis and the uniform load pattern distribution, U) do not change considering an aggregate of 5, 7 or 9 S.U.s., especially in the transversal direction.

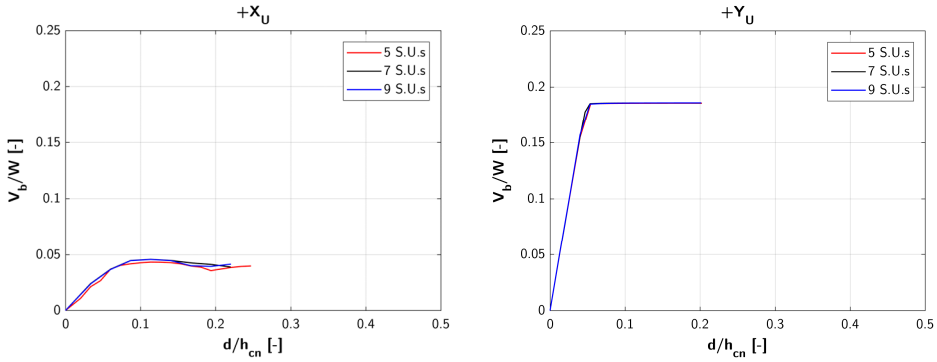

Figure 4-23: Row aggregate – internal S.U.: pushover curves comparison at S.U.- level in function of the n° S.U.s.

As an example, the average values of the percentage changes, in terms of maximum base shear V_{bu} and stiffness k^*, obtained in reference to the 5 S.U. aggregate, are shown in Table 4-5. You might notice that the changes are minimal, especially in the transversal direction Y.

Table 4-5: Row aggregate – internal S.U.: percentage changes of k^* and V_{bu} in reference to 5 S.U. aggregate.

		Δ% k*	**Δ% V_{bu}**
X direction	**7 S.U.s**	7%	2%
	9 S.U.s	8%	2%
Y direction	**7 S.U.s**	0%	0%
	9 S.U.s	0%	0%

The same conclusions can be drawn for an external S.U. and for a corner S.U. in an L aggregate, for which only the pushover curves are compared in Figure 4-24 and Figure 4-25, respectively.

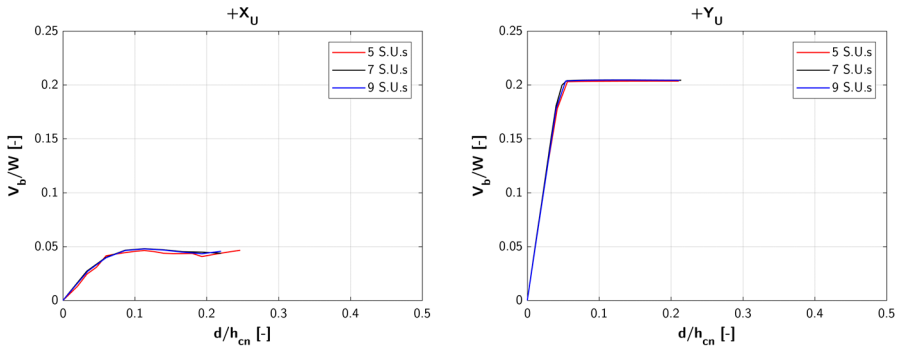

Figure 4-24: Row aggregate – external S.U.: pushover curves comparison at S.U.-level in function of the n° S.U.s.

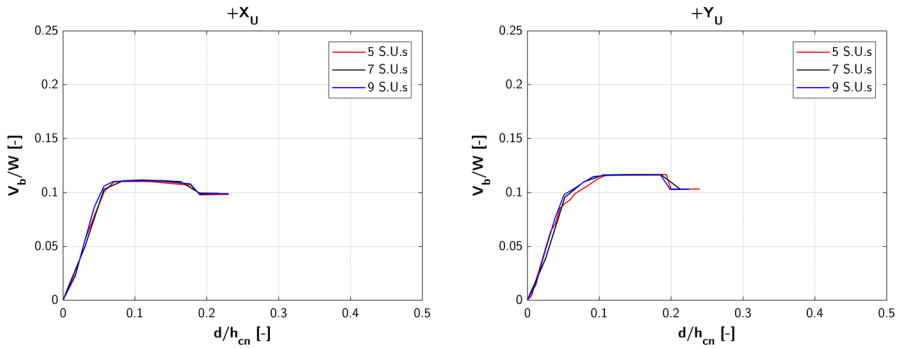

Figure 4-25: L aggregate – corner S.U.: pushover curves comparison at S.U.-level in function of the n° S.U.s.

4.6 SENSITIVITY TO FLOORS STIFFNESS

In this paragraph, the sensitivity to the stiffness of the floors is deepened by showing some comparisons for the modelling configurations of the 5 S.U.s aggregates in function of the floors typologies, shown in Figure 4-7:

- **R**: all rigid floors.
- **F**: all flexible floors;
- Combinations (RRFFF/RFF, FFRFF, FRRRF/FRR).

The results are in terms of percentage changes and pushover curves, at both global- level (§4.6.1) and S.U.- level (§4.6.2), trend of the maximum normalized base shear V_{bu} on each S.U. and base shear distribution among the walls (§4.6.3).

4.6.1 Global- level

4.6.1.1 Percentage changes

The sensitivity to the floors stiffness at global- level is assessed for both aggregate typologies, by evaluating the percentage changes, in terms of the maximum normalized base shear V_{bu} and the stiffness k^*, in reference to the case of rigid floors (R). The presence of flexible floors (F) generally produces a reduction of both maximum base shear and stiffness, but the variations are not relevant.

With reference to the row aggregate (Figure 4-26), the changes are null in term of V_{bu} and in the order of 5% in terms of k^*. The seismic capacity of L aggregate (Figure 4-27) is more influenced, with variations that however do not exceed 15%.

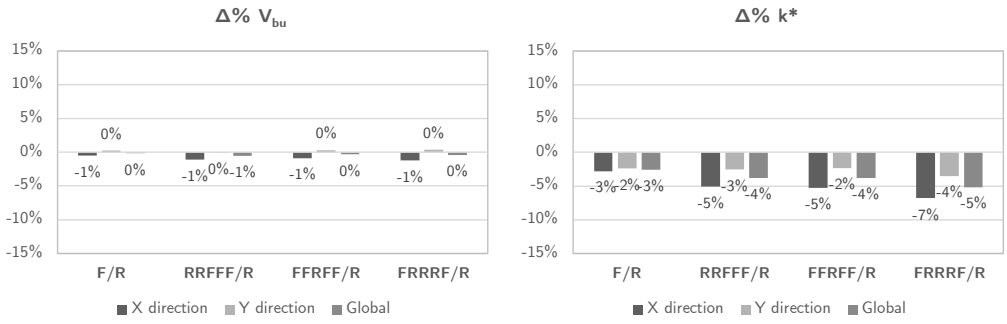

Figure 4-26: Row aggregate – sensitivity to floors stiffness at global- level, in terms of V_{bu} and k^*.

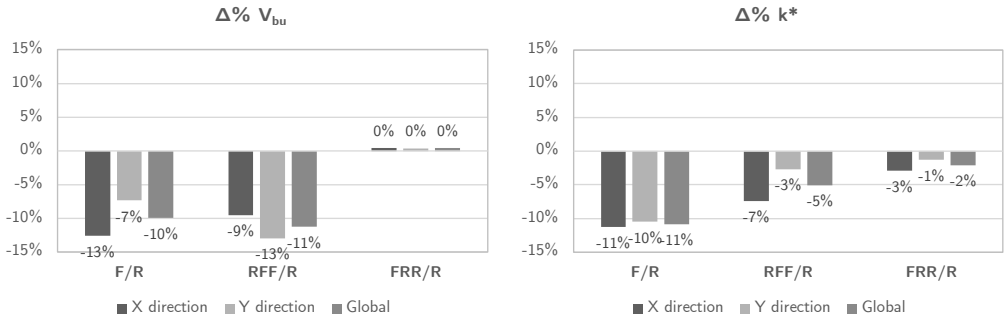

Figure 4-27: L aggregate – sensitivity to floors stiffness at global- level, in terms of V_{bu} and k^*.

4.6.1.2 Pushover curves

In the following, some comparisons of the pushover curves, obtained for both directions of analysis and the uniform load pattern distribution (U), are shown in function of the floors stiffness for the row aggregate (Figure 4-28) and the L aggregate (Figure 4-29).

As previously observed, the variation of the floors typology is not significant for both aggregate typologies. Indeed, for the row aggregates the pushover curves have the same trend, especially in Y direction. In X direction, there is a difference between the positive and the negative direction, with greater capacity in this last case; this fact can be attributed to the position of the openings in the X-walls.

Considering the L aggregates, instead, a more relevant difference between the pushover curves can be observed. In general, the trend is similar for R and FRR cases and for F and RFF ones, that have inferior values V_b/W and k^*.

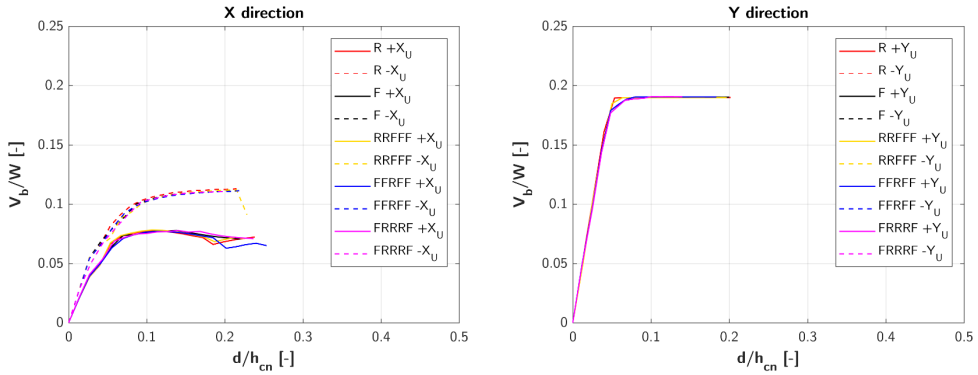

Figure 4-28: Row aggregate – Pushover curves comparison at global- level in function of floors stiffness.

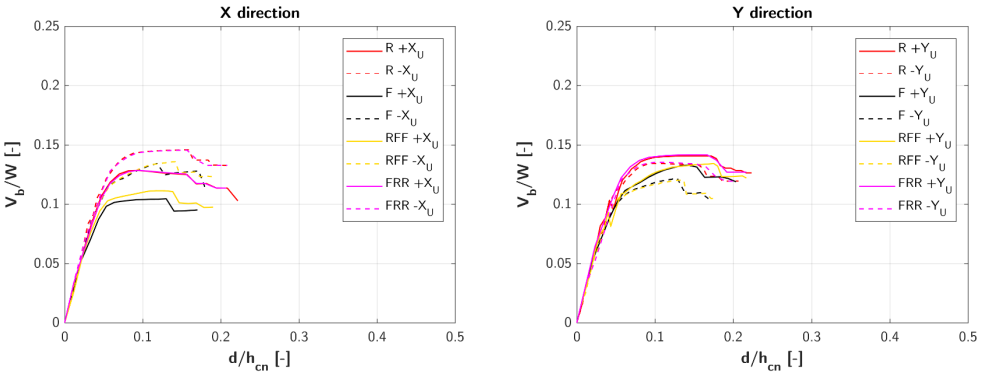

Figure 4-29: L aggregate – Pushover curves comparison at global- level in function of floors stiffness.

4.6.2 S.U.- level

The influence of the floors stiffness on the seismic behaviour of aggregate structures is deepened by evaluating the response of different S.U.s., highlighted in Figure 4-22, in terms of percentage changes, pushover curves and base shear trend.

4.6.2.1 Percentage changes

The sensitivity to the floors stiffness at S.U.- level (Figure 4-30) is assessed as function of the S.U. position (Figure 4-20), by evaluating the percentage changes of the maximum normalized base shear V_{bu} and the stiffness k^* in reference to the case of rigid floors (R).

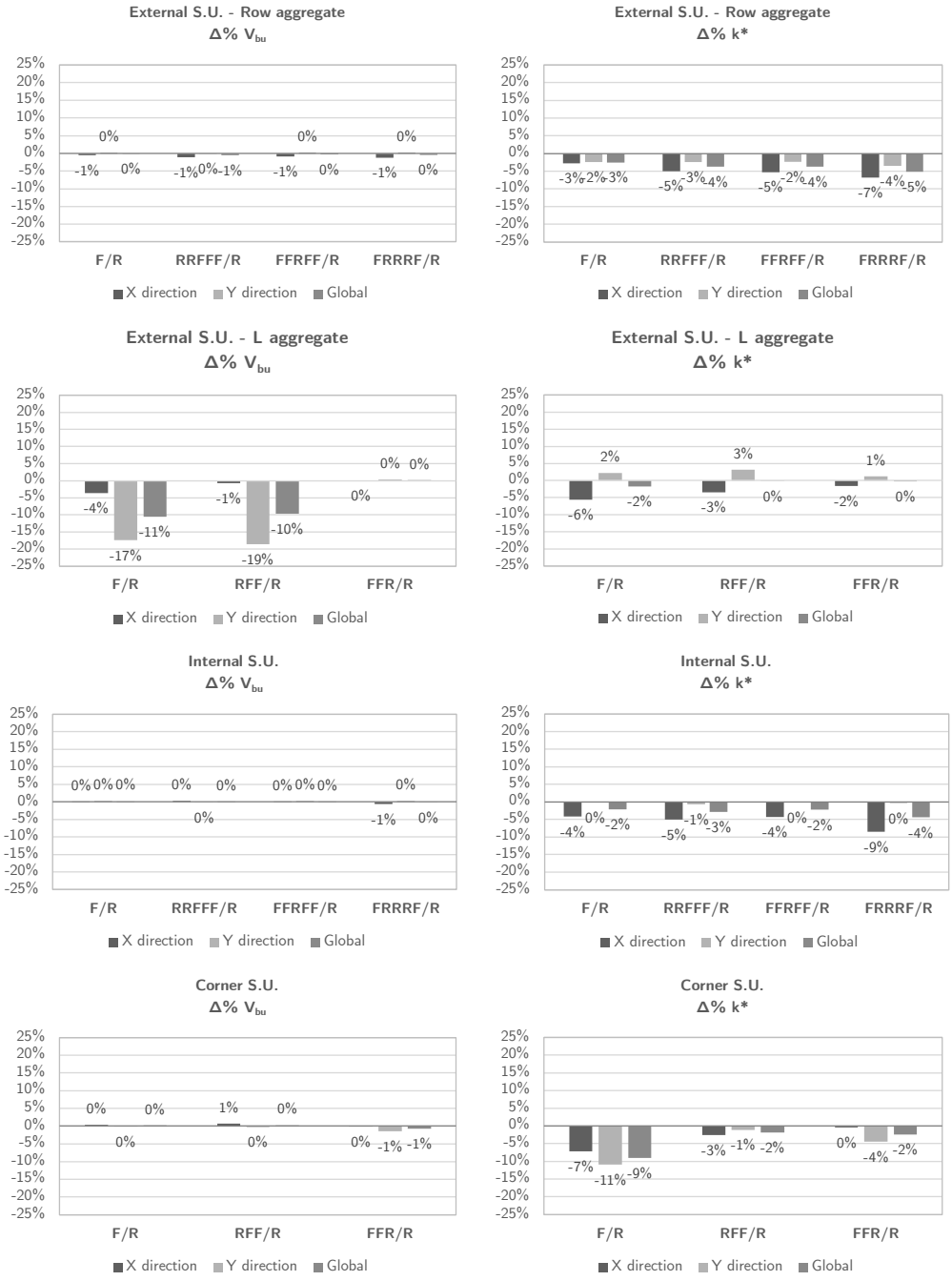

Figure 4-30: S.U.- level: sensitivity to floors stiffness for an external S.U. (upper rows), an internal S.U. (middle row) and a corner S.U. (bottom row), in terms of V_{bu} and k^*.

The presence of flexible floors (F) generally produces a reduction of stiffness, but the variations are not relevant, in the order of 5%, regardless of the S.U. position.

Considering the row aggregate, the reduction is minor in Y direction. On the contrary, the external S.U. of the L aggregate presents a slight increment of stiffness in this direction. The greatest reduction of stiffness can be observed for the corner S.U. in presence of flexible floors, in both directions.

In terms of maximum base shear V_{bu}, there are no changes; only the external S.U. of the L aggregate presents a reduction of the capacity, especially in Y direction, with values around 20%.

4.6.2.2 Pushover curves

A comparison of the pushover curves obtained for the row aggregate is shown in Figure 4-31, considering an external S.U. (S.U.1) and an internal one (S.U.3), as indicated in Figure 4-22.
As can be noticed, the floors typology does not influence the trend of the pushover curves. Moreover, in Y direction the internal S.U. has inferior values of V_b/W in comparison to the external one.

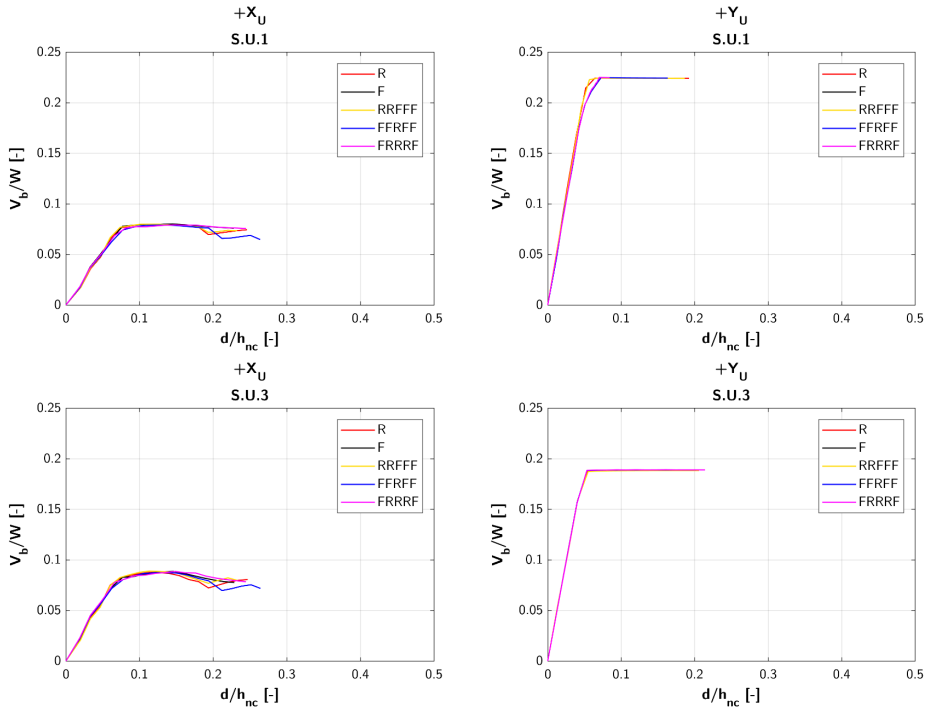

Figure 4-31: Row aggregate – Pushover curves comparison at S.U.-level for an external (S.U.1) and an internal (S.U.3) S.U., in function of floors stiffness.

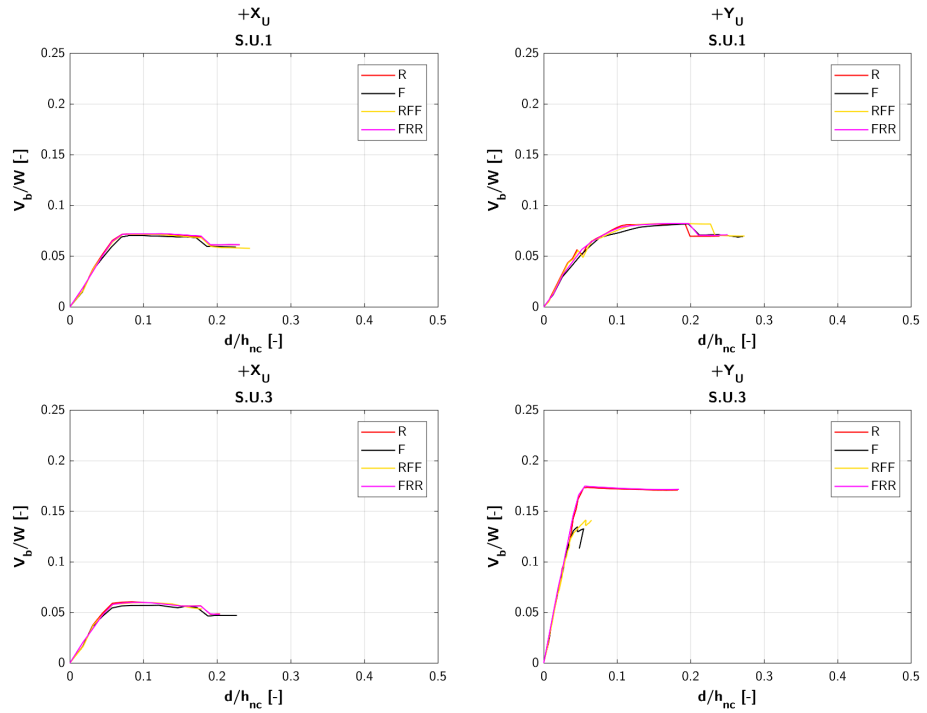

Figure 4-32: L aggregate – Pushover curves comparison at S.U.-level for a corner (S.U.1) and an external (S.U.3) S.U. in function of floors stiffness.

The same conclusions can be drawn from Figure 4-32, in which the comparison is shown for the L aggregate, considering the corner S.U. (S.U.1) and an external one (S.U.3). For the latter, a considerable difference can be observed between the pushover curves of the F/RFF cases and the others: their ultimate base shears and displacements have lower values.

4.6.2.3 Base shear trend

The last comparison at the S.U.- level regards the trend of the maximum normalized base shear (V_{bu}) on each S.U., by considering the uniform pattern distribution (U) in both directions of analysis.

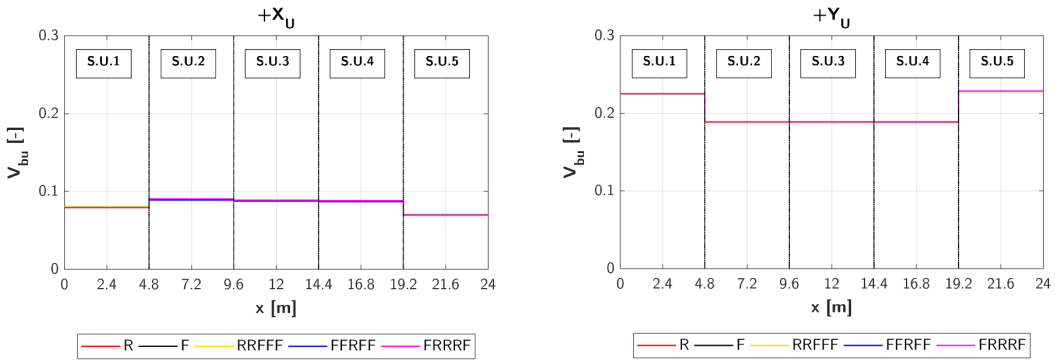

Figure 4-33: Row aggregate – Base shear trend on each S.U. in function of the floors stiffness.

With reference to the row aggregate (Figure 4-33), generally, there is no sensitivity to the stiffness of the floors. It can be noticed that, in X direction, V_{bu} is slightly greater in the internal S.U.s. On the contrary, in Y direction, the major values are in the external S.U.s, confirming the previous results.

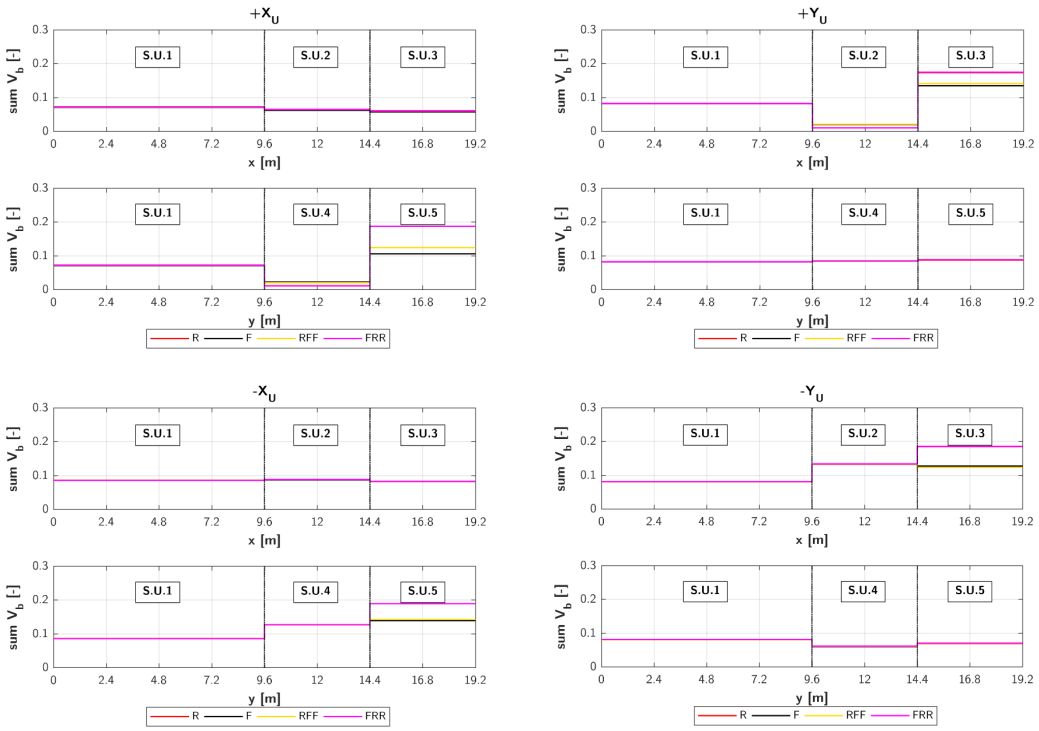

Figure 4-34: L aggregate – Base shear trend on each S.U. in function of the floors stiffness.

For the L aggregate (Figure 4-34), the results are shown for both positive and negative directions of analysis. The major values of V_{bu} are for the external S.U.s placed in the transversal row in respect of the analysis direction (S.U.5 for $+X_U$, S.U.3 for $+Y_U$). On the contrary, the lowest values are in correspondence to the internal S.U.s in the transversal row, when the direction of analysis is positive (S.U.4 for $+X_U$, S.U.2 for $+Y_U$). For the negative direction, the minimum V_{bu} is for the S.U.s placed in the longitudinal row in respect of the analysis direction (S.U.2 and S.U.3 for $-X_U$, S.U.4 and S.U.5 for $-Y_U$). The corner S.U.1 present intermediate values.

4.6.3 Wall- level

The distribution of the maximum base shear V_{bu} is evaluated at wall- level, by considering its percentage distribution among all walls in both directions of analysis, in function of the floors typology. The walls are highlighted in Figure 4-35 for both row and L aggregate.

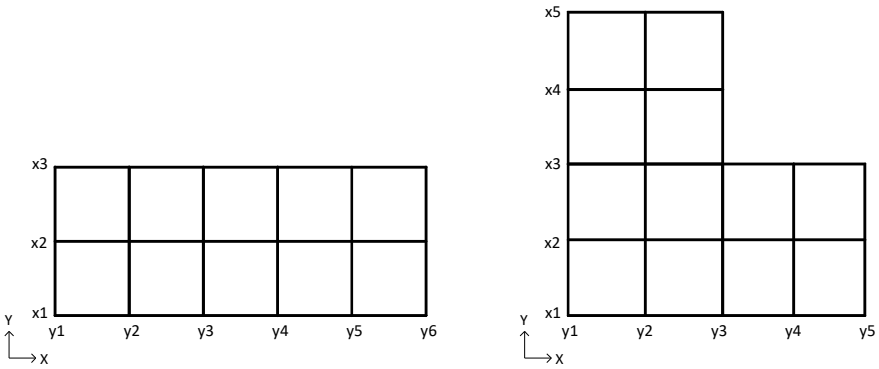

Figure 4-35: Scheme of the walls in the row (left) and L (right) aggregate.

In the case of the row aggregate (Figure 4-36), the base shear is mainly redistributed among the walls placed in the longitudinal direction in refers to that of the analysis.
In X direction, the internal wall x2 has the highest values, since it is characterized by an inferior openings area; the difference with the external S.U.s grows in presence of rigid floors.
The base shear is lower for the external walls y1 and y6 in Y direction too, as the loads they carry are inferior. It should be noticed again that the floors stiffness in this direction is irrelevant.

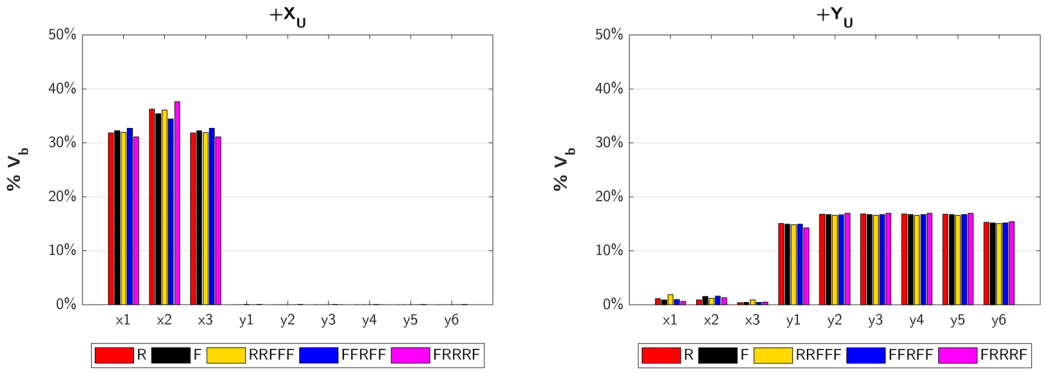

Figure 4-36: Row aggregate – Base shear percentage distribution among walls in function of the floors stiffness.

When considering the L aggregate (Figure 4-37), the base shear V_{bu} is redistributed not only among the longitudinal walls, but also among the transversal ones. The walls that show the greatest values are

the longitudinal internal ones (i.e., x2 and x4 for the analysis in X direction, y2 and y4 for those in Y direction), while the lowest are for the transversal ones, especially for y3 in X direction and x3 in Y direction. Finally, the internal longitudinal walls reach greater values of V_{bu} in presence of flexible floors; on the contrary, the external longitudinal walls and the transversal ones are more stressed in presence of rigid floors.

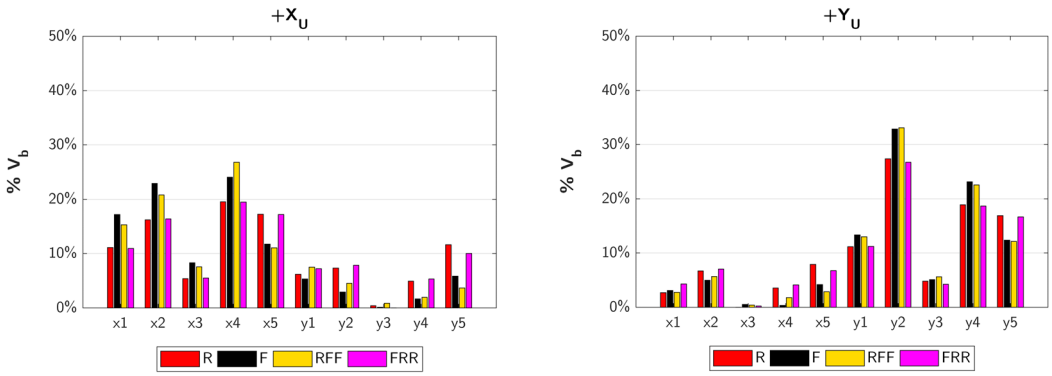

Figure 4-37: L aggregate – Base shear percentage distribution among walls in function of the floors stiffness.

4.7 SENSITIVITY TO MATERIAL HETEROGENEITIES

In this paragraph, the sensitivity to the presence of material heterogeneities is deepened by showing some comparisons for all the considered models (Figure 4-8):

- **murA**: all the S.U.s are in stone masonry.
- **murB**: the internal/corner S.U.s are in hollow brick masonry (more rigid);
- **murC**: the external S.U.s are in hollow brick masonry (more rigid).

As for the previous case, the results are in terms of percentage changes and pushover curves, at both global- level (§4.7.1) and S.U.- level (§4.7.2), maximum normalized base shear trend on each S.U. and base shear distribution among the walls (§4.7.3).

4.7.1 Global- level

4.7.1.1 Percentage changes

The sensitivity to the presence of material heterogeneities at global- level is assessed for both aggregate typologies, by evaluating the percentage changes, in terms of the maximum normalized base shear V_{bu} and the stiffness k^*, in reference to the murA case (i.e., absence of material heterogeneities). The results are shown only for rigid (R) floors, as the floors stiffness results to be the least influential factor (§4.6).

The presence of more rigid S.U.s generally produces a relevant variation in the seismic capacity of the masonry aggregates, especially in terms of stiffness; moreover, the changes are greater in presence of rigid floors.

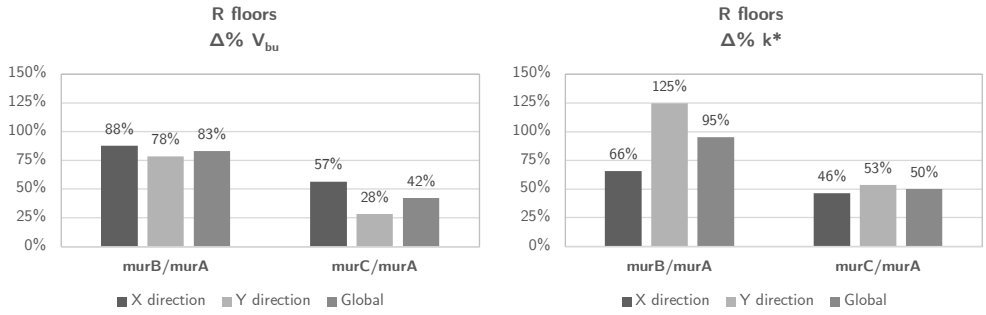

Figure 4-38: Row aggregate – sensitivity to material heterogeneities at global- level, in terms of V_{bu} and k^*, in presence of rigid floors.

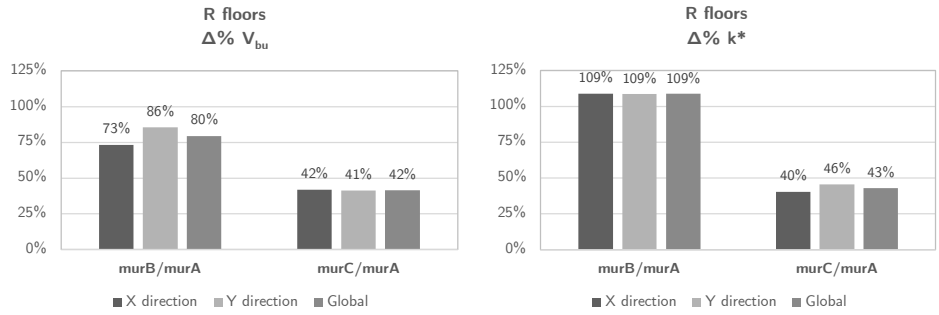

Figure 4-39: L aggregate – sensitivity to material heterogeneities at global- level, in terms of V_{bu} and k^*, in presence of rigid floors.

With reference to the row aggregate (Figure 4-38), the changes are greater for the murB case, in which the internal S.U.s are more rigid, with values in the order of 80% in terms of V_{bu} and of 95% in terms of k^*. The same conclusions can be drawn for the L aggregate (Figure 4-39), for which the major variation is due to the presence of a more rigid S.U. in the corner position (murA) and rigid floors, with changes greater than 100% in terms of k^*.

4.7.1.2 *Pushover curves*

The pushover curves of the row aggregate (Figure 4-40) and L aggregate (Figure 4-41) are compared in function of the presence of material heterogeneities, considering both directions of analysis and the uniform load pattern distribution (U). The graphs are shown for rigid (R) floors.
As previously observed, the presence of different masonry typologies between the S.U.s is a significant factor for both row and L aggregate. Indeed, the capacity in terms of V_b/W and the stiffness k^* increases as more S.U.s of better mechanical characteristics are present, as happens for murB case and, gradually, for murC case.

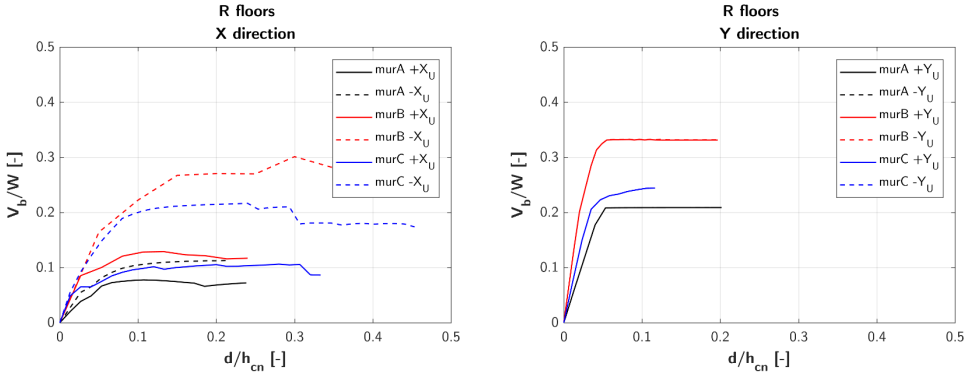

Figure 4-40: Row aggregate – Pushover curves comparison at global- level in presence of material heterogeneities for rigid (R) floors.

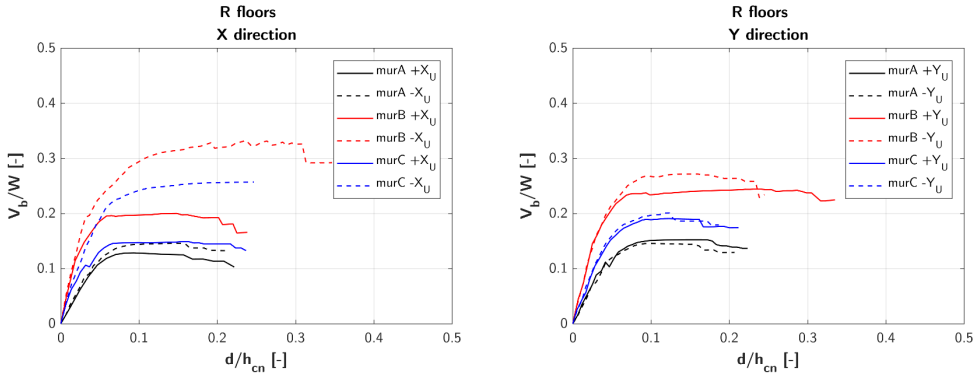

Figure 4-41: L aggregate – Pushover curves comparison at global- level in presence of material heterogeneities for rigid (R) floors.

4.7.2 S.U.- level

The influence of the presence of material heterogeneities is deepened by evaluating the response of different S.U.s., highlighted in Figure 4-22, in terms of percentage changes, pushover curves and base shear trend.

4.7.2.1 Percentage changes

The sensitivity to the material heterogeneities at S.U.- level (Figure 4-42) is assessed as function of the S.U. position, by evaluating the percentage changes of the maximum normalized base shear V_{bu} and the stiffness k^* in reference to the murA case (absence of material heterogeneities). The results are shown for rigid (R) floors.

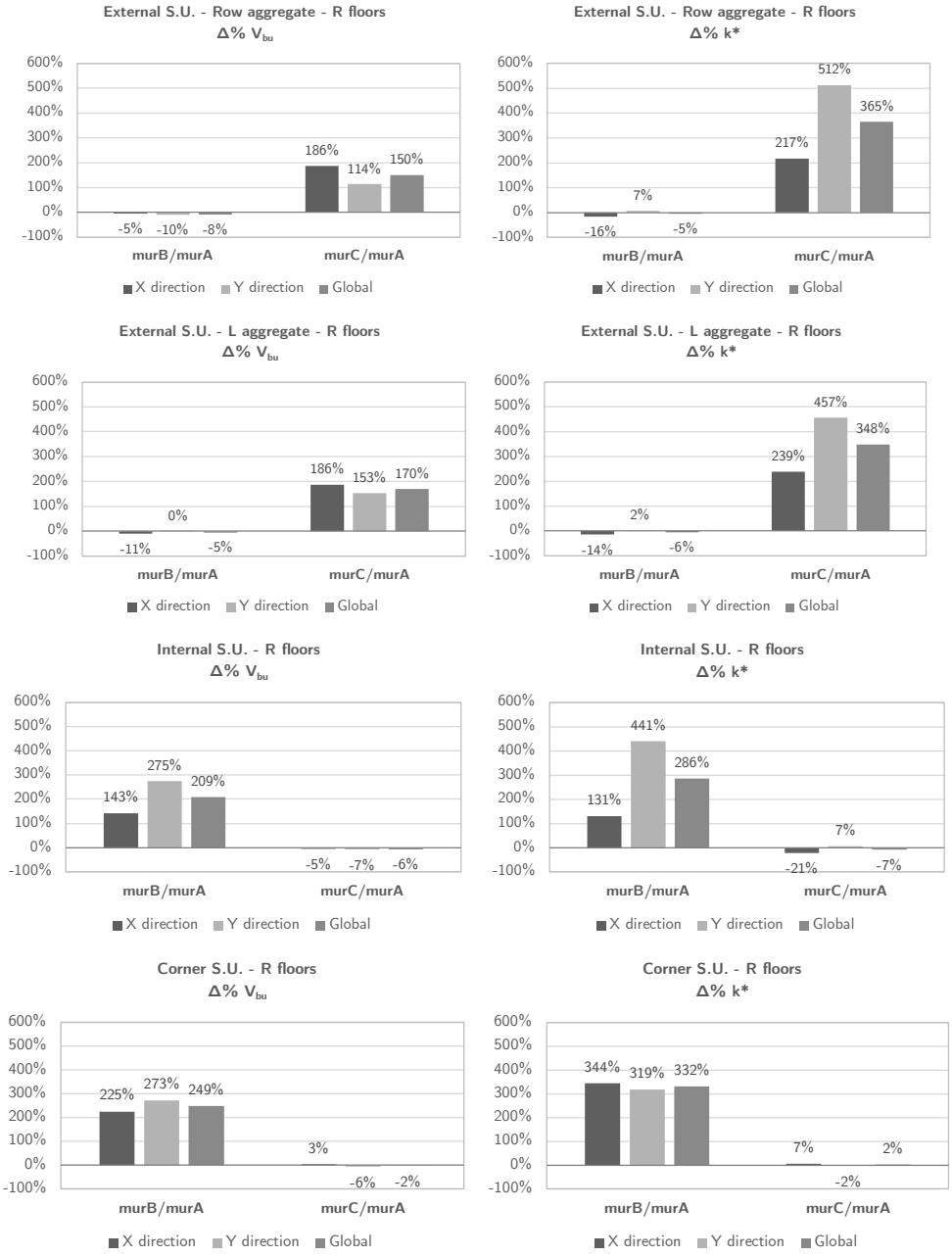

Figure 4-42: S.U.- level: sensitivity to material heterogeneities, in terms of V_{bu} and k^*, for an external (upper row), an internal (middle row) and a corner S.U. (bottom row).

The increment of the base shear and stiffness is also evident at S.U.- level. The S.U.s composed of more rigid masonry present an increase of base shear in the order of 200% and of stiffness in the order of 300%. On the contrary, it is possible to observe a slight reduction of the capacity (in the order of 5%) in the adjacent S.U.s. In terms of stiffness, the major changes are for the external S.U., while the lowest are for

the internal S.U.; Y direction is the most sensitive. In terms of base shear, the corner S.U. presents the major deviations, while the external ones show the lowest values.

4.7.2.2 Pushover curves

The comparison of the pushover curves of the row aggregate in function of the material heterogeneities is shown in Figure 4-43, considering both external (S.U.1 and S.U.5) and internal (S.U.3) S.U.s., in presence of rigid floors.

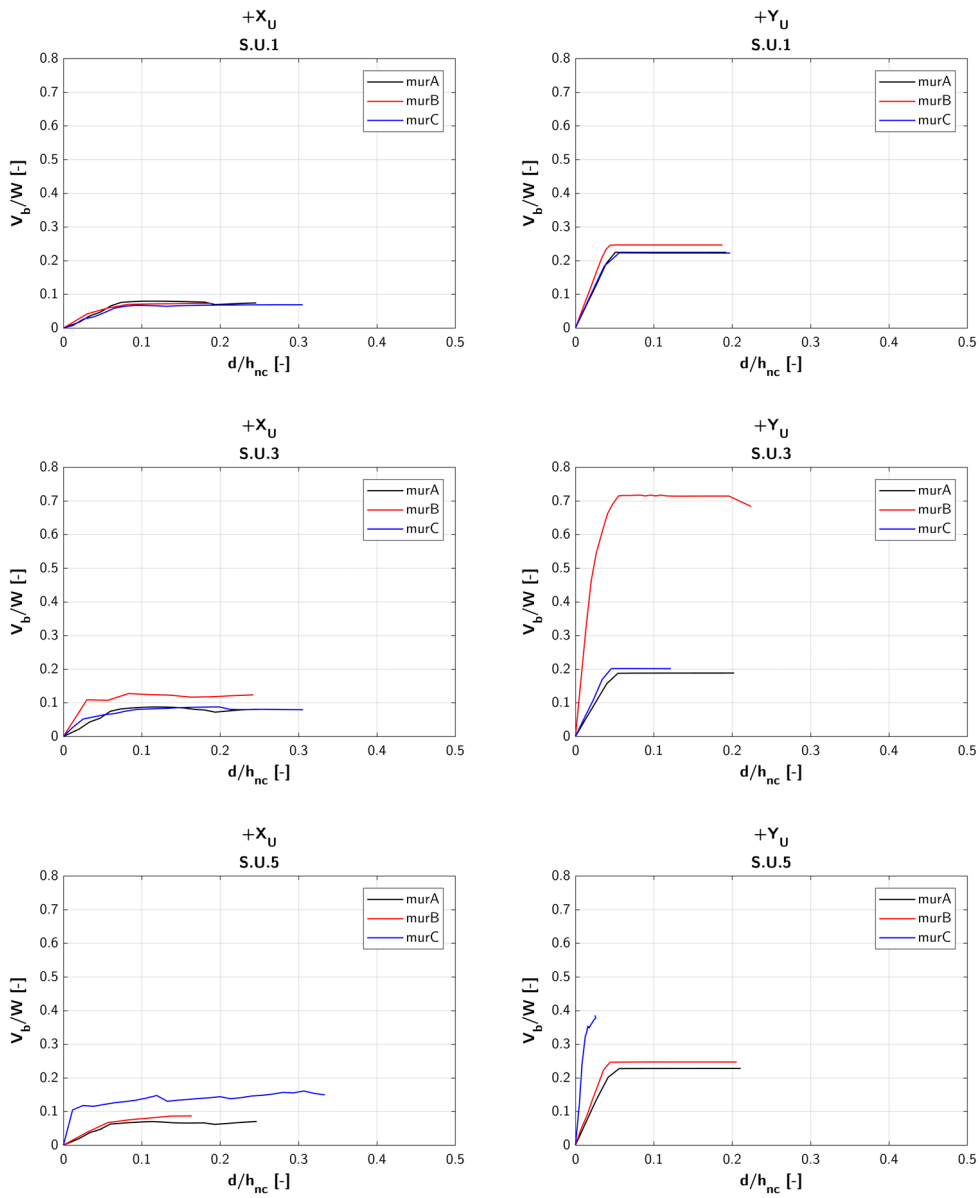

Figure 4-43: Row aggregate – Pushover curves comparison at S.U.- level in function of material heterogeneities, for the external S.U.s (S.U.1 and S.U.5) and an internal one (S.U.3).

As can be noticed, for the external S.U. on the left side (S.U.1), which is not subject to changes in material, the trend of the pushover curves is similar for the 3 cases. On the contrary, the internal S.U.3 shows a relevant increase of the capacity, especially in Y direction, when it is composed of a more rigid masonry, together with the immediately adjacent S.U.s (murB case). The same can be noticed in the case of the external S.U. on the right (S.U.5), for which the capacity is the greatest for the murC case.

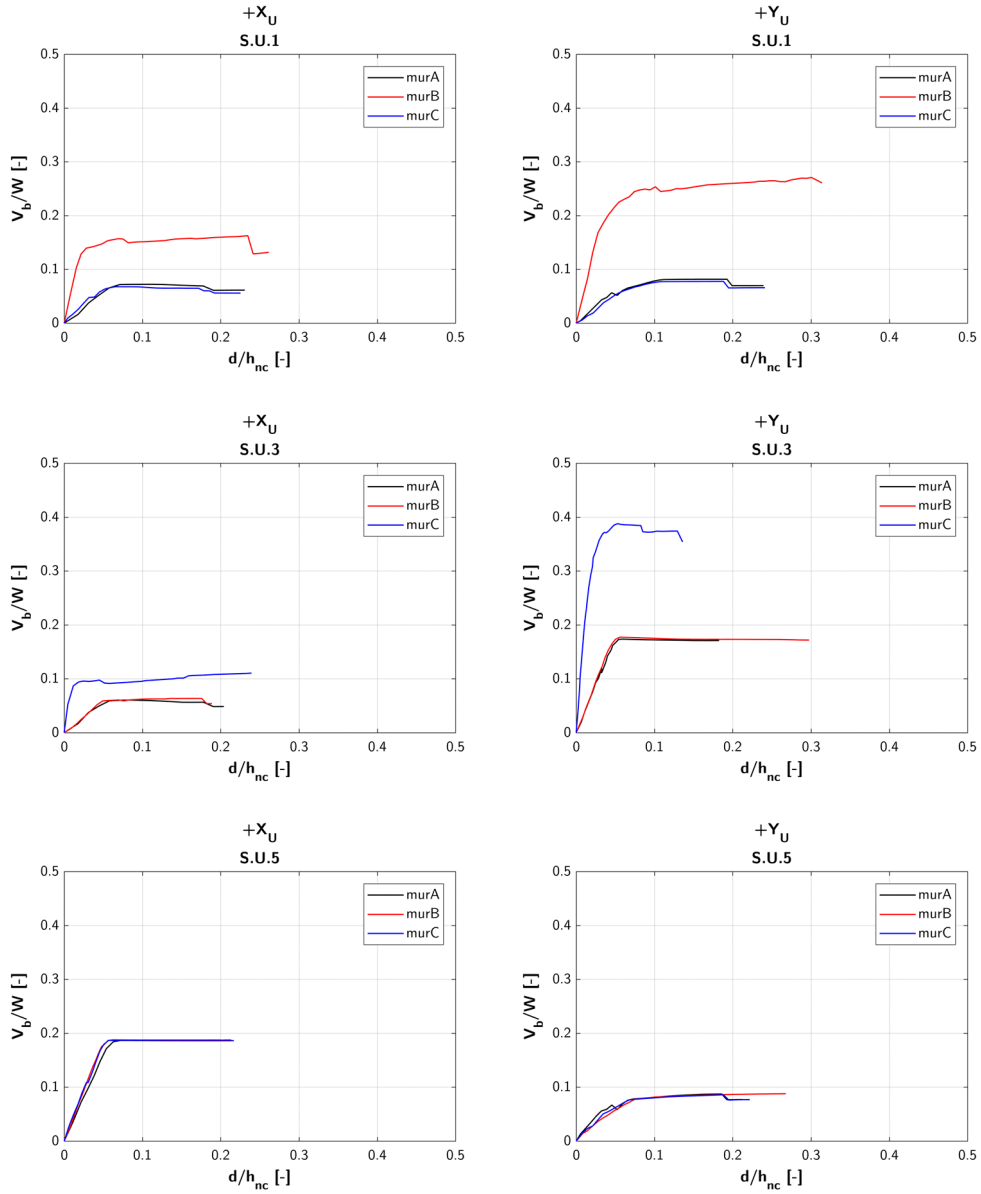

Figure 4-44: L aggregate – Pushover curves comparison at S.U.- level in function of material heterogeneities, for the corner S.U. (S.U.1) and the external ones (S.U.3 and S.U.5).

Referring to the L aggregate, in Figure 4-44 the pushover curves are compared for the corner S.U. (S.U.1) and the external ones (S.U.3 and S.U.5).

Similarly to the previous conclusions, the S.U.s show an increase in the capacity if composed of the most rigid masonry: that means for the corner S.U.1 in murB case and for the external S.U.3 in murC case. The capacity of the S.U.5, that is composed of stone masonry in all cases, is not influenced by the material variations in the adjacent S.U.s.

4.7.2.3 Base shear trend

The last comparison at the S.U.- level regards the trend of the maximum normalized base shear (V_{bu}) on each S.U., by considering the uniform pattern distribution (U) in both directions of analysis, in presence of rigid floors.

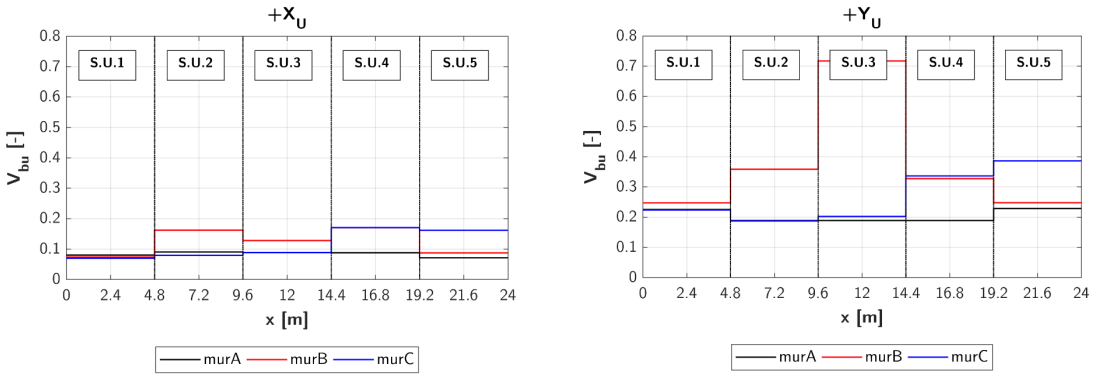

Figure 4-45: Row aggregate – Base shear trend on each S.U. in function of the masonry heterogeneities.

With reference to the row aggregate (Figure 4-45), in general, higher values are in correspondence to the S.U. composed of more rigid masonry. The difference is more accentuated in Y direction, especially for the murB case, for which the central S.U.3 reaches the highest values of V_{bu}. As previously noticed, the S.U.s not subject to the material variation are not influenced by the presence of material heterogeneities in the adjacent ones.

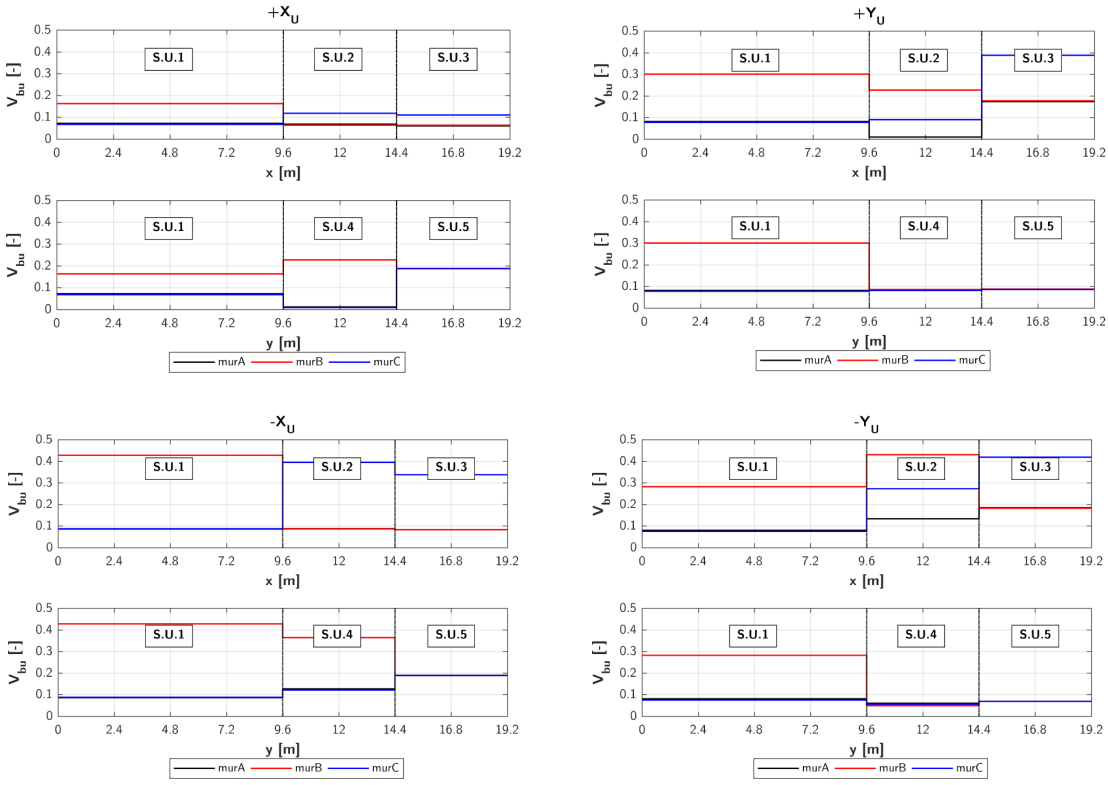

Figure 4-46: L aggregate – Base shear trend on each S.U. in function of the masonry heterogeneities.

For the L aggregate (Figure 4-46), the results are shown for both positive and negative directions of analysis. As previously highlighted, the highest values of V_{bu} are for the most rigid S.U.s
Considering the murB case, in which the corner S.U. is the most rigid, the major values of V_{bu} are for this one and the S.U. adjacent in the transversal direction in respect of the analysis direction, that means for S.U.4 in X direction and S.U.2 in Y direction. Referring to the negative direction, the trends are the same, but the differences are more evident. For the murC case, in which the external S.U.2 and S.U.3 are the

most rigid, it is noticeable that the increase of the V_{bu} is inferior to the previous case. The influence is visible for these S.U.s especially in the negative directions of analysis.

4.7.3 Wall- level

The distribution of the maximum base shear V_{bu} is evaluated at wall- level, by considering its percentage distribution among all walls, in presence of material heterogeneities. The walls are highlighted in Figure 4-35 for both row and L aggregate. Only the case of rigid floors is considered.

In the case of the row aggregate (Figure 4-47), in X direction the base shear V_{bu} decreases on the internal wall x2 for both murB and murC case, while it increases on the external walls x1 and x3. The changes are greater for the murC case. In Y direction, when the most rigid S.U.s are in internal position (murB), V_{bu} considerably increases on the central walls y3 and y4, while decreases on the other ones. The same happens for the murC case, when the external S.U.s on the right side are the most rigid: the base shear substantially increases in the wall between the most rigid S.U.s, but it decreases in the others.

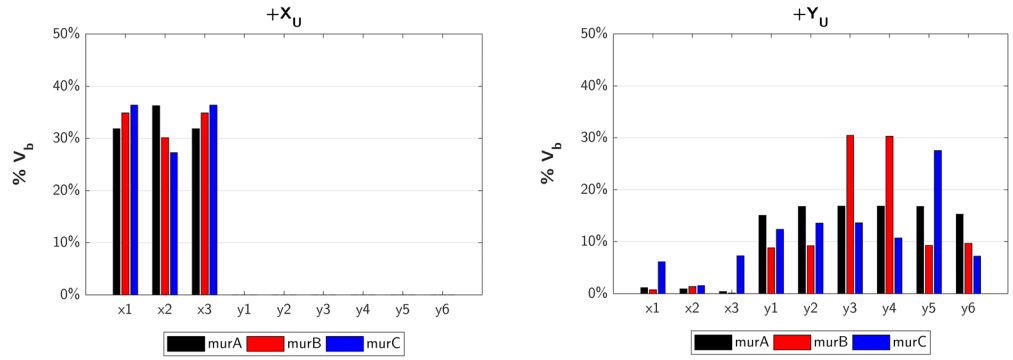

Figure 4-47: Row aggregate – Base shear percentage distribution among walls in presence of material heterogeneities.

In Figure 4-48 the percentage distributions are shown for the L aggregate. For the murB case, when the corner S.U. is the most rigid, in X direction the base shear V_{bu} slightly decreases in all longitudinal walls, with the exception of the façade x1 and of the transversal walls y1 and y2. The influence of the corner S.U. is more evident in Y direction, where the longitudinal walls y1 and y2 suffer a great increment of V_{bu}. Referring to murC case, when the external S.U.s 4 and 5 are the most rigid, in X direction there is an increment of V_{bu} on the longitudinal walls x1 and x3, while on x2 it decreases. In Y direction, V_{bu} grows on the wall y4, between the most rigid S.U., and on the transversal wall x2.

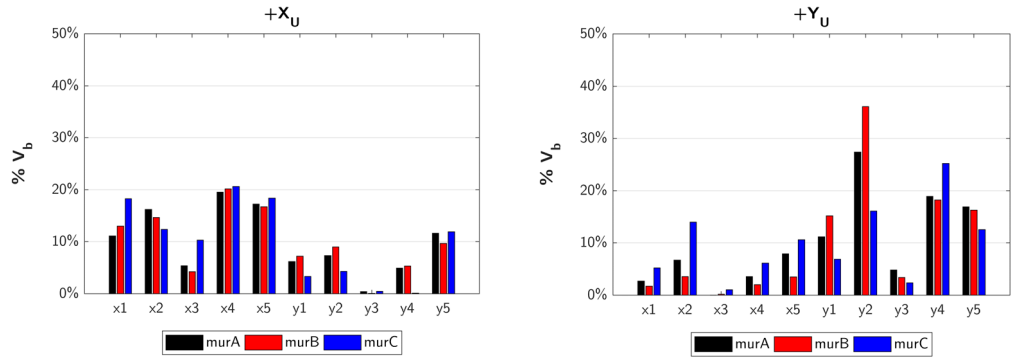

Figure 4-48: L aggregate – Base shear percentage distribution among walls in presence of material heterogeneities.

4.8 SENSITIVITY TO DIFFERENCES IN HEIGHT

In this paragraph, the sensitivity to the presence of differences in height is deepened by showing some comparisons for the considered models shown in Figure 4-10:

- **hA**: all the S.U.s have 2 storeys;
- **hB**: the internal/corner S.U.s have 3 storeys,
- **hC**: the external S.U.s has 3 storeys.

As for the previous case, the results are in terms of percentage changes and pushover curves, at both global- and S.U.- level, trend of the maximum normalized base shear on each S.U. and base shear distribution among the walls.

4.8.1 Global- level

4.8.1.1 Percentage changes

The sensitivity to the presence of differences in height at global- level is assessed for both aggregate typologies, by evaluating the percentage change, in terms of the maximum normalized base shear V_{bu} and the stiffness k^*, in reference to the hA case (i.e., absence of differences in height). The results are shown only for rigid (R) floors.

The presence of taller S.U.s generally produces a reduction of the capacity, especially in terms of stiffness.

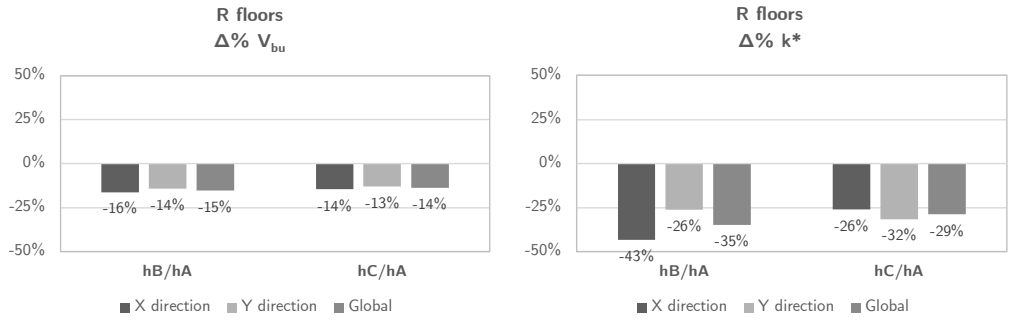

Figure 4-49: Row aggregate – sensitivity to differences in height at global- level, in terms of V_{bu} and k^*, in presence of rigid floors.

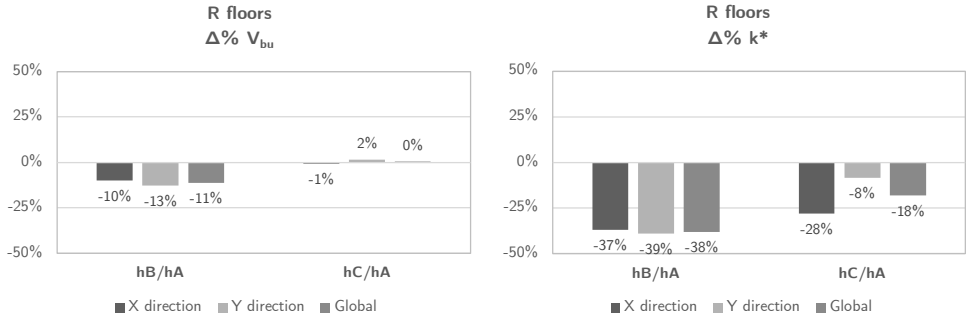

Figure 4-50: L aggregate – sensitivity to differences in height at global- level, in terms of V_{bu} and k^*, in presence of rigid floors.

With reference to the row aggregate (Figure 4-49), the reduction of the base shear is in the order of 15%, regardless the floors typology and the position of the highest S.U.s within the aggregate. Considering the stiffness, its reduction is slightly greater for the hB case, with values of around 40%.

The same trends can be observed for the L aggregate (Figure 4-50).

4.8.1.2 Pushover curves

The pushover curves of the row aggregate (Figure 4-51) and L aggregate (Figure 4-52) are compared in function of the presence of the differences in height, considering both directions of analysis and the uniform load pattern distribution (U). The graphs are shown for both rigid (R) and flexible (F) floors.

As previously observed, the presence of difference in height between the S.U.s is a significant factor for both row and L aggregate; moreover, the trend is the same for both floors typology.

With reference to the row aggregate (Figure 4-51), in both directions of analysis, the capacity decreases as the number of taller S.U.s increases. Therefore, the minor capacity is for the hB case.

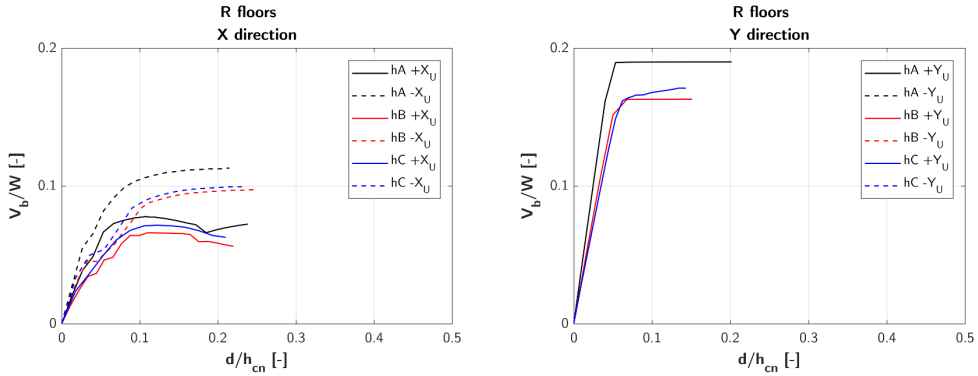

Figure 4-51: Row aggregate – Pushover curves comparison at global- level in presence of differences in height.

Looking at the pushover curves of the L aggregate (Figure 4-52), the cases hB and hC show a similar trend in X direction, with the minor capacity in terms of V_b/W and the stiffness k^*. In Y direction, instead, the trend of hC case is similar to that obtained for the hA case, characterized by capacity, in terms of base shear and stiffness, greater than that of the hB case.

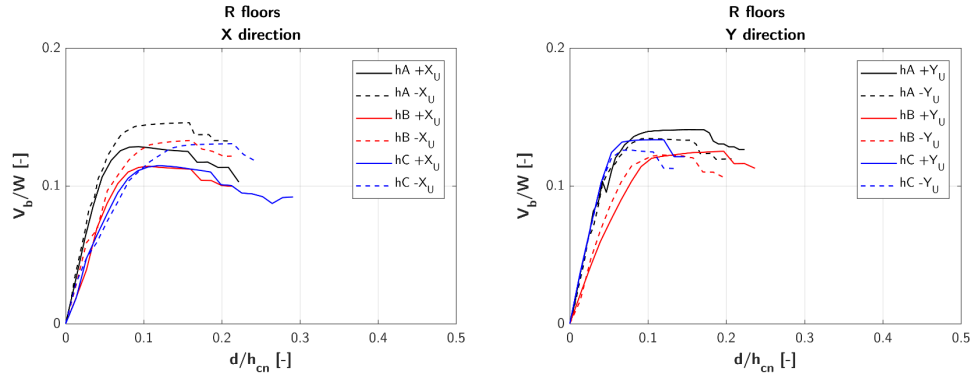

Figure 4-52: L aggregate – Pushover curves comparison at global- level in presence of differences in height.

4.8.2 S.U.- level

The influence of the differences in height is deepened by evaluating the response of different S.U.s, highlighted in Figure 4-22, in terms of percentage changes, pushover curves and base shear trend.

4.8.2.1 Percentage changes

The sensitivity to the differences in height at S.U.- level (Figure 4-53) is assessed as function of the S.U. position, by evaluating the percentage changes of the maximum normalized base shear V_{bu} and the stiffness k^* in reference to the hA case (absence of differences in height). The results are shown for rigid (R) floors.

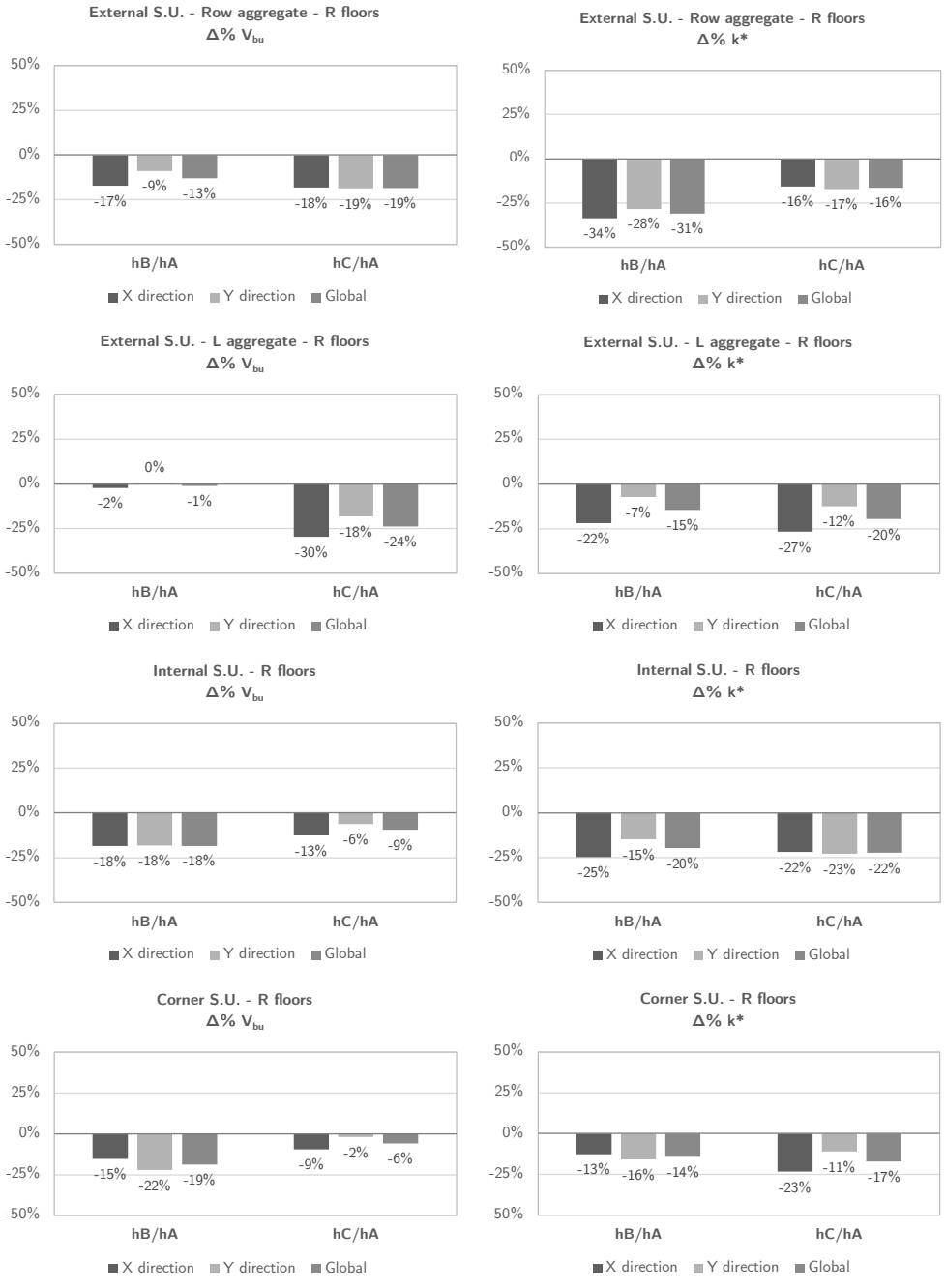

Figure 4-53: S.U.- level: sensitivity to differences in height, in terms of V_{bu} and k^*, for the corner (upper row), an internal (middle row) and an external S.U. (bottom row).

As previously observed, the presence of taller S.U.s generally determines a reduction of both base shear and stiffness at S.U.- level too. Considering the tallest S.U.s, the reduction is in the order of 20% for both quantities; the major deviations are for the external S.U. of the L aggregate in the hC case. The S.U.s

adjacent to a taller one also suffer a reduction of the capacity, especially in terms of stiffness; in this case, the greatest changes are for the external S.U. of the row aggregate in the hB case.

4.8.2.2 Pushover curves

In Figure 4-54, a pushover curves comparison is shown for the row aggregate, considering the external S.U.s (S.U.1 and S.U.5) and the central one (S.U.3). The results are shown for rigid floors and for the uniform load pattern distribution (U) in both positive directions of analysis.

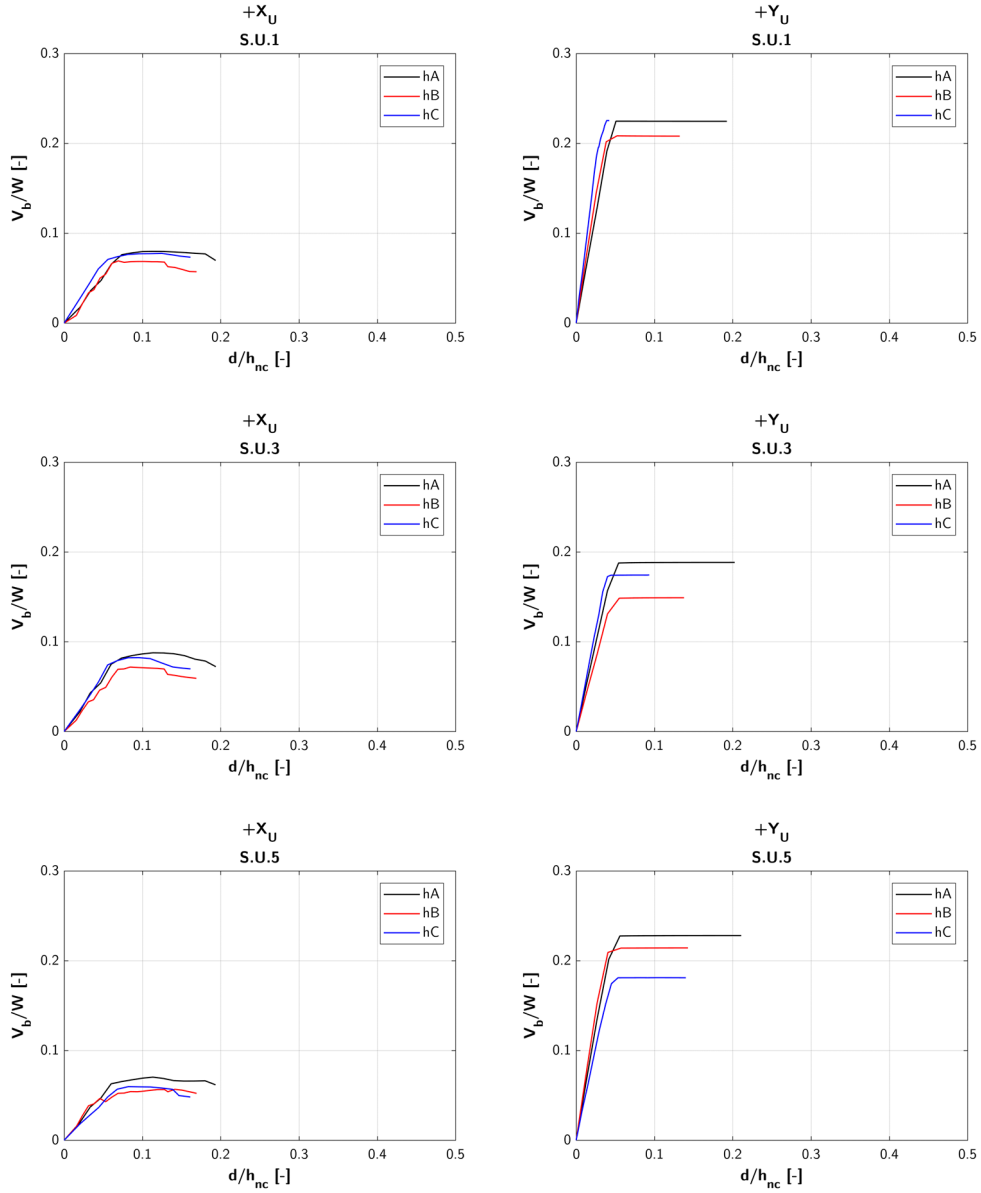

Figure 4-54: Row aggregate – Pushover curves comparison at S.U.- level in function of differences in height, for the external S.U.s (S.U.1 and S.U.5) and an internal one (S.U.3).

As previously highlighted, the presence of taller S.U.s leads in general to a reduction of the base shear capacity, regardless of the S.U. position and the case. If the analysed S.U. is one of the tallest, the reduction is more accentuated and also involve a relevant decrease of stiffness.

Referring to the L aggregate, in Figure 4-55 the pushover curves are compared for the corner S.U. (S.U.1) and the external ones (S.U.3 and S.U.5). The same previous considerations are valid for this aggregate typology.

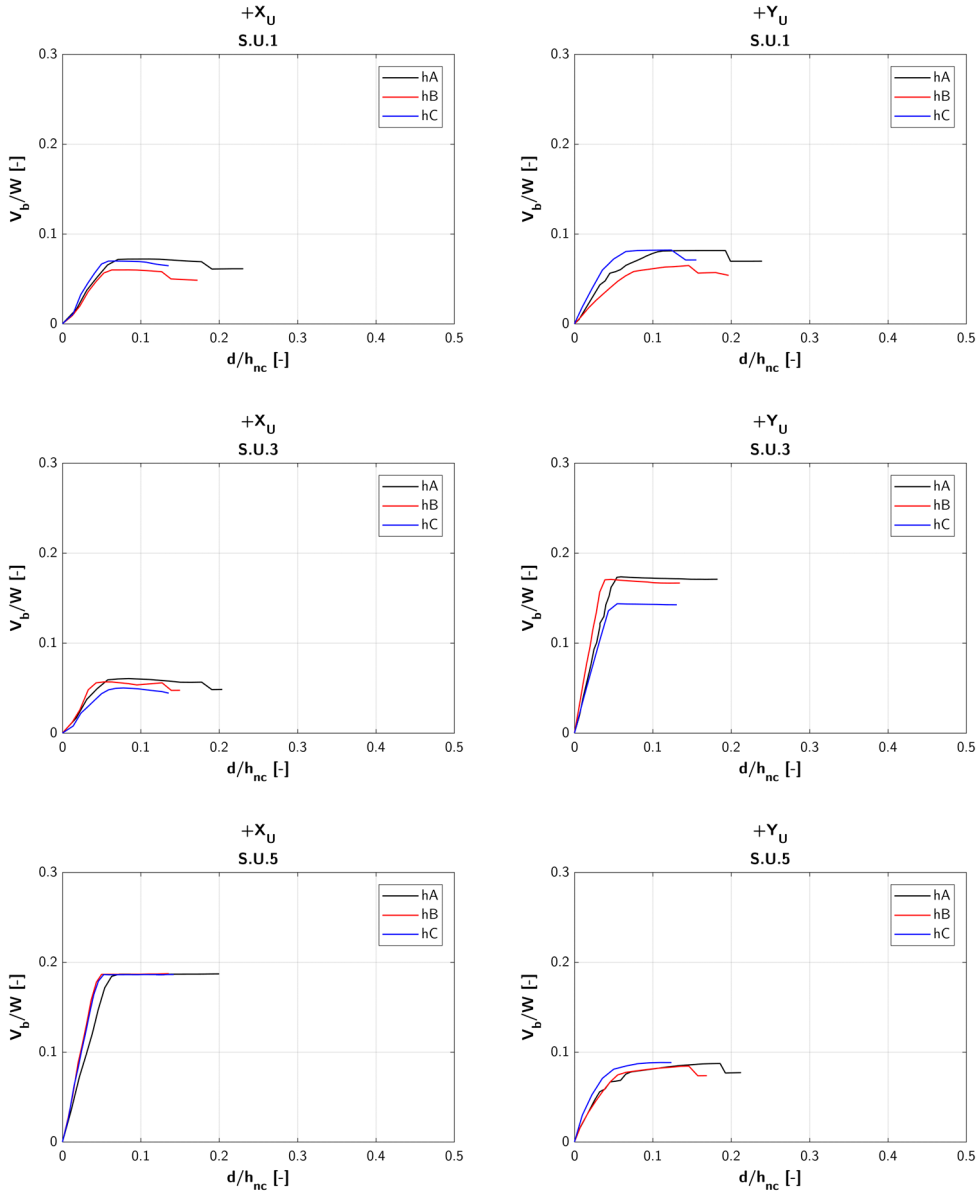

Figure 4-55: L aggregate – Pushover curves comparison at S.U.- level in function of differences in height, for the corner S.U. (S.U.1) and the external ones (S.U.3 and S.U.5).

4.8.2.3 Base shear trend

The last comparison at the S.U.- level refers to the distribution of the maximum normalized base shear (V_{bu}) on each S.U., by considering the uniform pattern distribution (U) in both directions of analysis.

With reference to the row aggregate (Figure 4-56), it can be noticed that the trends are in accordance with the previous conclusions: the presence of taller buildings leads to a reduction of the maximum value of the base shear. When they are placed in the central part of the aggregate (hB case, S.U.2, 3 and 4) there is a general reduction of V_{bu} on all the S.U.s, especially in Y direction. When the tallest S.U.s are in the external portion of the aggregate (hC case, S.U.4 and 5), the reduction influences not only these S.U.s, but also the internal one S.U.3, immediately adjacent to them.

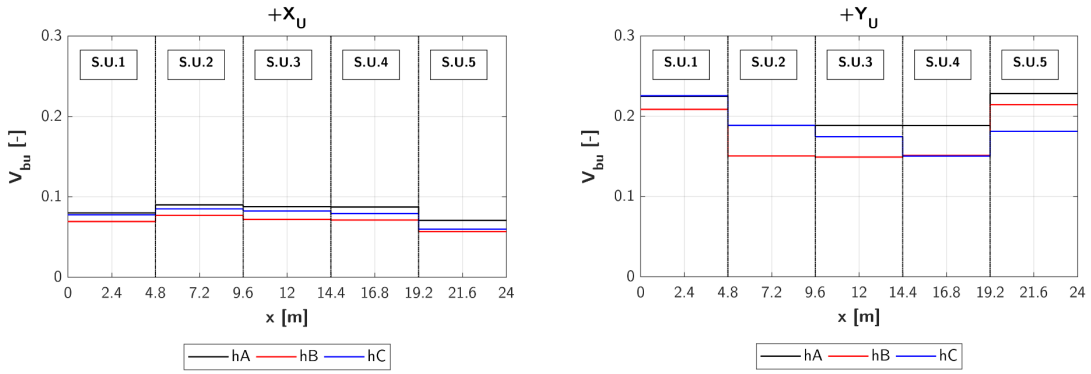

Figure 4-56: Row aggregate – Base shear trend on each S.U. in function of differences in height.

For the L aggregate (Figure 4-46), the results are shown for both positive and negative directions of analysis. With reference to the hB case, the presence of the corner S.U. taller than the others produces a small reduction of V_{bu}, especially in this S.U. The change is more visible in Y direction. The same trend can be observed for the hC case: the reduction affects the tallest S.U.2 and S.U.3, especially in Y direction. It is possible to conclude that the presence of differences in height mainly influences the seismic response of the row aggregates.

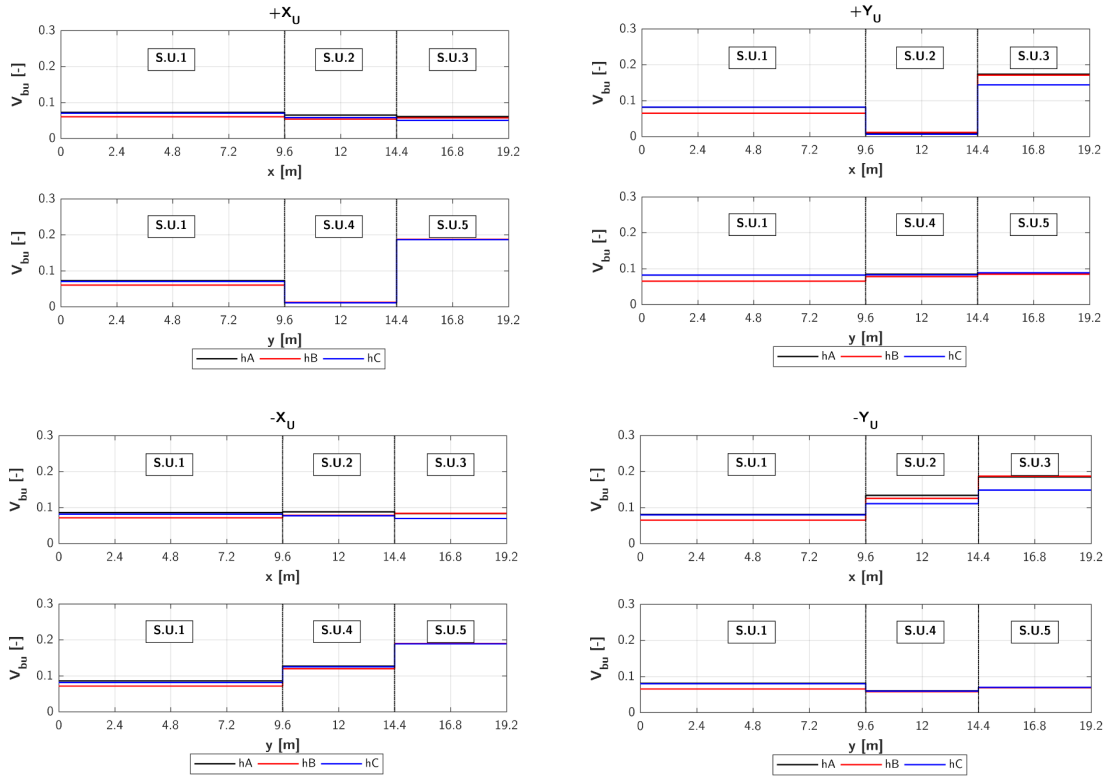

Figure 4-57: L aggregate – Base shear trend on each S.U. in function of differences in height.

4.8.3 Wall- level

The distribution of the maximum base shear V_{bu} is evaluated at wall- level, by considering its percentage distribution among all walls in both directions of analysis. The walls are highlighted in Figure 4-35 for both row and L aggregate. Only the case of rigid floors is considered.

Considering the row aggregate (Figure 4-58), in X direction the base shear V_{bu} grows on the central wall x2 for both hB and hC case, vice versa it decreases on the external walls x1 and x3.
In Y direction, when the tallest S.U.s are in internal position (hB), the base shear on the corresponding walls (from y2 to y5) does not change, but it decreases in the external walls (y1 and y6). For the hC case, when the external S.U.s on the right side are the tallest, the base shear slightly increases in the corresponding walls (from y4 to y6), but it decreases in the others, especially in the opposite wall y1.

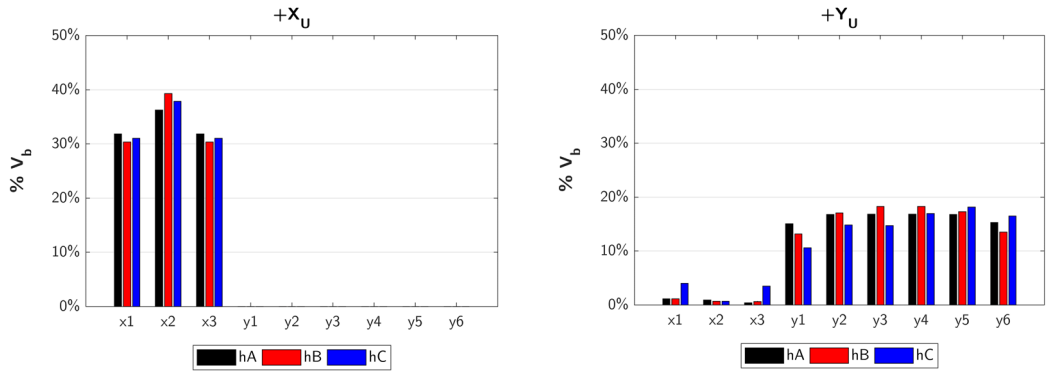

Figure 4-58: Row aggregate – Base shear percentage distribution among walls in presence of differences in height.

With reference to the L aggregate (Figure 4-59), in X direction the base shear V_{bu} increases in all the longitudinal walls (from x1 to x4) both hB and hC case, with the exception of the external wall x5. The same can be noticed in Y direction, in which all the longitudinal walls (from y1 to y4) are characterized by an increment, except for the external one y5.

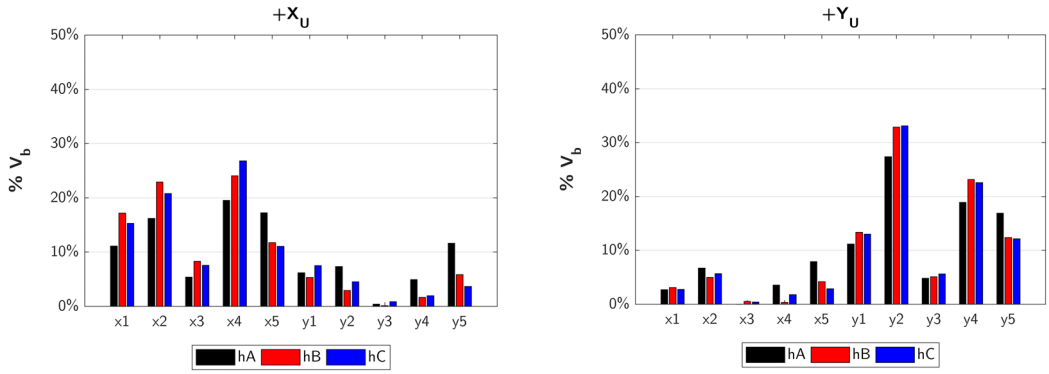

Figure 4-59: L aggregate – Base shear percentage distribution among walls in presence of differences in height.

4.9 CONCLUDING REMARKS

In this chapter, the results of a sensitivity analysis performed on prototype aggregates are shown and discussed, by considering different levels of detail: global-, S.U.- and wall- level. The investigated factors are:

- the aggregate typology,
- the number of S.U.s,
- the position of the S.U. in the aggregate,
- the floors typology,
- the presence of material heterogeneities,
- the presence of differences in height.

They are considered separately in order to evaluate their influence independently; moreover, the analysed combinations of models are those that maximize the effects.
The results are presented in terms of sensitivity indexes and percentage changes (both related to the maximum base shear, V_{bu}, and the stiffness, k^*), pushover curves at both global- and S.U.- level, base shear trend on each S.U. and base shear distribution among the walls.

Firstly, some aspects related to the general behaviour of the masonry aggregates are evaluated. Considering a row aggregate, the capacity in the transversal direction doubles that in the longitudinal one. In the longitudinal direction, the internal S.U.s have greater base shear and stiffness in comparison to the external ones, while the opposite happens in the transversal direction. At wall-level, the base shear is redistributed among the walls parallel to the analysis direction and the internal ones are the most stressed. Considering the L aggregate, the capacity is comparable in the two analysis directions. For both, the external S.U. placed in the transversal row has the highest base shear and stiffness, while the corner S.U. presents an intermediate capacity, similar to that of the S.U.s immediately adjacent in the longitudinal direction. The behaviour of the internal S.U. placed in the transversal row changes in function of the way of the analysis: in the positive direction, it presents the lowest capacity, while in the negative this is slightly inferior to the greatest value. At wall-level, the base shear is redistributed not only among the walls parallel to the direction of analysis but also on the orthogonal ones; the most stressed walls are the internal longitudinal ones.

Evaluating the general results of the sensitivity analysis (§4.4), the stiffness k^* results to be more sensitive than the maximum base shear, V_{bu}.
The most influential factor in the seismic behaviour of masonry aggregates at global- level (§4.4.1) is the number of S.U.s, especially for the row aggregate; it produces a general variation of around 70% in terms of V_{bu} and more than 100% in terms of k^*. On the contrary, the floors typology results to be the least relevant, with a global sensitivity in the order of 30% for V_{bu} and 40% for k^*. The material heterogeneities and the differences in height have a similar influence on the response, producing global variations of V_{bu} greater than 50% and of k^* in the order of 90%, and result to be more influential for the row aggregates.
The sensitivity analysis at S.U.- level (§4.4.2) is performed by considering 3 different conditions: external S.U., internal S.U. and corner S.U (Figure 4-20). The most sensitive position is the external one, while the corner is the least affected. At S.U.- level, the presence of material heterogeneities is the most influential factor, while the n° S.U.s does not significantly affect the response, since the influence of the other buildings on the target S.U. decreases with distance. Indeed, as shown in 4.5, the seismic capacity

of the S.U. is unvaried by considering an aggregate composed of 5, 7 or 9 S.U.s., regardless of its position and the typology of the aggregate. Consequently, with the aim to deepen the sensitivity to floors stiffness, material heterogeneities and differences in height, two main aggregate typologies are investigated: the row aggregate and the L aggregate composed of 5 S.U.s. (Figure 4-22).

Referring to the variation of the stiffness of the floors (§4.6), this factor is not significant at global-level, especially for the row aggregate. The presence of flexible floors generally produces a reduction of both maximum base shear and stiffness that is, however, inferior to 15%. The greatest changes at S.U.-level are for the external S.U.s in the L aggregate (around 20%).

In presence of material heterogeneities (§4.7), the more rigid S.U.s are present, the more the capacity at global- level increases; the changes are superior to 80% in terms of both stiffness and base shear. This increment is also evident at S.U.- level, especially for the most rigid S.U.s; on the contrary, the behaviour of those not subject to material changes is not influenced. At wall- level, the increment of the base shear is in correspondence of the walls between the most rigid S.U.s.

The seismic behaviour is significantly influenced by the differences in height too (§4.8), especially that of the row aggregate, particularly in the transversal direction. The presence of taller S.U.s generally produces a reduction of the capacity, especially in terms of stiffness (around 40%), because of the rapid damage of the walls. At S.U.- level, both the base shear and the stiffness decrease in correspondence of the tallest S.U.s of around 20%. When they are placed in the central part of the aggregate, the reduction is uniform on all the S.U.s.; when the tallest S.U.s are in the external position, the reduction also concerns the immediately adjacent buildings. At wall- level, the base shear increases in the tallest walls.

Chapter 5.

The proposed *"target structural unit approach"*

In this chapter, a new procedure, referred to as ***"target structural unit approach"****, allowing the definition of the* ***M.U.A.*** *for masonry buildings in aggregate is presented. It is applied on prototype aggregates, in order to provide general schemes in function of the analysed case.*

Contents

5.1 DEFINITION OF THE PROCEDURE

The procedure herein proposed is based on a multi-level analysis of the seismic response of the target structural unit to define its M.U.A. Two are the main features of this approach: the definition of several boundary conditions for the target S.U., that consists in defining different modelling configurations, and the execution of the seismic assessment at 3 different levels of detail:

- **Global- level**: analysis of the global response of each modelling configuration of the aggregate;
- **S.U.- level**: analysis of the response of the target S.U. in each modelling configuration;
- **Wall- level**: analysis of the response of the boundary walls of the target S.U. in each modelling configuration.

The need to consider simultaneously different levels of analysis depends on the fact that the "aggregate effect" is not adequately captured by only evaluating the global response of different modelling configurations. Moreover, the *S.U.– level* is introduced as a fundamental verification level to understand the variability of the seismic response of the case study building in function of different boundary conditions and to identify the MUA. For this reason, the procedure is referred to as *"**target structural unit approach**"*. The procedure, schematized in Figure 5-1, is divided into several phases, which are explained in detail in the next paragraphs. The assumptions of this work are illustrated in §3.3.

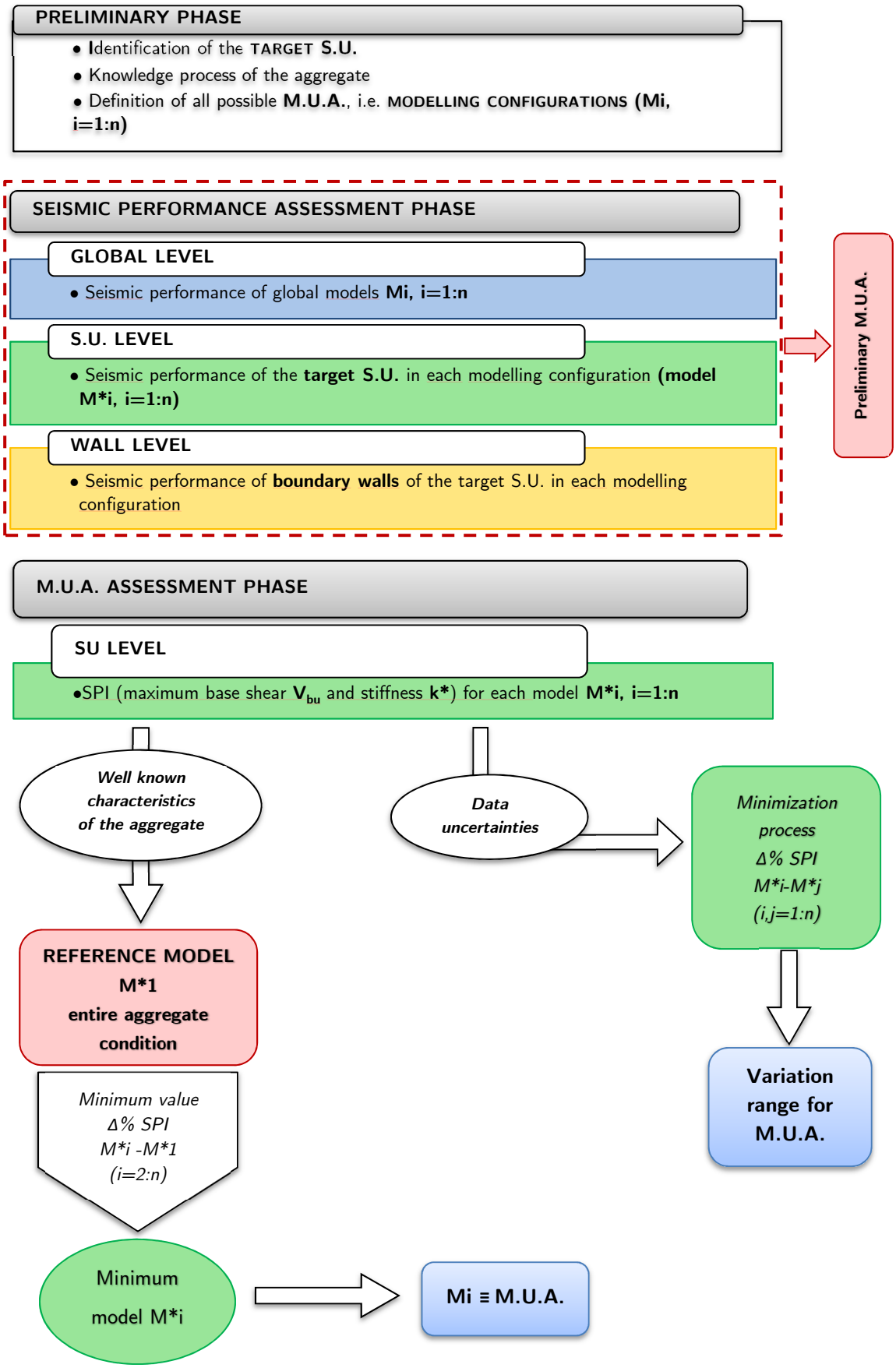

Figure 5-1: Scheme of the proposed "target structural unit approach".

5.1.1 Preliminary phase

In this phase, the first step consists in defining the target S.U. (i.e., **Minimum Intervention Unit, M.I.U.)**, whose seismic performance needs to be assessed.

Then, the investigation of the aggregate is performed, including the analysis of the masonry types and quality, the analysis of building typologies and constructions details, and the analysis of the cracking pattern, where possible. We remember that the preliminary "critical reading" of the constructive techniques and of the diachronic construction process of the aggregate is a fundamental step of the knowledge process (Carocci, 2001), that allows, inter alia, to identify the complete aggregate condition and all the S.U.s.

Finally, all the possible **Minimum Units of Analysis (M.U.A.)** should be settled, on the basis of the morphological characteristics of the aggregate and of the position of the target S.U., identifying several modelling configurations $\boldsymbol{M_i}$ (i=1:n), with the aim to evaluate the variability of the seismic behaviour at the varying of the boundary conditions. It should be noticed that the isolated condition is not considered since, as expected and as also shown in the following results, it represents an excessive simplification, that neglects the effects of interactions.

5.1.2 Seismic performance assessment phase

In this phase, the seismic performance of each modelling configuration M_i is assessed by performing nonlinear static analyses, not only at global- but also at both S.U.- and wall- levels, as illustrated in §3.3.1. This approach allows understanding how the seismic capacity of the target S.U. and of its load-bearing walls changes in function of the surrounding.

To this end, the capacity curves are reproduced for the target S.U. (models $\boldsymbol{M^*_i}$, where the apex * indicates that the target S.U. is evaluated, while the subscript i refers to the considered model configuration) and for its boundary walls, by considering displacements and base shear forces of the related points, extracted by the results of the analyses performed on the global models M_i.

As introduced in §3.3.2, to allow a more reliable comparison of the results, the same control node is selected for all the models and analyses, chosen in a barycentric position of the target S.U., and the pushover curves are normalised. In particular, the displacements at the control node (d_{cn}) are normalized by its height (h_{cn}), while the total base shear strength (V_b) is divided by the weight of the considered structure (W_{Mi} of global model M_i, W_{M^*i} of target S.U. M^*_i or W_w of the boundary wall), producing the normalized base shear V_b/W. Its calculation for all the analysis levels is shown in Table 5-1.

Table 5-1: Evaluation of the normalized base shear.

Base shear coefficient		
Global level	$V_{b,Mi}/W_{Mi}$	
Target S.U. level	$V_{b,M^*i}/W_{M^*i}$	
Wall level	$V_{b,w}/W_{Mi}$	for comparison among pushover curves at global- and wall- level
	$V_{b,w}/W_w$	for comparison among pushover curves at wall- level

The seismic performance of each configuration is then evaluated in terms of normalized maximum base shear V_{bu} and stiffness k^* for each level of analysis. Indeed, as previously stated in paragraph 3.3, the

"aggregate effect" on the target S.U. is evaluated in terms of seismic capacity; moreover, these parameters can be evaluated directly from the pushover curve. However, at global- and S.U.- level the assessment can be also performed in terms of safety, by means of code-oriented seismic performance-based assessment.

This phase would allow the identification of a preliminary M.U.A., based on the structural features and vulnerabilities of the S.U.s adjacent to the target one.

5.1.3 M.U.A. assessment phase

The M.U.A. is identified by comparing the seismic performance at S.U.- level of the configurations M^*_i. This procedure assumes that the reference configuration for the target S.U., namely the one that best represents its seismic performance, coincides with the complete aggregate condition (i.e., model M^*_1). As introduced in paragraph 3.3, this assumption is true when the investigated aggregate is well-known.
Then, the M.U.A. will correspond to the global configuration M_i, for which the model M^*_i results to have the closest seismic response to that of the reference configuration M^*_1. This means looking for the minimum value of the percentage changes of the SPI (maximum base shear V_{bu} and stiffness k^*) of models M^*_i in reference to M^*_1, calculated as in Eq. 51:

$$\Delta\% SPI = \frac{SPI_{M^*_i}}{SPI_{M^*_1}} - 1 \quad i=2:n \tag{51}$$

Of course, the identification of the M.U.A. must consider both the results of the minimization process and the preliminary conclusions of the previous phase.

5.1.3.1 Data uncertainties

As previously stated, the complete aggregate condition is defined on the basis of the knowledge process. Naturally, the knowledge can decrease as the number of S.U.s increases; indeed, often some parts of the aggregate may be inaccessible, or the collected information may be insufficient to define a reliable model. Consequently, when the complete aggregate condition is affected by uncertainties, the reference configuration for the target S.U. can be undefined.
In this case, the minimization process (Eq. 52) of the SPI performed for all models M^*_i, changing in rotation the reference configuration M^*_j, allows identifying the variation range of the M.U.A., excluding the extreme conditions.

$$\Delta\% SPI = \frac{SPI_{M^*_i}}{SPI_{M^*_j}} - 1 \qquad i,j=1:n \tag{52}$$

In the following, some examples of the application of the procedure on prototype aggregates are shown. Both the row and L aggregates previously described in section 4.2 are considered.

5.2 Application on the prototype aggregates

In accordance with the conclusions of the previous chapter, the procedure is applied to the prototype row and L aggregates composed of 5 S.U.s, shown in Figure 5-2, by considering all the cases previously introduced and resumed in Table 5-2, in function of the floors typology (Figure 4-7), the material heterogeneities (Figure 4-8) and the differences in height (Figure 4-10).

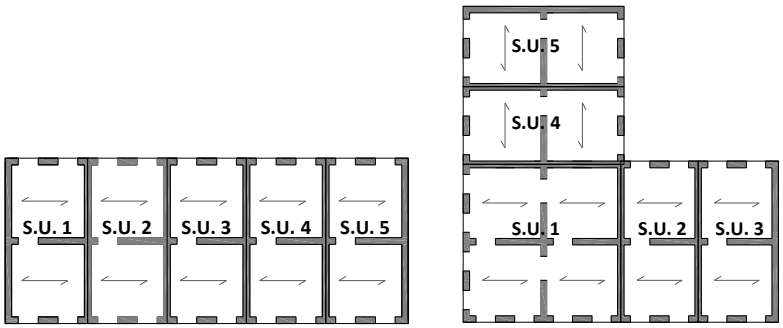

Figure 5-2: Plan view of the row (left) and of the L aggregate (right) case studies.

Table 5-2: Resume of the analysed cases.

Analysed cases		
Floors typology	R	Rigid floors
	F	Flexible floors
	RFF / RRFFF	
	FFRFF	
	FRR / FRRRF	
Material heterogeneities	murA	all the S.U.s are in stone masonry
	murB	the internal/corner S.U.s are in hollow brick masonry
	murC	the external S.U.s are in hollow brick masonry
Differences in height	hA	all the S.U.s have 2 storeys
	hB	the internal/corner S.U.s have 3 storeys
	hC	the external S.U.s has 3 storeys

For each aggregate typology, 2 different target S.U.s are analysed: the external and the internal (for the row aggregate) or the corner S.U. (for the L aggregate).
The considered modelling configurations for each case study are described in the next paragraph.

5.2.1 Modelling configurations

The analysed modelling configurations, presented in the next paragraphs, are fixed for each type of S.U.; for each case, the target S.U. is highlighted in red.

5.2.1.1 Row aggregate

In the case of the row aggregate, the investigated S.U.s are 1 internal (the central one) and 1 external (on the right side).
The analysis of the internal S.U. is performed by defining 8 modelling configurations, presented in Figure 5-3:

- A: complete aggregate condition;
- A1: 3 S.U. X-row configuration, in which the target S.U. is central;
- A2: 3 S.U. X-row configuration, in which the target S.U. is the external one on the left side;
- A3: 3 S.U. X-row configuration, in which the target S.U. is the external one on the right side;
- A4: 2 S.U. X-row configuration, with the adjacent building on the right side,
- A5: 2 S.U. X-row configuration, with the adjacent building on the left side;
- A6: 4 S.U. X-row configuration, with 1 adjacent building on the left side,
- A7: 4 S.U. X-row configuration, with 1 adjacent building on the right side.

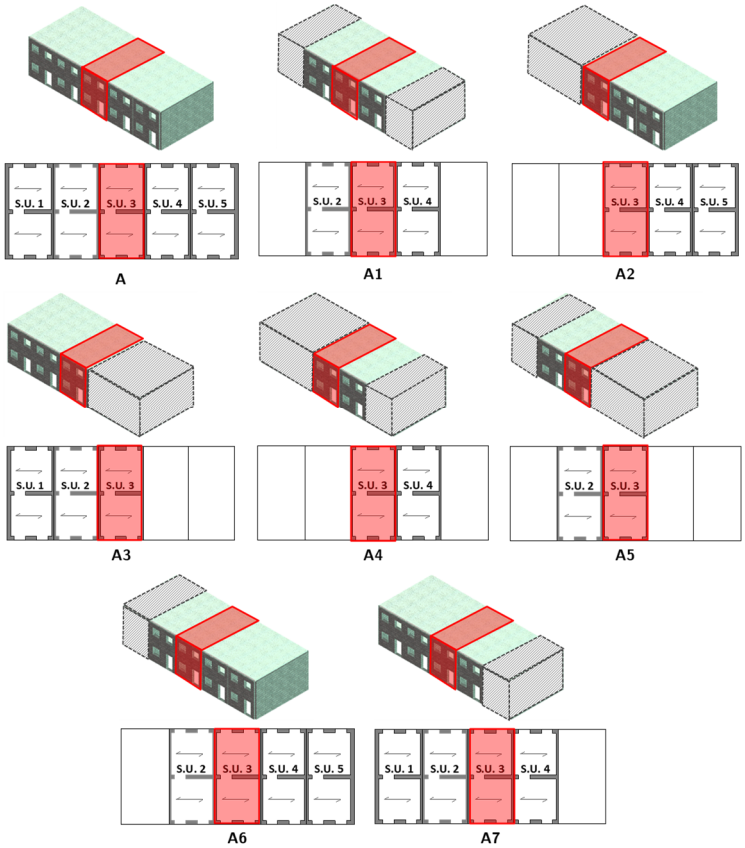

Figure 5-3: Modelling configurations Mi: row aggregate – internal S.U.

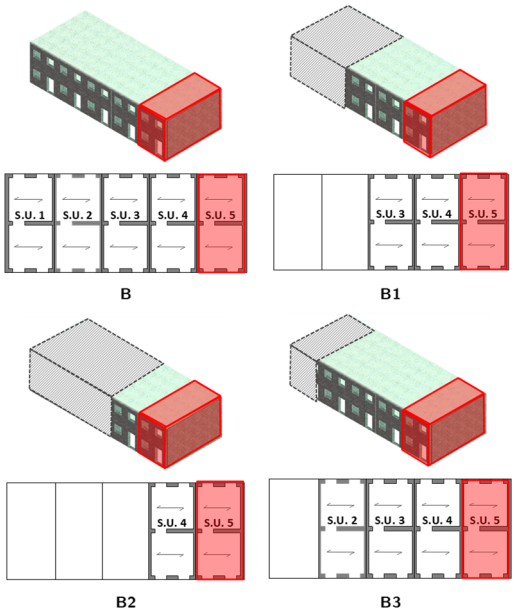

Figure 5-4: Modelling configurations Mi: row aggregate – external S.U.

For the analysis of the external S.U., 4 modelling configurations are considered (Figure 5-4):

- B: complete aggregate condition;
- B1: 3 S.U. X-row configuration;
- B2: 2 S.U. X-row configuration;

- B3: 4 S.U. X-row configuration.

5.2.1.2 L aggregate

In the case of the L aggregate, the target S.U.s are the corner one and the external on the left side. With reference to the corner S.U., the following 8 modelling configurations are defined (Figure 5-5):

- L: complete aggregate condition,
- L1: intermediate configuration, with the immediately adjacent S.U.s,
- L2: 3 S.U. X-row configuration;
- L3: 3 S.U. Y-row configuration;
- L4: 2 S.U. intermediate X-row configuration, with 1 adjacent building in X direction;
- L5: 2 S.U. intermediate Y-row configuration, with 1 adjacent building in Y direction;
- L6: 3 S.U. X-row configuration with 1 adjacent building in Y direction;
- L7: 3 S.U. Y-row configuration with 1 adjacent building in X direction.

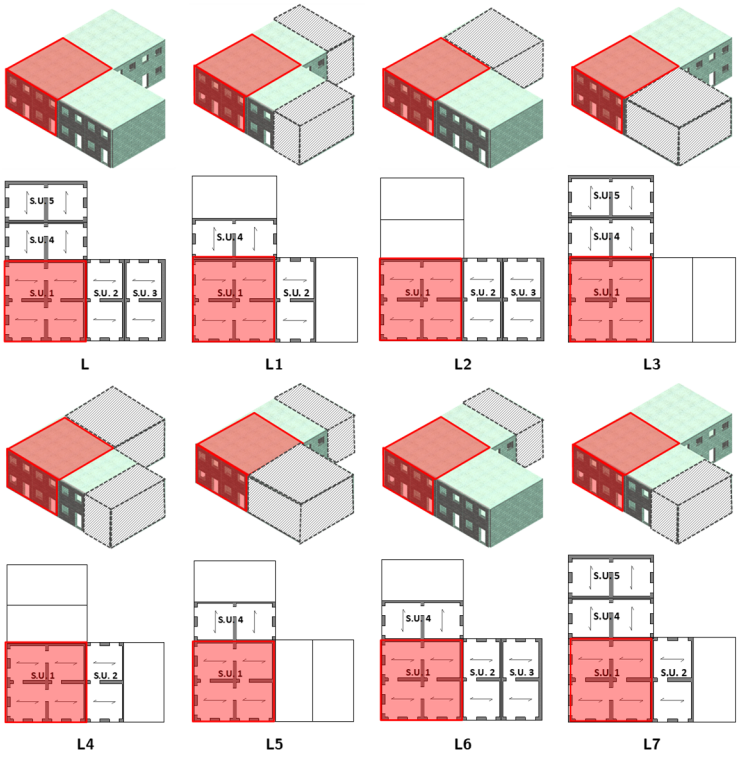

Figure 5-5: Modelling configurations Mi: L aggregate – corner S.U.

Considering the external S.U., 4 modelling configurations are generated (Figure 5-6):

- M: complete aggregate condition;
- M1: 3 S.U. X-row configuration;
- M2: 2 S.U. intermediate X-row configuration, with 1 adjacent building in X direction;
- M3: 3 S.U. X-row configuration with 1 adjacent building in Y direction.

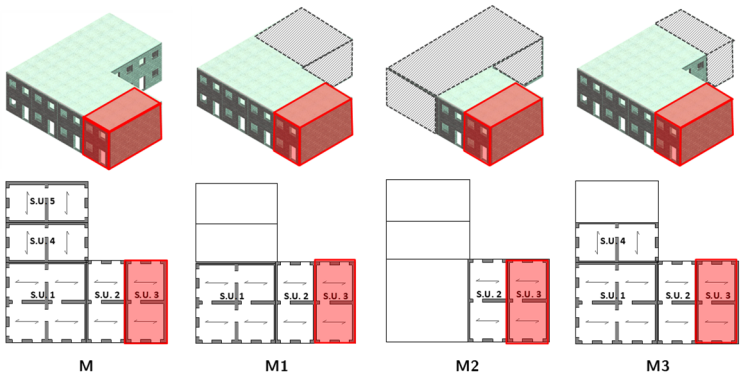

Figure 5-6: Modelling configurations Mi: L aggregate – external S.U.

5.2.2 Example of application of the procedure

The results obtained from the application of the procedure to the internal S.U. (highlighted in red in Figure 5-7) of the row aggregate with rigid (R) floors are illustrated below.

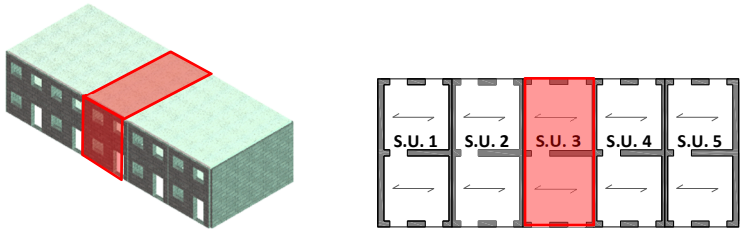

Figure 5-7: Internal S.U. of the row aggregate – R floors.

As previously introduced, 8 modelling configurations M_i are defined for this case (from configuration A to A7, as shown in Figure 5-3). For each model, the seismic assessment is performed at global-, S.U.- and wall- level, considering the same control node, highlighted in Figure 5-8, where the analysed walls are also shown. According to Figure 5-8, wall 1 (W1) and wall 3 (W3) correspond to the façades of the target S.U. in the X direction; wall 2 (W2) and wall 4 (W4) correspond to the mid-walls along the Y direction.

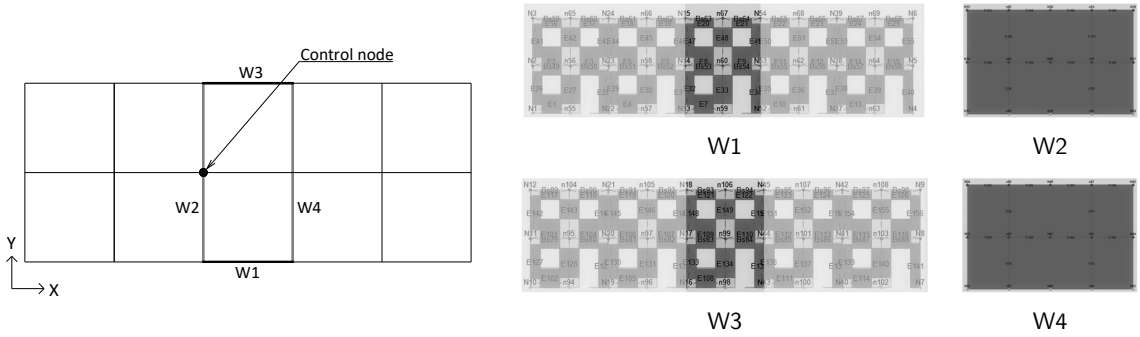

Figure 5-8: Internal S.U. of the row aggregate: location of the evaluated walls and the selected control node.

5.2.2.1 Seismic performance assessment

In this phase, the seismic performance of each modelling configuration M_i is assessed by performing nonlinear static analyses, by considering global-, S.U.- and wall- levels.

Global- level

In Figure 5-9, the global pushover curves are compared for all modelling configurations by direction, considering the uniform load pattern distribution (U). Firstly, the base shear capacity in Y direction is double than in X direction, since the walls in Y direction have no openings. Then, it should be noticed that in Y direction the pushovers are the same regardless the way, while in X direction the seismic capacity is slightly greater for the negative direction; this depends on the distribution of openings on the X-walls.

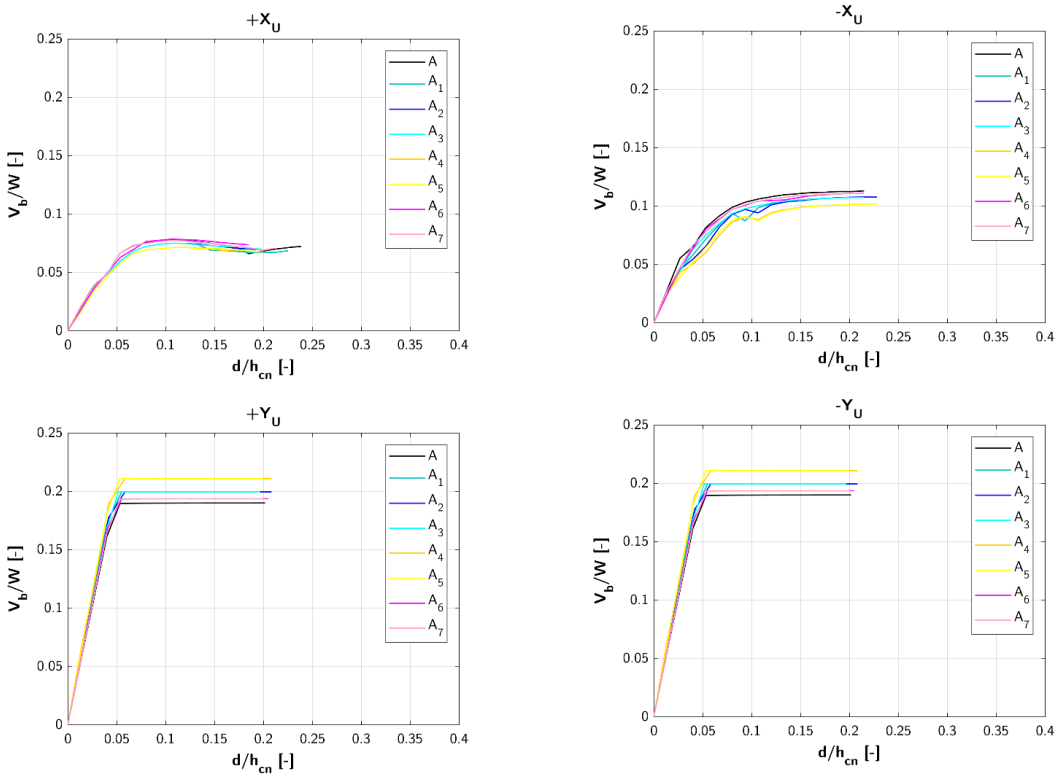

Figure 5-9: Internal S.U. of the row aggregate – R floors: pushover curves at global- level.

Wall- level

As previously mentioned, in order to investigate the actual influence of the different modelling configurations on the seismic response of target S.U., the variability on capacity is also compared at the wall- level, namely for the façades and mid-walls identified in Figure 5-8. Hence, Figure 5-10 presents the pushover curves of walls W1 and W3, and W2 and W4, obtained for the uniform load pattern distribution in both positive and negative directions of analysis.

The difference in terms of capacity between façades and mid-walls is quite significant; indeed, the base shear capacity of the mid-walls in Y direction is triple than that of the façades in X direction. These results depend on the fact that the mid-walls are blind (with no openings) and they carry the loads from the floors. The variability of the pushover curves in function of the modelling configuration is lower in X direction, where there is no difference of capacity between the walls W1 and W3. In this direction, their contribution is way more relevant in the case of modelling configurations A6, A7 and A, while they have an intermediate behaviour in configuration A1.

In Y direction it is possible to note a difference of capacity between W2 and W4 in models A2 and A4 (where the target S.U. is external on the left side), and A3 and A5 (where the target S.U. is external on

the right side), depending on the different carried loads by the walls. Moreover, if A2 and A4 are the configurations to which an inferior base shear capacity corresponds, A3 and A5 show the highest values. This result depends on the influence of the distribution of the openings on the modal behaviour, as shown in the following Figure 5-16. Finally, the contribution of W2 and W4 is intermediate and equal for the other configurations.

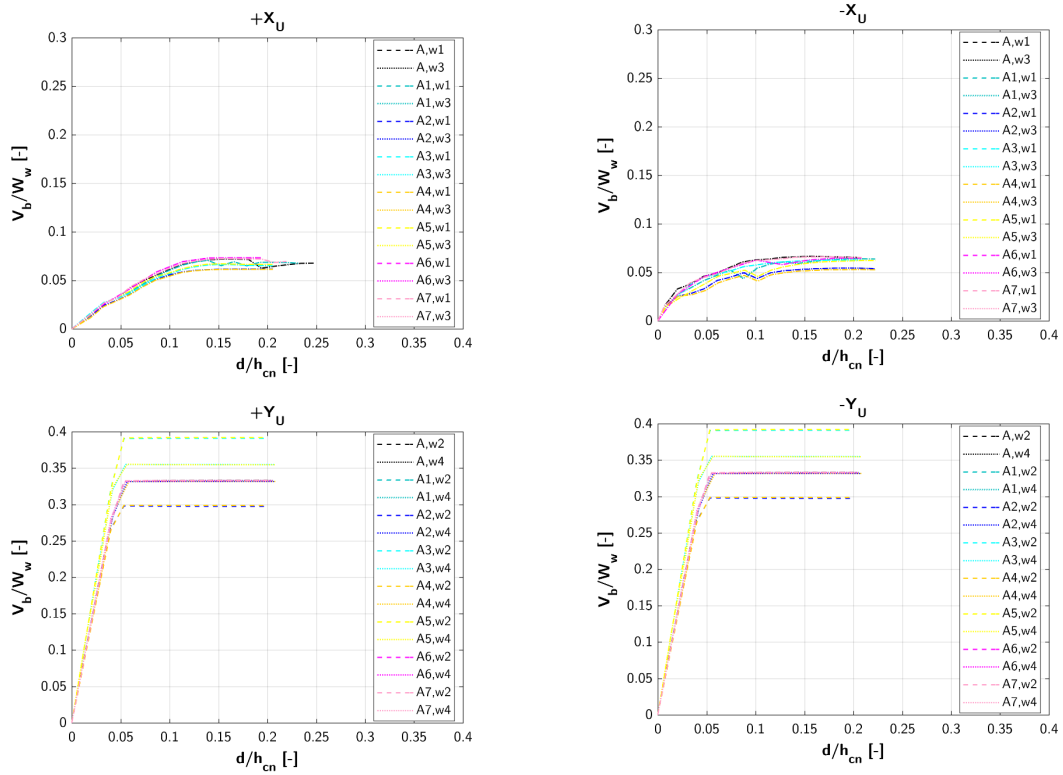

Figure 5-10: Internal S.U. of the row aggregate – R floors: pushover curves at wall- level.

S.U.- level

In the following Figure 5-11, the pushover curves obtained for the target S.U. are compared for each different modelling configuration.

As previously noticed at both global- and wall- level, the seismic capacity in Y direction doubles that in X direction; moreover, in Y direction the difference between the configurations is more evident. However, the trend is the same for both directions: the pushover curve of the reference model A* (from the complete aggregate condition) coincides with that of models A*1, A*6 and A*7, in which the target S.U. has an internal position; in these configurations, the base shear capacity has the lowest value. On the contrary, the highest capacity is reached in configurations A*2 and A*4; A*3 and A*5 are in intermediate position.

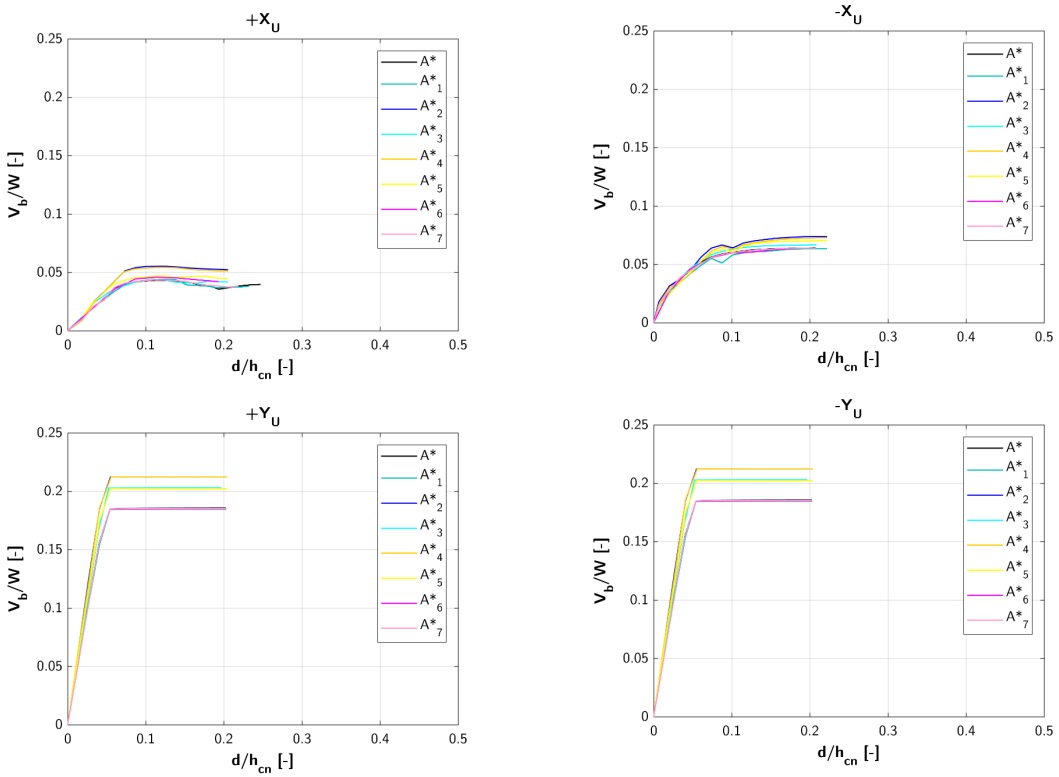

Figure 5-11: Internal S.U. of the row aggregate – R floors: pushover curves at S.U.- level.

5.2.2.2 M.U.A. assessment phase

In order to identify the M.U.A., the percentage changes of the ultimate base shear coefficient V_{bu} and of the stiffness k^* of each configuration (from A*1 to A*7) are compared with those of the reference configuration A*, as expressed in Eq. 51. As shown in Figure 5-12, the mean values and respective standard deviations for direction of analysis are considered. For both the SPI, the minimum changes are observed for configurations A*1 and A*7, in both directions of analysis. As confirmed from the trend of the pushover curves in Figure 5-11, the changes between these configurations are minimum; in particular, in Y direction, they result to be equivalent.

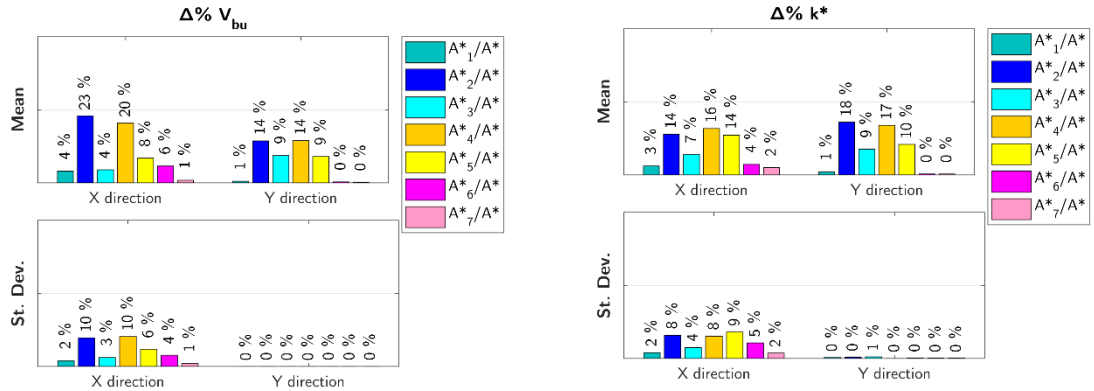

Figure 5-12: Internal S.U. of the row aggregate – R floors: mean value (upper row) and standard deviation (bottom row) of the percentage change of V_{bu} (left) and k (right) for A^*_i/A^* in both analysis directions.*

Considering these results and the structural characteristics of the case study, that is basically symmetric, configuration A1 (in which the target S.U. is modelled with the adjacent buildings, as shown in Figure 5-13) results to be the best M.U.A.

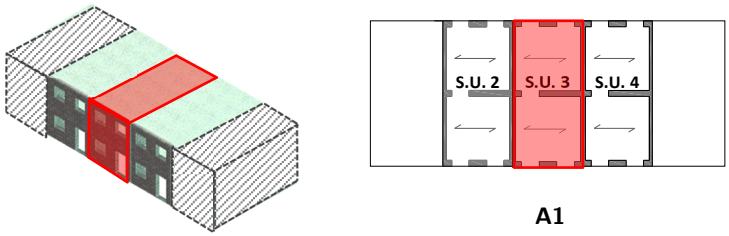

Figure 5-13: M.U.A. for the internal S.U. of the row aggregate – R floors.

5.2.2.3 Comparison with the isolated conditions

With the aim to quantify the error that an excessive simplification can produce, the results obtained from the individuated M.U.A. (Figure 5-13) are compared with:

- the isolated S.U.,
- the isolated S.U. with the pertinent masses deriving from the immediately adjacent structure (hereinafter referred as "isolated + q/2"), simplification suggested by NTC 2008; in detail, the masses are modelled as linear loads on the common walls.

The results obtained for the 3 conditions are compared in Figure 5-14, in terms of α_{PGA}, maximum base shear V_{bu} and stiffness k^*.

It is possible to notice that, while in X direction the seismic behaviour benefits from the aggregation, the results are reversed in Y direction, in which the capacity of M.U.A. is visibly inferior to that of the isolated conditions.

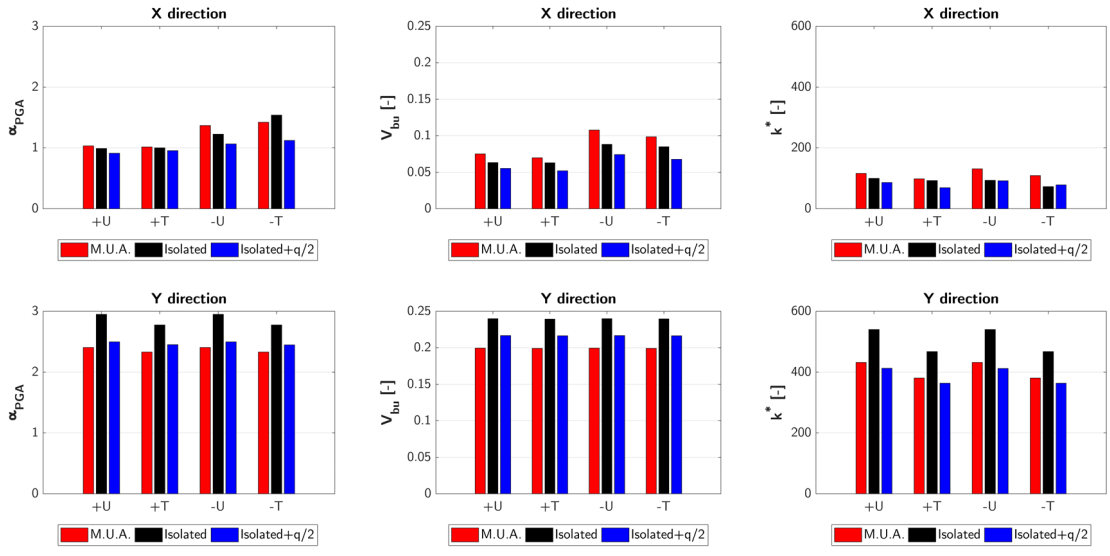

Figure 5-14: Row aggregate – internal S.U. – R floors: comparison between the M.U.A. and the isolated conditions.

In the following, only the analyses of each direction with the lowest value of α_{PGA} for M.U.A. are considered, that means +X and +Y triangular distribution.

In Figure 5-15, the pushover curves are compared; moreover, Table 5-3 shows the percentage changes, obtained in reference to the M.U.A., for the isolated conditions.

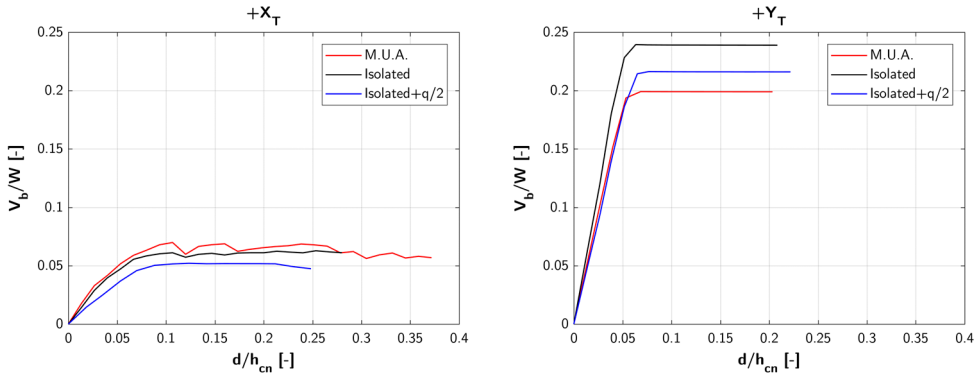

Figure 5-15: Row aggregate – internal S.U. – R floors: pushover curves comparison between the M.U.A. and the isolated conditions.

Table 5-3: Row aggregate – internal S.U. – R floors: percentage changes of α_{PGA}, k^* and V_{bu} for the isolated conditions in reference to M.U.A.

		Δ% α_{PGA}	Δ% k*	Δ% V_{bu}
X direction	**Isolated**	-1%	-6%	-10%
	Isolated + q/2	-6%	-30%	-25%
Y direction	**Isolated**	19%	23%	20%
	Isolated + q/2	5%	-4%	9%

As previously observed, the isolated conditions present a reduction of the capacity in X direction and an increment in Y direction. In detail, the α_{PGA} is reduced in X direction of 1% for the isolated S.U. and of 6% for the isolated S.U. + q/2; on the contrary, it is increased of 19% for the first condition and of 5% for the second. Resuming, the isolated conditions result to be in favour of safety in the longitudinal direction, but not in the transversal one.

§

The resulting M.U.A. for the case studies illustrated in Table 5-2 are resumed in the following paragraphs. Considering the large number of models and the amount of results to be shown, a table containing the scheme of the M.U.A. and the percentage changes of the maximum base shear V_{bu} and stiffness k^* (only with reference to the rigid floors) is presented for each case. Of course, the identification of M.U.A. has followed the procedure previously illustrated.
The complete results are shown in Annex A.

5.2.3 M.U.A. in presence of different floors typology

In this paragraph, the results obtained from the procedure for the row and L aggregate are shown at the varying of the stiffness of the floors.
The M.U.A. identified for all cases are resumed in the following tables.

5.2.3.1 Row aggregate

The presence of different floors typology influences the response of the row aggregate, especially in Y direction.

In Figure 5-16, a comparison of the first 3 modal shapes for all cases is shown. As we can observe, the 1st modal shape is translational in X direction regardless of the floors typology. On the contrary, the translational modal shape in Y direction changes in function of the floors stiffness: for example, in presence of R floors, it is purely translational and all the S.U.s react together, while, in presence of F floors, the internal S.U.s suffer greater displacements.

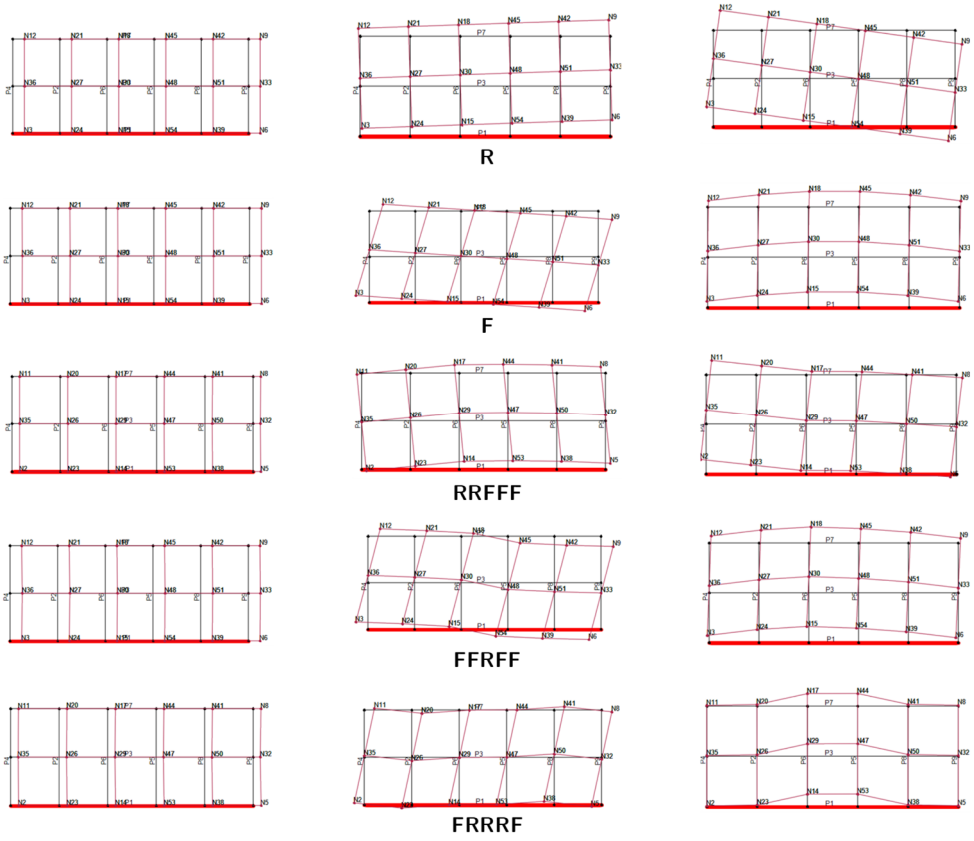

Figure 5-16: Row aggregate – First 3 modal shapes of the row aggregate in presence of different floors typology.

Figure 5-17 shows a comparison of the deformed configurations in Y direction obtained from the pushover analyses, with indication of the value of the modal participation factor Γ. As we can observed, the displacements are in general greater for the internal S.U.s, except for the RRFFF case, for which the external S.U. with flexible floors is the most stressed. The deformed configuration in X direction is equal to the 1st modal shape for all cases.

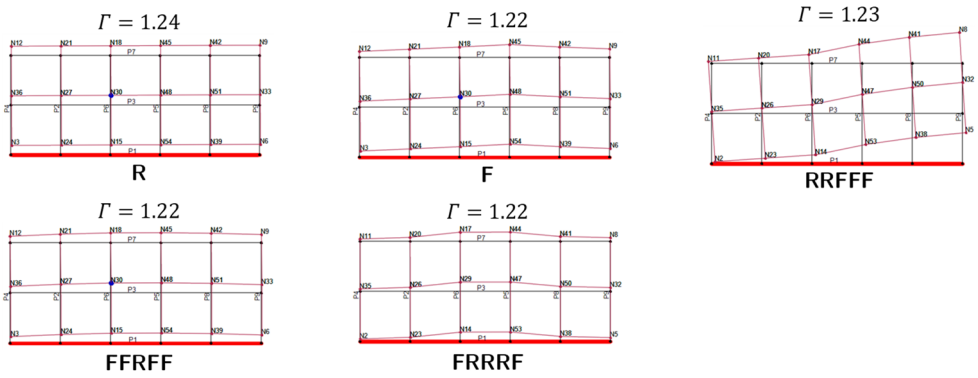

Figure 5-17: Row aggregate – Deformed configuration in Y direction from pushover analysis in function of the floors typology.

The M.U.A. individuated for the internal S.U. and for the external S.U. are shown in the following, together with the percentage changes of the maximum base shear V_{bu} and the stiffness k^* in respect to the reference configuration, and the comparison of the results with those of the isolated conditions.

The M.U.A. for the internal S.U. (Table 5-4) is model A1 (i.e., the configuration that considers the target S.U. with the immediately adjacent ones and excludes the external buildings) regardless of the floors typology, with the exception of the RRFFF case, for which the M.U.A. is model A7, that only excludes the external S.U. with flexible floors.

Considering the external S.U. (Table 5-5), the M.U.A. results to be model B3 (in which the opposite external S.U. is excluded) for all cases, but it should be noticed that model B1 (i.e., the configuration composed of 2 adjacent S.U.s to the target one) provides similar results. Actually, this is the M.U.A. for the FRRRF case.

With reference to the comparison of the results of M.U.A. with those of the isolated conditions, for both internal and external S.U.s, the isolated conditions present a reduction of the capacity in X direction and an increment in Y direction.

Table 5-4: M.U.A. for different floors typology: row aggregate – internal S.U.

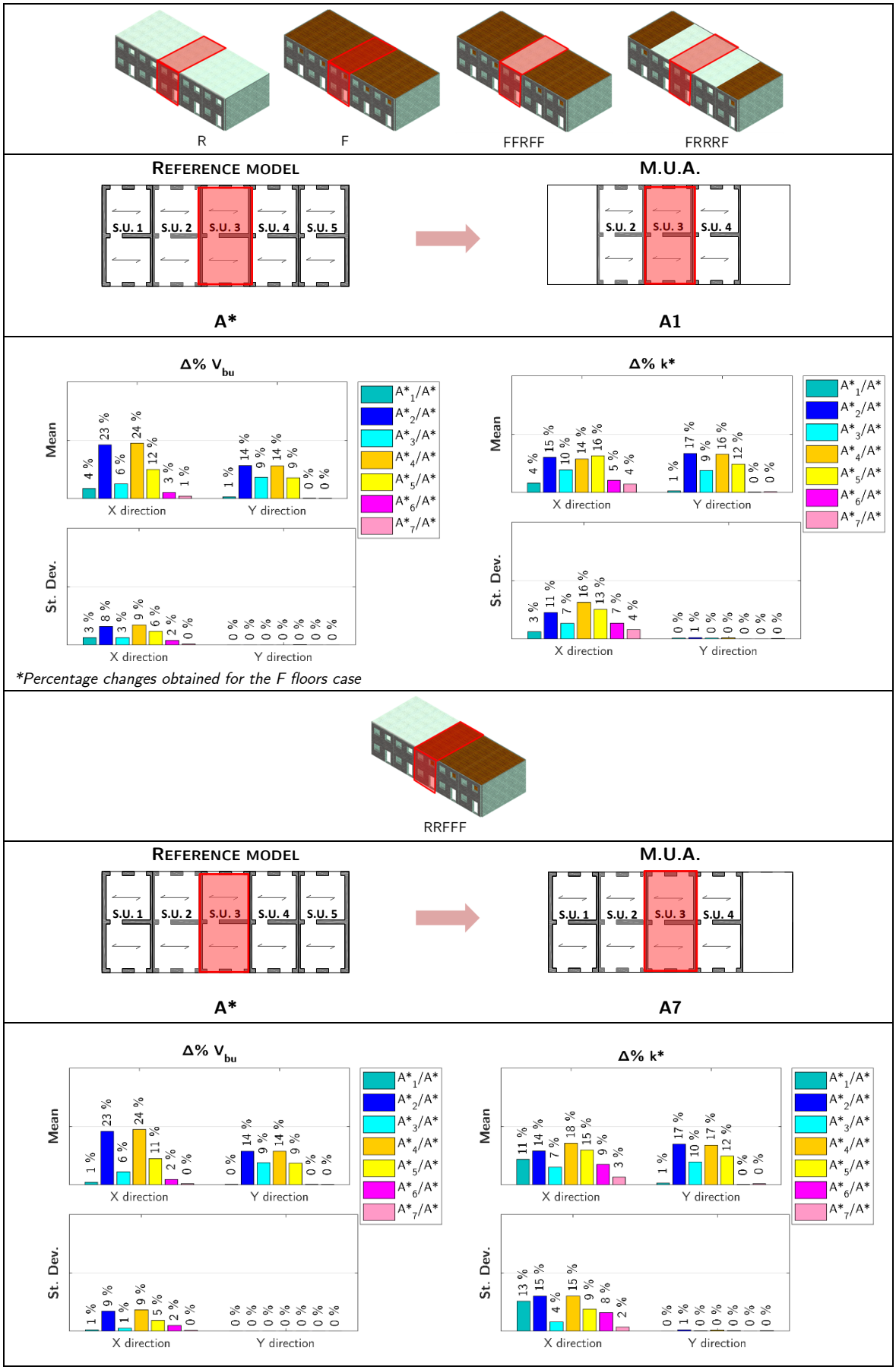

Table 5-5: M.U.A. for different floors typology: row aggregate – external S.U.

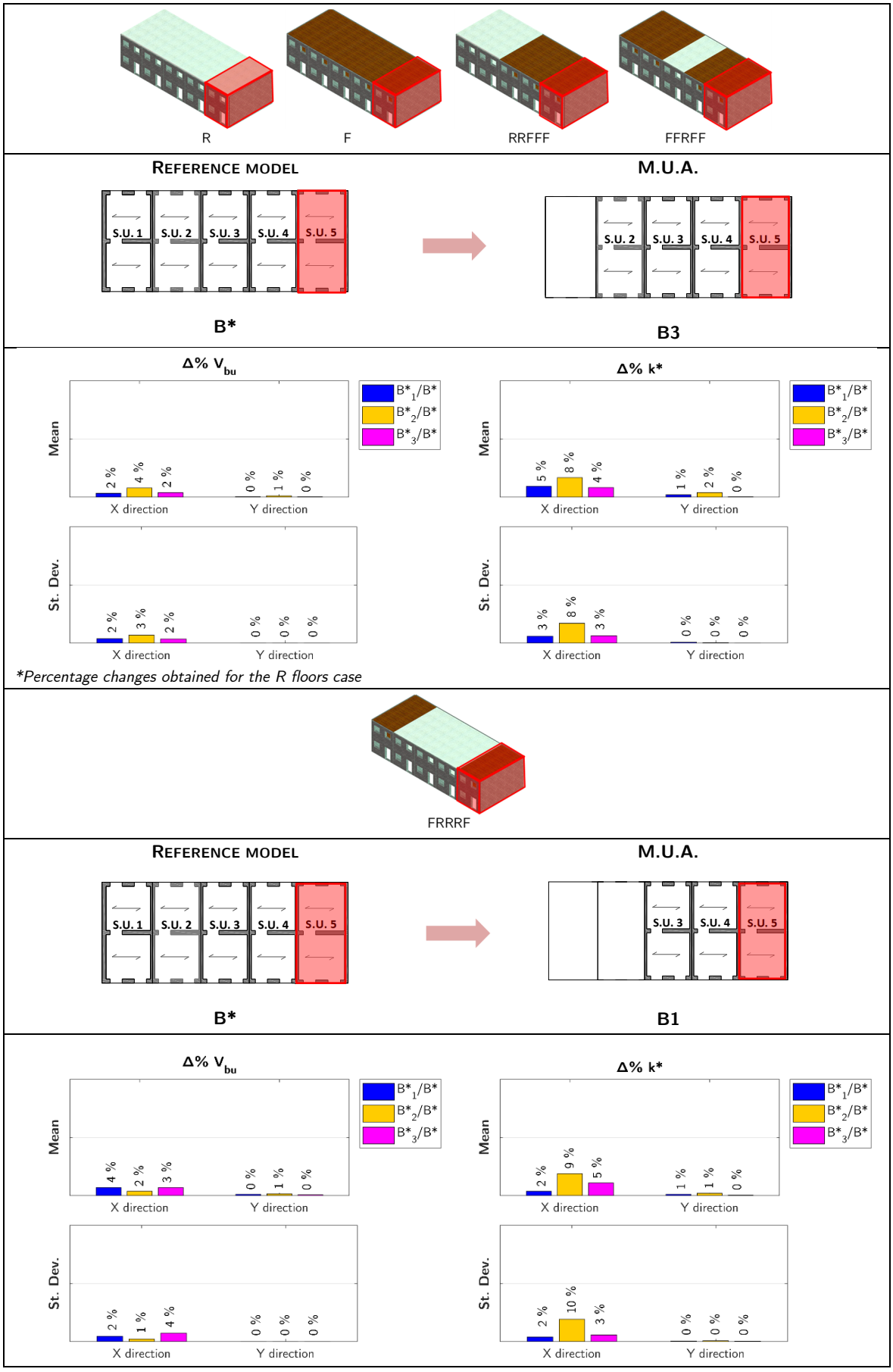

Comparison with the isolated conditions

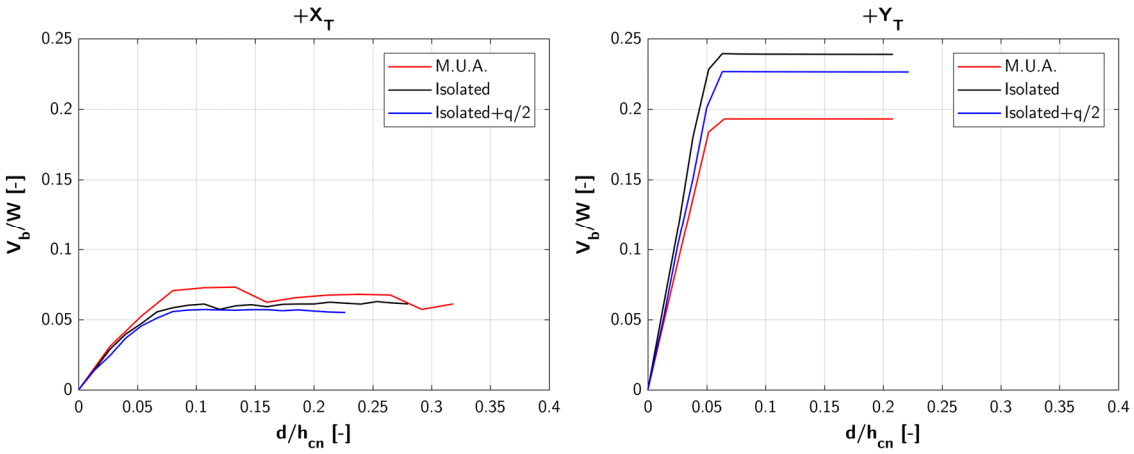

		Δ% α_{PGA}	Δ% k*	Δ% V_{bu}
X direction	**Isolated**	-5%	-7%	-14%
	Isolated + q/2	-11%	-10%	-22%
Y direction	**Isolated**	19%	31%	24%
	Isolated + q/2	14%	11%	17%

**Results obtained for the R floors case*

5.2.3.2 L aggregate

In Figure 5-18, a comparison of the first 3 modal shapes for all cases is shown. As we can observe, in general, there is a differentiated translation between the S.U.s arranged in X direction and those arranged in Y direction, meaning that the two parts of the aggregate behave as almost independent structures. Only in presence of R floors, the translation is rigid, and the complete aggregate moves together. This fact is also confirmed by the deformed configurations obtained from the pushover analyses, that are shown in Figure 5-19 and Figure 5-20 for X and Y direction, respectively.

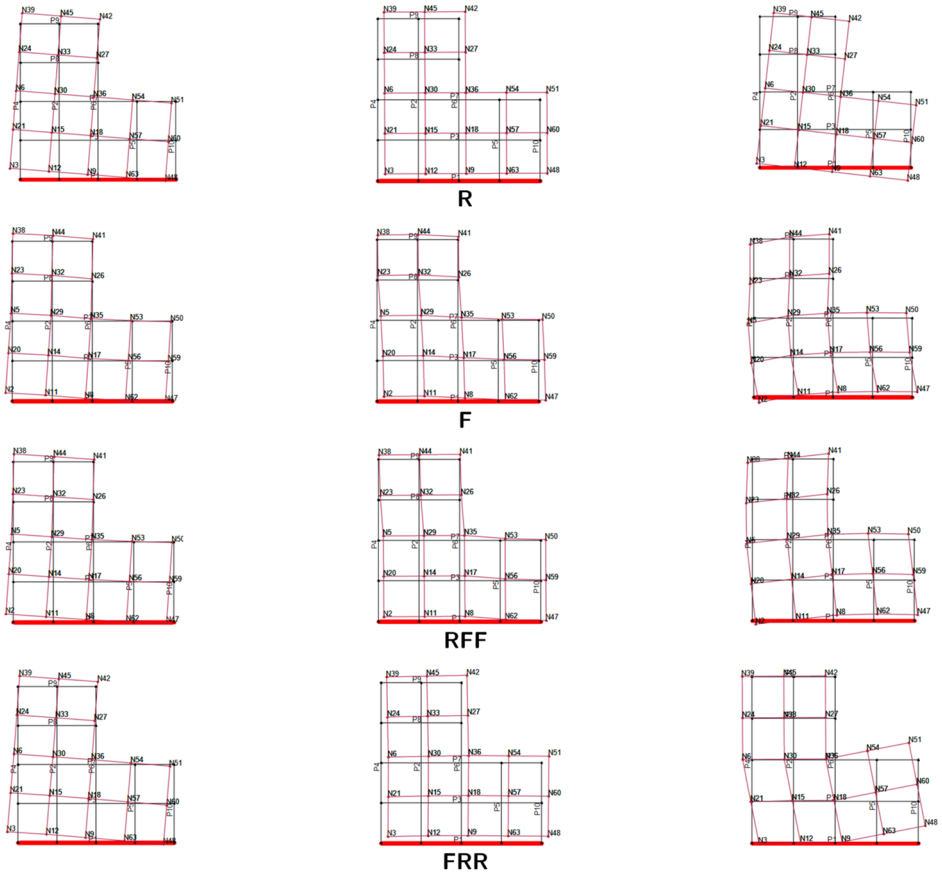

Figure 5-18: L aggregate – First 3 modal shapes of the row aggregate in presence of different floors typology.

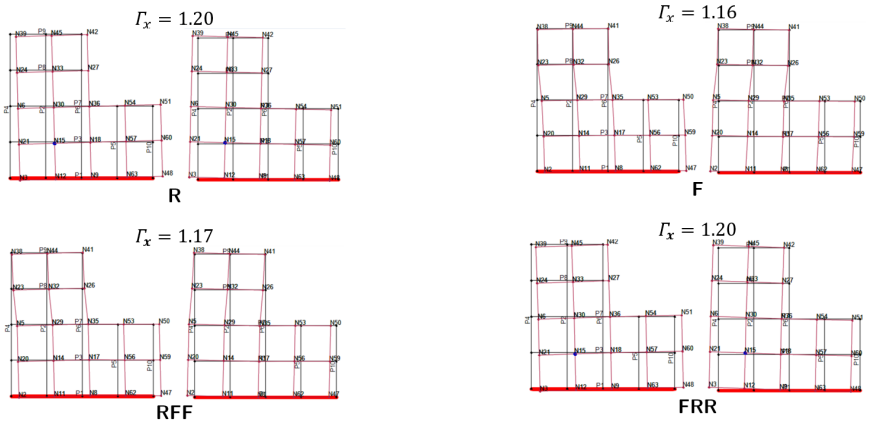

Figure 5-19: L aggregate – Deformed configuration in X direction (+X left, -X right) from pushover analysis in function of the floors typology.

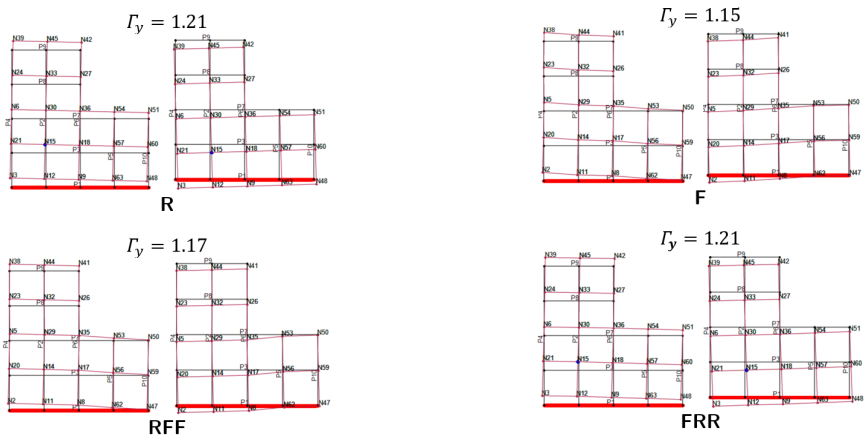

Figure 5-20: L aggregate – Deformed configuration in Y direction (+Y left, -Y right) from pushover analysis in function of the floors typology.

The M.U.A. individuated for the corner S.U. and for the external S.U. are shown in the following, together with the percentage changes of the maximum base shear V_{bu} and the stiffness k^* in respect to the reference configuration and the comparison of the results with those of the isolated conditions.

Referring to the corner building (Table 5-6), the M.U.A. differs by direction of analysis: indeed, configuration L6 (i.e., 3 S.U. X-row configuration with 1 adjacent S.U. in Y direction) is suitable for the analyses in X direction, while configuration L7 (i.e., 3 S.U. Y-row configuration with 1 adjacent S.U. in X direction) in Y direction, regardless the floors typology. However, it should be noticed that the complete aggregate condition L should be chosen as general M.U.A., regardless of the direction of analysis.

For the external S.U. (Table 5-7), the M.U.A. results to be configuration M3 (in which the opposite external S.U. is excluded) regardless of the floors typology.

From the comparison of the results of M.U.A. with those of the isolated conditions, it is possible to notice that, for the corner S.U., the isolated conditions present a similar capacity to that of the M.U.A. in both directions; the changes of α_{PGA} are inferior to 5%, except for the isolated S.U. in Y direction, for which it increases by 15%.

Considering the external S.U., instead, a relevant difference can be observed. In X direction the capacity of the isolated conditions is the half of that of the M.U.A.; on the contrary, in Y direction this is almost double. In detail, the α_{PGA} is reduced by about 30% in X direction, while it increases by more 65% in Y direction.

Table 5-6: M.U.A. for different floors typology: L aggregate – corner S.U.

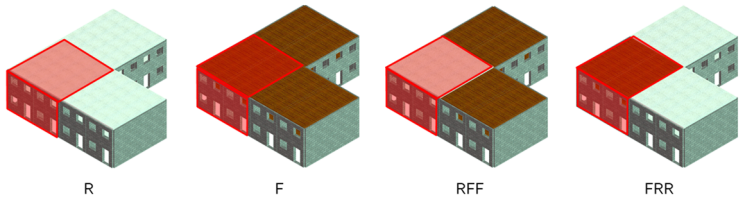

REFERENCE MODEL **M.U.A.**

L* **L6 in X direction** **L7 in Y direction** **L for both directions**

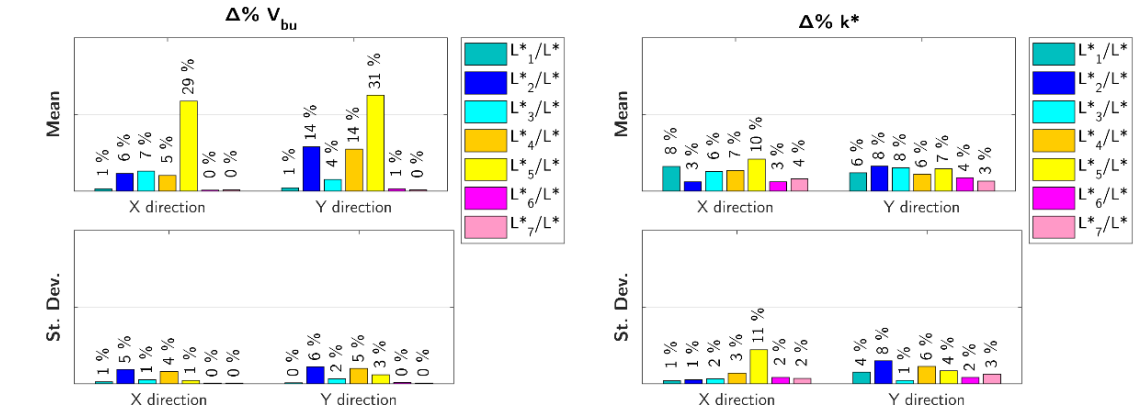

*Percentage changes obtained for the R floors case

Comparison with the isolated conditions

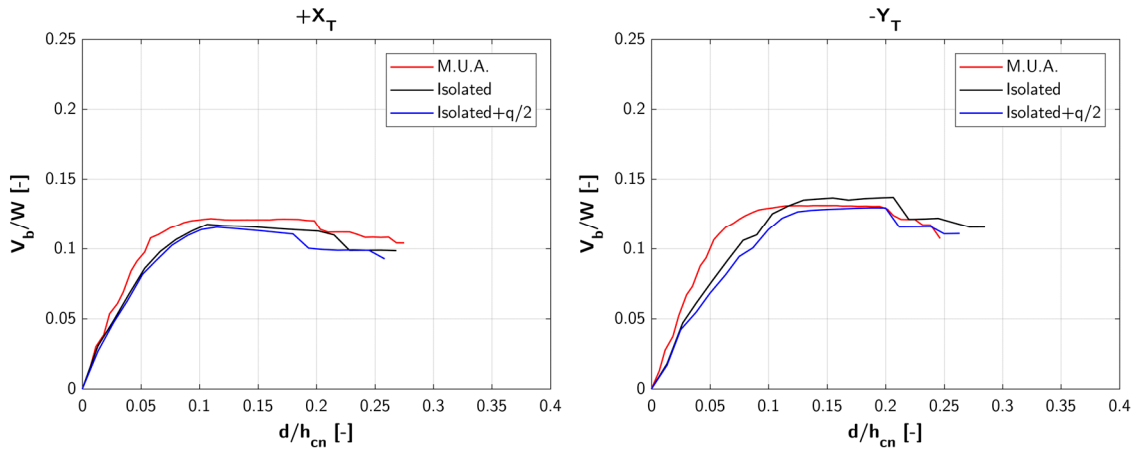

		Δ% α_{PGA}	Δ% k*	Δ% V_{bu}
X direction	**Isolated**	1%	-19%	-3%
	Isolated + q/2	-4%	-21%	-5%
Y direction	**Isolated**	15%	-31%	4%
	Isolated + q/2	2%	-38%	-1%

*Results obtained for the R floors case

Table 5-7: M.U.A. for different floors typology: L aggregate – external S.U.

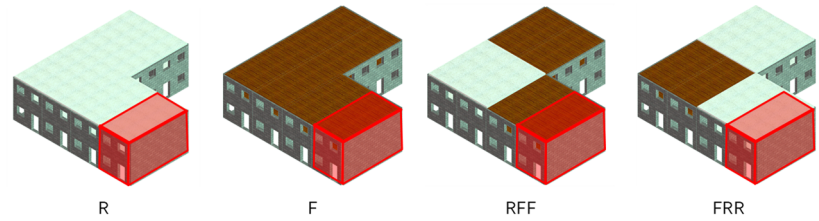

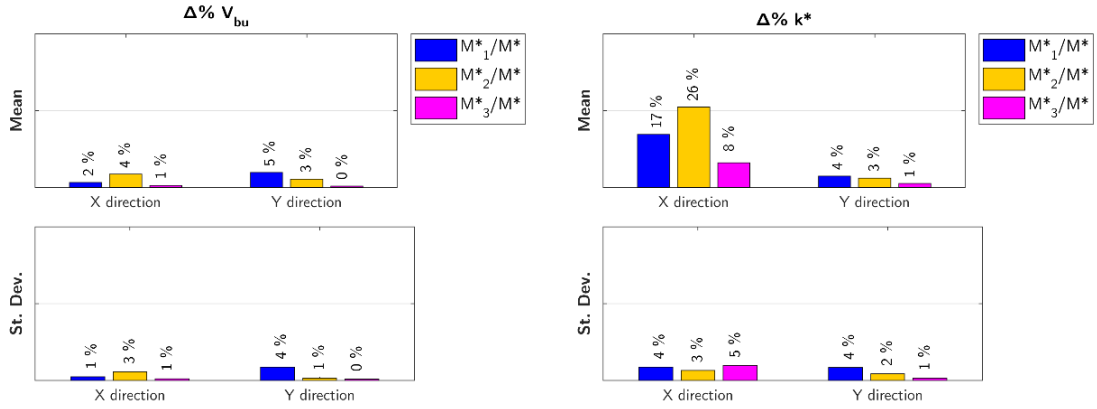

*Percentage changes obtained for the R floors case

Comparison with the isolated conditions

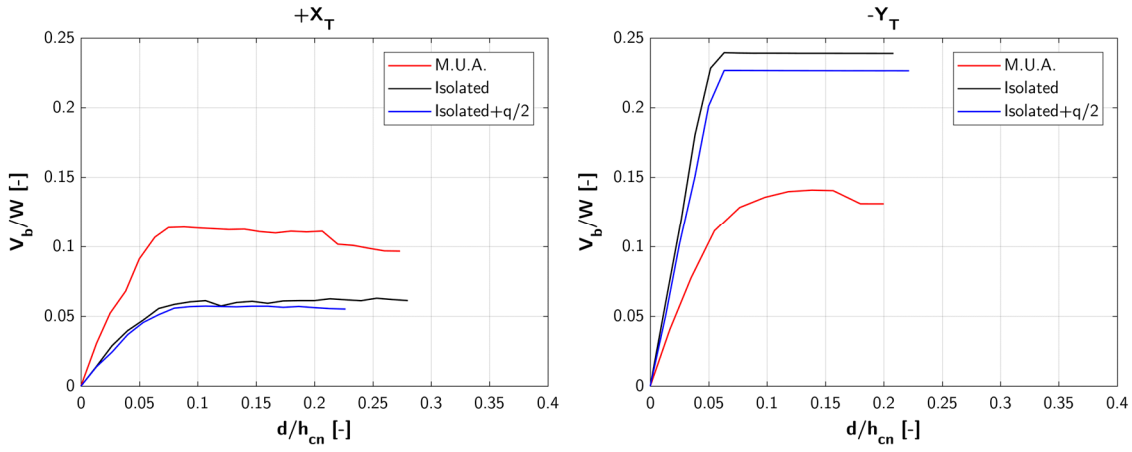

		Δ% α_{PGA}	Δ% k*	Δ% V_{bu}
X direction	**Isolated**	-24%	-49%	-45%
	Isolated + q/2	-29%	-51%	-50%
Y direction	**Isolated**	71%	125%	70%
	Isolated + q/2	64%	90%	61%

*Results obtained for the R floors case

5.2.3.3 Conclusions

As evidenced by the sensitivity analysis (§4.6), the variation of the stiffness of the floors is not significant for the identification of the M.U.A. compared to the other factors.

Considering a row aggregate, the M.U.A. for an internal S.U. is generally the configuration that includes the immediately adjacent S.U.s on each side (Table 5-4), except for the RRFFF case, for which the M.U.A. also including the next external S.U. with rigid floors results to be more suitable.
For an external S.U., 3 adjacent S.U.s should be modelled, even if the configuration composed of 2 adjacent S.U.s provides similar results (Table 5-5).

For a corner building of an L aggregate, the M.U.A. differs by direction of analysis, regardless the floors typology: indeed, the X-row configuration with 1 adjacent S.U. in Y direction is suitable for the analyses in X direction, while the Y-row configuration with 1 adjacent S.U. in X direction is suitable for those in Y direction (Table 5-6).
For an external S.U., the M.U.A. includes the longitudinal row in which this is placed and the first S.U. in the transversal row, adjacent to the corner building (Table 5-7).

With the aim to evaluate the error that an excessive simplification can produce, the results obtained for the individuated M.U.A. are compared with those obtained for the isolated target S.U. and this one modelled with the pertinent masses deriving from the immediately adjacent structure.
For the row aggregate, both in the case of internal (Table 5-4) and external S.U. (Table 5-5), the isolated conditions present a reduction (inferior to 10%) of the capacity in X direction and an increment (in the order of 20%) in Y direction.
For the corner S.U., the isolated conditions present a similar capacity to that of the M.U.A. in both directions, with changes of α_{PGA} inferior to 5% (Table 5-6).
Considering the external S.U. of the L aggregate, the capacity of the isolated conditions in X direction is the half of that of the M.U.A., with a reduction of α_{PGA} of about 30%; on the contrary, in Y direction this is almost double, with an increase of α_{PGA} major than 65% (Table 5-7).

5.2.4 M.U.A. in presence of material heterogeneities

In this paragraph, the results obtained from the procedure for the row and L aggregate are shown for the case of material heterogeneities.
The M.U.A. defined for all cases are resumed in the following tables.

5.2.4.1 Row aggregate

As for different floors typologies, the presence of material heterogeneities influences the modal behaviour of the row aggregate, especially in Y direction. In Figure 5-21 the first 3 modal shapes are shown for murB and murC cases, in presence of both flexible (F) and rigid (R) floors. It is possible to note that the modal shape in X direction is the same for all cases and in general is the 2nd one. The modal shape in Y direction is very different from one model to another and this influence the deformed configuration obtained from the pushover analysis, as shown in Figure 5-22. In fact, in this direction, the external S.U.s, characterized by inferior values of masonry and floors stiffness, suffer the highest displacements. In the case murB – R floors, the displacements are equal for all the S.U.s. With reference to the deformed configuration in X direction, this is equivalent to the first modal shape for all cases also in presence of material heterogeneities.

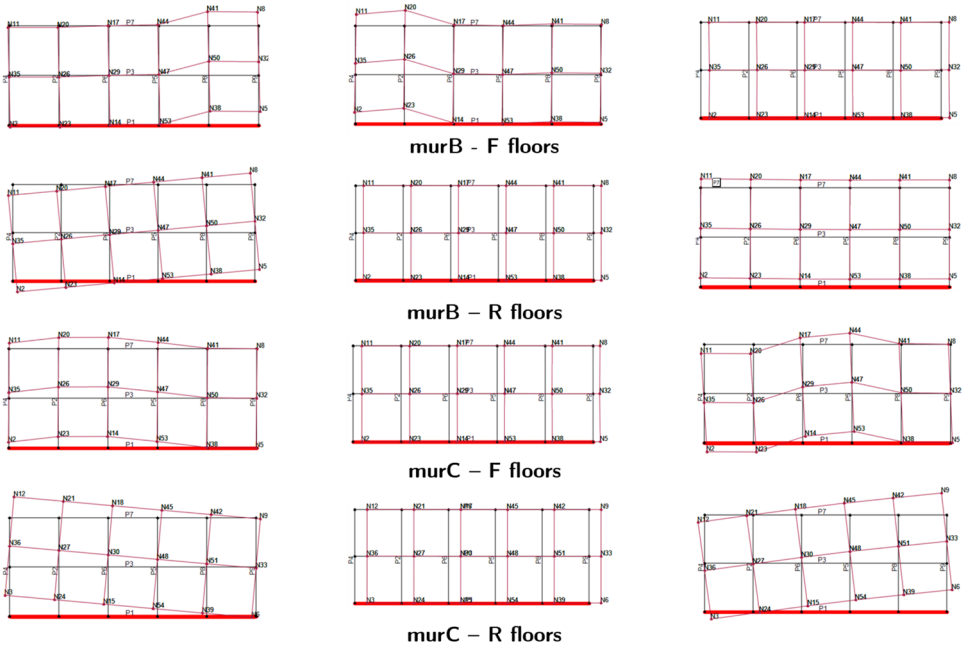

Figure 5-21: First 3 modal shapes of the row aggregate in presence of material heterogeneities, for F and R floors.

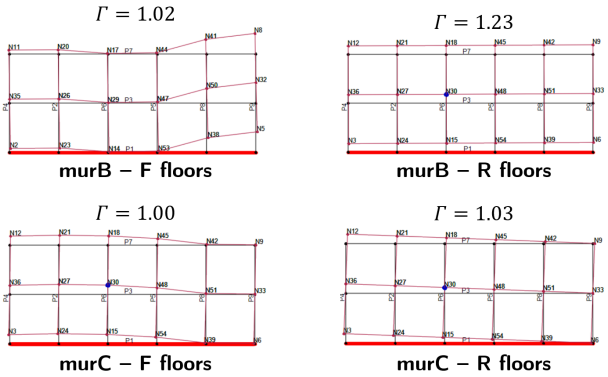

Figure 5-22: Deformed configuration in Y direction from pushover analysis in presence of material heterogeneities, for F and R floors.

For both murB and murC case, the M.U.A. individuated for the internal S.U. and for the external S.U. are shown in the following, together with the percentage changes of the maximum base shear V_{bu} and the stiffness k^* in respect to the reference configuration and the comparison of the results with those of the isolated conditions.

With reference to the murB case, in which the internal S.U.s are the most rigid, for the internal S.U. (Table 5-8), there is no a clear trend in the pushover curves at S.U.- level; for this reason, in accordance to the deformed configurations previously shown in Figure 5-22, the complete aggregate condition results to be the optimal M.U.A., regardless the floors typology.

Considering the external S.U. (Table 5-9), the M.U.A. results to be model B1 (i.e., the configuration composed of 2 adjacent S.U.s to the target one) for both R and F floors.

Considering the murC case, in which the external S.U.s are the most rigid, the M.U.A. for the internal S.U. (Table 5-10) is configuration A6, that excludes the external less rigid S.U., regardless of the floors typology.

For the external S.U (Table 5-11), the M.U.A. results to be model B3 (that excludes the opposite not rigid S.U.) for both R and F floors.

With reference to the comparison of the results of the M.U.A. with those of the isolated conditions, they are closely linked to the type of masonry of the target S.U. In general, the capacity of the isolated S.U., if composed of more rigid masonry, is greater than that of the M.U.A.

For the internal S.U., when this is one of the most rigid (murB case), in X direction the α_{PGA} of M.U.A. is inferior to that of the isolated S.U. of 20%, while is major respect that of the isolated S.U. + q/2 of about 30%. Instead, in Y direction is inferior of almost 50%. On the contrary, when it is adjacent to more rigid S.U.s (murC case), the α_{PGA} of the isolated conditions is reduced of about 5% in X direction and it increases in Y direction, especially for the isolated S.U.

For the external S.U., when this is adjacent to more rigid S.U.s (murB case), the capacity of M.U.A. is major in comparison to that of the isolated S.U.s. Vice versa, when the external S.U. is one of the most rigid (murC case), the capacity of M.U.A. is considerably inferior in Y direction.

Table 5-8: M.U.A. in presence of material heterogeneities: row aggregate – internal S.U. – murB.

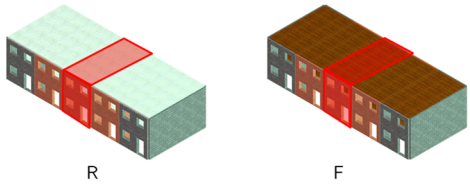

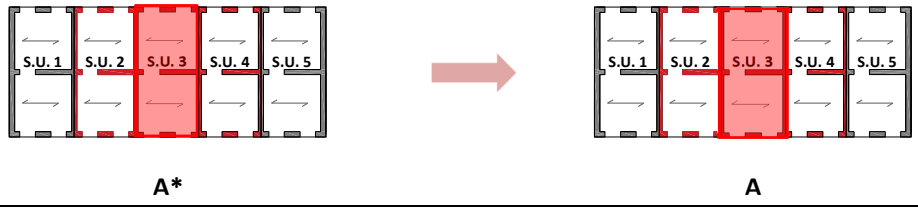

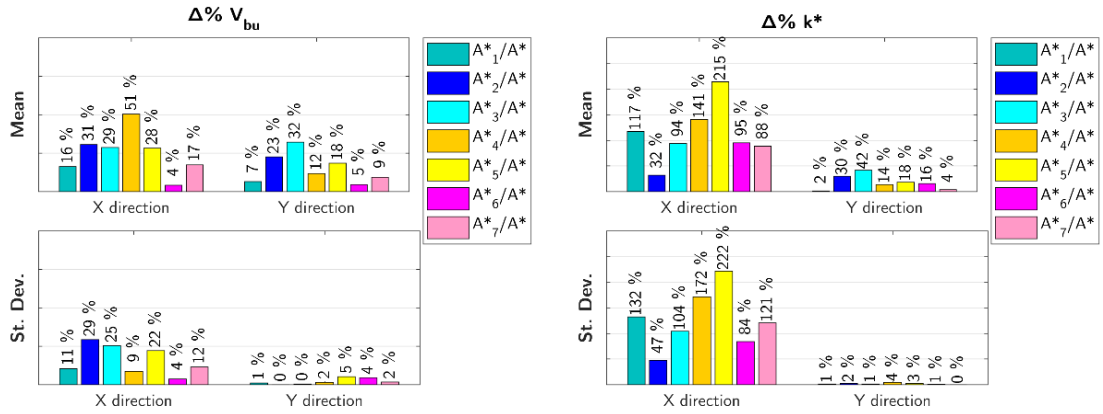

*Percentage changes obtained for the R floors case

Comparison with the isolated conditions

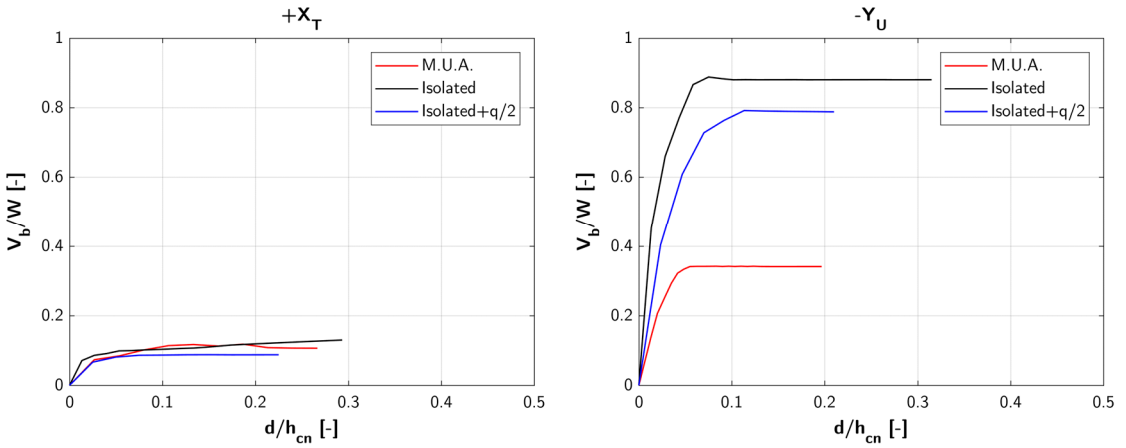

		Δ% α_{PGA}	Δ% k*	Δ% V_{bu}
X direction	**Isolated**	20%	37%	10%
	Isolated + q/2	-29%	58%	-26%
Y direction	**Isolated**	205%	160%	160%
	Isolated + q/2	53%	46%	132%

*Results obtained for the R floors case

Table 5-9: M.U.A. for in presence of material heterogeneities: row aggregate – external S.U. – murB.

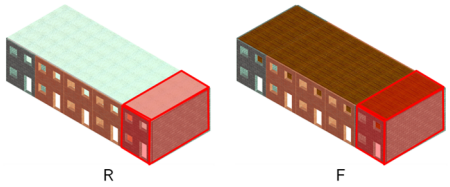

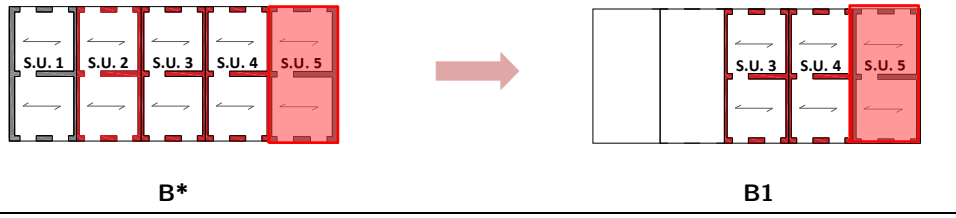

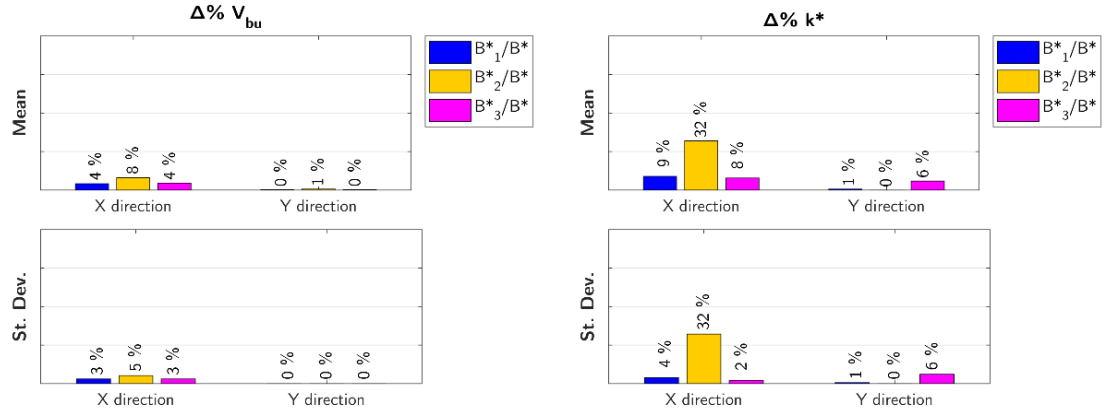

*Percentage changes obtained for the F floors case

Comparison with the isolated conditions

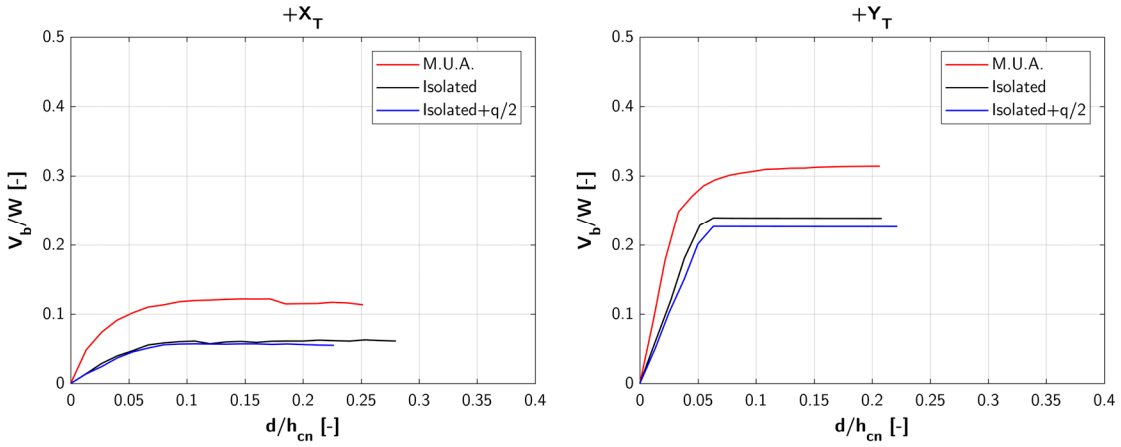

		Δ% α_{PGA}	Δ% k*	Δ% V_{bu}
X direction	**Isolated**	-28%	-62%	-48%
	Isolated + q/2	-33%	-63%	-53%
Y direction	**Isolated**	-1%	-37%	-26%
	Isolated + q/2	-9%	-47%	-30%

*Results obtained for the R floors case

Table 5-10: M.U.A. in presence of material heterogeneities: row aggregate – internal S.U. – murC.

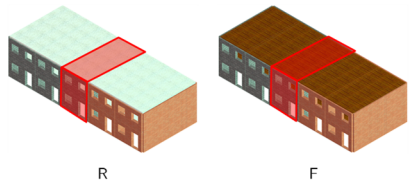

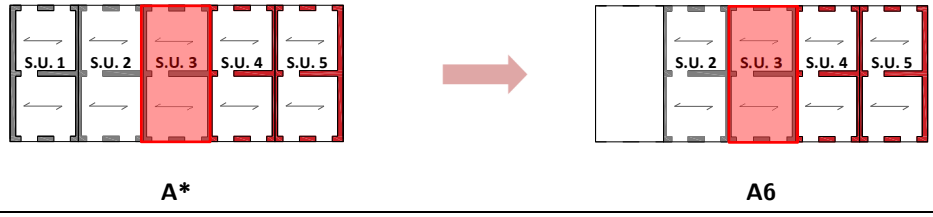

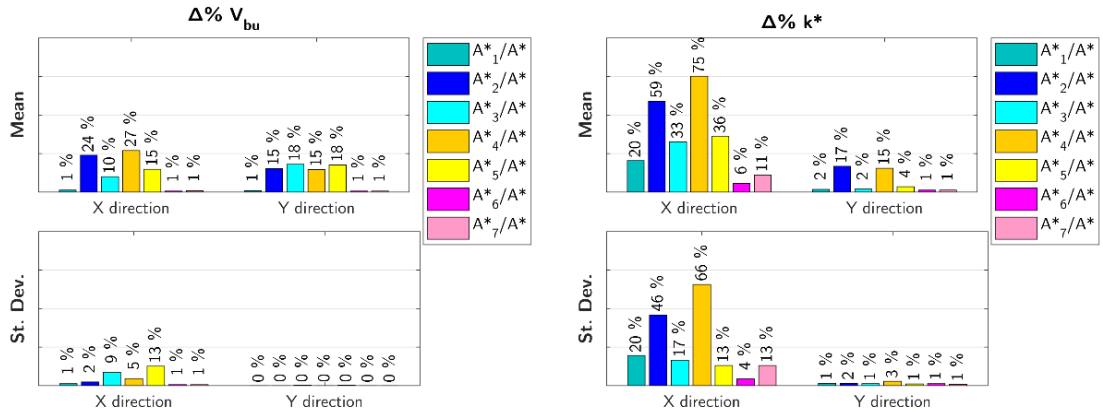

*Percentage changes obtained for the R floors case

Comparison with the isolated conditions

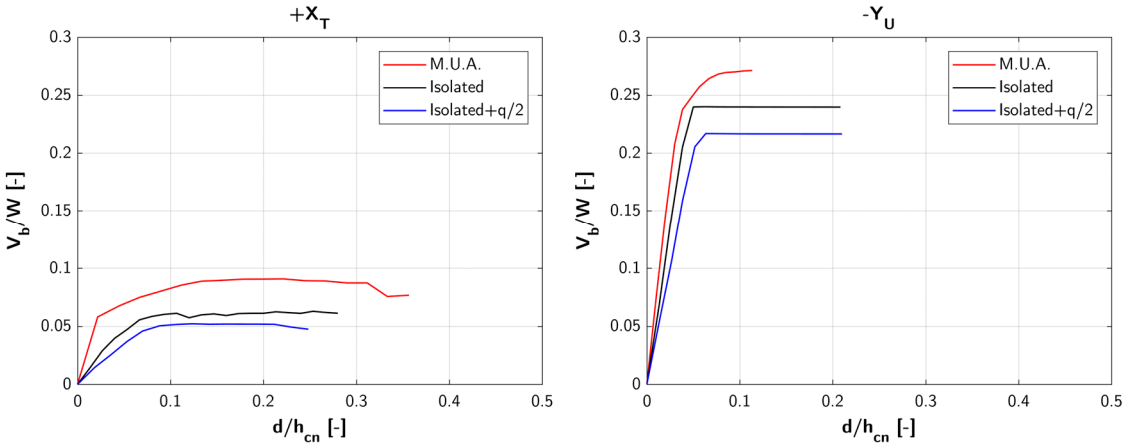

		Δ% α_{PGA}	Δ% k*	Δ% V_{bu}
X direction	**Isolated**	-2%	-49%	-31%
	Isolated + q/2	-6%	-62%	-43%
Y direction	**Isolated**	22%	-20%	-12%
	Isolated + q/2	3%	-39%	-20%

*Results obtained for the R floors case

Table 5-11: M.U.A. in presence of material heterogeneities: row aggregate – external S.U. – murC.

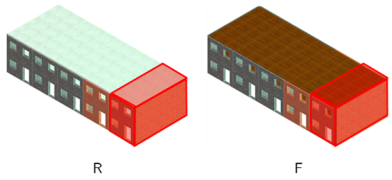

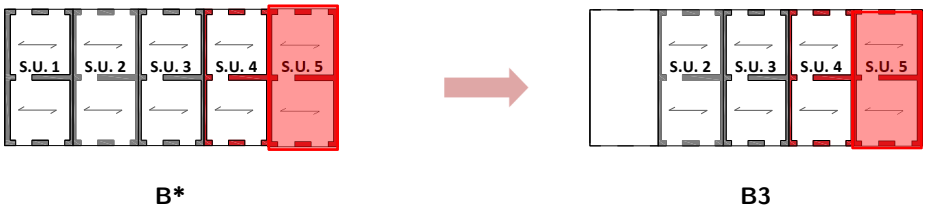

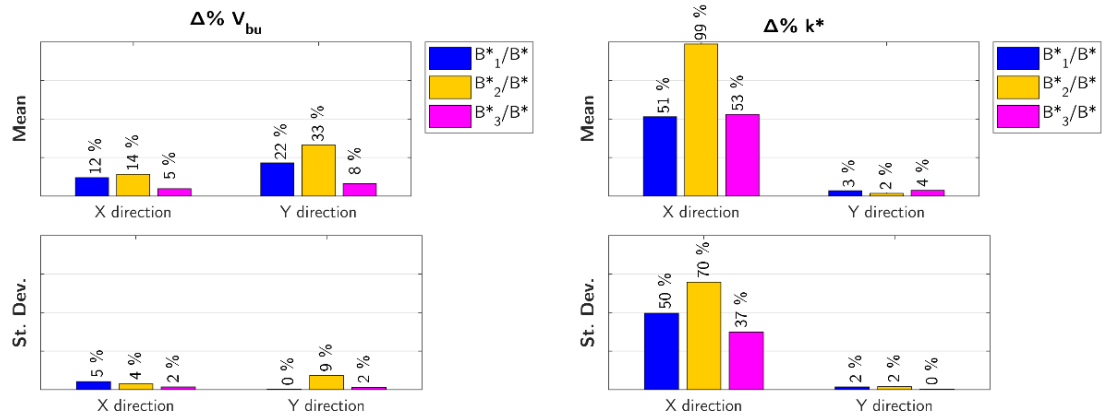

*Percentage changes obtained for the R floors case

Comparison with the isolated conditions

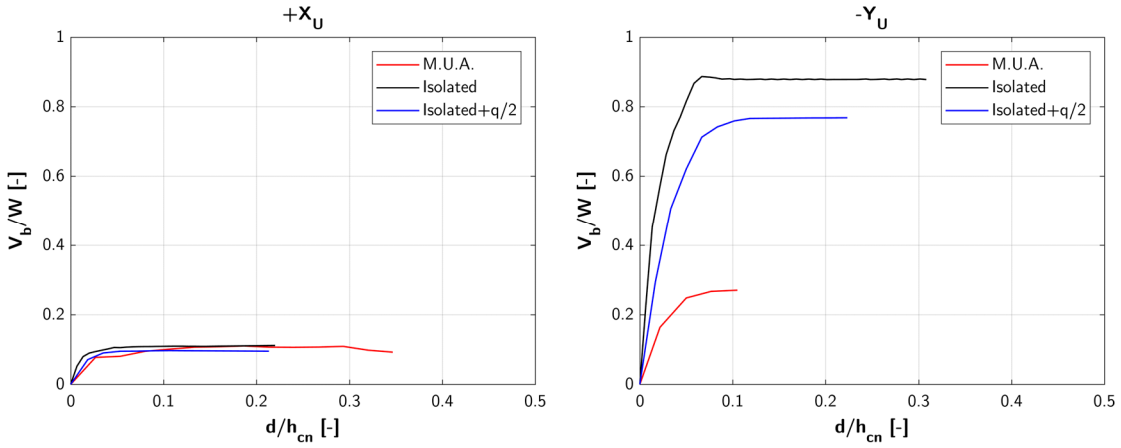

		Δ% α_{PGA}	Δ% k*	Δ% V_{bu}
X direction	**Isolated**	7%	108%	1%
	Isolated + q/2	-10%	33%	-12%
Y direction	**Isolated**	441%	293%	228%
	Isolated + q/2	199%	127%	184%

*Results obtained for the R floors case

5.2.4.2 L aggregate

The first 3 modal shapes of the L aggregate for the murB and murC cases, in presence of both R and F floors, are shown in Figure 5-23. As we can observe, when the floors are rigid, the S.U.s are subject to rigid translation and the 1st modal shape is a rigid rotation around the most rigid S.U.s. For flexible floors, the two parts of the aggregate moves in a differentiated way and the less rigid S.U.s suffer the greatest displacements. This fact is also confirmed by the deformed configurations obtained from the pushover analyses, that are shown in Figure 5-24 and Figure 5-25 for X and Y direction, respectively.

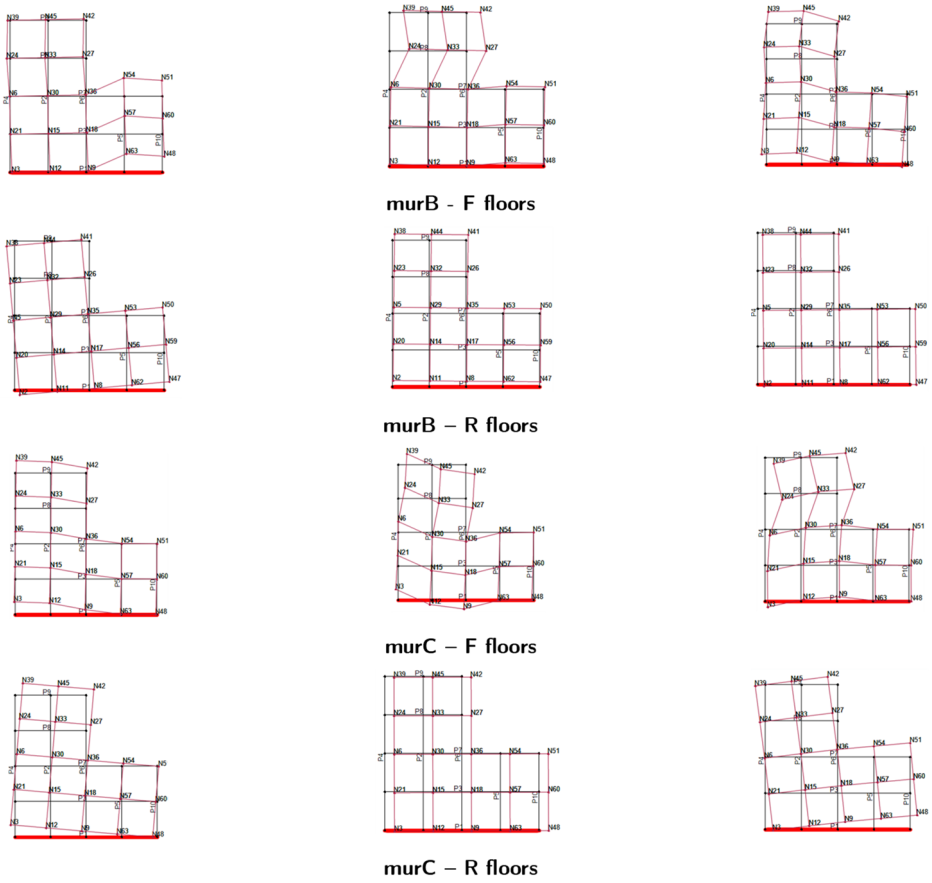

Figure 5-23: First 3 modal shapes of the row aggregate in presence of material heterogeneities, for F and R floors.

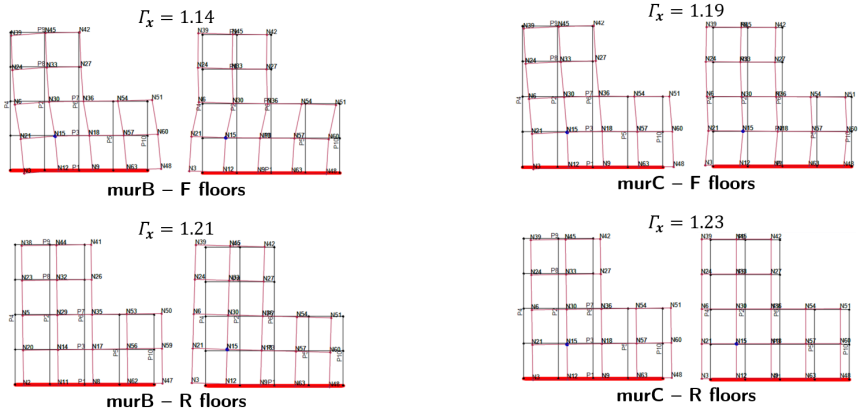

Figure 5-24: L aggregate – Deformed configuration in X direction (+X left, -X right) from pushover analysis in presence of material heterogeneities, for F and R floors.

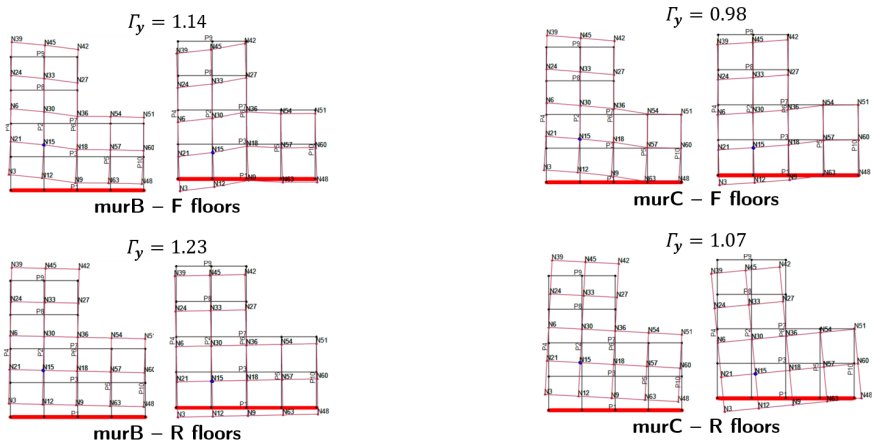

Figure 5-25: L aggregate – Deformed configuration in Y direction (+Y left, -Y right) from pushover analysis in presence of material heterogeneities, for F and R floors.

For both murB and murC case, the M.U.A. individuated for the corner S.U. and for the external S.U. are shown in the following, together with the percentage changes of the maximum base shear V_{bu} and the stiffness k^* in respect to the reference configuration and the comparison of the results with those of the isolated conditions.

Considering the corner S.U., the M.U.A. differs by direction of analysis but is the same for murB (Table 5-12) and murC (Table 5-14) case; as previously seen, configuration L6 (i.e., 3 S.U. X-row configuration with 1 adjacent S.U. in Y direction) is suitable for the analyses in X direction, while configuration L7 (i.e., 3 S.U. Y-row configuration with 1 adjacent S.U. in X direction) in Y direction. However, the complete aggregate condition results to be the general M.U.A.

The results are in accordance to those of the previous paragraph also for the external S.U. For both murB case (Table 5-13) and murC (Table 5-15), the M.U.A. results to be configuration M3 (in which the opposite external S.U. is excluded). Only for the murB case in presence of flexible floors the M.U.A. differs and coincides with configuration M1 (i.e., X-row configuration).

With reference to the comparison of the results of M.U.A. with those of the isolated conditions, also for the L aggregate the results are closely linked to the type of masonry of the target S.U.

In general, considering the corner S.U., the capacity of the isolated S.U., if composed of more rigid masonry (murB case), is greater than that of the M.U.A. Vice versa, when it is adjacent to more rigid S.U.s (murC case), the α_{PGA} of the isolated conditions is inferior at least of 15%.

For the external S.U., the capacity of the M.U.A is major in comparison to that of the isolated S.U.s. if more rigid (murB case).

Table 5-12: M.U.A. in presence of material heterogeneities: L aggregate – corner S.U. – murB.

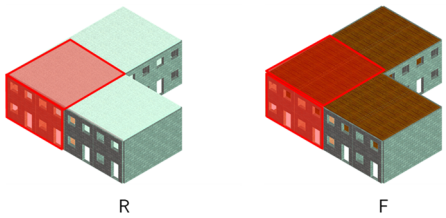

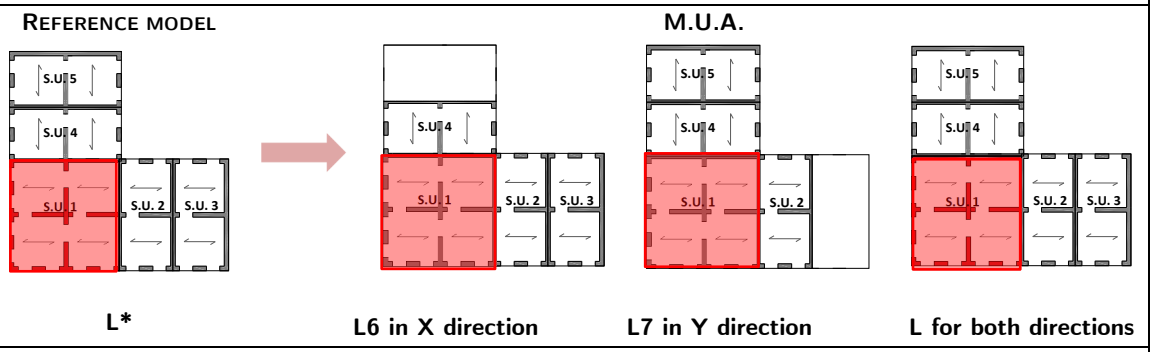

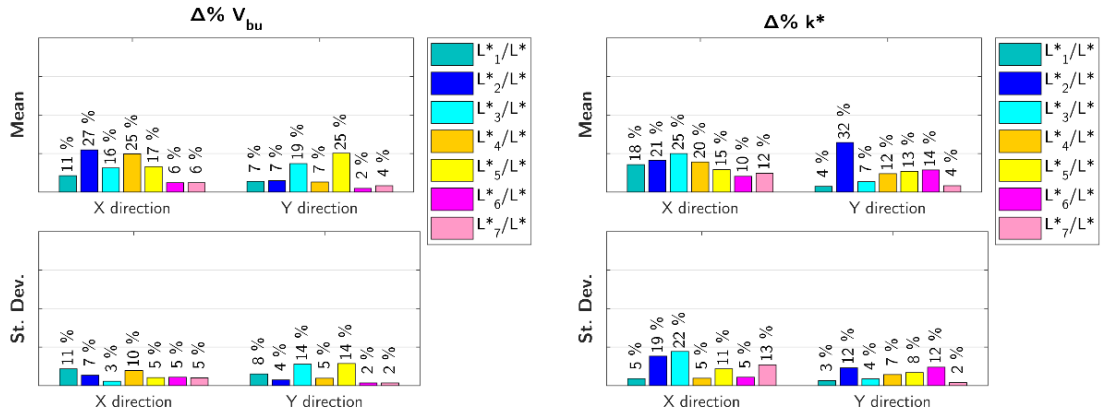

*Percentage changes obtained for the R floors case

Comparison with the isolated conditions

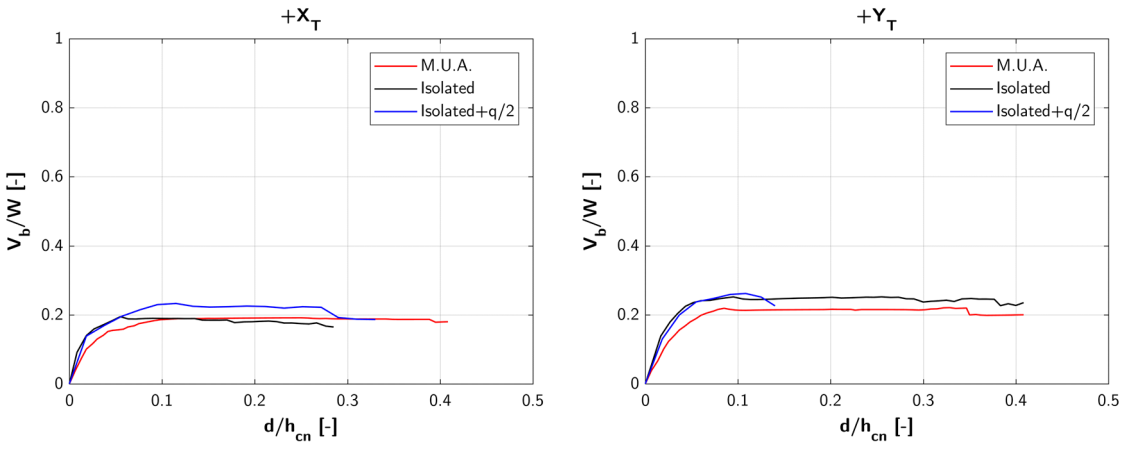

		Δ% α_{PGA}	Δ% k*	Δ% V_{bu}
X direction	**Isolated**	1%	88%	2%
	Isolated + q/2	16%	17%	22%
Y direction	**Isolated**	18%	59%	14%
	Isolated + q/2	-14%	33%	19%

*Results obtained for the R floors case

Table 5-13: M.U.A. in presence of material heterogeneities: L aggregate – external S.U. – murB.

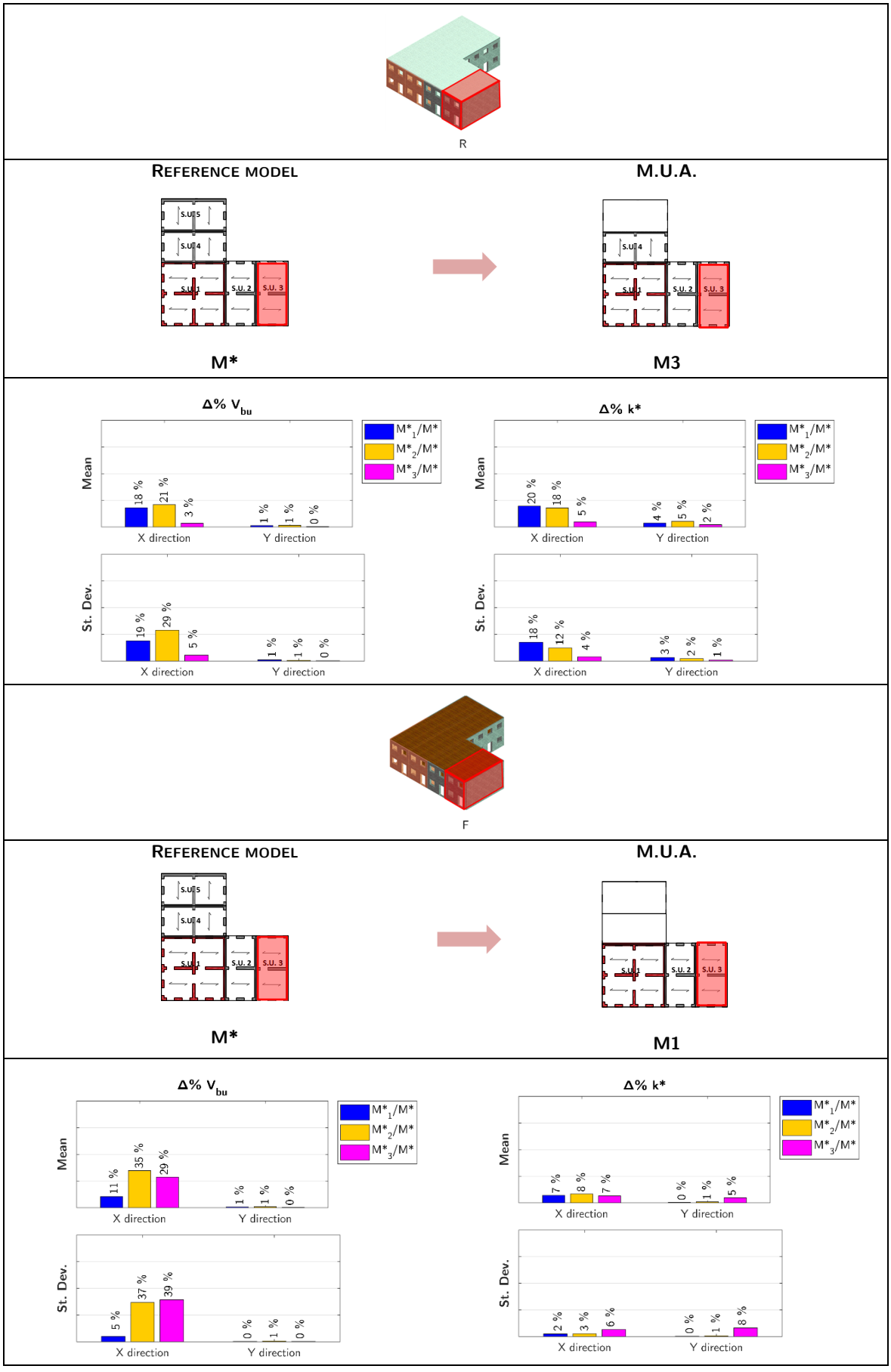

Comparison with the isolated conditions

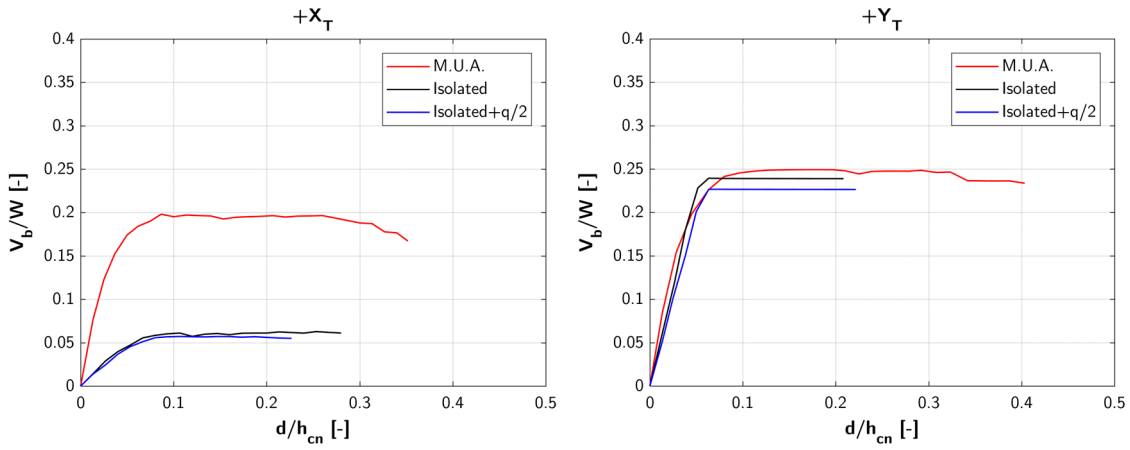

		Δ% α_{PGA}	Δ% k*	Δ% V_{bu}
X direction	**Isolated**	-56%	-79%	-68%
	Isolated + q/2	-59%	-80%	-71%
Y direction	**Isolated**	-5%	-3%	-4%
	Isolated + q/2	-9%	-18%	-9%

**Results obtained for the R floors case*

Table 5-14: M.U.A. in presence of material heterogeneities: L aggregate – corner S.U. – murC.

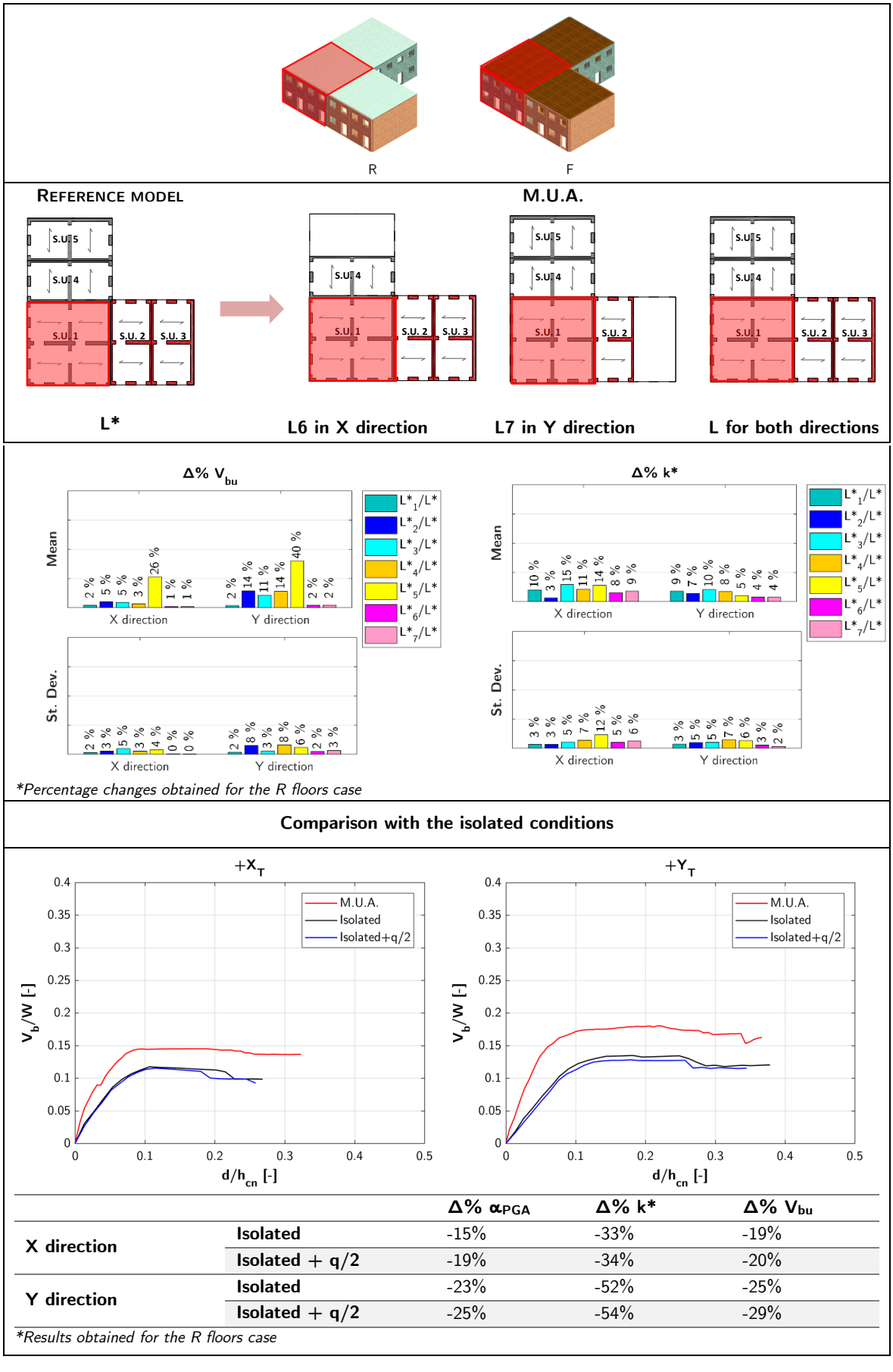

		Δ% α_{PGA}	Δ% k*	Δ% V_{bu}
X direction	**Isolated**	-15%	-33%	-19%
	Isolated + q/2	-19%	-34%	-20%
Y direction	**Isolated**	-23%	-52%	-25%
	Isolated + q/2	-25%	-54%	-29%

Results obtained for the R floors case

Table 5-15: M.U.A. in presence of material heterogeneities: L aggregate – external S.U. – murC.

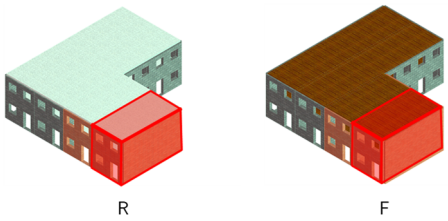

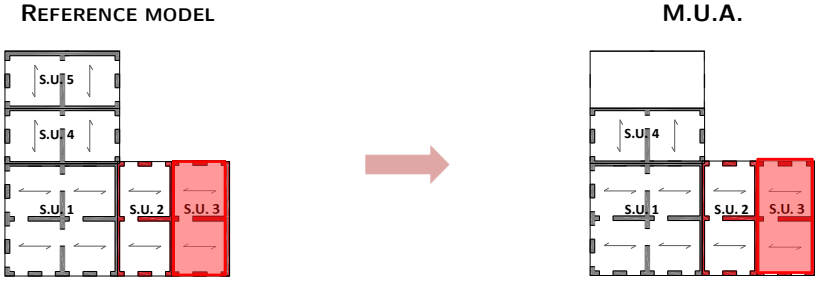

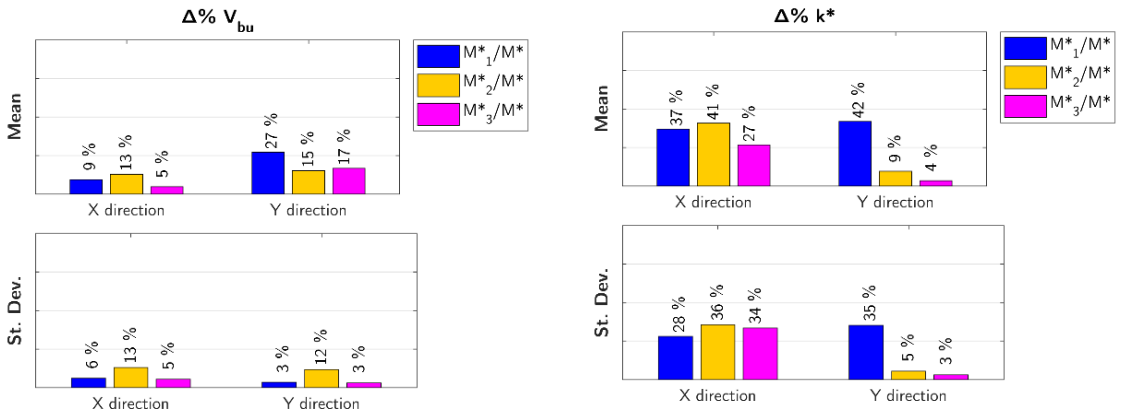

*Percentage changes obtained for the R floors case

Comparison with the isolated conditions

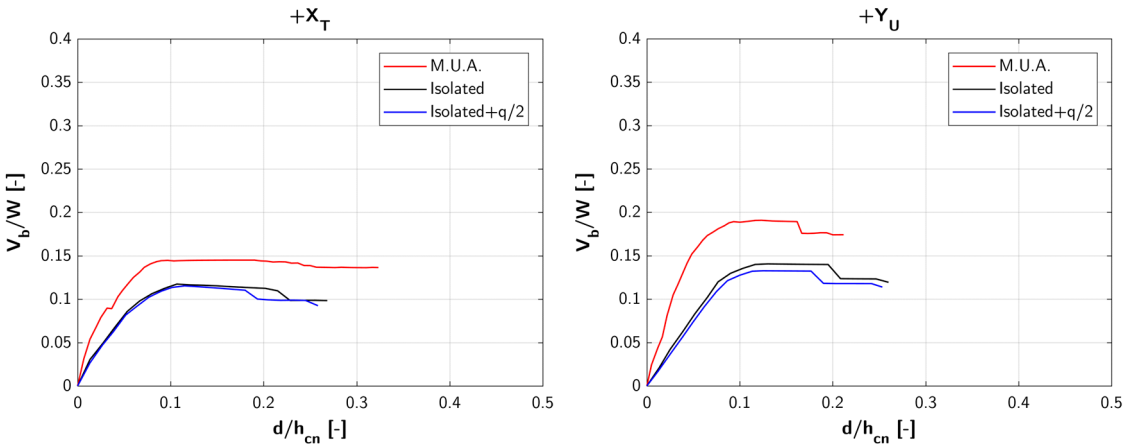

		Δ% α_{PGA}	Δ% k*	Δ% V_{bu}
X direction	**Isolated**	4%	6%	-5%
	Isolated + q/2	-33%	30%	-29%
Y direction	**Isolated**	418%	703%	357%
	Isolated + q/2	187%	417%	310%

*Results obtained for the R floors case

5.2.4.1 Conclusions

As evidenced by the sensitivity analysis (§4.7), the presence of material heterogeneities is very influent. The identification of M.U.A. changes in function of the position of the most rigid S.U.s, regardless of the floors typology.

Considering a row aggregate, when the internal S.U.s are the most rigid, for the central one the M.U.A. should include not only the immediately adjacent structures characterized by the same masonry type, as previously seen in paragraph 5.2.3.3, but also the next ones less resistant (Table 5-8). This fact can be explained by considering that, excluding the less resistant S.U.s, the M.U.A. would present a too high seismic capacity in comparison to the reference configuration.

In this configuration, for an external S.U. that is so adjacent to more rigid ones, the M.U.A. results to be composed of 2 adjacent S.U.s. (Table 5-9).

Instead, when the most rigid S.U.s in the aggregate are the external and, consequently, the internal S.U. is adjacent to these on just one side, the M.U.A. includes the immediately adjacent S.U.s on each side and the next more rigid one (Table 5-10).

In this configuration, for the external more rigid S.U., the M.U.A. excludes the opposite less resistant S.U. (Table 5-11).

Considering an L aggregate (§5.2.4.2), the results do not change respect to the previous case. For the corner building, the M.U.A. differs by direction of analysis also in presence of material heterogeneities, regardless the floors typology: indeed, the X-row configuration with 1 adjacent S.U. in Y direction is suitable for the analyses in X direction, while the Y-row configuration with 1 adjacent S.U. in X direction is suitable for those in Y direction.

For an external S.U., the M.U.A. generally includes the longitudinal row in which this is placed and the first S.U. in the transversal row, adjacent to the corner building. The only exception is the case in which the corner building is the most rigid in the aggregate and the floors are flexible (Table 5-13): in this configuration, the transversal row can be excluded from the M.U.A.

Finally, comparing the results obtained for the individuated M.U.A. and those of the isolated target S.U. and this one modelled with the pertinent masses deriving from the immediately adjacent structure, it can be observed that they are closely linked to the masonry type of the target S.U. In general, the capacity of the isolated S.U., if composed of more rigid masonry, is greater than that of the M.U.A.

For the row aggregate, when the internal S.U. is one of the most rigid, in X direction the α_{PGA} of M.U.A. is inferior to that of the isolated S.U. of 20%, while is major respect that of the isolated S.U. + q/2 of about 30%; instead, in Y direction is inferior of almost 50% (Table 5-8). Moreover, when the internal S.U. is adjacent to more rigid S.U.s, the α_{PGA} of the isolated conditions is reduced of about 5% in X direction, while it increases in Y direction (Table 5-10).

For the external S.U., when this is adjacent to more rigid S.U.s, the capacity of M.U.A. is major in comparison to that of the isolated S.U.s (Table 5-9). On the contrary, when this is one of the most rigid in the aggregate, the capacity of M.U.A. is considerably inferior in Y direction (Table 5-11).

Finally, considering the corner S.U., the capacity of the isolated S.U., if more rigid, is greater than that of the M.U.A. (Table 5-12). Vice versa, when this is less rigid, the α_{PGA} of the isolated conditions is inferior at least of 15% (Table 5-14). For the external S.U., if more rigid, the capacity of the M.U.A is major in comparison to that of the isolated S.U.s (Table 5-13).

5.2.1 M.U.A. in presence of differences in height

In this paragraph, the results obtained from the procedure for the row and L aggregate are shown for differences in height.
The M.U.A. defined for all cases are resumed in the following tables.

5.2.1.1 Row aggregate

The modal behaviour of the row aggregate is influenced by the presence of differences in height, especially in Y direction. In Figure 5-26 the first 3 modal shapes are shown for hB and hC cases, in presence of both flexible (F) and rigid (R) floors. It is possible to note that the modal shape in X direction is the same for all cases and is the 1st one. With regards to the modal shape in Y direction, the greatest displacements are in correspondence of the highest S.U.s, as confirmed by the deformed configurations derived from the pushover analyses, as shown in Figure 5-27.

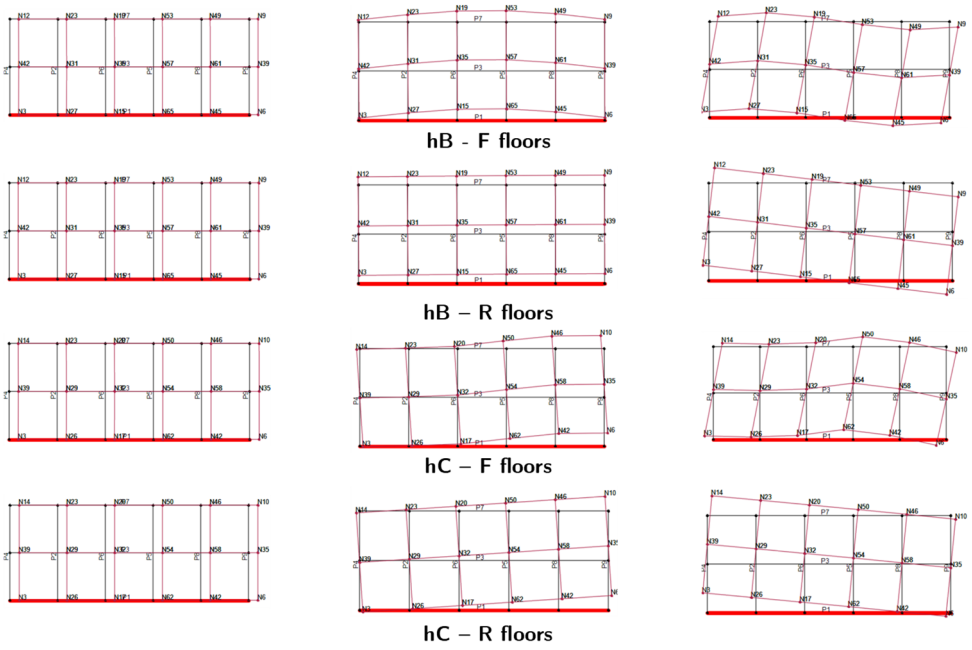

Figure 5-26: First 3 modal shapes of the row aggregate in presence of differences in height, for F and R floors.

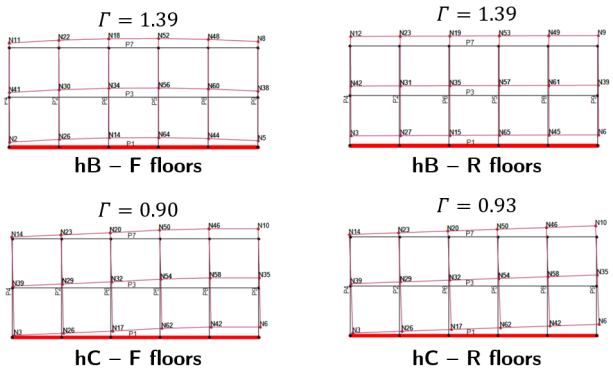

Figure 5-27: Deformed configuration in Y direction from pushover analysis in presence of differences in height, for F and R floors.

For both hB and hC case, the M.U.A. individuated for the internal S.U. and for the external S.U. are shown in the following, together with the percentage changes of the maximum base shear V_{bu} and the stiffness k^* in respect to the reference configuration and the comparison of the results with those of the isolated conditions.

With reference to the hB case, in which the internal S.U.s are the tallest, for the internal S.U. (Table 5-16) the M.U.A. results to be model A1 (i.e., the intermediate configuration with 1 adjacent S.U. on each side).

For the external S.U. (Table 5-19), the M.U.A. can be represented by model B3 (that excludes the opposite external S.U.), even if model B1 (that considers the 2 S.U.s adjacent to the target one) presents similar results.

With reference to the hC case, in which the external S.U.s are the tallest, the M.U.A. for the internal S.U. (Table 5-18) is model A7 (that excludes the external tallest S.U.), while for the external S.U. (Table 5-20) is model B1 (that considers the 2 S.U.s adjacent to the target one).

Considering the comparison of the results of M.U.A. with those of the isolated conditions, the results are closely linked to the height of the target S.U.

Considering the internal S.U., when this is one of the tallest (hB case), in both directions the α_{PGA} of M.U.A. is inferior to that of the isolated S.U., while is major respect that of the isolated S.U. + q/2; however, the deviations are inferior to 16%. On the contrary, when it is adjacent to a taller S.U. (hC case), the α_{PGA} of the isolated conditions is reduced in X direction of 13% for the isolated S.U. and of 30% for the isolated S.U. + q/2; instead, it increases in Y direction, especially for the isolated S.U.

For the external S.U., when it is adjacent to taller S.U.s (hB case), the capacity of M.U.A. is major in both directions of analysis, apart from the isolated S.U. in Y direction, that present a percentage change of α_{PGA} of 74%. Vice versa, when the external S.U. is one of the tallest (hC case), the α_{PGA} value changes in Y direction, with an increment especially in Y direction.

Table 5-16: M.U.A. in presence of differences in height: row aggregate – internal S.U. – hB.

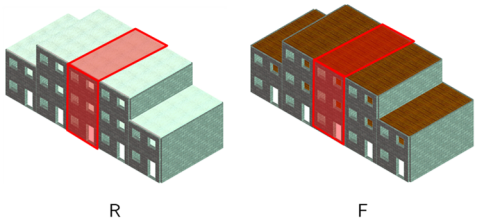

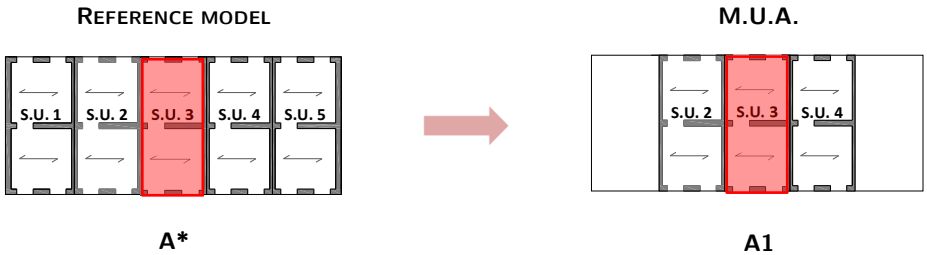

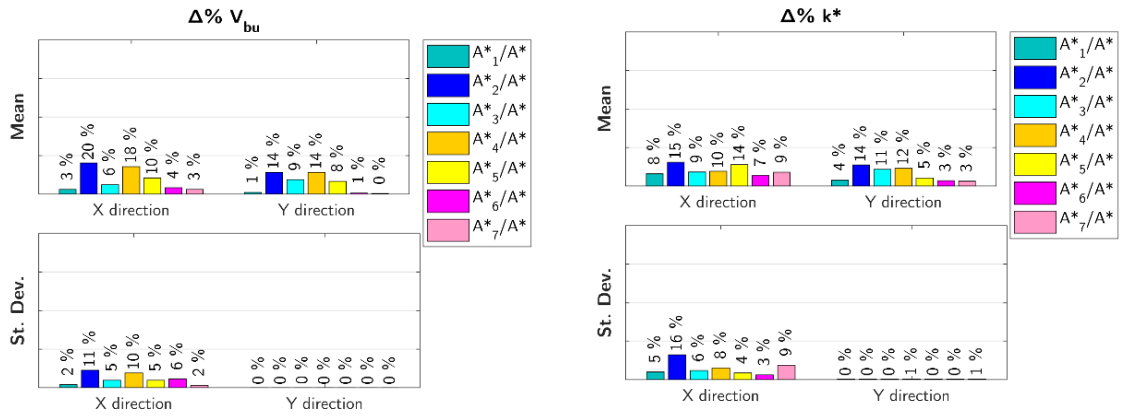

*Percentage changes obtained for the R floors case

Comparison with the isolated conditions

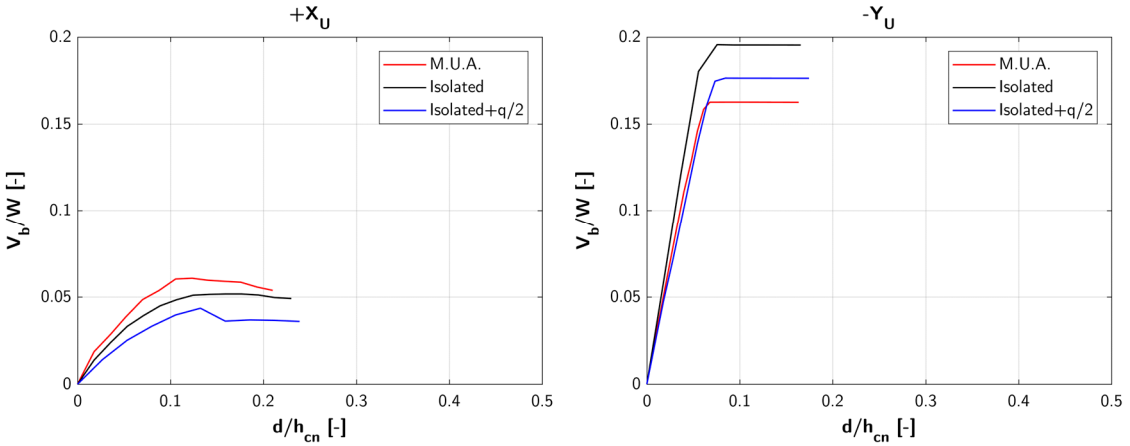

		Δ% α_{PGA}	Δ% k*	Δ% V_{bu}
X direction	**Isolated**	1%	-7%	-18%
	Isolated + q/2	-6%	-52%	-34%
Y direction	**Isolated**	16%	19%	20%
	Isolated + q/2	-1%	-8%	9%

*Results obtained for the R floors case

Table 5-17: M.U.A. in presence of differences in height: row aggregate – external S.U. – hB.

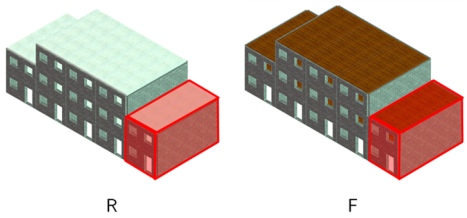

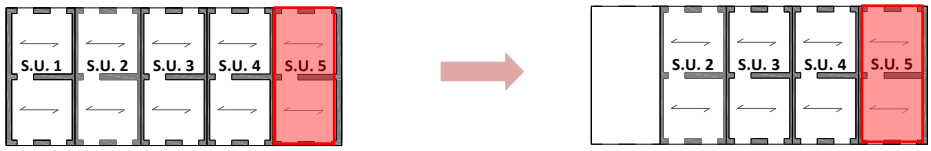

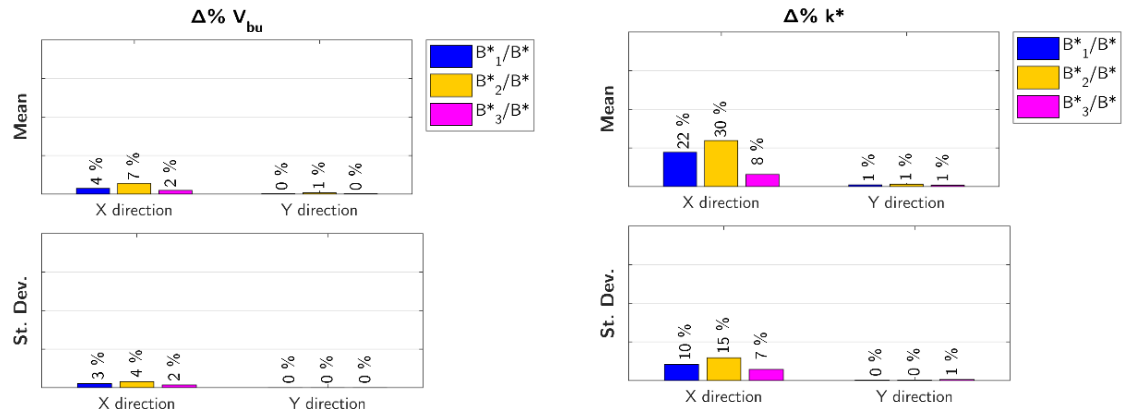

*Percentage changes obtained for the R floors case

Comparison with the isolated conditions

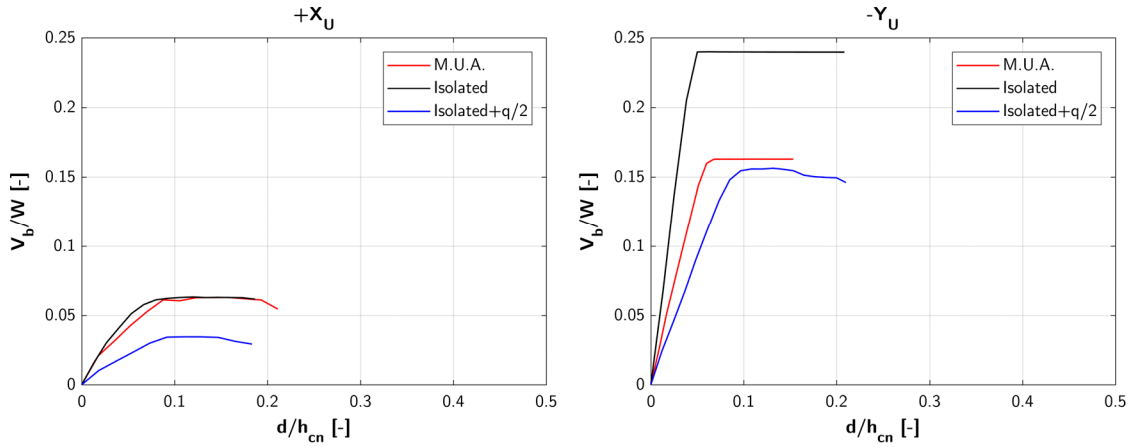

		Δ% α_{PGA}	Δ% k*	Δ% V_{bu}
X direction	**Isolated**	-14%	25%	0%
	Isolated + q/2	-45%	-47%	-45%
Y direction	**Isolated**	74%	90%	47%
	Isolated + q/2	-5%	-35%	-4%

*Results obtained for the R floors case

Table 5-18: M.U.A. in presence of differences in height: row aggregate – internal S.U. – hC.

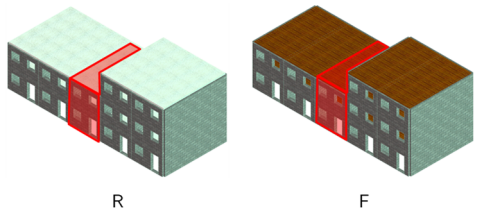

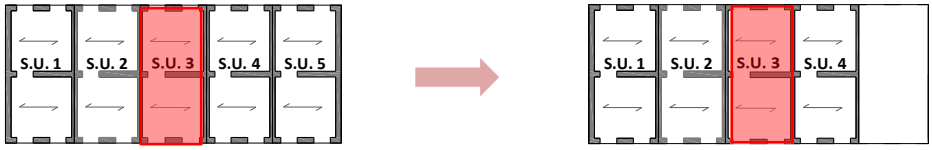

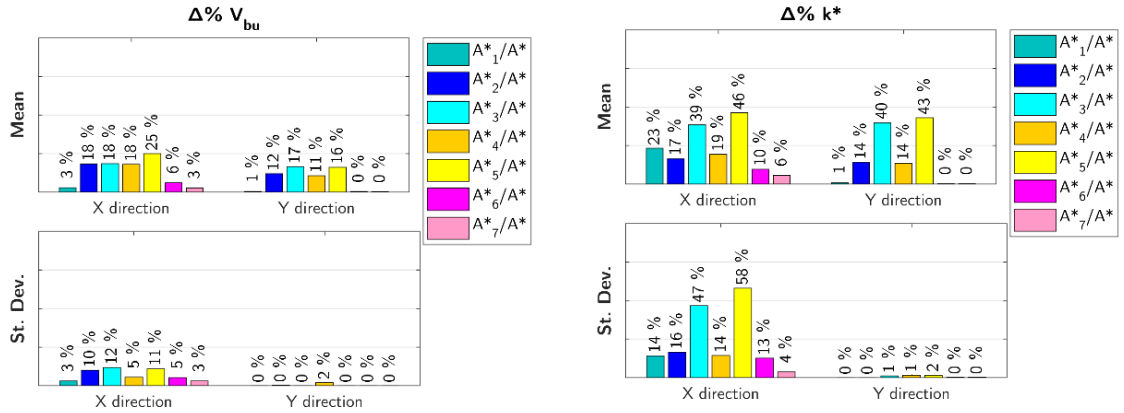

*Percentage changes obtained for the R floors case

Comparison with the isolated conditions

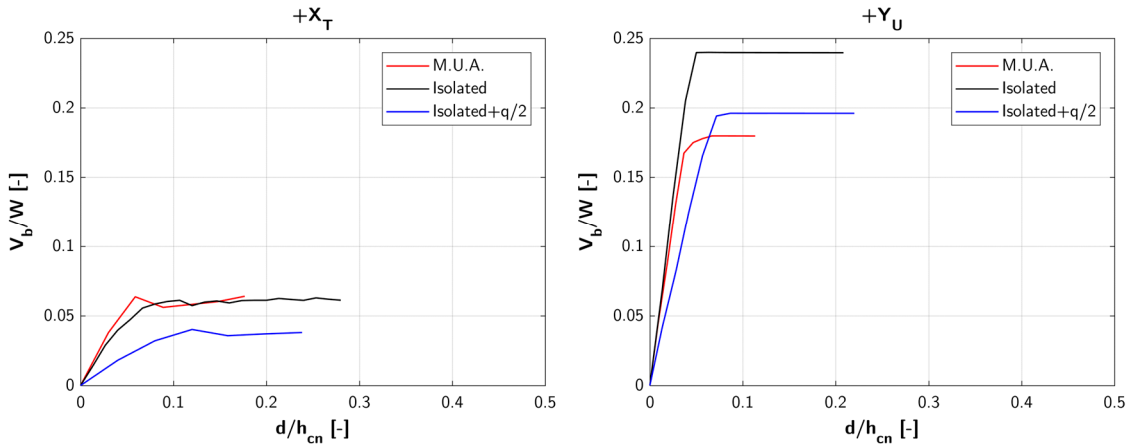

		Δ% α_{PGA}	Δ% k*	Δ% V_{bu}
X direction	**Isolated**	-13%	8%	-2%
	Isolated + q/2	-30%	-52%	-37%
Y direction	**Isolated**	42%	15%	33%
	Isolated + q/2	4%	-37%	9%

*Results obtained for the R floors case

Table 5-19: M.U.A. in presence of differences in height: row aggregate – external S.U. – hC.

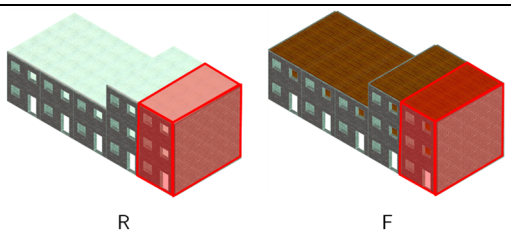

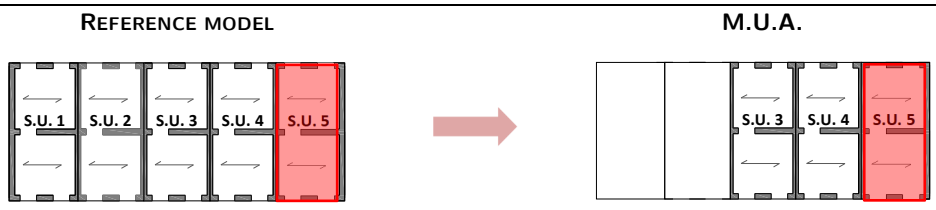

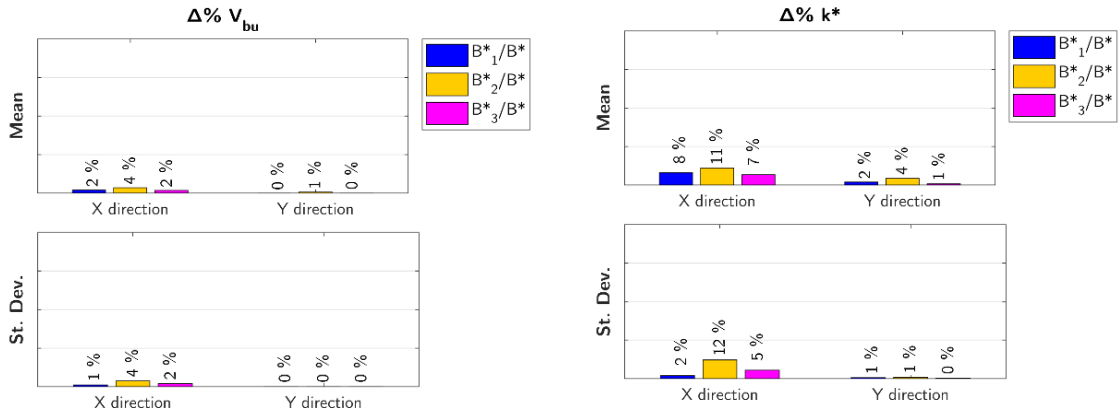

*Percentage changes obtained for the R floors case

Comparison with the isolated conditions

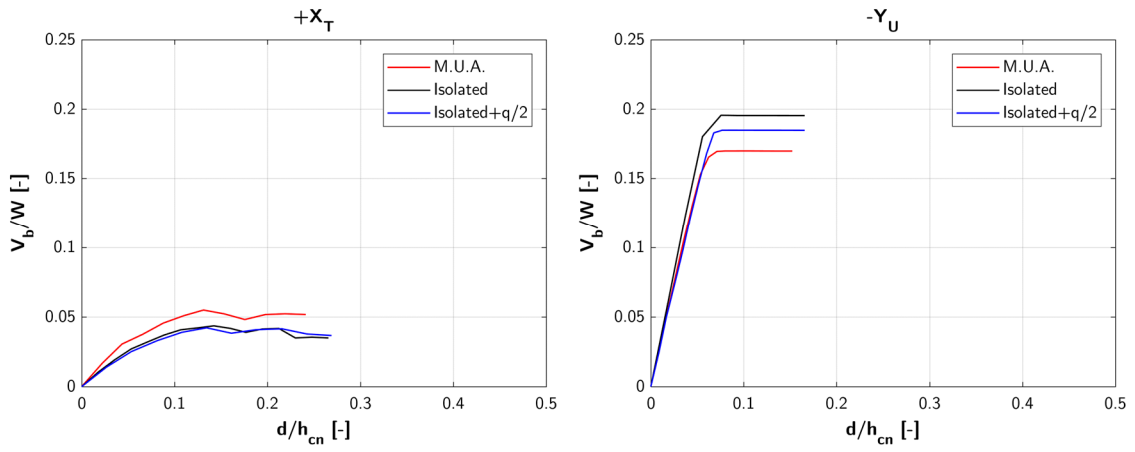

		Δ% α_{PGA}	Δ% k*	Δ% V_{bu}
X direction	**Isolated**	-1%	-17%	-21%
	Isolated + q/2	-1%	-24%	-23%
Y direction	**Isolated**	16%	12%	15%
	Isolated + q/2	4%	-3%	9%

*Results obtained for the R floors case

5.2.1.2 L aggregate

The first 3 modal shapes of the L aggregate for the hB and hC cases, in presence of both R and F floors, are shown in Figure 5-28. As previously observed for the row aggregate, the greatest displacements are in correspondence of the highest S.U.s. Also in this case, when the floors are rigid, the S.U.s are subject to rigid translation while, when they are flexible, the two parts of the aggregate moves in a differentiated way. This can also be noticed in the deformed configurations obtained from the pushover analyses, that are shown in Figure 5-29 and Figure 5-30 for X and Y direction, respectively.

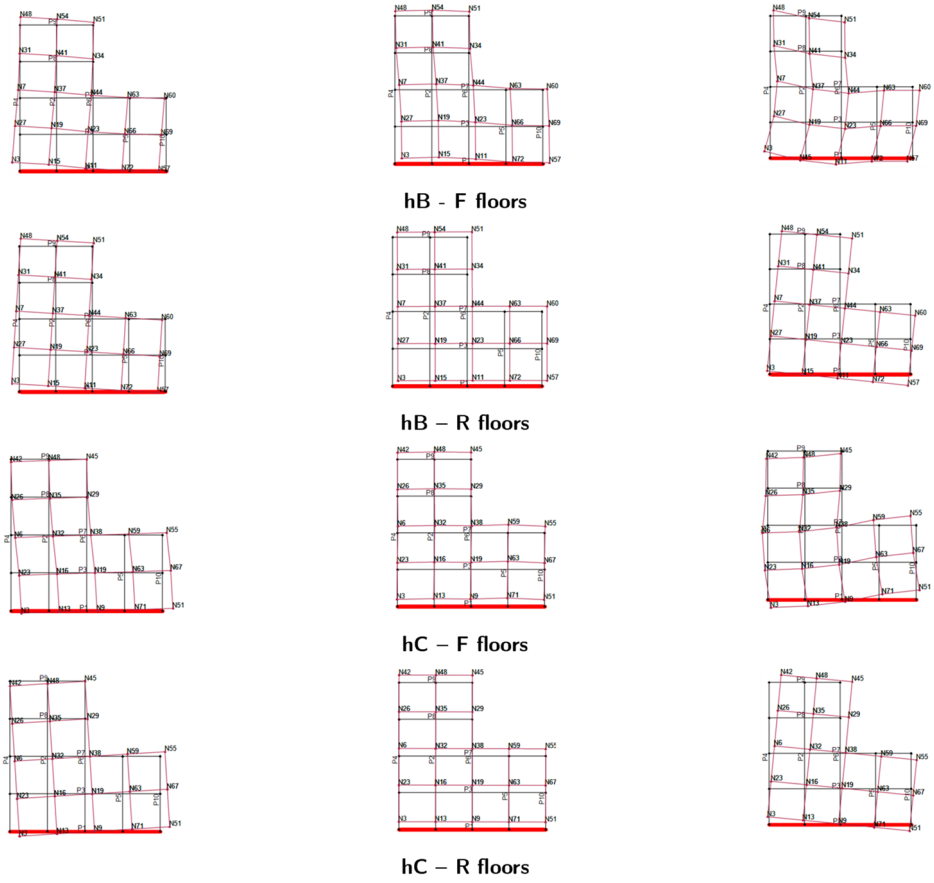

Figure 5-28: First 3 modal shapes of the row aggregate in presence of differences in height, for F and R floors.

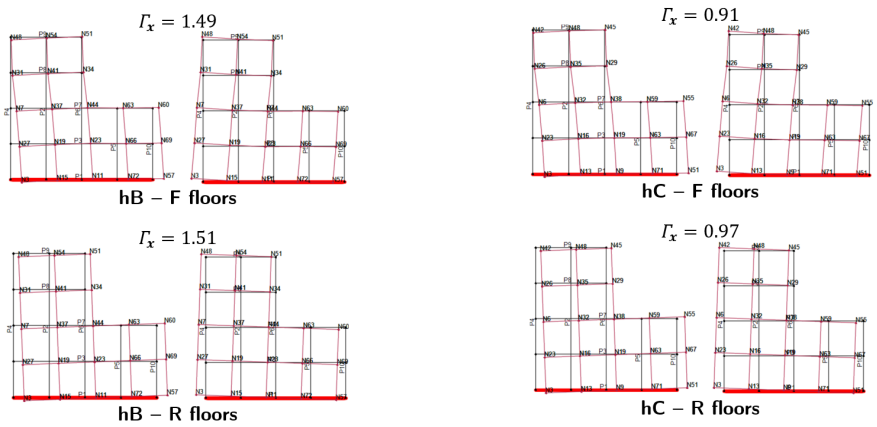

Figure 5-29: L aggregate – Deformed configuration in X direction (+X left, -X right) from pushover analysis in presence of differences in height, for F and R floors.

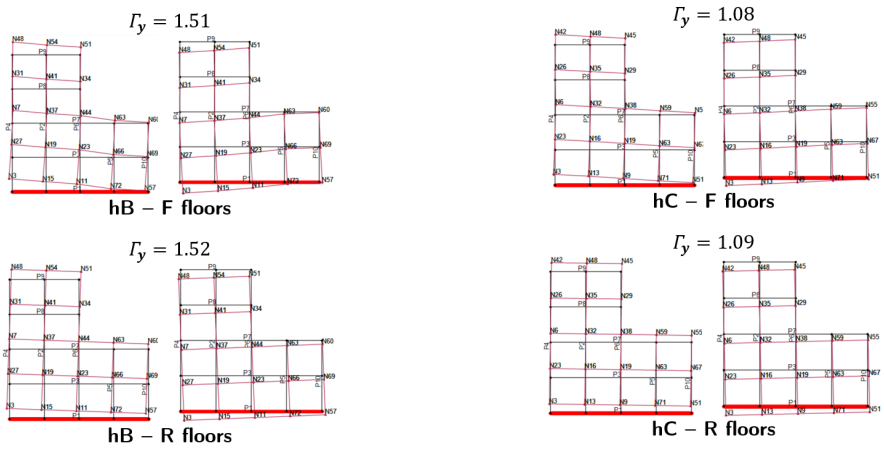

Figure 5-30: L aggregate – Deformed configuration in Y direction (+Y left, -Y right) from pushover analysis in presence of differences in height, for F and R floors.

For both hB and hC case, the M.U.A. individuated for the corner S.U. and for the external S.U. are shown in the following, together with the percentage changes of the maximum base shear V_{bu} and the stiffness k^* in respect to the reference configuration and the comparison of the results with those of the isolated conditions.

Considering the corner S.U., both for hB (Table 5-20) and for hC (Table 5-22) case, the M.U.A. differs by direction of analysis; as expected, configuration L6 (i.e., 3 S.U. X-row configuration with 1 adjacent S.U. in Y direction) is suitable for the analyses in X direction, while configuration L7 (i.e., 3 S.U. Y-row configuration with 1 adjacent S.U. in X direction) in Y direction.

However, for both cases hB and hC, model L1 (i.e., intermediate configuration with the immediately adjacent S.U.s) can be chosen as general M.U.A., regardless the direction of analysis, since the seismic behaviour of the target S.U. in this configuration is very similar to that of the reference model, both in X and Y direction.

Finally, model M3 (that excludes the opposite external S.U.) is the M.U.A. for the external S.U., for both cases (hB, Table 5-21; hC, Table 5-23), regardless of the floors stiffness.

From the comparison of the results of the M.U.A. with those of the isolated conditions, it is possible to notice that, also for the L aggregate the results are closely linked to the height of the target S.U.

In general, considering the corner S.U., the capacity of the isolated S.U., if taller (hB case), is inferior to that of the M.U.A. of about 10%. The same happens in X direction when it is adjacent to taller S.U.s (hC case). On the contrary, in Y direction the α_{PGA} of the isolated conditions increases.

For the external S.U., in hB case, the capacity of the M.U.A is major in comparison to that of the isolated S.U.s. in X direction of about 30%, but it is inferior in Y direction of about 100%. Moreover, in hC case, the capacity of the isolated conditions increases of more than 35% in both directions.

Table 5-20: M.U.A. in presence of differences in height: L aggregate – corner S.U. – hB.

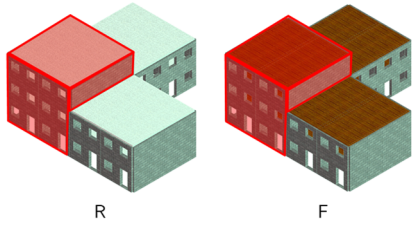

REFERENCE MODEL **M.U.A.**

L* **L6 in X direction** **L7 in Y direction** **L for both directions**

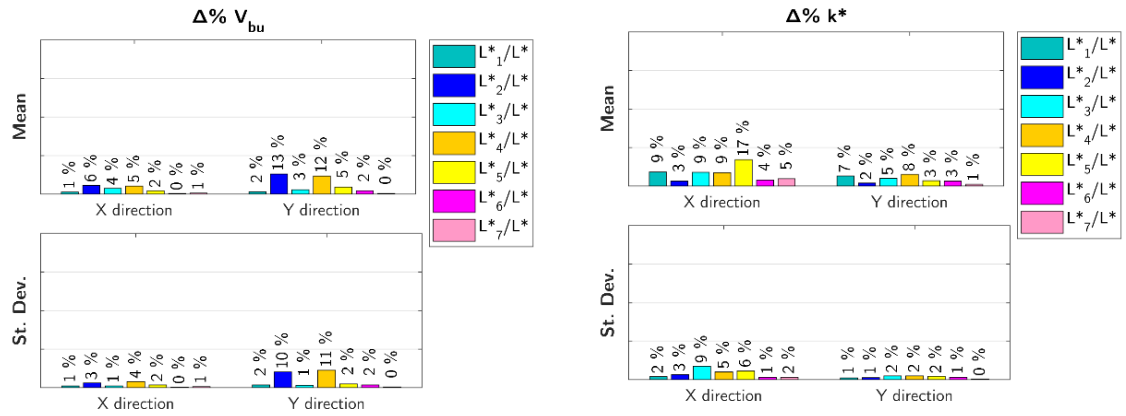

*Percentage changes obtained for the R floors case

Comparison with the isolated conditions

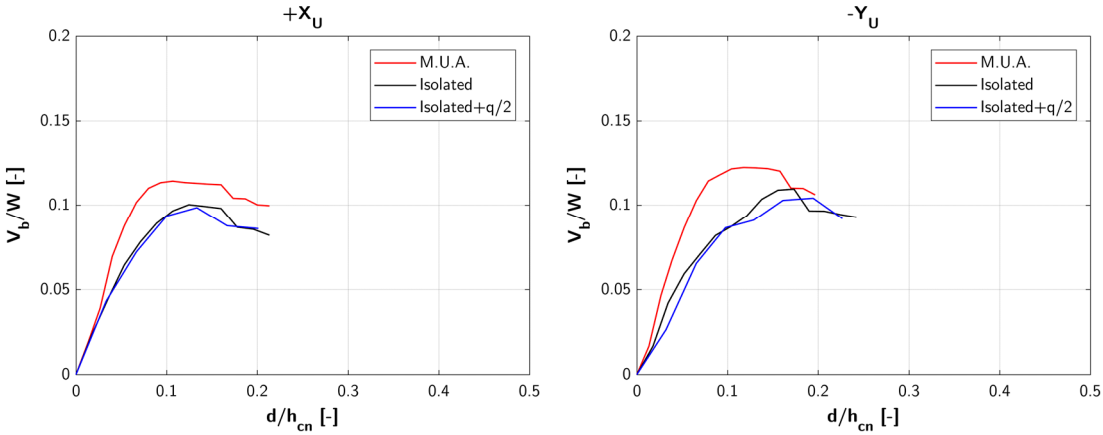

		Δ% α_{PGA}	Δ% k*	Δ% V_{bu}
X direction	**Isolated**	-1%	-31%	-12%
	Isolated + q/2	-12%	-35%	-14%
Y direction	**Isolated**	1%	-52%	-10%
	Isolated + q/2	-9%	-55%	-15%

*Results obtained for the R floors case

Table 5-21: M.U.A. in presence of differences in height: L aggregate – external S.U. – hB.

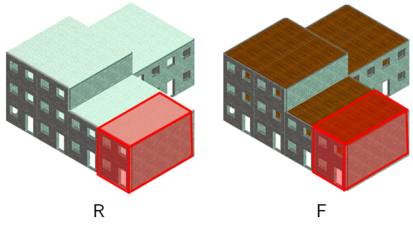

REFERENCE MODEL **M.U.A.**

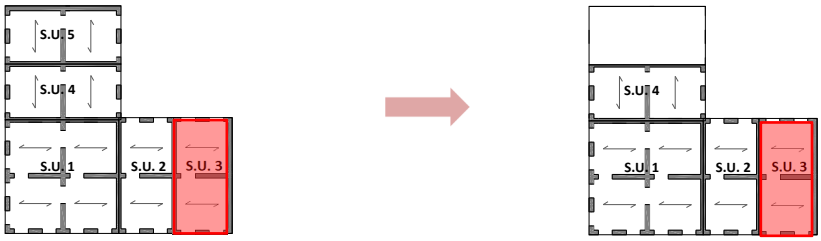

M* **M3**

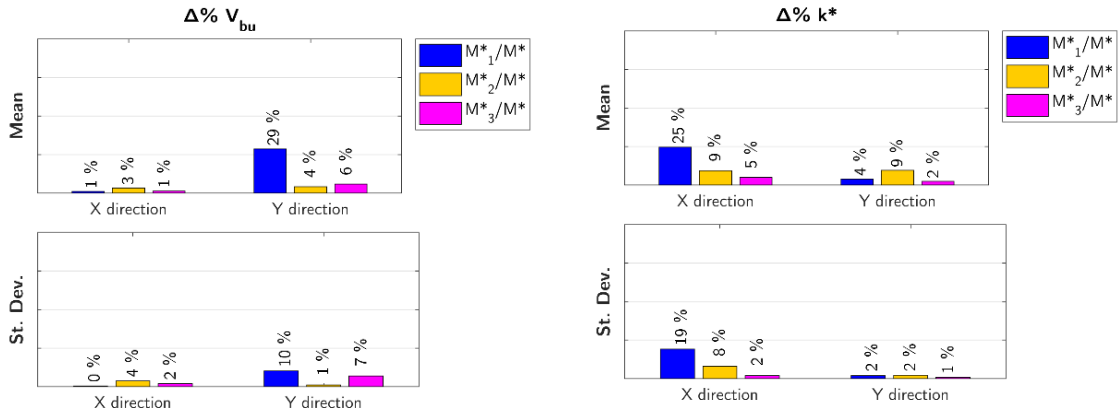

*Percentage changes obtained for the R floors case

Comparison with the isolated conditions

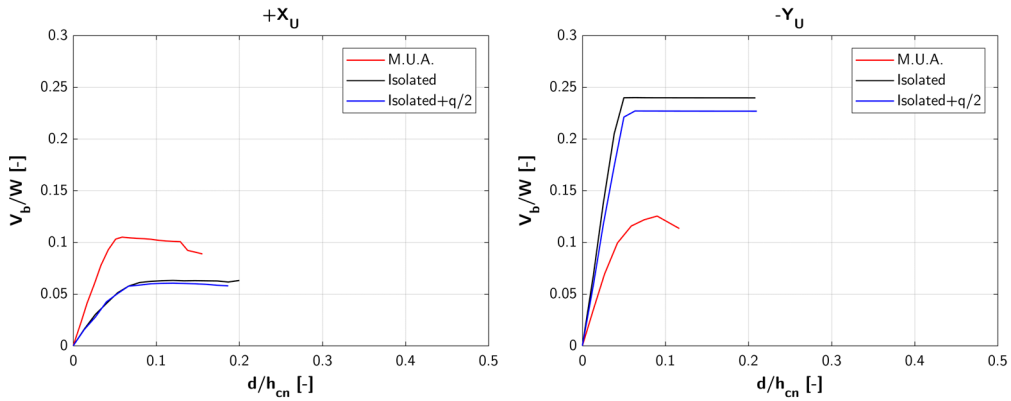

		Δ% α_{PGA}	Δ% k*	Δ% V_{bu}
X direction	**Isolated**	-31%	-57%	-40%
	Isolated + q/2	-37%	-55%	-42%
Y direction	**Isolated**	110%	123%	91%
	Isolated + q/2	94%	88%	81%

*Results obtained for the R floors case

Table 5-22: M.U.A. in presence of differences in height: L aggregate – corner S.U. – hC.

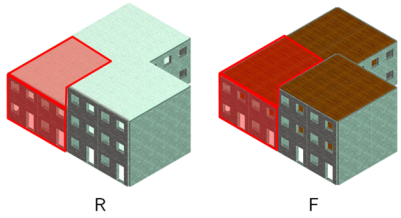

REFERENCE MODEL **M.U.A.**

L* **L6 in X direction** **L7 in Y direction** **L for both directions**

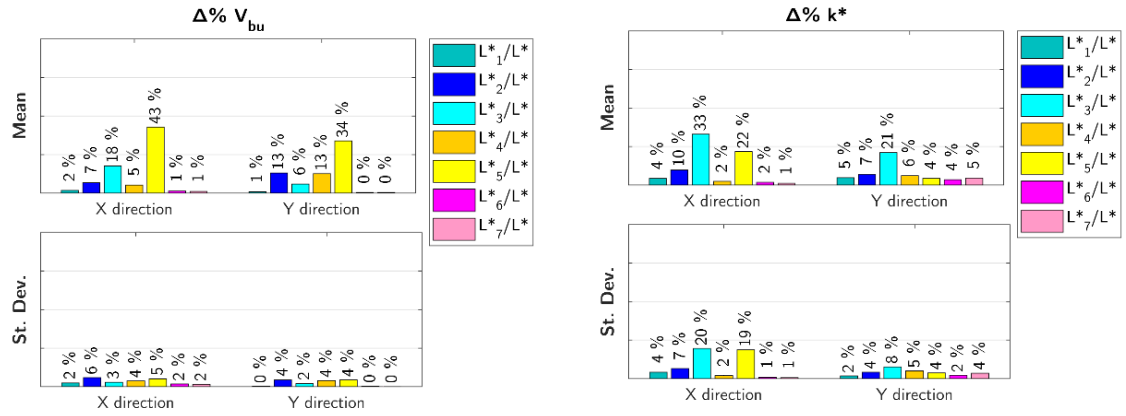

*Percentage changes obtained for the R floors case

Comparison with the isolated conditions

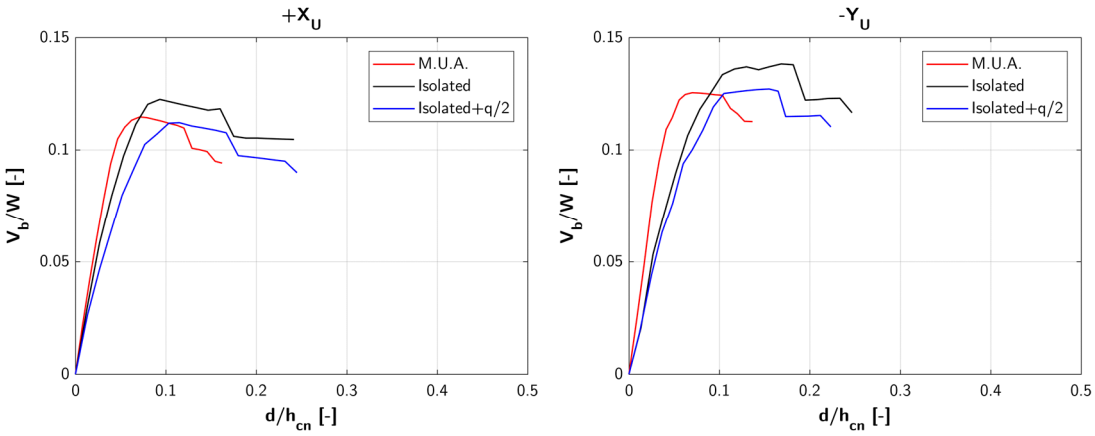

		Δ% α_{PGA}	Δ% k*	Δ% V_{bu}
X direction	**Isolated**	-8%	-23%	7%
	Isolated + q/2	-13%	-38%	-2%
Y direction	**Isolated**	12%	-48%	10%
	Isolated + q/2	1%	-56%	1%

*Results obtained for the R floors case

Table 5-23: M.U.A. in presence of differences in height: L aggregate – external S.U. – hC.

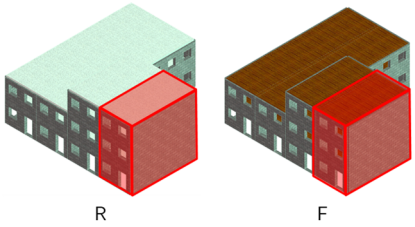

REFERENCE MODEL **M.U.A.**

M* **M3**

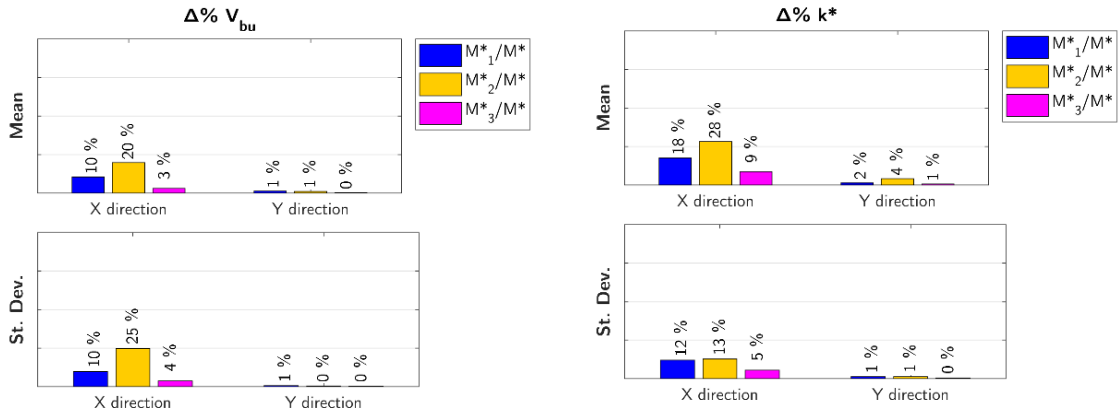

**Percentage changes obtained for the R floors case*

Comparison with the isolated conditions

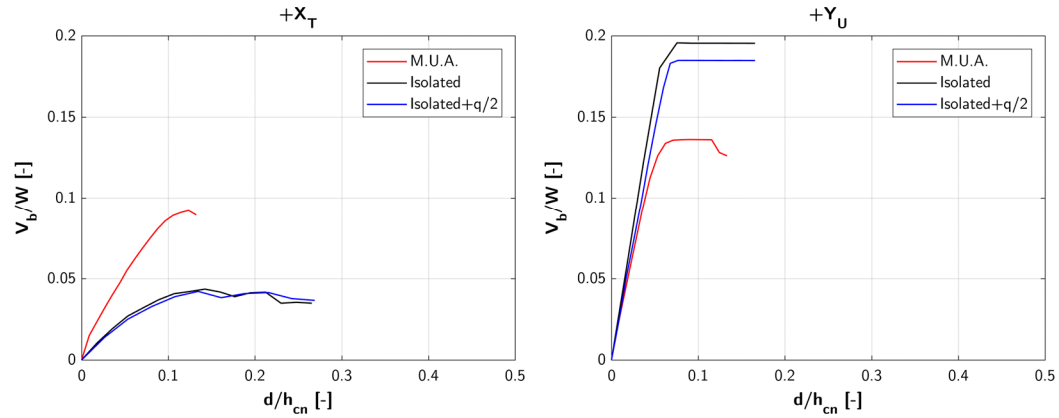

		Δ% α_{PGA}	Δ% k*	Δ% V_{bu}
X direction	**Isolated**	40%	-53%	-53%
	Isolated + q/2	39%	-57%	-54%
Y direction	**Isolated**	50%	27%	44%
	Isolated + q/2	36%	10%	36%

**Results obtained for the R floors case*

5.2.1.1 Conclusions

The differences in height are an influential factor too, as demonstrated by the sensitivity analysis (§4.8). The identification of M.U.A. changes in function of the position of the tallest S.U.s, regardless of the floors typology, in this case too.

Considering a row aggregate, when the internal S.U.s are the tallest in the aggregate, for the central one the M.U.A. should include the immediately adjacent buildings of the same height (Table 5-16).
In this configuration, for an external lower S.U., the M.U.A. results to be composed of the 3 adjacent taller S.U.s. (Table 5-17), even if the model with only 2 S.U.s presents similar results.
Instead, when the external S.U.s are the tallest in the aggregate and, consequently, the internal S.U. is adjacent to these on just one side, the M.U.A. excludes the external tallest S.U. (Table 5-18).
In this case, for the external taller S.U., the M.U.A. just includes 2 adjacent S.U.s (Table 5-19).

Considering a L aggregate (§5.2.1.2), the results do not change respect to the previous cases. For the corner building, the M.U.A. differs by direction of analysis as expected, regardless the floors typology: indeed, the X-row configuration with 1 adjacent S.U. in Y direction is suitable for the analyses in X direction, while the Y-row configuration with 1 adjacent S.U. in X direction is suitable for those in Y direction.
For an external S.U., the M.U.A. includes the longitudinal row in which this is placed and the first S.U. in the transversal row, adjacent to the corner building.

Finally, comparing the results obtained for the individuated M.U.A. and those of the isolated target S.U. and this one modelled with the pertinent masses deriving from the immediately adjacent structure, it can be observed that the results are closely linked to the height of the target S.U.
Considering the internal S.U. of the row aggregate, when this is one of the tallest, in both directions the α_{PGA} of M.U.A. is inferior to that of the isolated S.U., while is major respect that of the isolated S.U. + q/2; however, the deviations are inferior to 16% (Table 5-16). On the contrary, when it is adjacent to a taller S.U.s, the α_{PGA} of the isolated conditions is reduced in X direction, while it increases in Y direction (Table 5-17).
For the external S.U., when this is adjacent to taller S.U.s, the capacity of M.U.A. is major in both directions of analysis, apart from the isolated S.U. in Y direction (Table 5-18). Vice versa, when the external S.U. is one of the tallest, the α_{PGA} value changes in Y direction, with an increment especially in Y direction (Table 5-19).
Considering the corner S.U., the capacity of the isolated S.U., if taller, is inferior to that of the M.U.A. of about 10% (Table 5-20). The same happens in X direction when it is adjacent to taller S.U.s (Table 5-22). On the contrary, in Y direction the α_{PGA} of the isolated conditions increases.
For the external S.U., if lower, the capacity of the M.U.A is major in comparison to that of the isolated S.U.s. in X direction of about 30%, but it is inferior in Y direction of about 100% (Table 5-21). On the contrary, if this is taller, the capacity of the isolated conditions increases by more than 35% in both directions (Table 5-23).

5.3 CONCLUDING REMARKS

In this chapter, a new procedure, referred to as ***"target structural unit approach"***, is presented for the definition of the M.U.A. for the S.U. of interest (§5.1). It is a multi-level analysis procedure characterized by two main features: the definition of several intermediate boundary conditions for the target S.U. (in addition to the complete aggregate configuration) and the assessment of the seismic performance at:

- **Global- level**: analysis of the global modelling configurations;
- **S.U.- level**: analysis of the target S.U. in each modelling configuration;
- **Wall- level**: analysis of the boundary walls of the target S.U. in each modelling configuration.

The isolated condition is not analysed because it is an excessive simplification, that neglects the effects of interactions.

The S.U.- level is considered as the most important verification level, in which the M.U.A. is identified as the intermediate configuration providing the best representation of the seismic performance of the target S.U. in the aggregate. For this reason, the procedure is referred to as *"target structural unit approach"*.

The procedure consists of several phases.

1. **Preliminary phase**

This phase (§5.1.1) consists in the identification of the target S.U. and in the knowledge process of the aggregate. Moreover, all the possible modelling configurations $\boldsymbol{M_i}$ (i.e. all the possible M.U.A.) are defined.

2. **Seismic performance assessment phase**

The seismic performance of each modelling configuration M_i is assessed for the 3 levels of analysis previously mentioned (§5.1.2) by performing nonlinear static analyses. In particular, the seismic response of models $\boldsymbol{M^*_i}$ refers to that of the target S.U. (apex *) evaluated in the i model configuration. In detail, the pushover curves at S.U.- and wall- level are reproduced by considering displacements and base shear forces of the nodes belonging to the considered structure, as results of the analyses performed on the global models M_i. The maximum normalized base shear V_{bu} and the stiffness k^* are evaluated as SPI, as they are directly related to the seismic capacity variability. This phase allows identifying a preliminary M.U.A.

3. **M.U.A. assessment phase**

The seismic performance at S.U.- level of the configurations M^*_i (i=2:n) is compared with that of the complete aggregate condition (referred to as model M^*_1), that represents the **reference configuration**, namely the one that best represents the seismic performance of the target S.U. in the aggregate. In particular, the percentage changes of the SPI (maximum base shear V_{bu} and stiffness k^*) of models M^*_i in reference to M^*_1 (Eq. 51) are evaluated and the minimum values are sought. In fact, the M.U.A. corresponds to the global configuration M_i for which the model M^*_i results to have the closest seismic response to that of the reference configuration M^*_1.

The application of the procedure is meaningful only if the aggregate is exhaustively investigated and the modelling configurations are reliable. If the knowledge of the complete aggregate condition is affected by uncertainties, the reference configuration for the target S.U. can be unknow; in this case, the minimization process (Eq. 52) of the SPI performed for all models M^*_i, changing in rotation the reference configuration M^*_j, allows identifying the variation range of the M.U.A., excluding the extreme conditions.

The procedure is applied on the prototype aggregates (§5.2), considering both absence and presence of heterogeneities (of material and in height), and general schemes for the M.U.A. are provided. It should be highlighted that the only variation of the stiffness of the floors is equated with the absence of heterogeneities as its influence is not relevant, as shown in the previous Chapter 5.

With reference to the **row aggregate,** the M.U.A. for an **internal S.U.** should at least consist of the immediately adjacent S.U. on each side. This is suitable in the absence of heterogeneities (Table 5-4) or when this is between S.U.s of the same height (hB case, Table 5-16). In presence of material heterogeneities, if the target S.U. and the immediately adjacent ones are the most resistant and rigid in the aggregate (murB case, Table 5-8), the M.U.A. should also include the next less resistant one on each side; otherwise, its seismic capacity would be too much increased compared to the reference configuration. Moreover, when the internal S.U. is between equivalent S.U.s on one side and more resistant ones on the other side (murC case, Table 5-10), the M.U.A. should also incorporate the next more resistant one. Finally, if the internal S.U. is adjacent to taller S.U.s on one side (hC case, Table 5-18), the next one of the same height should also be included in the M.U.A., in addition to the immediately adjacent S.U.s.
Considering the **external S.U.**, the M.U.A. should be composed of 2 or 3 adjacent S.U.s. In absence of heterogeneities (Table 5-5), or when it is one of the most resistant in the aggregate (murC case, Table 5-11), or adjacent to taller S.U.s (hB case, Table 5-17), the M.U.A generally includes 3 adjacent S.U.s., but the model with only 2 provides similar results. When the target S.U. is adjacent to more resistant S.U.s (murB case, Table 5-9) or it is one of the tallest in the aggregate (hC case, Table 5-19), the M.U.A. should incorporate 2 adjacent S.U.s.

For the **L aggregate**, the M.U.A. results to be the same for all the cases, suggesting that its complex plan configuration is more influential than the investigated factors.
Considering the **corner S.U.**, two distinct M.U.A are individuated depending on the analysis direction, each of them excludes the external S.U. in the transversal row; for this reason, the general M.U.A. includes at least 2 S.U.s on each side.
For the **external S.U.**, the M.U.A results to be the configuration that excludes the opposite external S.U.

With the aim to provide general indications for the M.U.A. definition, the distribution of the **conventional strength value, C,** of each S.U. in the aggregate is introduced. The conventional strength is the ratio between the shear resistance value and the weight; it is introduced in the GNDT II Level Form (§2.5.1.1) and, starting from Eq. 10, is here evaluated in a simplified way as follows:

$$C = \frac{A_0 \tau_k}{p} \tag{53}$$

in which: $A_0 = A_R/A_{tot}$ is the resistant area, τ_k is the shear resistance of the masonry and $p = W/A_{tot}$ is the average weight per unit area of the S.U.
The ratio between the C values of adjacent buildings can give an indication of the influence between them. With reference to the defined basic S.U.s (Figure 4-2), Table 5-24 resumes the corresponding value of the conventional strength, C, in X direction, since this is the direction of expansion of the aggregate and the "aggregate effect" is more relevant.

Table 5-24: Values of the conventional strength C in X direction for each basic S.U.

Basic S.U.	C
2 storeys - stone masonry	0.03
2 storeys – hollow brick masonry	0.54
3 storeys - stone masonry	0.02

Considering the **row aggregate**, Figure 5-31 shows the distribution of the conventional strength C in X direction for each S.U., in function of all the analysed cases. The investigated target S.U.s are highlighted in blue (internal S.U.) and green (external S.U.); moreover, the average value of the conventional strength, C_{av}, of the aggregate is indicated in red.

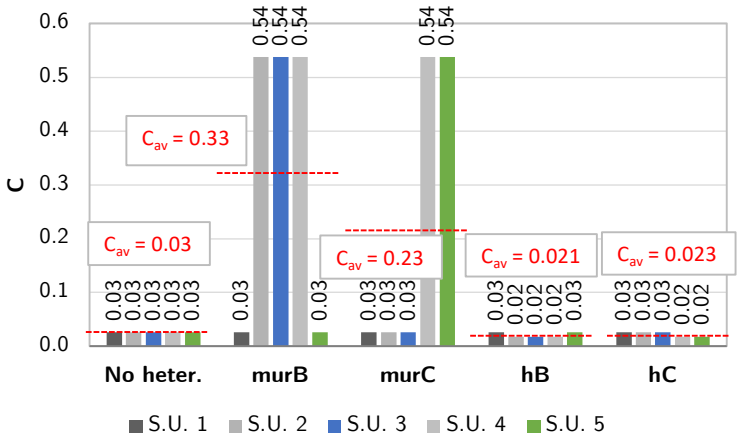

Figure 5-31: Row aggregate: distribution of the conventional strength C in X direction for the analysed cases.

With reference to the **internal S.U.**, the M.U.A. identified for each case are schematized in Figure 5-32. When the target S.U. is between S.U.s having the same value of C and the change respect to the average value is null (no heter.) or low (hB case), the M.U.A generally includes the immediately adjacent S.U. on each side. Vice versa, when the change is greater than 50% (murB case), the M.U.A. should also include the next less resistant S.U.s on each side. Moreover, if the internal S.U. is between S.U.s of equivalent C value on one side and S.U.s of different C value on the other (murC or hC case), the M.U.A. should also include, in addition to the immediately adjacent S.U.s, the next one more resistant (major C value).

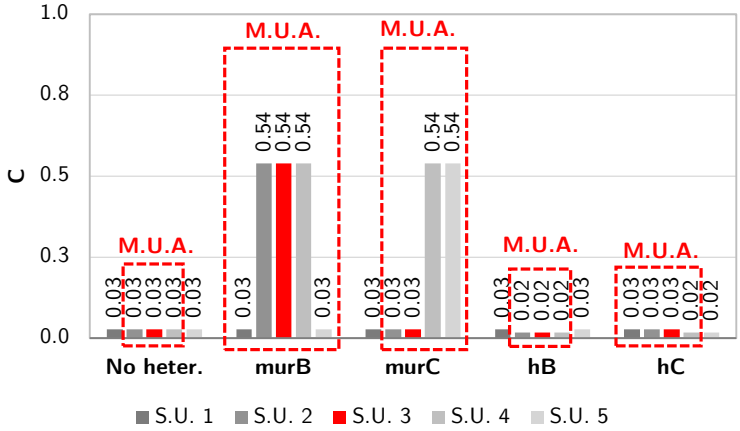

Figure 5-32: Row aggregate – internal S.U.: M.U.A. in terms of the conventional strength (C) distribution in X direction.

With reference to the **external S.U.**, the M.U.A. individuated for each case are schematized in Figure 5-33. When the target S.U. is adjacent to S.U.s of equivalent C (no heter.) or when it presents the major C value (hB and murC case), the M.U.A generally includes 3 adjacent S.U.s. but, as previously mentioned, the model with only 2 adjacent S.U.s provides similar results. Moreover, when the C value of the external S.U. is inferior to the average value of the aggregate and it is therefore adjacent to more resistant S.U.s (murB and hC case), the M.U.A. includes the 2 adjacent S.U.s.

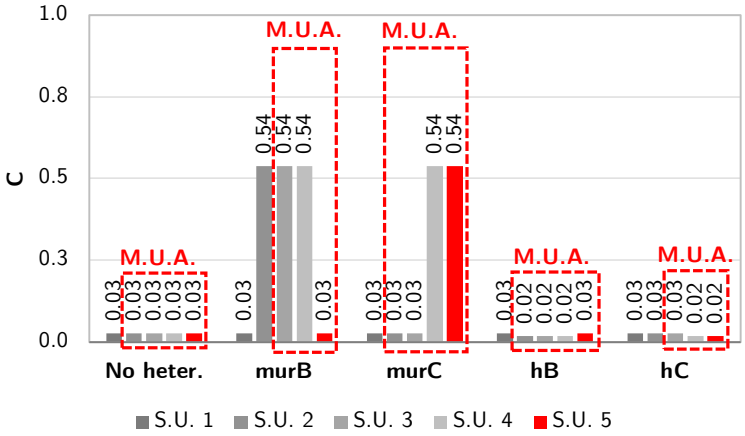

Figure 5-33: Row aggregate – external S.U.: M.U.A. in terms of the conventional strength (C) distribution in X direction.

Finally, in order to quantify the error that a too simplified modelling can produce, the results obtained for all the individuated M.U.A. are compared with those of the corresponding isolated condition (referred to as "isolated") and the isolated S.U. modelled with the loads deriving from the adjacent structures (referred to as "isolated+q/2"), as suggested by NTC 2008. The percentage changes are shown for the different investigated cases.

For the **internal S.U.** of the **row aggregate**, the percentage change of α_{PGA} is shown in Figure 5-34 for both directions of analysis.

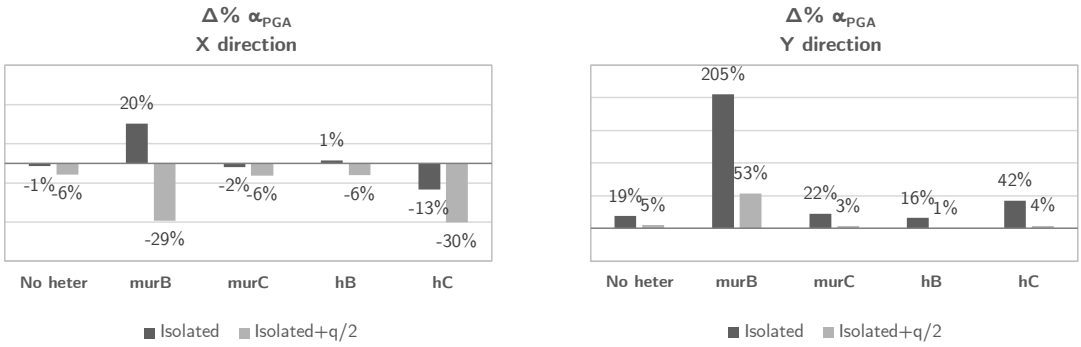

Figure 5-34: Row aggregate – internal S.U.: percentage changes of α_{PGA} for the isolated conditions in comparison to the M.U.A.

As it can be noticed, the isolated conditions generally present a reduction of the seismic capacity in the longitudinal direction and an increment in the transversal one, suggesting that a simplified model can be in favour of safety in the first direction, but not in the second one.

The lowest changes are in absence of heterogeneities (no heter.), while the greatest variation is when the internal S.U. is one of the most resistant in the aggregate (murB case); indeed, in this case, the isolated conditions do not consider the presence of less resistant S.U.s, that reduce the capacity of the M.U.A.

With reference to the **external S.U.** of the **row aggregate**, the percentage change of α_{PGA} is shown in Figure 5-35 for both directions of analysis.

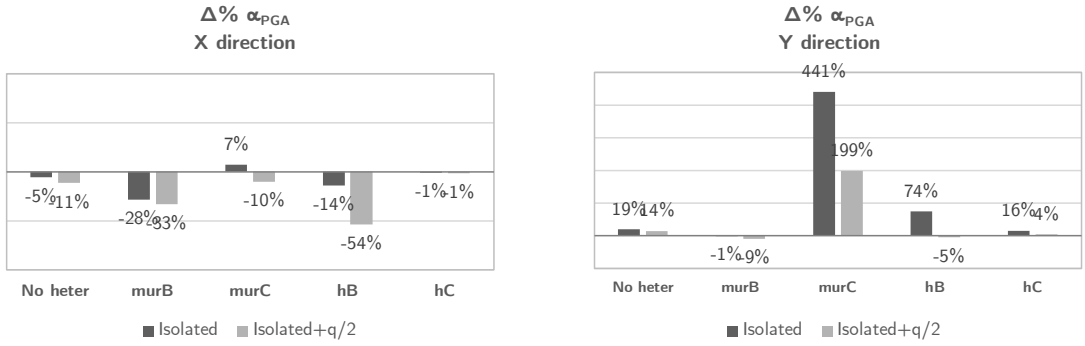

Figure 5-35: Row aggregate – external S.U.: percentage changes of α_{PGA} for the isolated conditions in comparison to the M.U.A.

It is evident that the trend is the same previously observed for the internal S.U.: the isolated conditions generally present a reduction of the seismic capacity in the longitudinal direction and an increment in the transversal one. However, the changes are major.

Finally, considering the **corner S.U.** of the **L aggregate**, the percentage change of α_{PGA} is shown in Figure 5-36 for both directions of analysis.

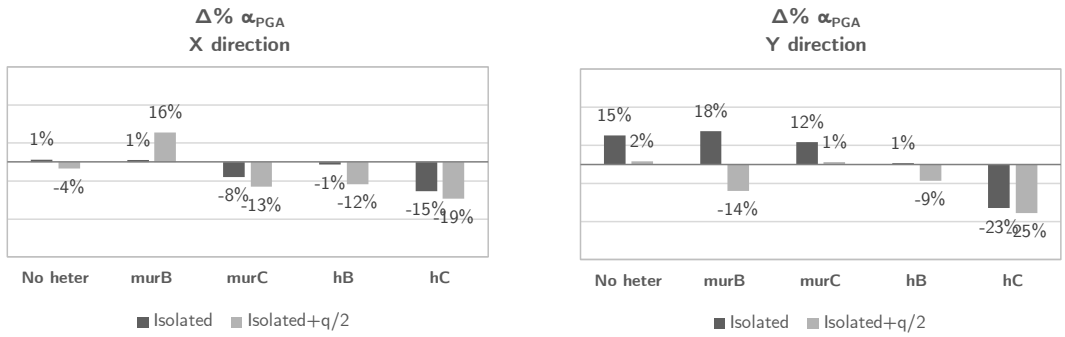

Figure 5-36: L aggregate – corner S.U.: percentage changes of α_{PGA} for the isolated conditions in comparison to the M.U.A.

It is possible to observe that, in this case, the changes are inferior to 25%. The major variation is for the case in which the corner S.U. is adjacent to taller S.U.s (hC case).

Chapter 6.
Validation of the proposed procedure

In this chapter, the proposed "target structural unit approach" is validated by considering two case studies. The first is an L aggregate located in Faro (Portugal); the second is a row aggregate located in Castelnuovo (L'Aquila). For both, the "aggregate effect" is investigated by analysing target S.U.s in different positions. The complete results are shown in Annex B.

Contents

6.1 L AGGREGATE IN FARO (PORTUGAL)

In this paragraph, a masonry aggregate located in the "Bairro Ribeirinho" neighbourhood in Faro (Portugal) is analysed, aiming at investigating the "aggregate effect" on different target S.U.s: the corner and the external one. Some preliminary results are illustrated in Bernardini et al. (2018, 2019).

6.1.1 Built environment

The "Bairro Ribeirinho" neighbourhood is part of the historical centre of the city and it was recently subject of study in the scope of a national project entitled "URBSIS: Assessing Vulnerability and Managing Earthquake Risk at Urban Scale", commissioned by the Faro City Council, (Vicente, et al., 2016).
The aggregate has a square shape and it is composed of a total of 11 S.U.s constructed in different time periods (Figure 6-1). In this study, however, only a part of it is considered, due to the presence of structural discontinuities with the remaining part.

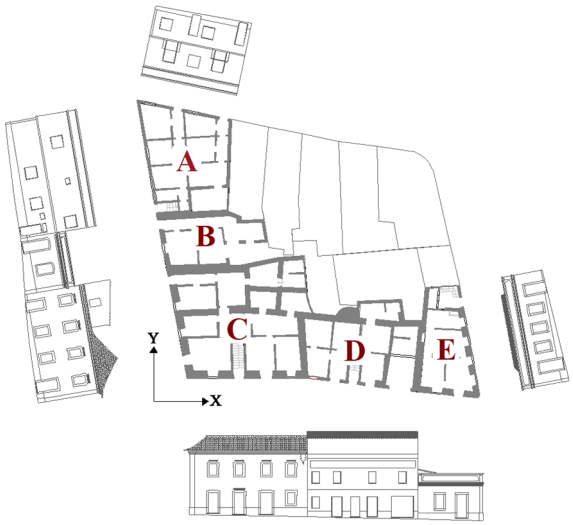

Figure 6-1: Faro aggregate: architectural plans with main façades.

The investigated S.U.s are:

- the corner S.U. C,
- the external S.U. A.

6.1.1 Knowledge process

6.1.1.1 Geometric survey

The aggregate is characterized by a square conformation with a small courtyard; each side is about 30 m and the maximum height is 9.30 m. The number of floors is generally 2 and they are slightly staggered, with an average inter-floor height of 3 m.

Figure 6-2: Faro aggregate: main façades.

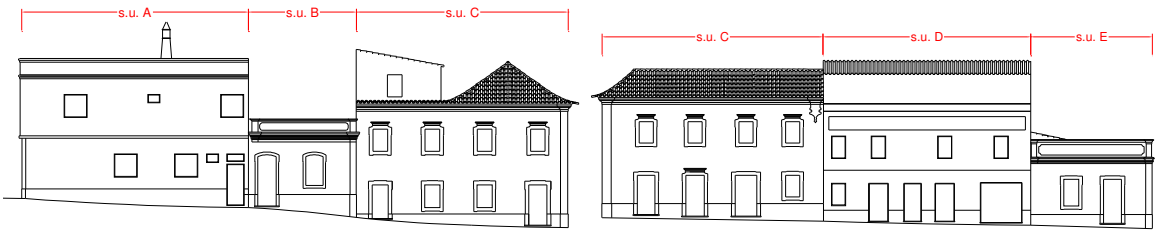

Figure 6-3: Faro aggregate: geometric survey.

6.1.1.2 Structural survey

The aggregate is mainly composed of limestone masonry, except for the partitional walls and the S.U. A, characterized by hollow clay bricks masonry. Several floors typologies are present, from wooden floors to that composed of prefabricated reinforced-concrete beams with voided concrete blocks. Moreover, the roofs are both traditional timber structures and "Santa Catarina" terrace typology (Maio et al., 2015). The structural drawings are illustrated in Figure 6-4.

S.U. A is a two-storey building presenting a rectangular layout of about 12x10 m^2 and a total height of 8.0 m. The thickness of load-bearing walls varies between 15 cm and 30 cm, respectively for partition and external walls, and are executed in hollow clay bricks masonry. While floors slabs are made of voided concrete slabs, the roof is a "Santa Catarina" terrace typology.

S.U. B, instead, is a single-storey limestone masonry building with a rectangular layout of about 6x11 m^2 and a total height of 5.0 m. The external walls are made of quite regular limestone masonry about 50 cm thick, partition walls are made of hollow clay brick masonry about 15 cm thick. The roof system is a traditional timber structure.

S.U. C has a total height of 9.0 m, presents a square-shaped layout of about 12x12 m^2 and bonds its sidewalls with the adjacent buildings. The façade walls are composed of quite regular limestone masonry, about 70 cm thick, with about 5 cm of lime-sand plaster on each side of the wall. Interior partition walls instead are executed in 11.5 cm thick hollow clay bricks. With regard to the horizontal structure, the

building presents both traditional timber floors and voided concrete slabs. The roof structure comprises a timber kingpost hip roof truss system of three hip rafters (known as "telhados de tesouro") and also "Santa Catarina" terraces.

S.U. D is a three-storey building with a rectangular layout of about 12x9 m^2 and a total height of 9.0 m. External walls at the ground floor level are made of limestone masonry about 30 cm thick, while the partition ones are executed in hollow clay bricks masonry about 15 cm thick. The horizontal structure consists of both traditional timber floors and roofs, and "Santa Catarina" terraces.

Finally, S.U. E is a single-storey limestone building presenting a rectangular layout of about 11x7 m^2 and a total height of 5.0 m. External walls are about 65 cm thick and partition walls are made of hollow clay brick masonry about 15 cm thick. The roof is a traditional timber truss structure.

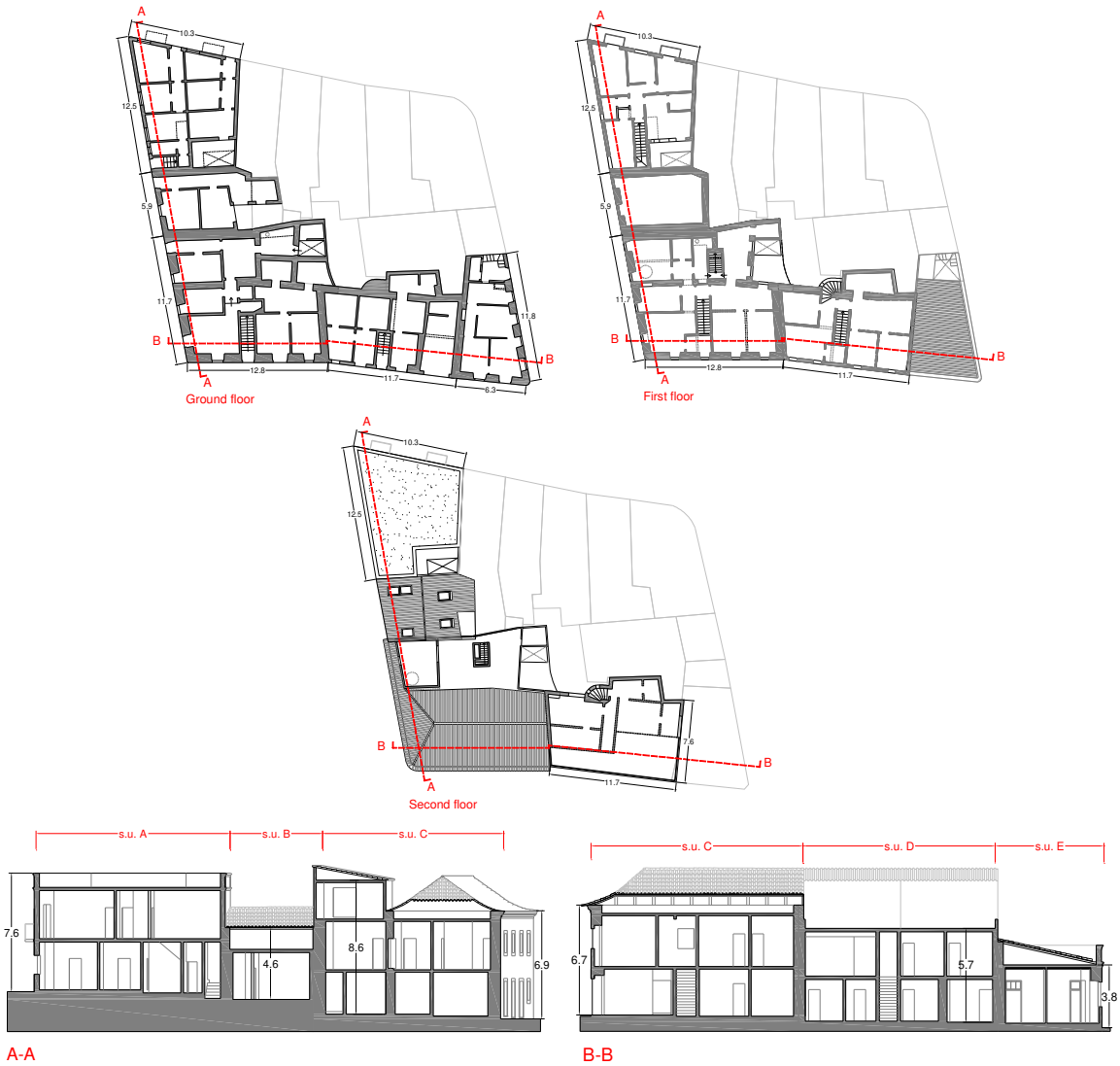

Figure 6-4: Faro aggregate: structural survey.

6.1.2 Numerical modelling

The three-dimensional model is developed by using the commercial release of 3Muri software code (STADATA, 2017). The geometry is defined accordingly to the plans.

With regards to the masonry typologies, the classification proposed by C.M. 617/2009 (Tab. C8A.2.1) is assumed. Hence, the typology "double-leaf stone masonry in rough-hewn with internal nucleus" (2nd category from Tab. C8A.2.1) is assigned to limestone masonry walls, while the typology "masonry in hollow brick blocks with a perforation percentage smaller than 45%" (8th category from Tab. C8A.2.1) is assigned to hollow clay brick masonry walls. As introduced in paragraph 3.3.2, a knowledge level KL1 is assumed. Additionally, due to the poor state of preservation of masonry fabric, a cracked stiffness condition is applied to the stiffness parameters. The values of the mechanical characteristics of the masonry typologies are resumed in Table 6-1.

Table 6-1: Faro aggregate: mechanical properties assigned to masonry panels.

Material	E [MPa]	G [MPa]	w [kN/m^3]	f_m [N/cm^2]	τ_0 [N/cm^2]
Limestone masonry	615	205	20	148.15	2.60
Hollow brick masonry	2250	675	12	296.30	22.20

Regarding the horizontal elements, the mechanical properties assigned to the diaphragms are resumed in Table 6-2. Timber floors and roofs are modelled as orthotropic finite element membranes with an equivalent thickness, s, equal to 5 cm. Voided concrete slabs (also referred to as mixed composite floors) are represented as a continuous concrete slabs 5 cm thick concrete class C16/20. Finally, "Santa Catarina" terraces are also represented as voided concrete slabs 4 cm thick.

Table 6-2: Faro aggregate: mechanical properties assigned to floors.

Floors	$E_{1,eq}$ [MPa]	$E_{2,eq}$ [MPa]	G [MPa]	ν [-]	G_k [kN/m^2]	Q_k [kN/m^2]
Timber floors	9000	5000	300	0	0.8	2
Timber roofs	9000	5000	300	0	1	0.4
Voided concrete slabs	43500	29000	12000	0.2	1.5	2
"Santa Catarina" terraces	36000	20000	8300	0	2	2

To allow a more reliable comparison of the results, for the different analysed S.U.s, the control node is selected in a barycentric position of the target building and the pushover curves are normalised, as illustrated in 3.3.2.

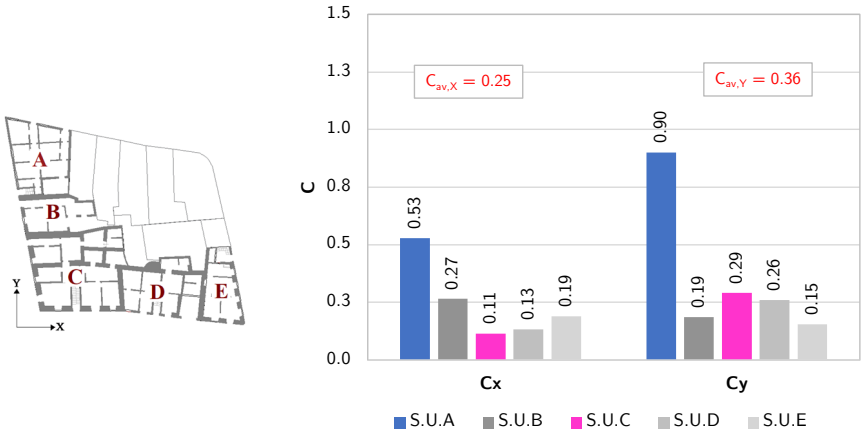

Figure 6-5: Faro aggregate: values of the conventional strength, C, for each S.U.

As shown in Figure 6-5, the conventional strength C is estimated from S.U. A to S.U. E, considering the two directions of analysis separately. The average value of the aggregate, C_{av}, is highlighted in red; moreover, the values of the investigated S.U.s A and C are highlighted in blue and pink, respectively.
It is possible to observe that, in general, the aggregate presents higher values of C in Y direction and S.U. A has the highest resistance. Considering the X direction, S.U. C presents the lowest value of C, while in Y direction S.U. B does.

6.1.3 Analysis of the corner S.U. C

The corner S.U. C is analysed. As it is possible to observe in Figure 6-6, where the distribution of the conventional strength C is shown, this is adjacent to S.U.s of similar C value, except for the external S.U. A. In this case, as noticed for the prototype aggregates, the M.U.A. is not influenced as much by the heterogeneities as by the plan configuration. Two distinct M.U.A should be individuated in function of the analysis direction, each of them excludes the external S.U. in the transversal row (highlighted in blue and green in the graphs); for this reason, the general M.U.A. should coincide with the complete aggregate (highlighted in red).

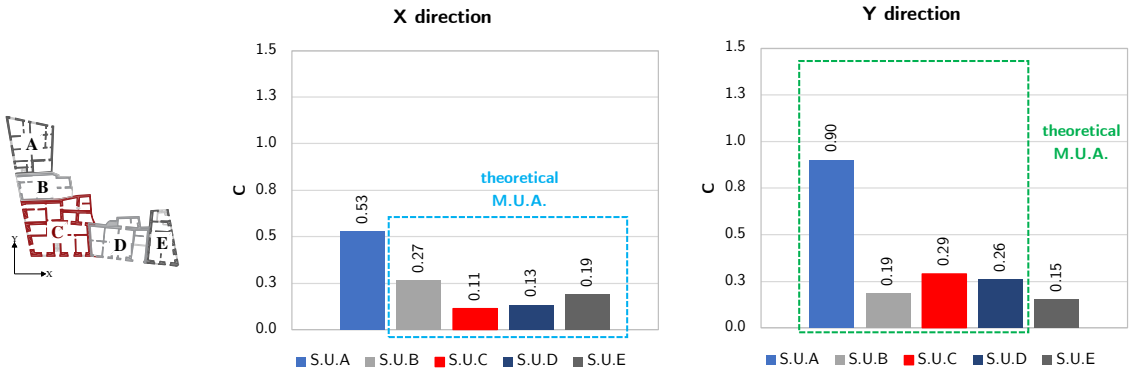

Figure 6-6: Faro aggregate – corner S.U. C: theoretical M.U.A. in terms of the conventional strength (C) distribution.

In order to validate this result, the proposed Procedure is applied to this target S.U. The considered modelling configurations and the results are shown in the following.

6.1.3.1 Modelling configurations

The location of the investigated walls and the control node is highlighted in Figure 6-7.
The modelling configurations investigated for the S.U.C are illustrated in the following Figure 6-8.

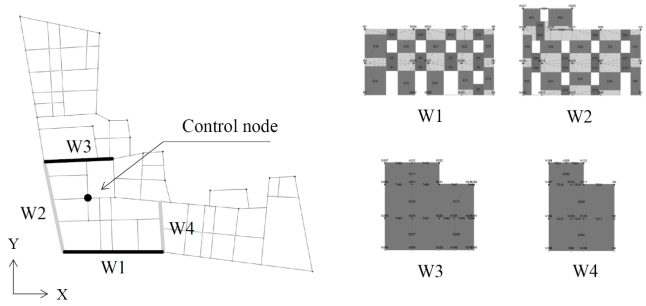

Figure 6-7: Faro aggregate – corner S.U. C: location of the investigated walls and the selected control node.

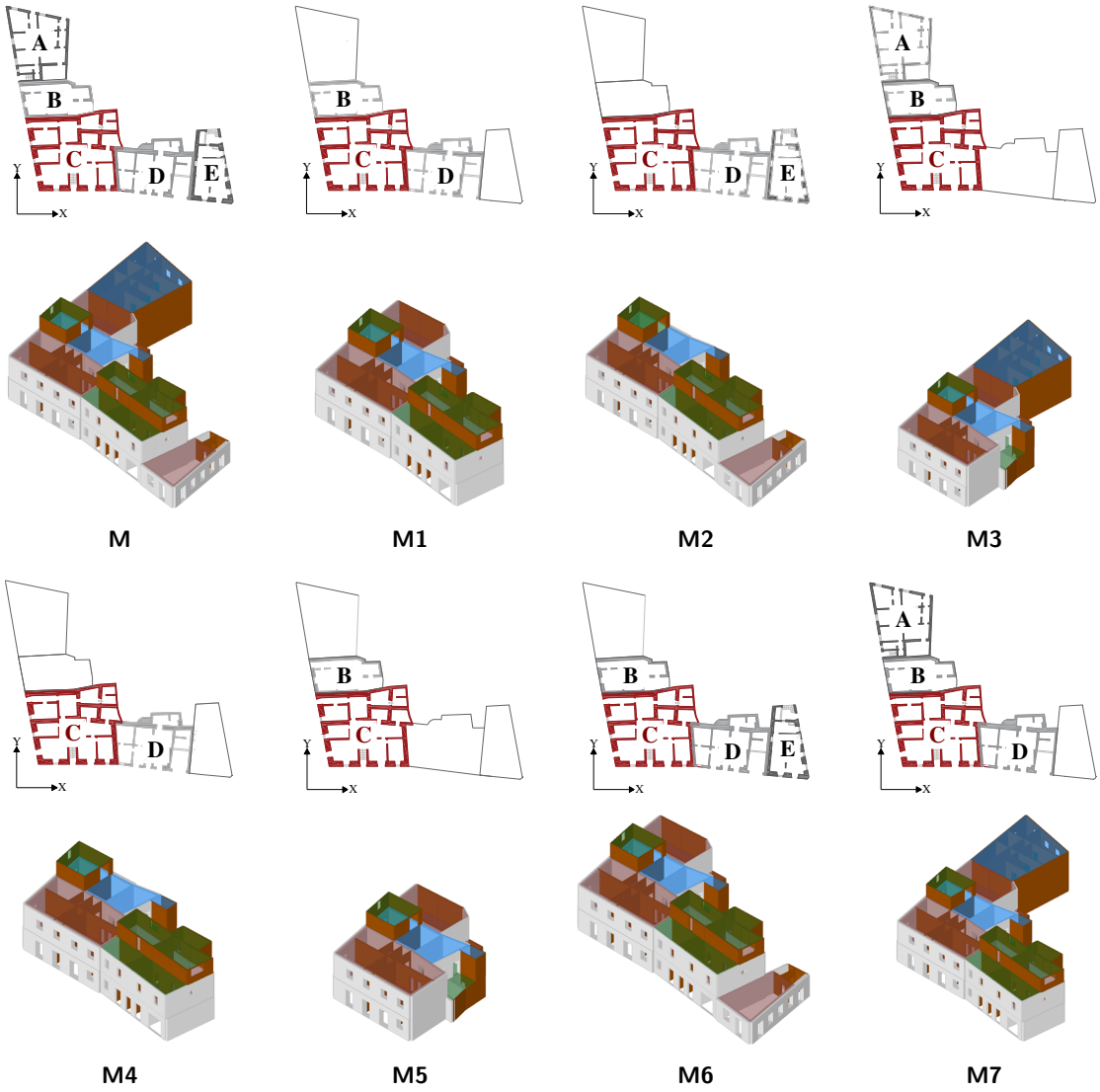

Figure 6-8: Faro aggregate – corner S.U. C: modelling configurations.

6.1.3.2 Seismic performance assessment phase

In this phase, the seismic performance of each modelling configuration M_i is assessed by performing nonlinear static analyses, by considering global-, S.U.- and wall- levels. The results are shown in the following.

Global- level

The pushover curves at global- level are compared in Figure 6-9 for all modelling configurations (from M to M7) by direction, considering the uniform load pattern distribution (U).

With reference to the X direction, models M and M7 present the highest capacity in terms of stiffness k^*, while model M5 results to be the most flexible. In terms of maximum base shear V_{bu}, the highest values are in general for M7, while the lowest are for M2. Moreover, the trend of the pushover curves of the intermediate condition M1 is similar to that of model M6; this indicates that the contribution of S.U. E is not relevant.

In Y direction, models M, M3 and M7 show the highest capacity, since all the S.U.s along the Y direction are modelled, while models M2 and M4, that do not consider them, have the lowest. Configurations M1, M5 and M6 have intermediate behaviour.

These first results indicate that the S.U. adjacent to the target building C along the X direction are a part of the aggregate in which damage is expected to be concentrated, which in turn might be originated either by a low thickness of masonry walls, a low ratio of effective resistant area in X direction, the presence of a single-storey building (S.U. E), or even by the apparent higher contribution of S.U. arranged along the Y direction (especially S.U. A) to the global stiffness.

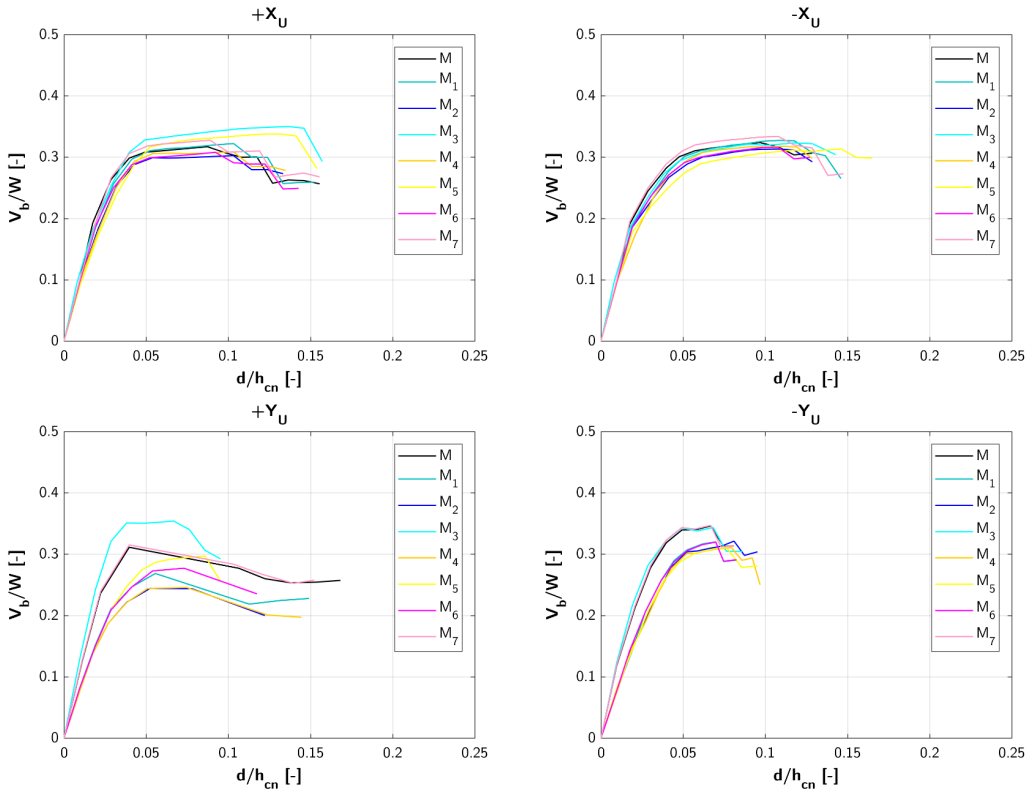

Figure 6-9: Faro aggregate – corner S.U. C: pushover curves at global- level.

In the light of these results and in accordance with the percentage distribution of the conventional strength C for each S.U. (Figure 6-5), it is possible to conclude that, globally, modelling configuration M7 presents the highest shear capacity, while models M2 and M5 the lowest.

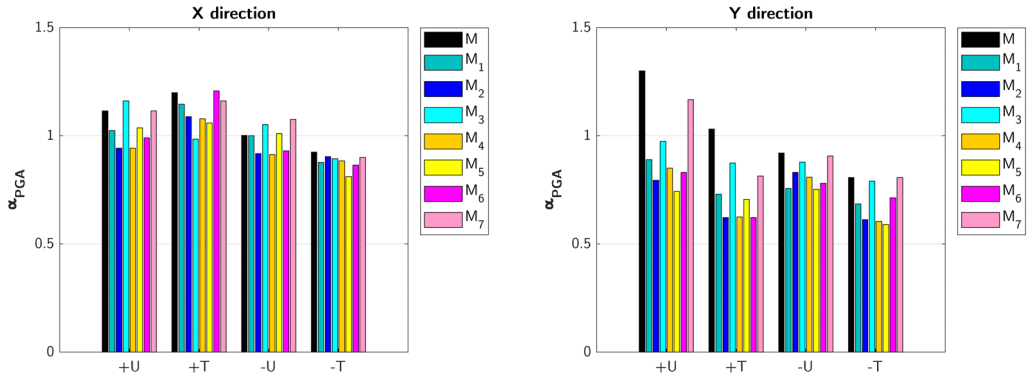

Figure 6-10: Faro aggregate – corner S.U. C: comparison of the α_{PGA} values for models M to M7, in X (left) and Y (right) direction.

Moreover, in Figure 6-10, the α_{PGA} values obtained for each modelling configuration are compared, from where it is possible to identify M2, M4 and M5 as the most vulnerable configurations in most of the analyses. Moreover, in the Y direction, practically none of the analyses verify safety, suggesting a higher vulnerability in this direction.

Wall- level

As previously mentioned, to investigate the actual influence of the different modelling configurations on the seismic response of S.U. C, the variability on capacity is also compared at the wall-scale level, namely for the façades and mid-walls identified in Figure 6-7. Hence, Figure 6-11 presents the pushover curves of walls W1 and W3, and W2 and W4, obtained for the uniform load pattern distribution in both directions of analysis.

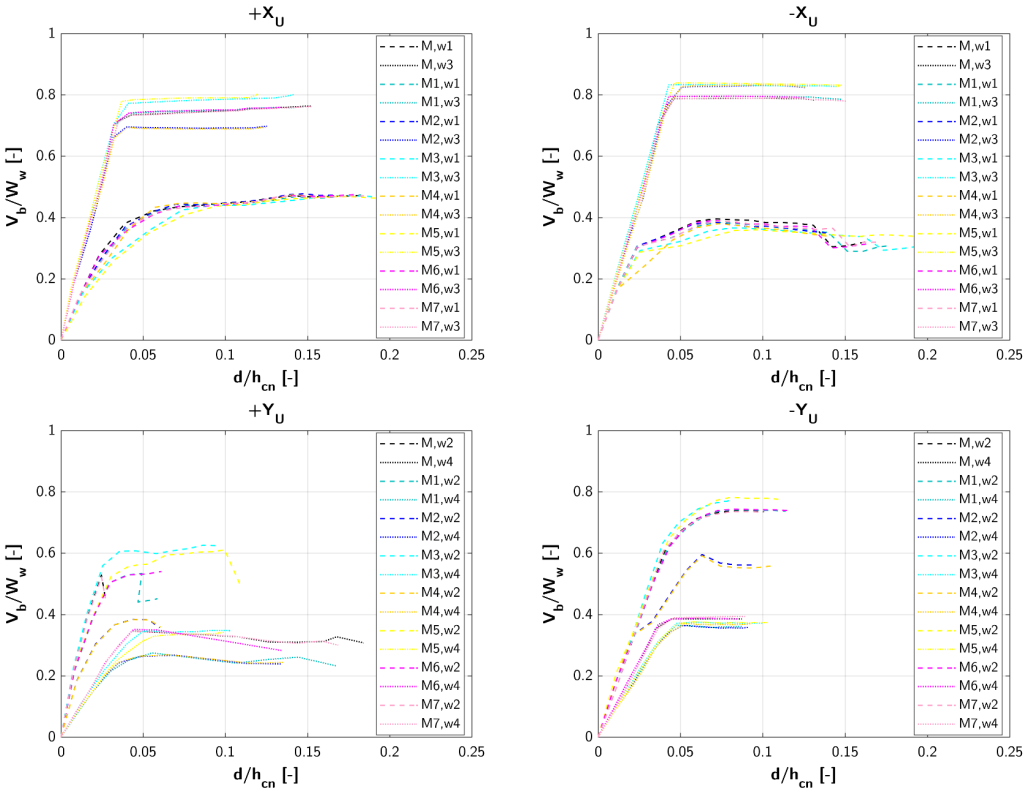

Figure 6-11: Faro aggregate – corner S.U. C: pushover curves at wall- level.

Firstly, the difference in terms of capacity between façades and mid-walls is quite significant. This is particularly evident in X direction, where the base shear capacity is practically doubled. In fact, these results can be partially explained by the fact that, being a blind-wall (with no openings), wall W3 carries part of the loads from S.U. B. The observed deviation with respect to façade W1 is indeed smaller in models M2 and M5, where S.U. B is not modelled. However, the contribution of wall W1 is way more relevant in the case of modelling configurations M1 and M2, while that of wall W3 in the case of M3 and M5. In Y direction, and despite the evident differences regarding the ratios of effective resistant area between the corresponding façade and mid-wall, façade W2 presents, in general, a higher stiffness and base shear capacity. This is due to the fact that wall W2 carries higher loads than the mid-wall W4. Moreover, wall W2 present the highest stiffness and shear capacity in models M3 and M5, while wall W4

in configurations M, M6 and M7. By contrast, the same walls present the lowest stiffness and base shear capacity in the case of modelling configuration M2 and M4.

S.U.- level

In the following Figure 6-12, the pushover curves obtained for the target S.U. C are compared for each modelling configuration, considering the uniform load pattern distribution (U) in both directions of analysis.

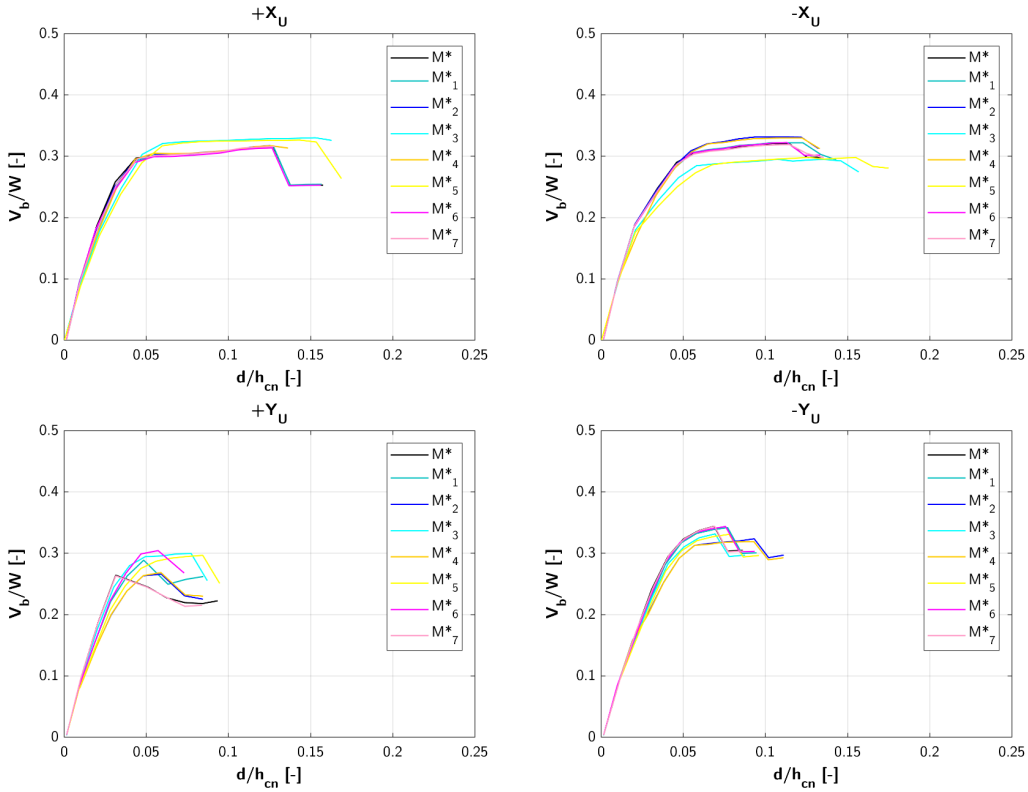

Figure 6-12: Faro aggregate – corner S.U. C: pushover curves at S.U.- level.

In X direction, the pushover curves of M*3 and M*5 have a similar trend, presenting the highest and the lowest base shear capacity, respectively in the positive and negative direction of X; however, in both cases, they show the lowest stiffness capacity. Moreover, M*2 and M*4 show very similar curves for most of the analyses, as also configurations M*, M*1, M*6 and M*7, and are characterized by the highest stiffness.
In Y direction, the results show a similar trend for the pushover curves of M*2 and M*4, with the lowest capacity in terms of stiffness and base shear. Moreover, the highest capacity in terms of base shear and stiffness is for models M* and M*7, and models M*1 and M*6, that show similar trends respectively. Finally, as previously noticed for the X direction, the trend of the curves of M*3 is similar to that of M*5.

In accordance with the previous results, the target S.U. C results to be more rigid when considered in the complete aggregate condition M and in the intermediate configurations M1, M6 and M7.
As can be noticed, its behaviour is not influenced by external S.U. E in any case.

Moreover, in Figure 6-13, the α_{PGA} values obtained for each modelling configuration are compared, from where it is possible to identify M*2 and M*4 (X-row conditions), M*3 and M*5 (Y-row conditions) as the most vulnerable configurations in the majority of the analyses. Moreover, in the Y direction, practically none of the analyses verify safety, confirming a higher vulnerability in this direction.

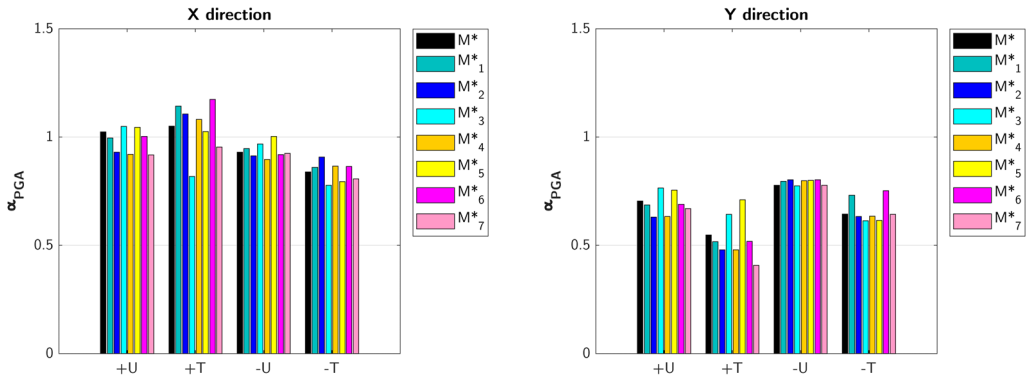

Figure 6-13: Faro aggregate – corner S.U. C: comparison of the α_{PGA} values for models M to M*7, in X (left) and Y (right) direction.*

6.1.3.3 M.U.A. assessment phase

With the aim to define the M.U.A., once that the seismic performance of the target S.U. C is assessed for all the considered modelling conditions, we are going to identify the model M*i characterized by the closest seismic capacity, in terms of stiffness and base shear, to that of the target S.U. modelled in the complete aggregate condition, namely model M*.

Figure 6-14 shows the mean values and respective standard deviations for each direction of the percentage changes of the maximum base shear V_{bu} and stiffness k^* for each configuration (M* to M*7), evaluated as given in Eq. 51.

In X direction, the minimum changes in terms of maximum base shear V_{bu} are observed for configurations M*1 and M*6, with an average value of 0% and a standard deviation of 0%, and also for M*4 and M*7, with an average value of 1% and a standard deviation of 1%. In terms of stiffness k^*, the minimum changes are for M*7, with an average value of 3%, and for M*1, M*2 and M*6, with average values of 4%. In Y direction, the minimum changes in terms of both maximum base shear V_{bu} and stiffness k^* are obtained for model M*7, with average values of 1%.

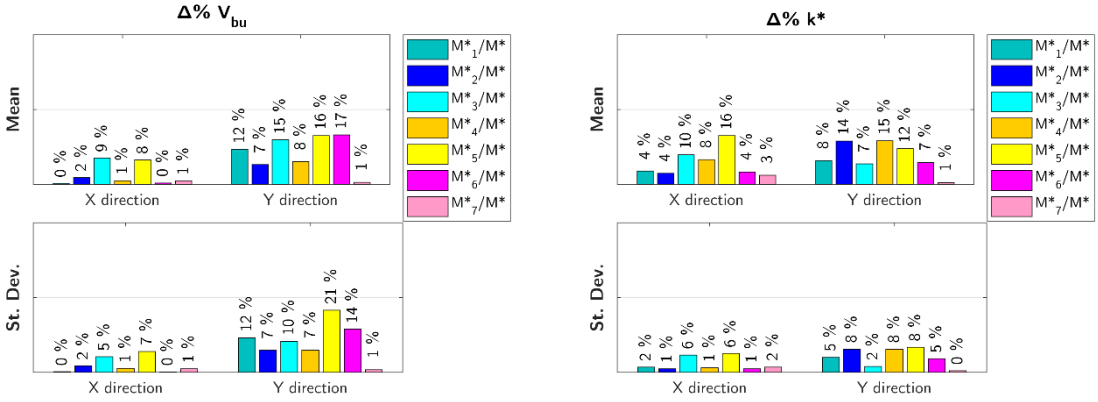

*Figure 6-14: Faro aggregate – corner S.U. C: mean and standard deviation of the percentage change of V_{bu} and k^* for M*i/M*.*

From these results, it is possible to conclude that the best M.U.A. in X direction are configurations M1, that includes the immediately adjacent S.U. B and D, and M7, that includes all the S.U.s along the Y direction (A, B and C) and the one (D) adjacent to the target S.U. along the X direction; this last is

also the best configuration in Y direction. For this reason, M7 can be chosen as the optimum M.U.A. for the corner S.U. C in both directions of analysis.

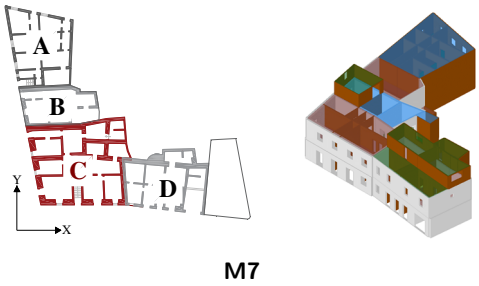

Figure 6-15: Faro aggregate – corner S.U. C: M.U.A.

In Figure 6-16, the theoretical M.U.A. and the one deriving from the procedure (highlighted in red) are compared in function of the distribution of the conventional strength, C. In X direction the M.U.A. should exclude the external S.U. A, placed in the transversal row; however, in this case study, S.U.A presents the major value of the conventional strength and it is very influent in the seismic response of the corner S.U. C. On the contrary, the external S.U. E does not influence it in any case, as previously observed from the pushover curve; therefore, it can be also excluded in the M.U.A. of the X direction.
Hence, the results are partially in accordance with those obtained for the prototype aggregates.

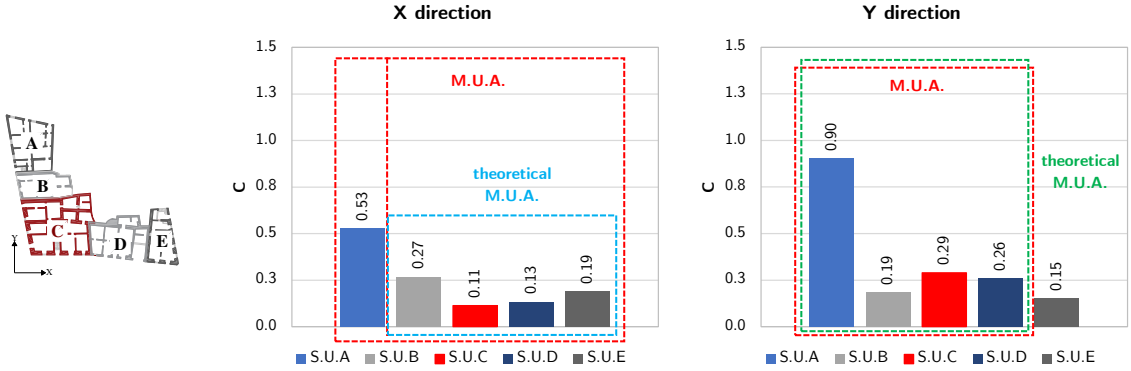

Figure 6-16: Faro aggregate – corner S.U. C: comparison between the theoretical and the individuated M.U.A. in terms of the conventional strength (C) distribution.

6.1.3.4 Comparison with the isolated conditions

The results obtained for the M.U.A. are compared with those of the isolated S.U.C and of this one modelled with the pertinent masses deriving from the immediately adjacent S.U.s B and D (hereinafter referred as "isolated + q/2" model).
The results obtained for the 3 conditions are compared in Figure 6-17, in terms of α_{PGA}, maximum base shear V_{bu} and stiffness k^*.
It should be noticed that the seismic capacity of the M.U.A. is very similar to that of the isolated conditions in both directions.

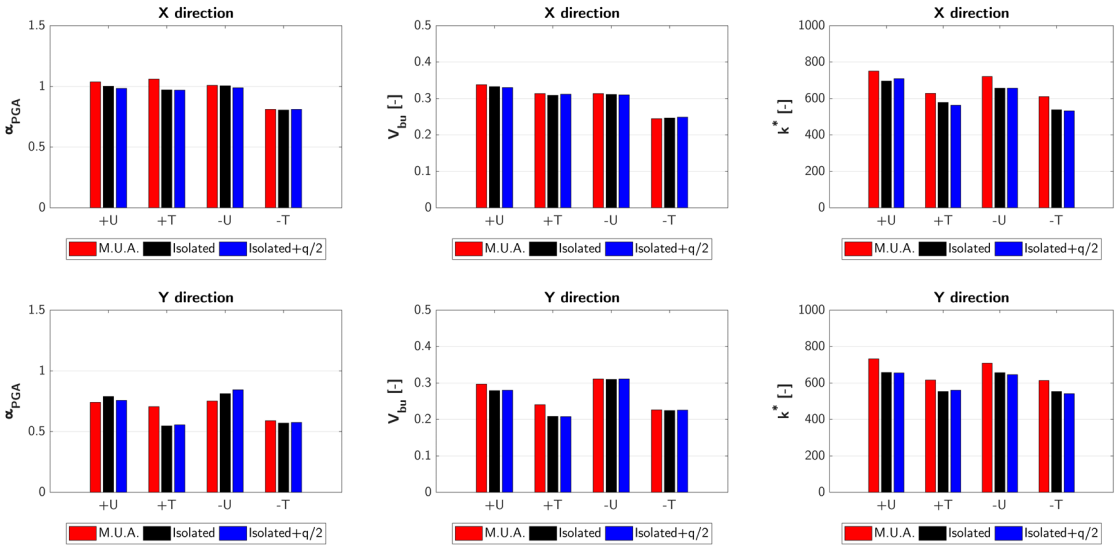

Figure 6-17: Faro aggregate – corner S.U. C: comparison of results between the M.U.A. and the isolated conditions.

In the following, only the analyses of each direction with the lowest value of α_{PGA} for M.U.A. are considered, that means -X and -Y triangular distribution.

In Figure 6-18, the pushover curves are compared; moreover, Table 6-3 shows the percentage changes, obtained in reference to the M.U.A., for the isolated conditions.

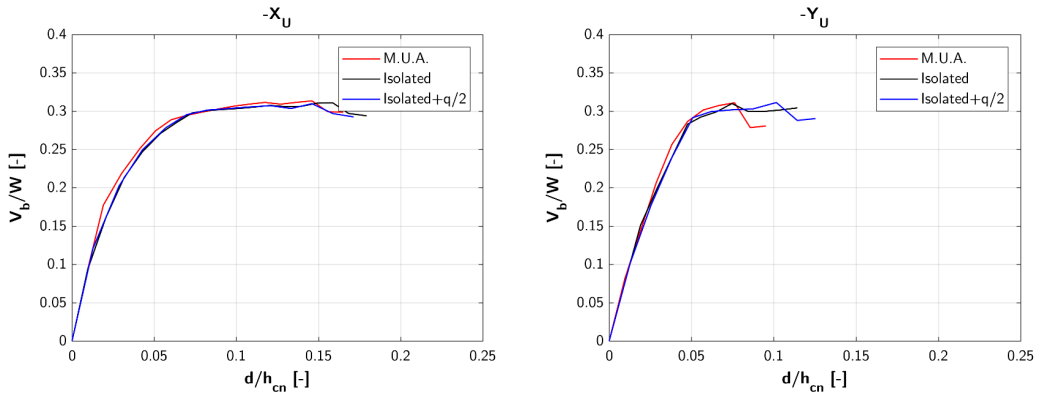

Figure 6-18: Faro aggregate – corner S.U. C: pushover curves comparison between the M.U.A. and the isolated conditions.

Table 6-3: Faro aggregate – corner S.U. C: percentage changes of α_{PGA}, k^* and V_{bu} for the isolated conditions in reference to the M.U.A.

		Δ% α_{PGA}	Δ% k*	Δ% V_{bu}
X direction	**Isolated**	-1%	-12%	1%
	Isolated + q/2	0%	-13%	2%
Y direction	**Isolated**	-3%	-10%	-1%
	Isolated + q/2	-2%	-12%	0%

As previously observed, the changes are generally small. The greatest variation is for the stiffness, that is reduced by about 10% passing from the M.U.A. to the isolated conditions.

6.1.4 Analysis of the external S.U. A

The S.U. A is external and is the most resistant in the aggregate, as can be observed in Figure 6-19, where the distribution of the conventional strength, C, is shown. Referring to the results obtained for the prototypes, in this case, the M.U.A. should exclude the opposite external S.U. E, as highlighted in the graphs.

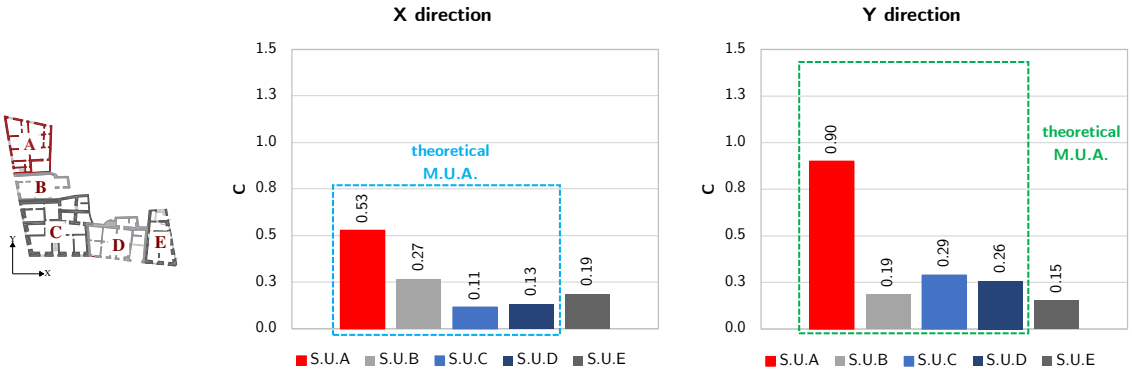

Figure 6-19: Faro aggregate – external S.U. A: identification of the theoretical M.U.A. in terms of the conventional strength (C) distribution.

In order to validate this result, the proposed Procedure is applied to this target S.U. The considered modelling configurations and the results are shown in the following.

6.1.4.1 *Modelling configurations*

The modelling configurations investigated for the S.U. A are illustrated in the following Figure 6-20. The location of the investigated walls and the control node is highlighted in Figure 6-21.

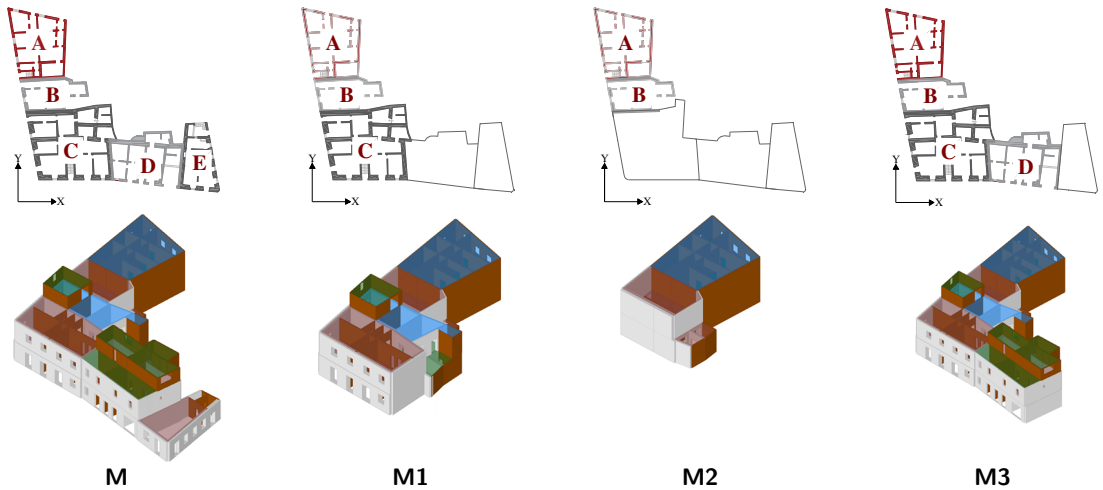

Figure 6-20: Faro aggregate – external S.U. A: modelling configurations.

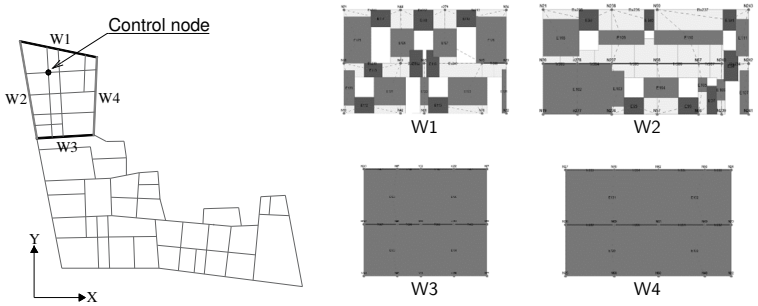

Figure 6-21: Faro aggregate – external S.U. A: location of the investigated walls and the selected control node.

6.1.4.2 Seismic performance assessment phase

In this phase, the seismic performance of each modelling configuration M_i is assessed by performing nonlinear static analyses, by considering global-, S.U.- and wall- levels.

Since the procedure has been already shown and the M.U.A. is individuated at S.U.- level, the following results are related only to the S.U.-level.

S.U.- level

In the following Figure 6-22, the pushover curves obtained for the target S.U. A are compared for each modelling configuration, considering the uniform load pattern distribution (U) in both directions of analysis.

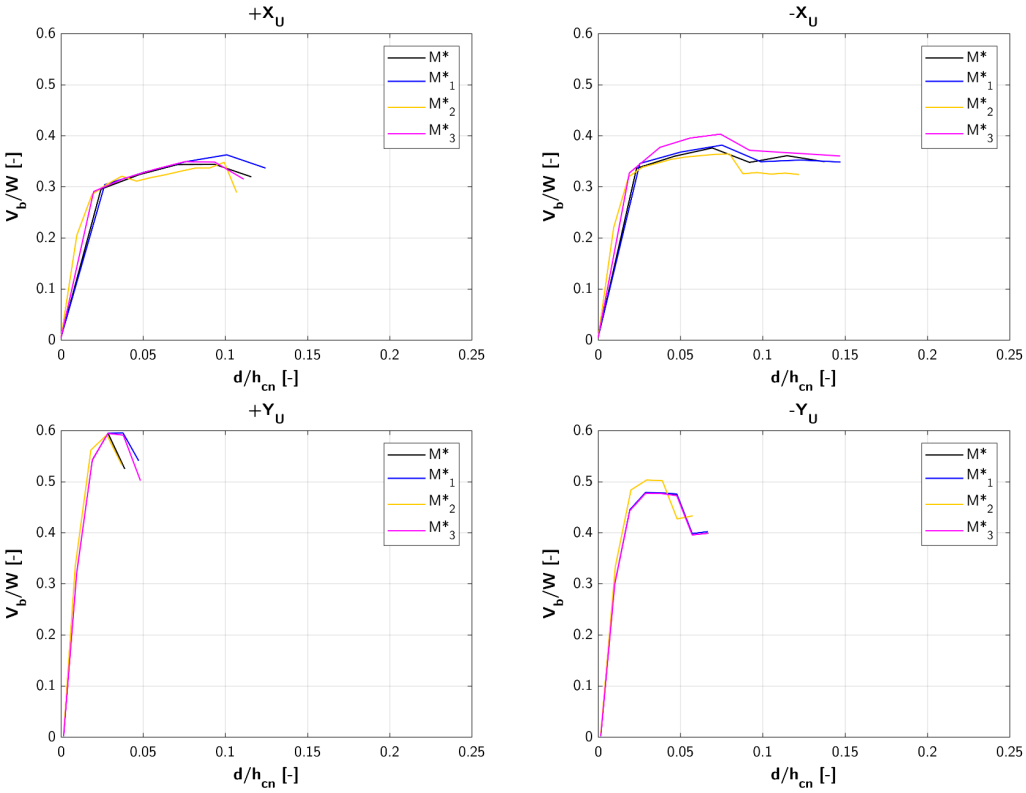

Figure 6-22: Faro aggregate – external S.U. A: pushover curves at S.U.- level.

As it can be noticed, the pushover curves have in general the same trend for all configurations, except for model M*2, which present the highest capacity in terms of stiffness in both directions, while the highest values base shear are for configuration M*1 and M*3.

In accordance with the previous results, the target S.U. A results to be more rigid if modelled with the immediately adjacent S.U. B; the buildings along the X direction, especially, S.U. E, do not improve its capacity.

6.1.4.3 M.U.A. assessment phase

Figure 6-23 shows the mean values and respective standard deviations for each direction of the percentage changes of the maximum base shear V_{bu} and stiffness k^* for each configuration (M* to M*3), evaluated in reference to model M*, as given in Eq. 51.

In X direction, the minimum changes in terms of both maximum base shear V_{bu} and stiffness k^* are observed for configuration M*1, with average values of 2% and 5%, respectively. However, it should be noticed that the values of V_{bu} obtained in the other configurations are very similar.

In Y direction, the minimum changes in terms of both maximum base shear V_{bu} and stiffness k^* are obtained for model M*3, with average values of in the order of 1%.

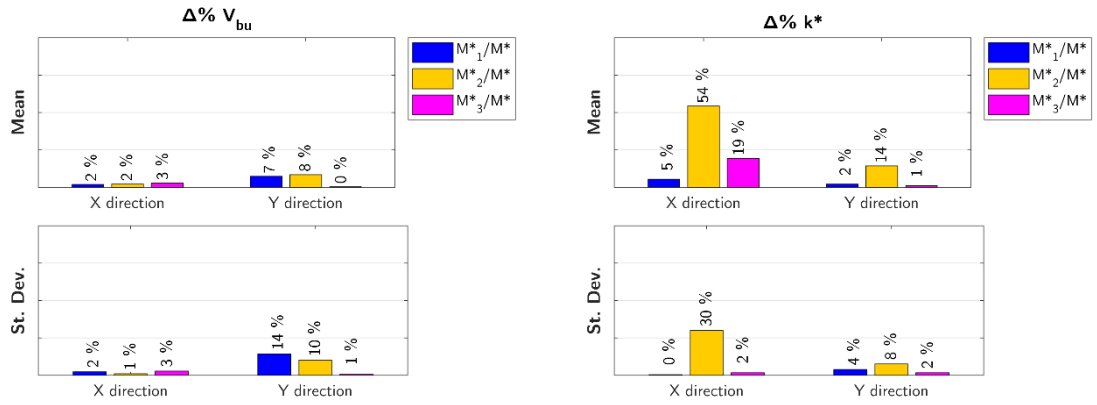

*Figure 6-23: Faro aggregate – external S.U. A: mean and standard deviation of the percentage change of V_{bu} and k^* for M*i/M*.*

From these results, it is possible to conclude that configuration M1, that includes all the S.U.s along the Y direction (A, B and C) is the best M.U.A. for the external S.U. A in both directions of analysis. Model M3, that also includes the S.U. D, perfectly represents the capacity of the target S.U. in Y direction, but not in X direction especially in terms of stiffness.

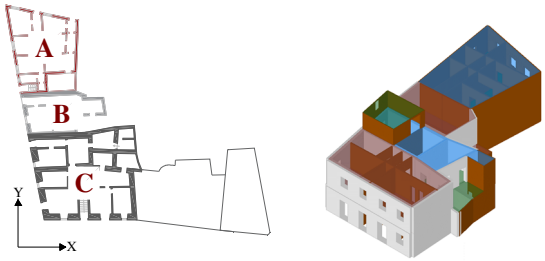

M1

Figure 6-24: Faro aggregate – external S.U. A: M.U.A.

In Figure 6-25, the theoretical M.U.A. (highlighted in blue in X direction and green in Y direction) and the one individuated by applying the procedure (i.e., model M1, highlighted in red) are compared in function of the distribution of the conventional strength, C. It can be noticed that this result partially validates the theoretical M.U.A., since in this case, S.U. D can be excluded from the M.U.A. too.

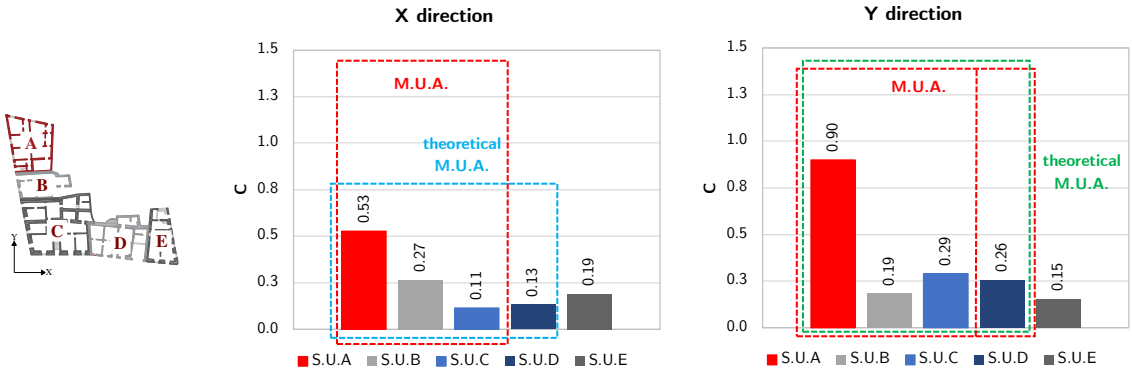

Figure 6-25: Faro aggregate – corner S.U. A: comparison between the theoretical and the individuated M.U.A. in terms of the conventional strength (C) distribution.

6.1.4.4 Comparison with the isolated conditions

The results obtained for the M.U.A. are compared with those of the isolated S.U.A and of this one modelled with the pertinent loads deriving from the immediately adjacent S.U.B (hereinafter referred to as "isolated + q/2").

The results obtained for the 3 conditions are compared in Figure 6-26, in terms of α_{PGA}, maximum base shear V_{bu} and stiffness k^*.

As we can observe, the seismic capacity of the M.U.A. is the greatest in X direction but the lowest in Y direction. Moreover, it is possible to notice that the isolated conditions present similar behaviour.

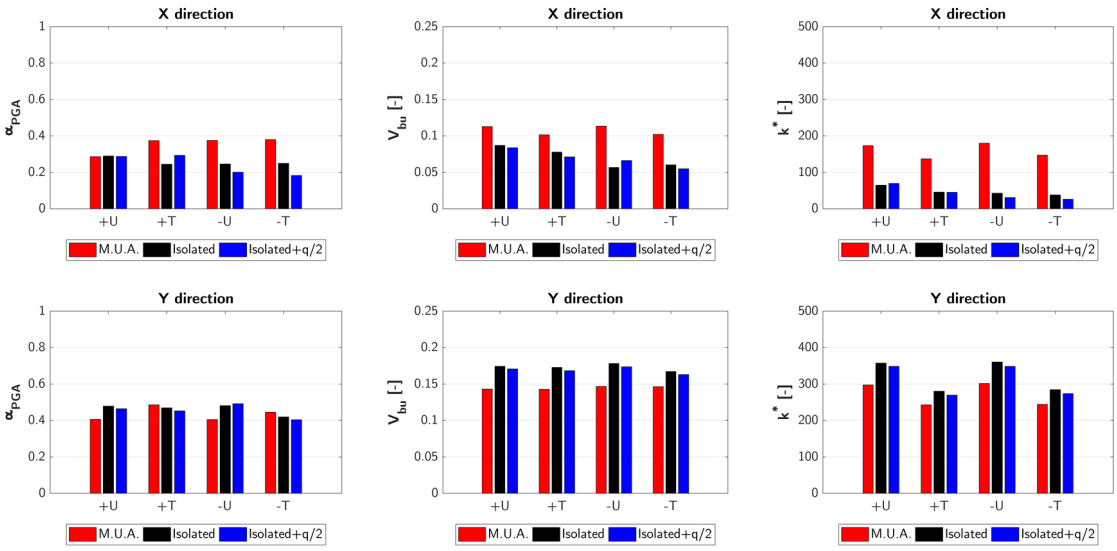

Figure 6-26: Faro aggregate – external S.U. A: comparison of results between the M.U.A. and the isolated conditions.

In the following, only the analyses of each direction with the lowest value of α_{PGA} for M.U.A. are considered, that means +X and -Y uniform distribution.

In Figure 6-27, the pushover curves are compared; moreover, Table 6-4 shows the percentage changes, obtained in reference to the M.U.A., for the isolated conditions.

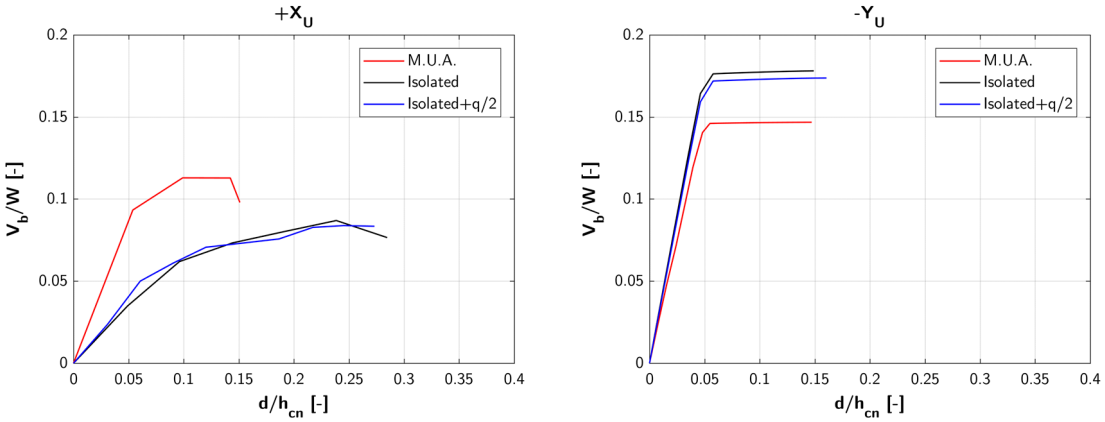

Figure 6-27: Faro aggregate – external S.U. A: pushover curves comparison between the M.U.A. and the isolated conditions.

Table 6-4: Faro aggregate – external S.U. A: percentage changes of α_{PGA}, k^* and V_{bu} for the isolated conditions in reference to the M.U.A.

		Δ% α_{PGA}	Δ% k*	Δ% V_{bu}
X direction	**Isolated**	1%	-63%	-23%
	Isolated + q/2	0%	-60%	-26%
Y direction	**Isolated**	19%	20%	21%
	Isolated + q/2	21%	16%	18%

As previously observed, in X direction the isolated conditions present a reduction of the capacity, especially in terms of stiffness, in the order of 60%; moreover, the α_{PGA} is unvaried. In Y direction, instead, they show an increment of the capacity, in the order of 20% for all parameters. Therefore, the analysis of the isolated S.U., modelled with or without the pertinent loads, implies a relevant variation of the seismic capacity in both directions of analysis.

6.1.5 Second hypothesis of complete aggregate condition

Given the different masonry typology of the load-bearing walls of building A, it is possible to suppose the presence of a material discontinuity among S.U.s A and B and, consequently, to neglect its contribution to the global base shear capacity.

Bearing that prospect in mind, in the analysis of the corner S.U. C, a second configuration can be chosen as the complete aggregate condition, in which S.U.A is not considered, namely model M6. Then, the new investigated modelling configurations are illustrated in the following Figure 6-28.

Figure 6-29 shows the mean values and respective standard deviations for each direction of the percentage changes of the maximum base shear V_{bu} and stiffness k^* for each configuration M*i, evaluated in reference to model M*. From these results, it is possible to conclude that configuration M1, that only considers S.U. B and D, immediately adjacent to the target one, is the best M.U.A. for the corner S.U. C in both directions of analysis for this complete aggregate condition (Figure 6-30).

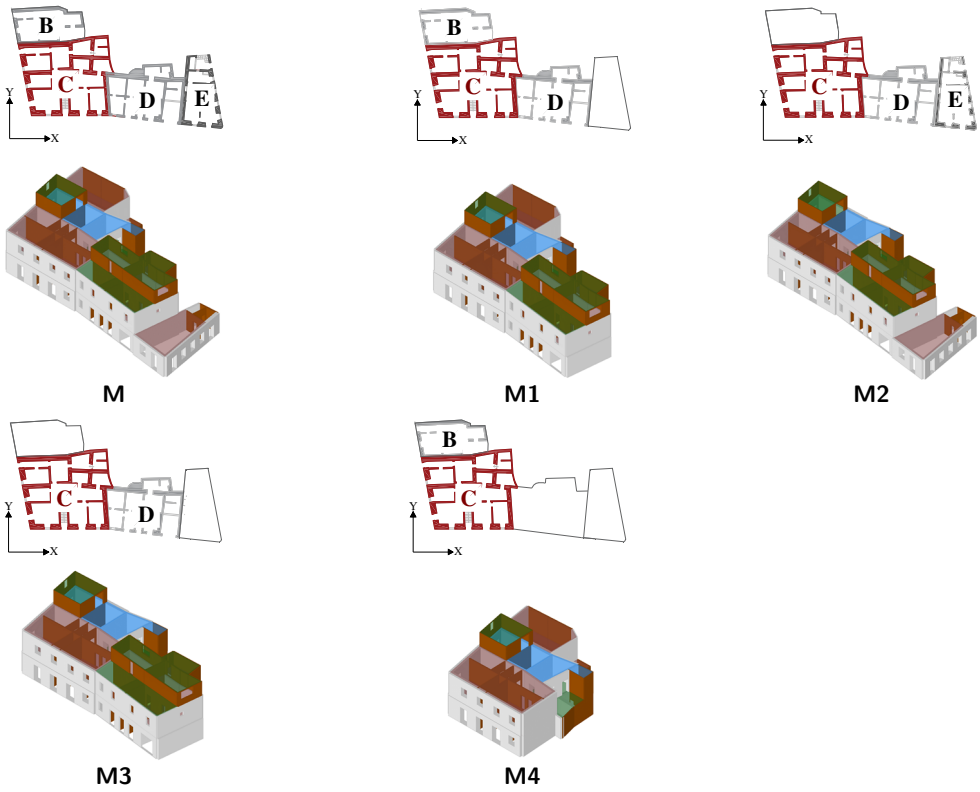

Figure 6-28: Faro aggregate – corner S.U. C: 2nd hypothesis of modelling configurations.

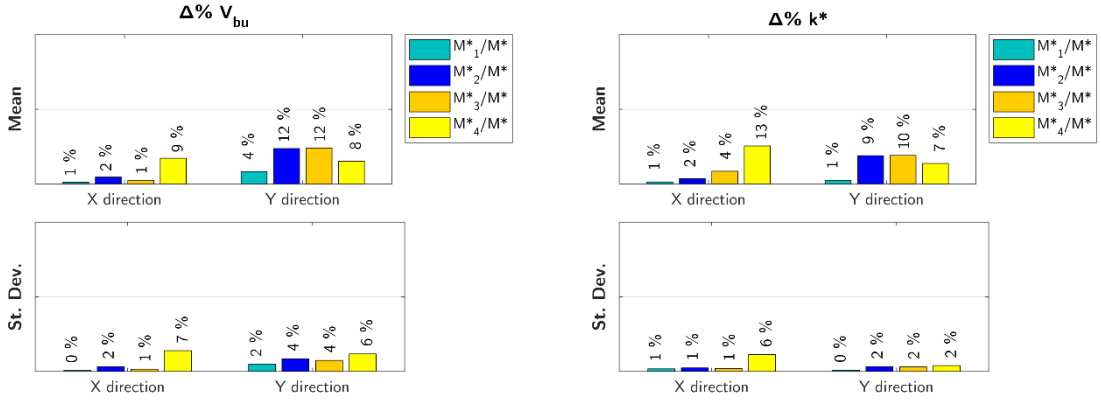

*Figure 6-29: Faro aggregate – corner S.U. C: mean and standard deviation of the percentage change of V_{bu} and k^* for M*i/M*.*

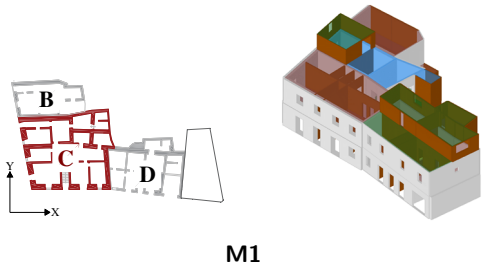

Figure 6-30: Faro aggregate – corner S.U. C: 2nd hypothesis of M.U.A.

6.2 Row aggregate in Castelnuovo (L'Aquila)

In this paragraph, a masonry aggregate located in Castelnuovo, a village in the L'Aquila valley, is analysed, aiming at investigating the "aggregate effect" on different target S.U.s: the internal and the external ones.

Castelnuovo was hit by L'Aquila earthquake of 06/04/2009. After this catastrophic event, the team of DICEA (Department of Civil and Environmental Engineering) performed surveys in this area, with the aim to better understand the seismic behaviour of masonry aggregates (Vignoli, 2012).

Figure 6-31: Castelnuovo: ante- and post-earthquake aerial view (google-maps).

6.2.1 Built environment

The investigated aggregate has a rectangular shape and consists of 9 S.U.s built in different time periods and, consequently, with different construction techniques. Because of its morphological and structural characteristics, this aggregate can be considered as representative of this area.

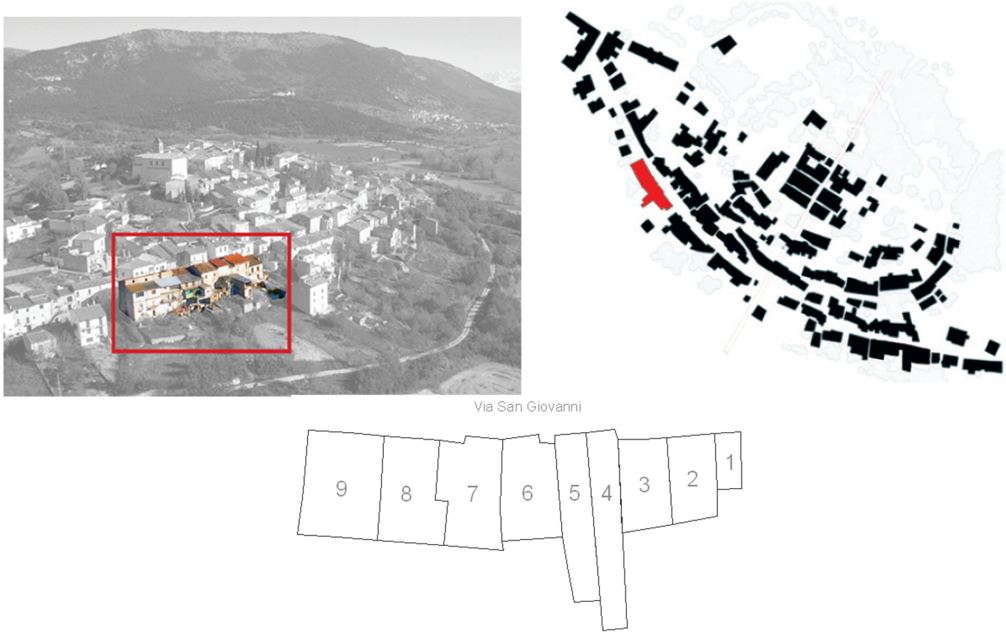

Figure 6-32: Castelnuovo aggregate: aerial view and identification.

The preliminary phase of the knowledge process included geometric, structural and damage survey.

6.2.2 Knowledge process

6.2.2.1 Geometric survey

The aggregate is characterized by a complex structural conformation, both in plan and in height. The length is about 60 m, the depth of about 15 m, the maximum height is about 10 m. The number of storeys is in general 3, characterized by an average height of 2.8 m; some S.U.s have a basement floor. Moreover, the floors are slightly staggered.

Figure 6-33: Castelnuovo aggregate: façades and internal rooms.

Figure 6-34: Castelnuovo aggregate: geometric survey.

6.2.2.2 Structural survey

The plans of the aggregate are shown in Figure 6-35, from the basement floors to the roof, with the indication of the structural elements.

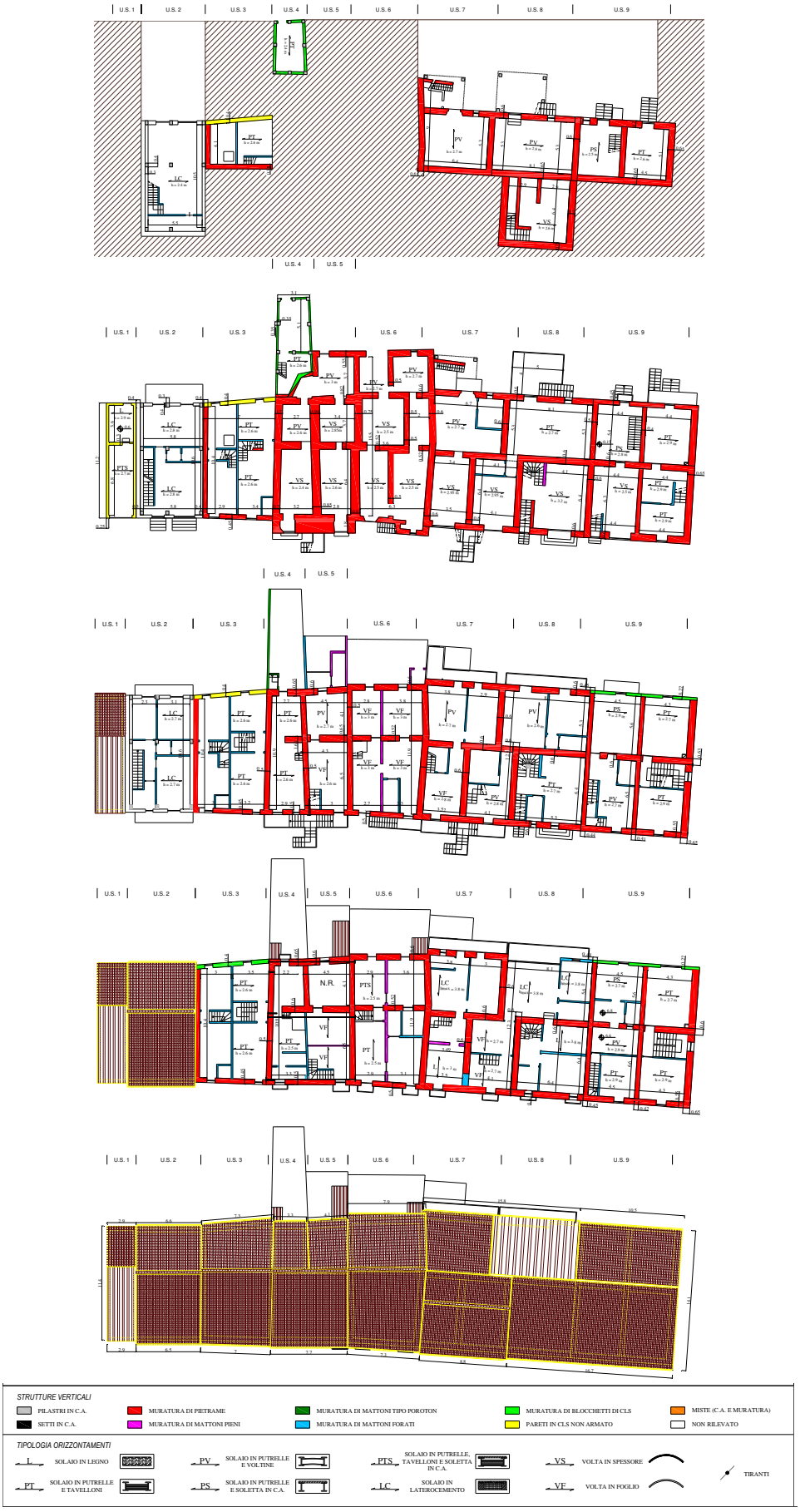

Figure 6-35: Castelnuovo aggregate: structural survey, from basement floor (upper row) to the roof (bottom row).

The aggregate is mainly composed of stone masonry (S.U. 4 - S.U. 9), except for the first 3 S.U.s, characterized by non-r.c. walls (S.U. 1 and S.U. 3) and by a r.c. frame (S.U. 2).
Considering the horizontal elements, S.U. 1 and 2 have concrete slabs. In the others, different typologies are present: masonry vaults on the ground and first floor, steel slabs (PT: I-beams and hollow tiles; PV: I-beams and hollow building tiles) on the upper floors. The roof is made of wood, separated from the lower level by vaults, with a false ceiling function. The floors typologies are highlighted in Figure 6-36.

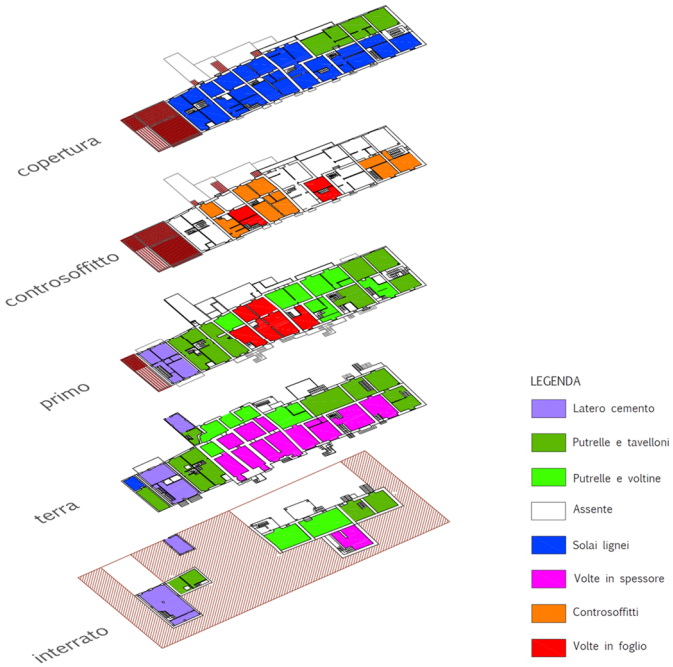

Figure 6-36: Castelnuovo aggregate: structural survey of the horizontal elements.

6.2.2.3 Hypothesis of the aggregate evolution

The analysis of the possible construction phases allows clarifying the aggregate morphology, leading to a careful assessment of structural discontinuities and material heterogeneities.
The original nucleus of the aggregate is represented by the S.U. 4, 5 and 6, characterized by a more ancient construction typology. Indeed, stone masonry vaults are present at the ground floor; furthermore, the walls are continuous along the height and are characterized by high thicknesses (around 90 cm at the base). The wall texture is irregular, with stones of various sizes and not rough, that implicates poor resistance characteristics. The hypothesis that this is the original nucleus of the aggregate is reflected in the crack pattern produced by the seismic action, which has highlighted the existence of joints between these S.U.s and those adjacent.
In the subsequent phases, the aggregate developed following the natural slope of the land, with the adding the S.U. 3 (on the left looking at the main front) and S.U.s 7, 8 and 9 (on the right looking at the main front). With reference to these last, they were built in two different times, as they are physically separated by a visible vertical line. The parts on the main façades were built first; then, the rear portions were added, showing different manufacture and a homogeneous masonry typology.
The last expansion dates from the 1980s and refers the construction of S.U.s 1 and 2, structurally independent from the rest of the aggregate by the presence of a seismic joint between the S.U. 2 and 3.

Finally, the current conformation of the aggregate has been achieved with the construction of some annexes and/or terraces on the backside.

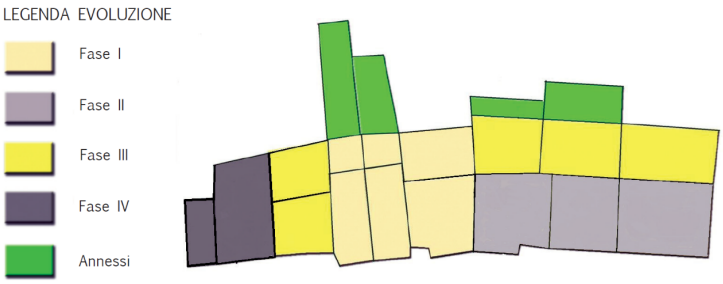

Figure 6-37: Castelnuovo aggregate: hypothesis of historical evolution.

6.2.2.4 Crack pattern and damage survey

The damage pattern is shown in the following figures.

Figure 6-38: Castelnuovo aggregate: diagonal cracking in S.U.4 (left), S.U.6 (centre) and S.U.9 (right).

Figure 6-39: Castelnuovo aggregate: damage in the spandrels in S.U.6 (upper row) and in S.U.7 (bottom row).

S.U.9 presents the greatest damage level (D4). The façade has diagonal lesions along the whole elevation and the activation of an overturning mechanism is evident. S.U.s 4, 5, 6 and 7 present a damage level D4 and D3, due to relevant cracks on all the perimeter walls, partial out-plane collapses and damages of the horizontal structures, as well as widespread damage on non-structural elements. In the other S.U.s the damage is lower (D2 and D1 in S.U. 3 and 8) or absent (D0 in S.U. 1 and 2). In conclusion, the greatest damage level is in correspondence of the S.U.s composed of stone masonry. Considering the horizontal elements, the masonry vaults are almost intact. The steel slabs suffered damage mainly due to the rotation of the support walls and the consequent extraction of the beams.

6.2.3 Numerical modelling

The three-dimensional model is developed by using the commercial release of 3Muri software code (STADATA, 2017). The geometry is defined accordingly to the plans. The basements are not modelled since they were not affected by failures.

With regards to the masonry typologies, referring to the classification proposed by C.M. 617/2009 (Tab. C8A.2.1), the typology "irregular stone masonry" (1st category) is assigned to the stone masonry walls, while the typology "brick masonry and lime mortar" (6th category) is assigned to brick masonry walls. Moreover, the typology "masonry in hollow brick blocks with a perforation percentage smaller than 45%" (8th category) is assigned to hollow brick masonry walls and the typology "masonry in hollow concrete blocks with a perforation percentage between 45% and 65%" (10th category) is assigned to non-r.c. walls. As introduced in paragraph 3.3.2, a knowledge level KL1 is assumed. Additionally, due to the poor state of preservation of masonry fabric, a cracked stiffness condition is applied to the stiffness parameters. The values of the mechanical characteristics of the masonry typologies are resumed in Table 6-5.

Table 6-5: Castelnuovo aggregate: mechanical properties assigned to masonry panels.

Material	E [MPa]	G [MPa]	w [kN/m^3]	f_m [N/cm^2]	τ_0 [N/cm^2]
Stone masonry	435	145	19	74.1	1.48
Brick masonry	750	250	18	177.8	4.44
Hollow brick masonry	2250	675	12	296.30	22.20
Hollow concrete masonry	700	175	12	222.2	13.3

Regarding the horizontal elements, the mechanical properties assigned to the diaphragms are resumed in Table 6-6. Steel and wood floors are modelled as orthotropic finite element membranes with an equivalent thickness, s, equal to 4 cm. Timber floors and roofs are modelled as orthotropic finite element membranes with an equivalent thickness, s, equal to 5 cm.

Table 6-6: Castelnuovo aggregate: mechanical properties assigned to floors.

Floors	$E_{1,eq}$ [MPa]	$E_{2,eq}$ [MPa]	G [MPa]	ν [-]	G_k [kN/m^2]	Q_k [kN/m^2]
Barrel masonry vaults	645	645	210	0.2	11.10	2.0
In folio masonry vaults	150	150	50	0.2	5.40	2.0
Steel slabs (PT)	0.0	0.0	10500	0.0	5.50	2.0
Steel slabs (PV)	0.0	0.0	11000	0.2	3.95	2.0
Wooden roof	0.0	0.0	780	0.0	1.50	1.55
PT roof	0.0	0.0	10500	0.0	2.90	1.55

To allow a more reliable comparison of the results, for the different analysed S.U.s, the control node is selected in a barycentric position of the target building and the pushover curves are normalised, as illustrated in 3.3.2.

As previously introduced, S.U.1 and 2 are structurally independent from the rest of the aggregate by the presence of a discontinuity between the S.U.2 and 3. For this reason, they are not considered in the model.

In the following, S.U.s 6 (the central one) and 9 (the external) are investigated in order to define their M.U.A.

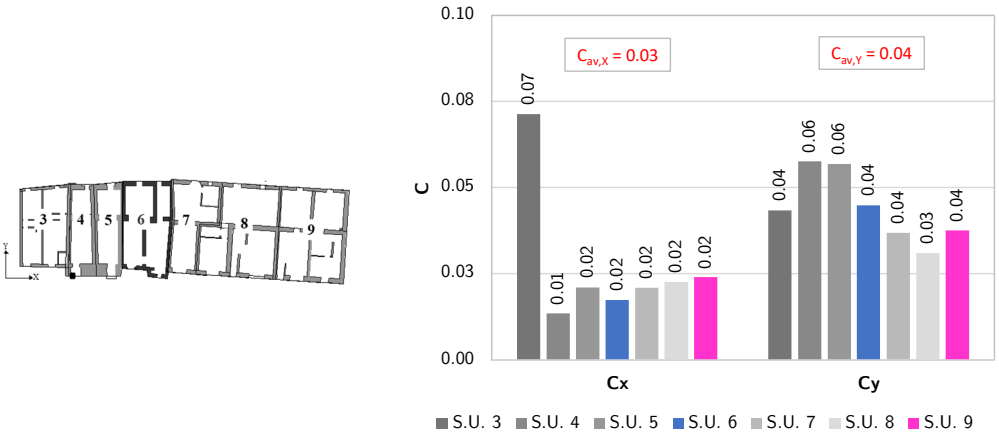

Figure 6-40: Castelnuovo aggregate: values of the conventional strength, C, for each S.U.

As shown in Figure 6-40, the conventional strength *C* is estimated from S.U. 3 to S.U. 9, considering the two directions of analysis separately. The average value of the aggregate, C_{av}, is highlighted in red; moreover, the values of the investigated S.U.s 6 and 9 are highlighted in blue and pink, respectively.

It is possible to observe that, in general, the aggregate is more resistant in the transversal direction Y. The internal S.U.s (from 4 to 8) present a similar global strength, around 0.06 and inferior to the average value, equal to 0.07. The most resistant S.U.s are the external ones, especially S.U.3, but they show the major resistance in X direction; indeed, in Y direction the greatest values of C are for S.U.s 4, 5, 6.

6.2.4 Analysis of the internal S.U. 6

The S.U. 6 is placed in the central part of the aggregate and is adjacent to S.U.s of similar resistance, as can be observed in Figure 6-41, where the distribution of the conventional strength C in X direction is shown, since in this direction the "aggregate effect" is more relevant. In this case, as noticed for the prototype aggregates, the M.U.A. should just include the immediately adjacent S.U.s on each side (S.U.5 and 7), as highlighted in red in the graph.

In order to validate this result, the proposed Procedure is applied to this target S.U. The considered modelling configurations and the results are shown in the following.

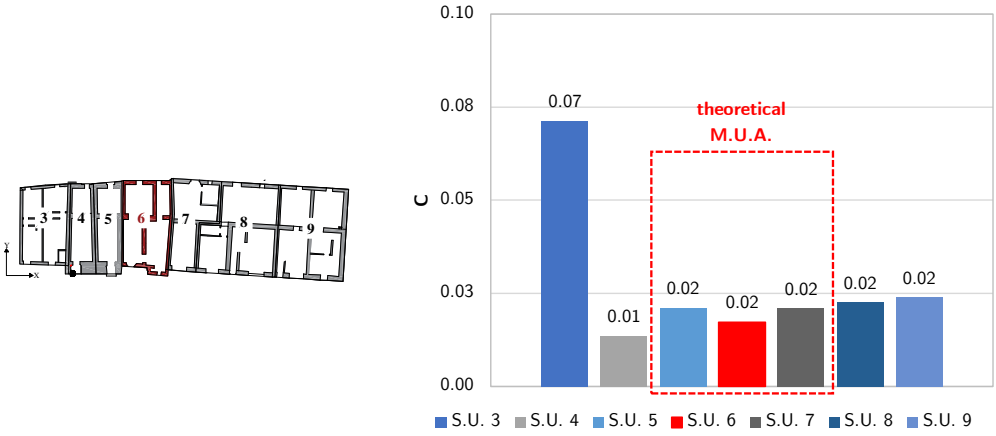

Figure 6-41: Castelnuovo aggregate – internal S.U. 6: identification of the theoretical M.U.A. in terms of the conventional strength (C) distribution.

6.2.4.1 *Modelling configurations*

The modelling configurations investigated for this S.U. are illustrated in Figure 6-43, considering all the possibilities starting from the complete aggregate condition (model M).
The location of the investigated walls and the control node is highlighted in Figure 6-42.

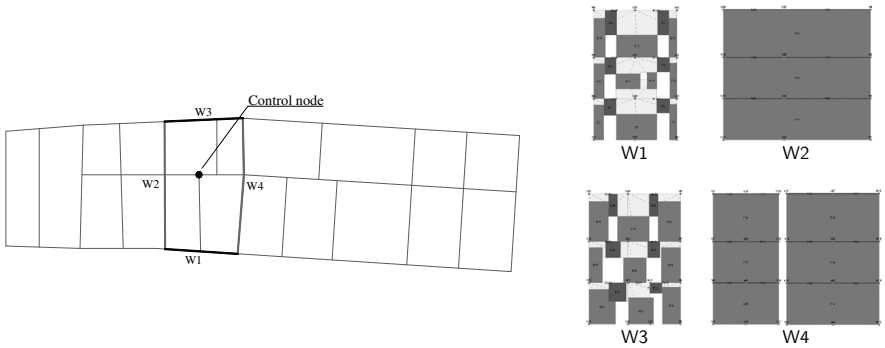

Figure 6-42: Castelnuovo aggregate – internal S.U. 6: location of the investigated walls and the selected control node.

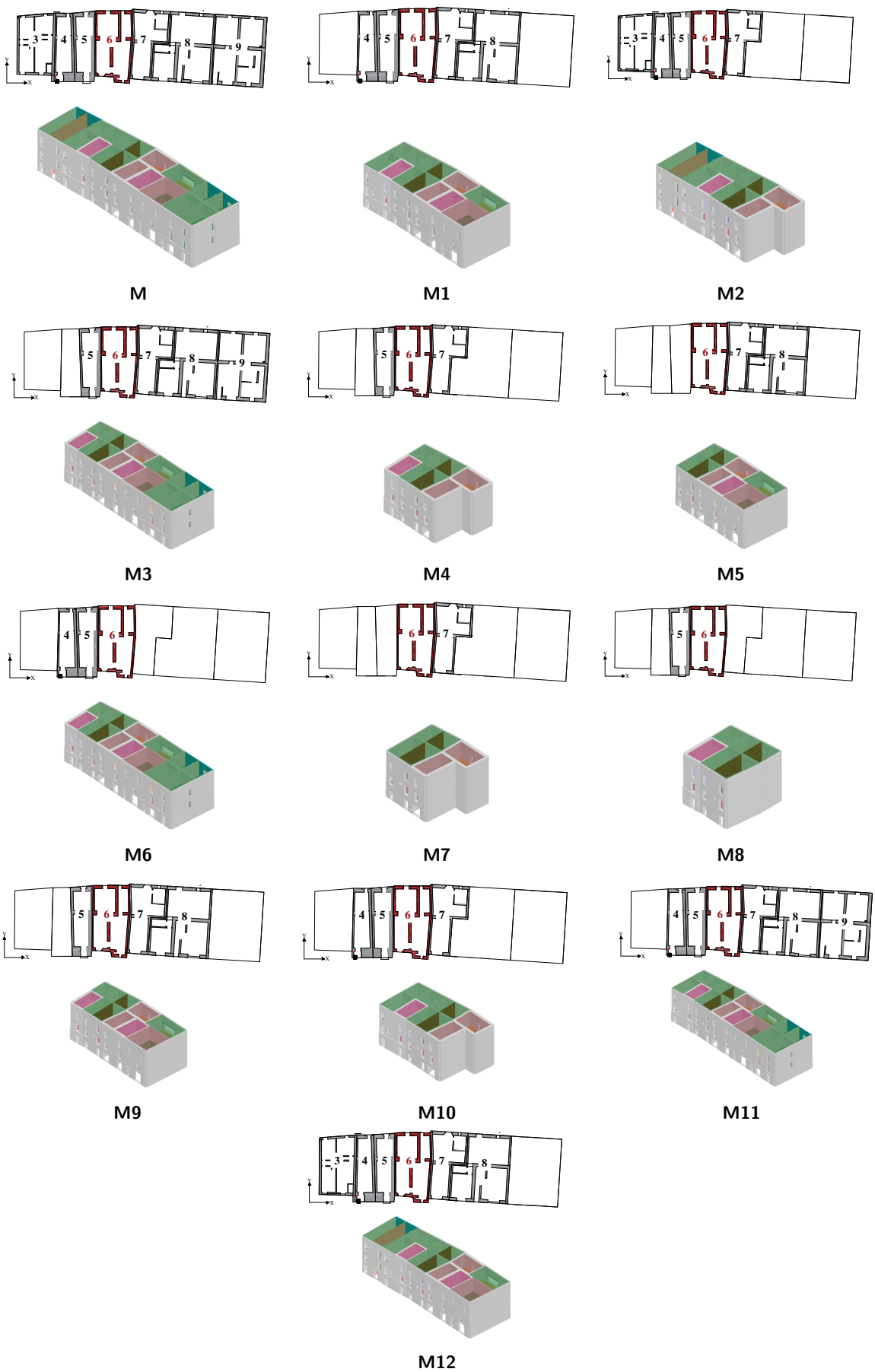

Figure 6-43: Castelnuovo aggregate – internal S.U. 6: modelling configurations.

6.2.4.2 Seismic performance assessment phase

In this phase, the seismic performance of each modelling configuration M_i is assessed by performing nonlinear static analyses, by considering global-, S.U.- and wall- levels.

With reference to the complete aggregate condition (model M), the damage pattern obtained from the modelling is compared with the real damage in the following Figure 6-44 and Figure 6-45.

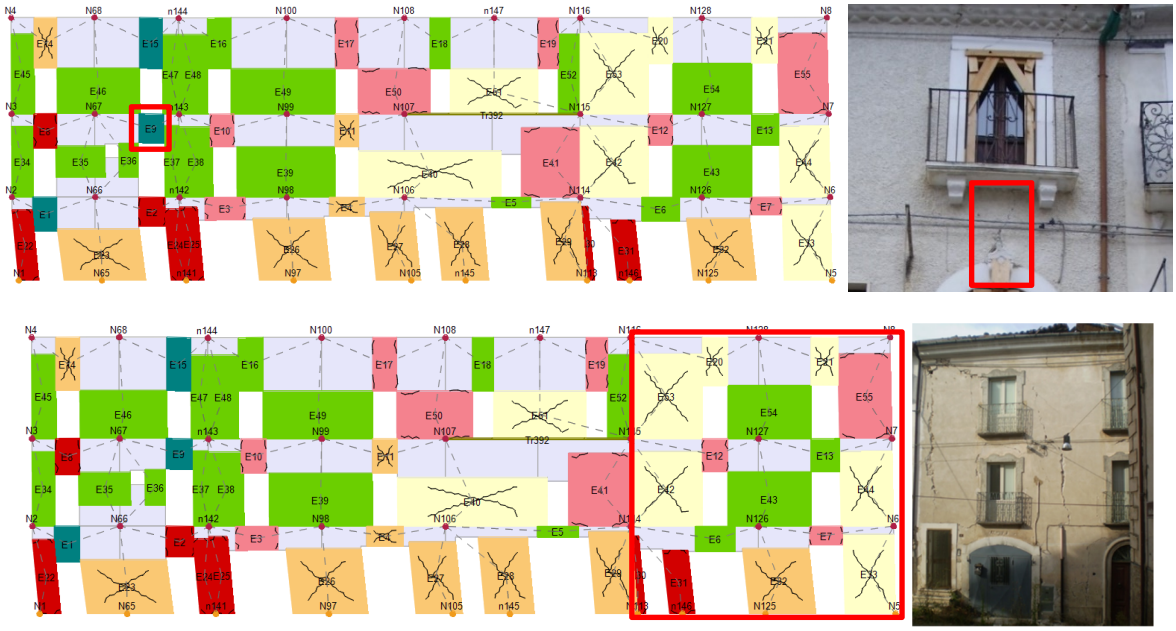

Figure 6-44: Castelnuovo aggregate: damage pattern of the frontal façade.

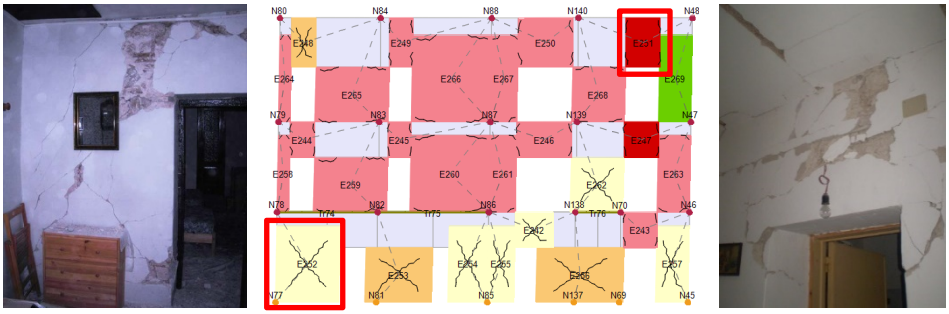

Figure 6-45: Castelnuovo aggregate: damage pattern of internal wall.

Since the procedure has been already shown and the M.U.A. is individuated at S.U.- level, the following results are related only to the S.U.-level.

S.U.- level

In the following Figure 6-46, the pushover curves obtained for the target S.U. 6 are compared for each modelling configuration, considering the uniform load pattern distribution (U) in both directions of analysis.

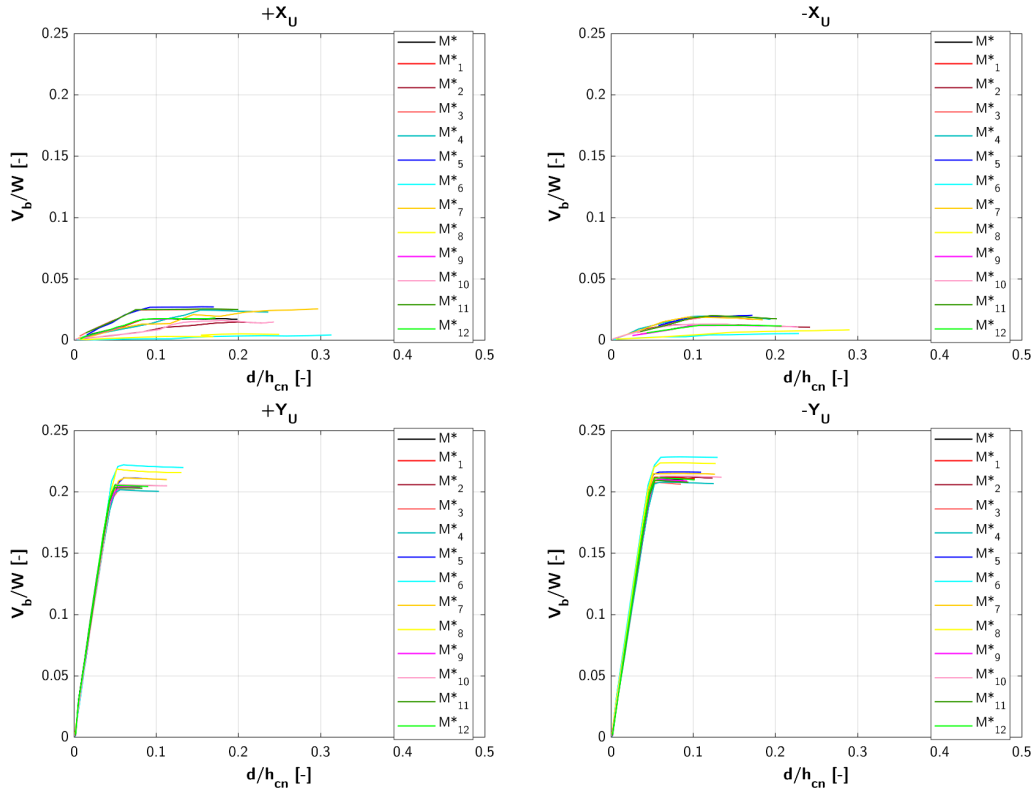

Figure 6-46: Castelnuovo aggregate – internal S.U. 6: pushover curves at S.U.- level.

Firstly, the capacity in Y direction quadruples that in X direction, confirming the results obtained for the prototype aggregates. Moreover, in X direction the variability of the pushover curves trend is more evident than in Y direction, where the capacity in terms of stiffness is not influenced by the modelling configuration. This result indicates that the "aggregate effect" is way more relevant in the longitudinal direction of the row aggregate.

In X direction, the lowest capacity, in term of both stiffness and base shear, is for models M*6 and M*8, in which the target S.U. is modelled as external S.U. on the right side; on the contrary, models M*3, M*5 and M*11 present the highest values. This indicates that, in this direction, S.U.s 7 and 8 have a great influence on the target S.U., contrary to S.U.s 3 and 4.

The results are reversed in Y direction, since model M*6 and M*8 present the highest capacity, while M*3 and M*4 the lowest. This means that both S.U.s 5 and 7 influence the seismic behaviour of the target S.U., while S.U.4 and 9 do not.

6.2.4.3 M.U.A. assessment phase

Figure 6-47 shows the mean values and respective standard deviations for each direction of the percentage changes of the maximum base shear V_{bu} and stiffness k^* for each configuration (M* to M*12), evaluated in reference to model M*, as given in Eq. 51.

The percentage changes are greater in X direction, with most of the values that exceed 50%, while in Y direction they are in the order of 3%. In terms of both maximum base shear V_{bu} and stiffness k^*, the minimum changes are for M*9, with average values of 3% in X direction and 0% in Y direction for V_{bu} and of 4% and 2% for k^*. Similar values are obtained for models M*1.

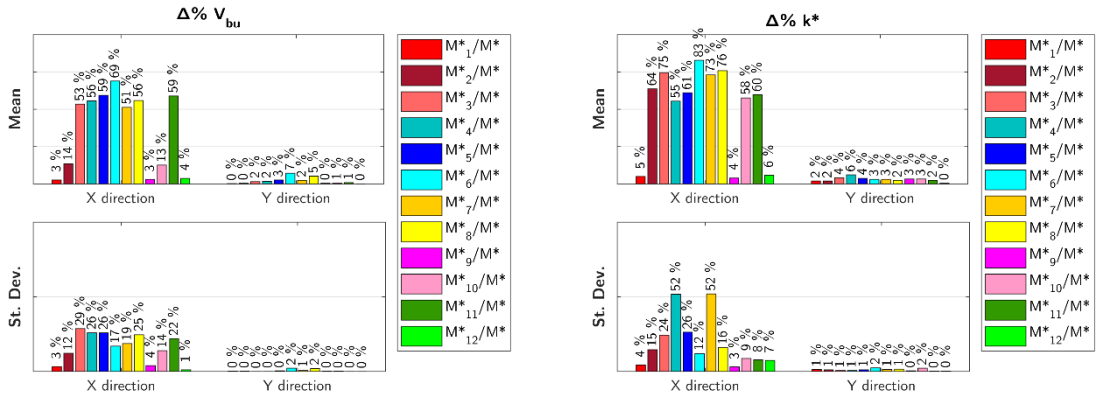

*Figure 6-47: Castelnuovo aggregate – internal S.U. 6: mean and standard deviation of the percentage change of V_{bu} and k^* for M*i/M**.

From these results and in accordance with the previous conclusions on the pushover curves trends, it is possible to individuate configuration M9, that excludes the external S.U.s 3, 4 and 9, as the best M.U.A. for the internal S.U. 6 in both directions of analysis.

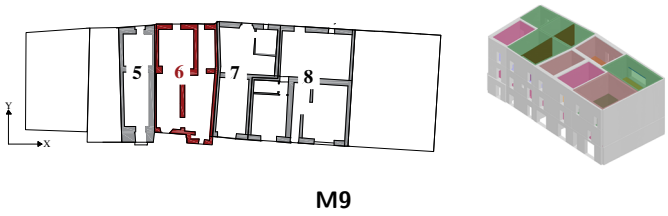

Figure 6-48: Castelnuovo aggregate – internal S.U. 6: M.U.A.

In Figure 6-49, the theoretical M.U.A. (highlighted in purple) and the one deriving from the procedure (i.e., model M9, highlighted in red) are compared in terms of the distribution of the conventional strength C in X direction.

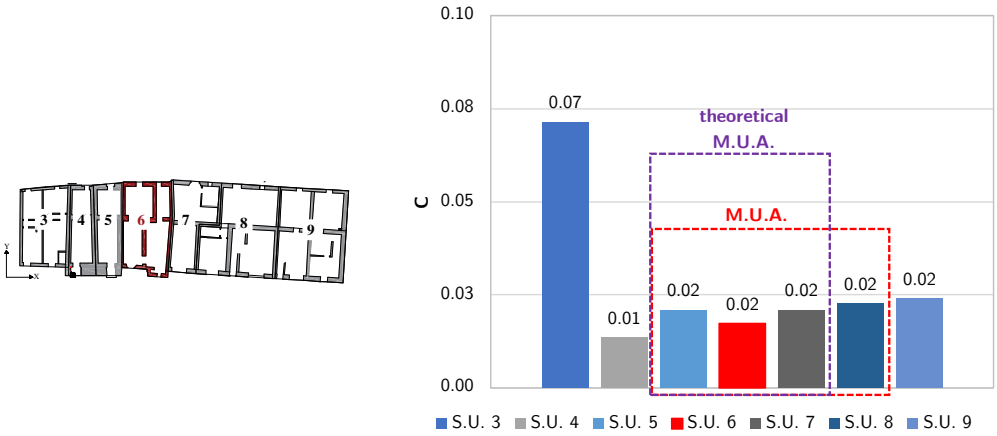

Figure 6-49: Castelnuovo aggregate – internal S.U. 6: comparison between the theoretical and the individuated M.U.A. in terms of the conventional strength (C) distribution.

Unlike the prototype aggregates, for which the M.U.A. should just include the immediately adjacent S.U.s on each side in presence of similar values of C, in this case study S.U.8 should also be included, despite it presents the lowest value of C. This can be explained by the fact that it is planimetrically complementary to S.U.7.

6.2.4.4 Comparison with the isolated conditions

With the aim to provide a vision of the error that an excessive simplification can produce, the results obtained for the M.U.A. are compared with those of the isolated S.U.6 and of this modelled with the pertinent loads deriving from the immediately adjacent S.U.s 5 and 7 (hereinafter referred as "isolated + q/2" model).

The results obtained for the 3 conditions are compared in Figure 6-50, in terms of α_{PGA}, maximum base shear V_{bu} and stiffness k^*.

As expected, the seismic capacity of the M.U.A. is the greatest in X direction but the lowest in Y direction. Moreover, it is possible to notice that the isolated conditions present similar behaviour.

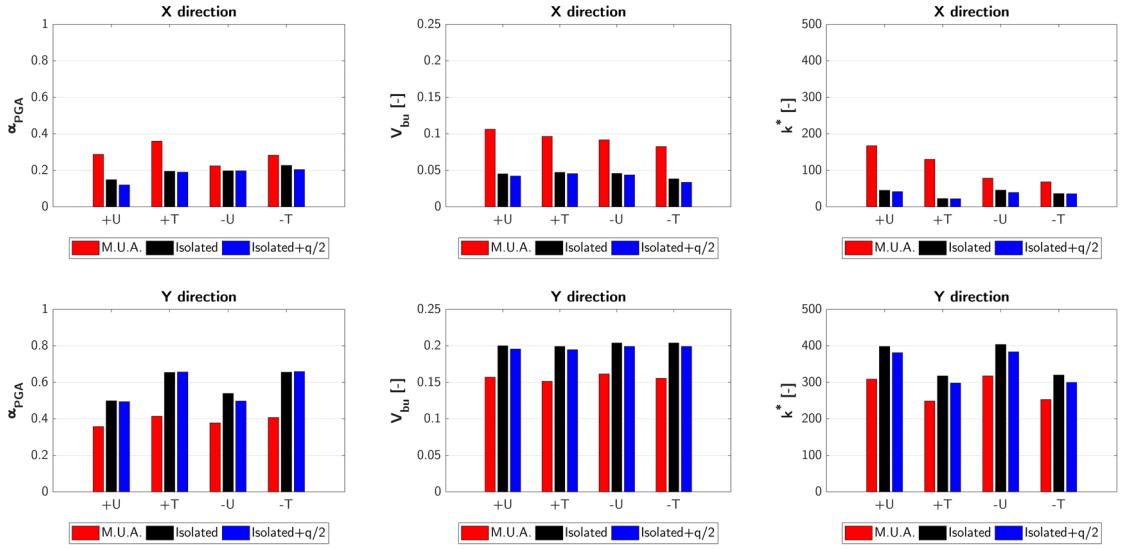

Figure 6-50: Castelnuovo aggregate – internal S.U. 6: comparison of results between the M.U.A. and the isolated conditions.

In the following, only the analyses of each direction with the lowest value of α_{PGA} for M.U.A. are considered, that means -X and +Y uniform distribution.

In Figure 6-5, the pushover curves are compared; moreover, Table 6-7 shows the percentage changes, obtained in reference to the M.U.A., for the isolated conditions.

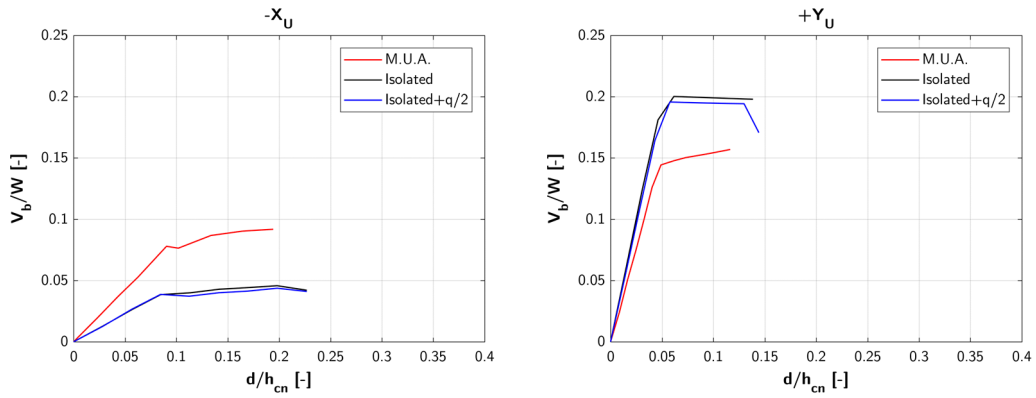

Figure 6-51: Castelnuovo aggregate – internal S.U. 6: pushover curves comparison between the M.U.A. and the isolated conditions.

Table 6-7: Castelnuovo aggregate – internal S.U. 6: percentage changes of α_{PGA}, k^* and V_{bu} for the isolated conditions in reference to M.U.A.

		Δ% α_{PGA}	Δ% k*	Δ% V_{bu}
X direction	**Isolated**	-12%	-42%	-50%
	Isolated + q/2	-12%	-50%	-52%
Y direction	**Isolated**	40%	29%	28%
	Isolated + q/2	38%	23%	25%

As previously observed, in X direction the isolated conditions present a reduction of the capacity, especially in terms of maximum base shear and stiffness, in the order of 50%; moreover, the α_{PGA} is reduced of 12%. In Y direction, instead, they show an increment of the capacity, especially in terms of α_{PGA}, in the order of 40%. Therefore, the analysis of the isolated S.U., modelled with or without the pertinent loads, implies a relevant variation of the seismic capacity in both directions of analysis.

6.2.5 Analysis of the external S.U. 9

The S.U. 9 is external on the right side and is adjacent to S.U.s of minor resistance, but the change respect of the average value is low (around 10%), as can be observed in Figure 6-52, where the distribution of the conventional strength C in X direction is shown. In this case, as noticed for the prototype aggregates, the M.U.A. should include 3 adjacent S.U.s. (S.U.6, 7 and 8), as highlighted in red in the graph; however, the model with only 2 adjacent S.U.s should provide similar results.

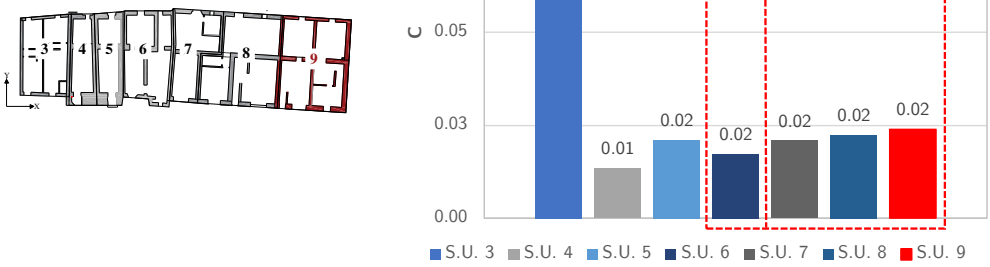

Figure 6-52: Castelnuovo aggregate – external S.U. 9: identification of the theoretical M.U.A. in terms of the conventional strength (C) distribution.

In order to validate this result, the proposed Procedure is applied to this target S.U. The considered modelling configurations and the results are shown in the following.

6.2.5.1 Modelling configurations

The modelling configurations investigated for this S.U., illustrated in Figure 6-53, go from the complete aggregate condition (model M) to the target S.U. modelled with the immediately adjacent one (model M5).

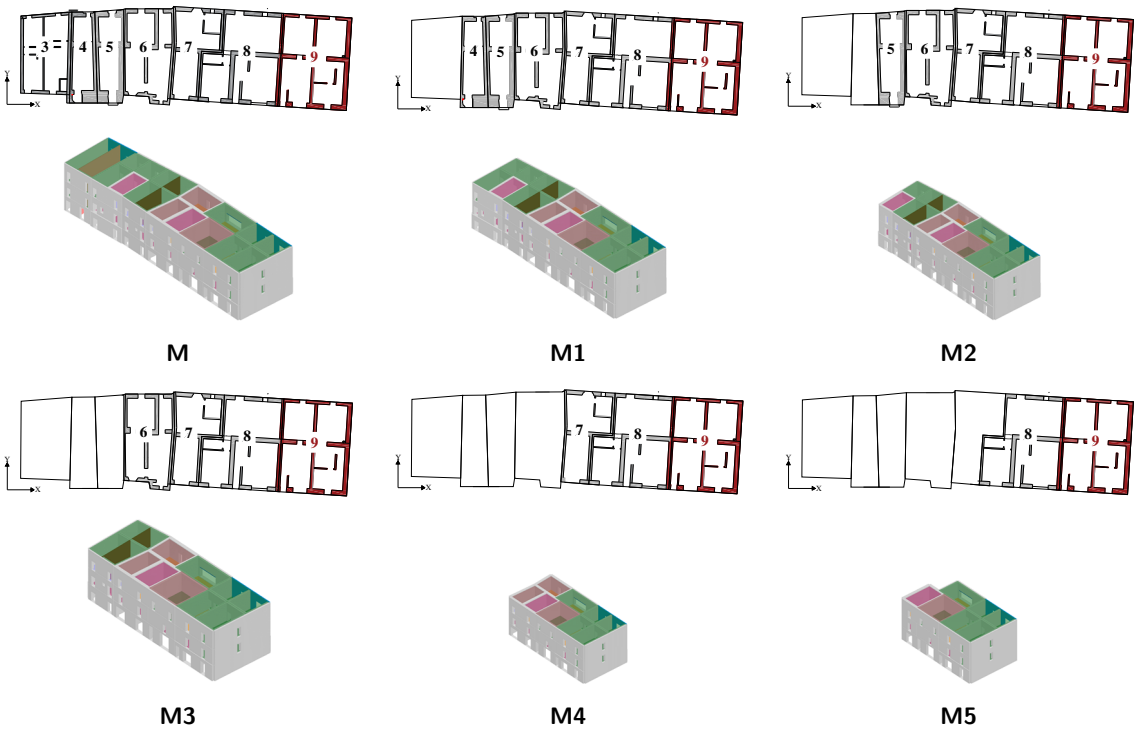

Figure 6-53: Castelnuovo aggregate – external S.U. 9: modelling configurations.

The location of the investigated walls and the control node is highlighted in Figure 6-54.

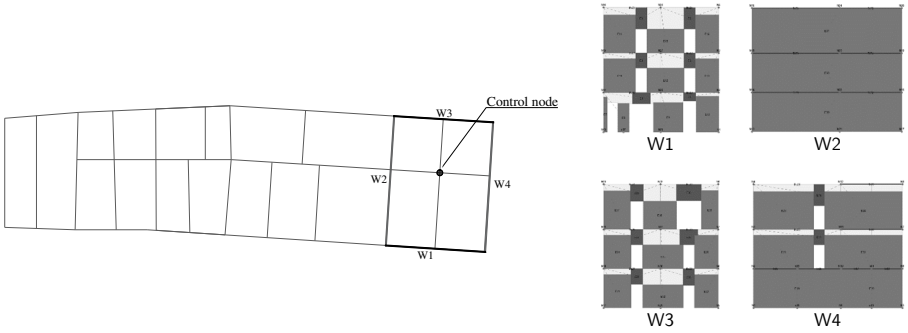

Figure 6-54: Castelnuovo aggregate – external S.U. 9: location of the investigated walls and the selected control node.

6.2.5.2 Seismic performance assessment phase

In this phase, the seismic performance of each modelling configuration M_i is assessed by performing nonlinear static analyses, by considering global-, S.U.- and wall- levels. Since the procedure has been already shown and the M.U.A. is individuated at S.U.- level, the following results are related only to the S.U.-level.

S.U.- level

In the following Figure 6-55, the pushover curves obtained for the target S.U. 9 are compared for each modelling configuration, considering the uniform load pattern distribution (U) in both directions of analysis.

As previously noticed, the capacity in X direction is lower than that in Y direction. The pushover curves have in general the same trend, especially in Y direction. It is possible to observe that model M*5 has the lowest and the highest capacity in the positive and negative X direction, respectively.

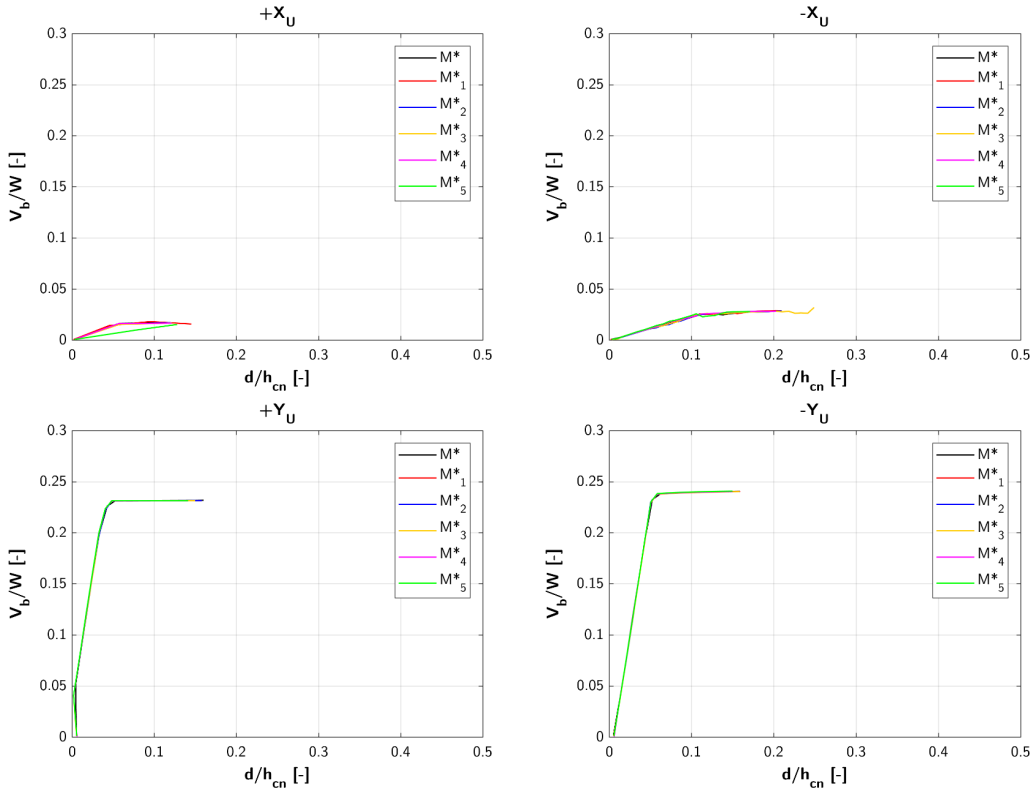

Figure 6-55: Castelnuovo aggregate – external S.U. 9: pushover curves at S.U.- level.

6.2.5.3 M.U.A. assessment phase

Figure 6-56 shows the mean values and respective standard deviations for each direction of the percentage changes of the maximum base shear V_{bu} and stiffness k^* for each configuration (M* to M*5), evaluated in reference to model M*, as given in Eq. 51.

Similar values are obtained for all models, in the order of 3% in X direction and 0% in Y direction, except for model M*5 in X direction. This indicates that the considered modelling configurations are equivalent to represent the "aggregate effect" on the external S.U. 9.

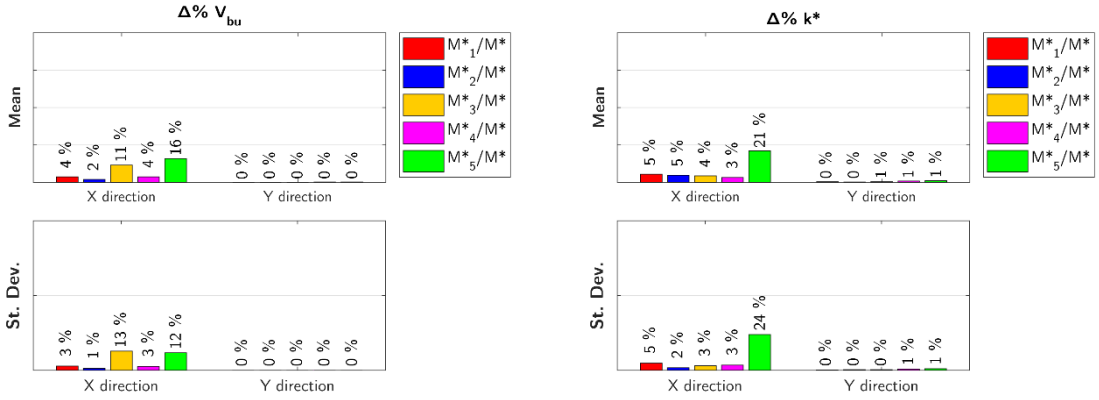

*Figure 6-56: Castelnuovo aggregate – external S.U. 9: mean and standard deviation of the percentage change of V_{bu} and k^* for M*i/M*.*

From these results it is possible to conclude that configuration M4, that only considers the 2 S.U.s immediately adjacent to the target one, is the best M.U.A. for the external S.U. 9 in both directions of analysis.

Figure 6-57: Castelnuovo aggregate – external S.U. 9: M.U.A.

In Figure 6-58, the theoretical M.U.A. (highlighted in purple) and the one individuated by applying the procedure (i.e., model M4, highlighted in red) are compared in function of the distribution of the conventional strength, C. It can be noticed that this result is in accordance with the theoretical M.U.A., considering that it should include 2 or 3 adjacent S.U.s., as the provided results are similar.

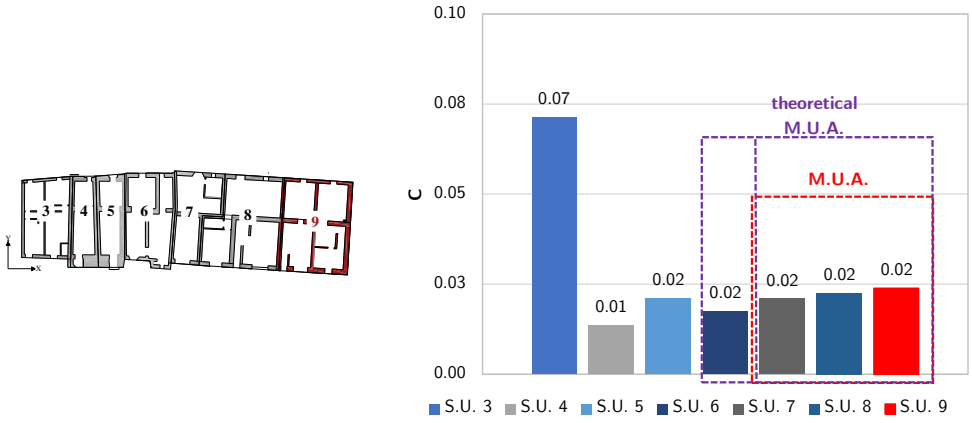

Figure 6-58: Castelnuovo aggregate – external S.U. 9: comparison between the theoretical and the individuated M.U.A. in terms of the conventional strength (C) distribution.

6.2.5.1 Comparison with the isolated conditions

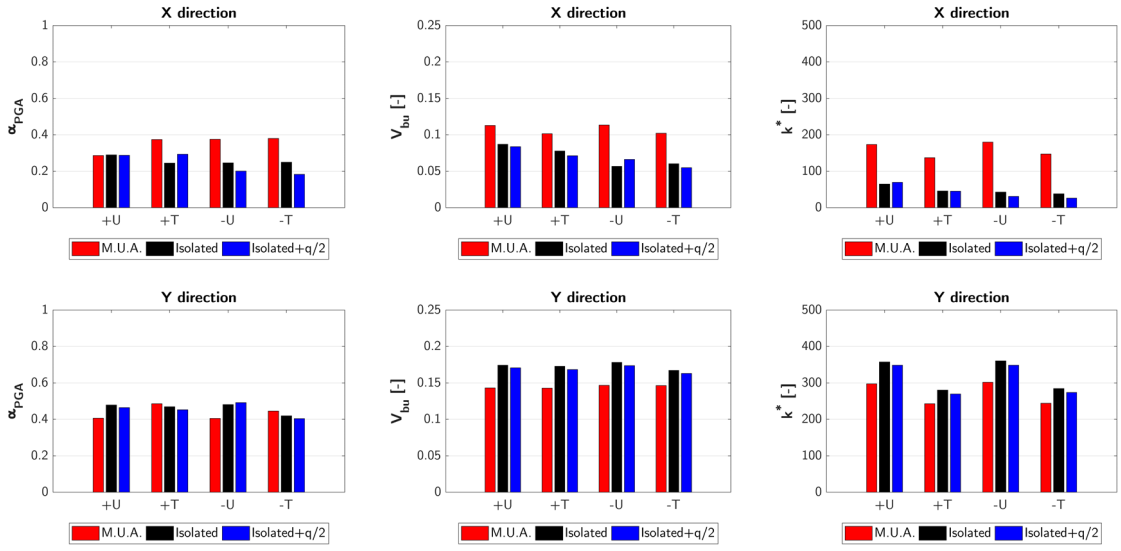

Figure 6-59: Castelnuovo aggregate – external S.U. 9: comparison of results between the M.U.A. and the isolated conditions.

The results obtained for the M.U.A. are compared with those of the isolated S.U.9 and of this modelled with the pertinent loads deriving from the immediately adjacent S.U. 8 (hereinafter referred as "isolated + q/2" model).

The results obtained for the 3 conditions are compared in Figure 6-59, in terms of α_{PGA}, maximum base shear V_{bu} and stiffness k^*.

The seismic capacity of the M.U.A. is the greatest in X direction, especially in terms of stiffness and maximum base shear; on the contrary, it is the lowest in Y direction. Moreover, it is possible to notice that the isolated conditions present a similar behaviour.

In the following, only the analyses of each direction with the lowest value of α_{PGA} for M.U.A. are considered, that means +X and -Y uniform distribution.

In Figure 6-60, the pushover curves are compared; moreover, Table 6-8 shows the percentage changes, obtained in reference to the M.U.A., for the isolated conditions.

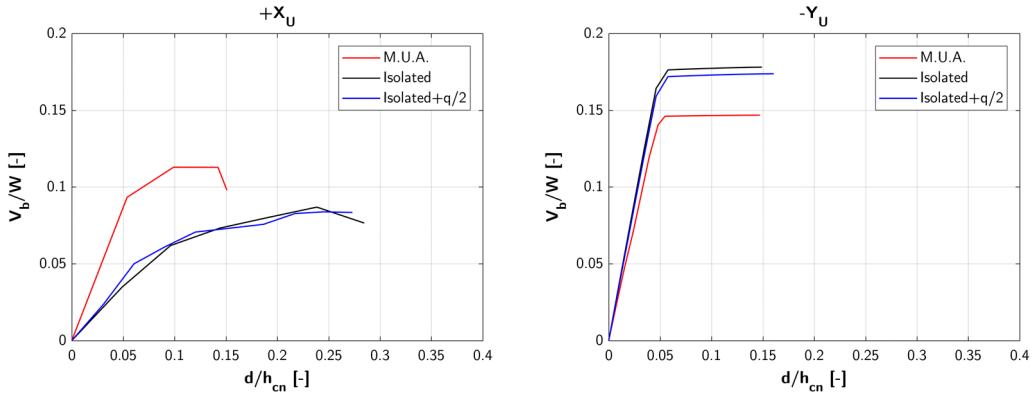

Figure 6-60: Castelnuovo aggregate – external S.U. 9: pushover curves comparison between the M.U.A. and the isolated conditions.

Table 6-8: Castelnuovo aggregate – external S.U. 9: percentage changes of α_{PGA}, k^* and V_{bu} for the isolated conditions in reference to M.U.A.

		Δ% α_{PGA}	Δ% k*	Δ% V_{bu}
X direction	**Isolated**	1%	-63%	-23%
	Isolated + q/2	0%	-60%	-26%
Y direction	**Isolated**	19%	20%	21%
	Isolated + q/2	21%	16%	18%

As previously observed, in X direction the isolated conditions present a reduction of the capacity, especially in terms of stiffness, in the order of 60%; the α_{PGA} is unvaried. In Y direction, instead, they show an increment of the capacity, in the order of 20% for all the quantities. Therefore, also for this external S.U., the analysis of the isolated S.U., modelled with or without the pertinent loads, implies a relevant variation of the seismic capacity in both directions of analysis.

6.3 CONCLUDING REMARKS

In this chapter, the proposed *"target structural unit approach"* procedure is applied to different S.U.s of two case studies, a L aggregate in Faro (Portugal) and a row aggregate in Castelnuovo (L'Aquila). The obtained M.U.A. are compared with the theoretical ones deriving from the analysis of the prototype aggregates, considering the distribution of the conventional strength, C, in the aggregates.

For the row aggregate in Castelnuovo, the results are in accordance with those of the prototypes. In detail, for the internal S.U.6 (§6.2.4), that is placed between structures presenting similar C values, the theoretical M.U.A. includes the immediately adjacent S.U.s on each side, but in this case the next S.U.8 on the right side should also be included since it is planimetrically complementary to S.U.7.
For the external S.U.9 (§6.2.5), that presents a C value slightly major in respect to the others, the M.U.A. is composed of 2 adjacent S.U.s, as observed for the prototype aggregates.

Referring to the L aggregate in Faro, the results are less predicted and partially validate the theoretical schemes. It should be remembered that for the prototypes the M.U.A. is not influenced as much by the heterogeneities as by the plan configuration.
For a corner building, two distinct theoretical M.U.A are individuated in function of the analysis direction, each of them excludes the external S.U. in the transversal row. Considering the corner S.U.C of Faro (§6.1.3), the results are partially in accordance with those obtained for the prototype aggregates, since the same M.U.A. is individuated for both directions, excluding the external S.U.E.: it just differs for the X direction.
Considering the external S.U.A (§6.1.4), the individuated M.U.A. is the longitudinal row in which it is placed (S.U.B and C). In this case, contrary to the theoretical M.U.A., the S.U.D adjacent in the transversal row is excluded.

Hence, it is possible to conclude that the theoretical M.U.A. proposed for the prototypes are partially validated. However, it is stressed that the M.U.A. must be individuated by considering, in addition to the conventional strength distribution, structural features that may influence the damage distribution, but that often cannot be represented by numerical values, as for example the planimetric configuration of the S.U.s in the aggregate and the distribution of the resistant area.

Chapter 7.
Conclusions and outlooks

In this chapter, the conclusions about the work are drawn. The main goals achieved are summarised and suggestions for the future steps of the research are given.

The present dissertation has focused on the global seismic performance of masonry buildings in aggregate, which are the most widespread structural typology in Italian historical centres (and across the world) and, for this reason, the evaluation of their seismic safety is a matter of great importance. Indeed, the significant damages occurred after the recent Italian earthquakes have highlighted the necessity of a specific methodology for the analysis of these structures and the planning of proper unitary interventions. The main aim of the work is understanding how the **"aggregate effect"**, that refers to the effects of interactions between adjacent buildings during a seismic event, should be modelled for a more accurate assessment of the seismic performance of these structures.
To this end, it has been shown how the analysis of a building in aggregate can concern just a restricted portion of the compound, reducing the difficulties and the uncertainties related to the knowledge process of a whole aggregate.
Hence, a new procedure has been proposed for identifying the **M.U.A.**, i.e. Minimum Unit of Analysis, that is the optimal portion of the aggregate that best represents the "aggregate effect" for the investigated building. It is important to underline that the procedure can be applied to buildings able to explicate a global box behaviour, therefore characterized by connections among orthogonal walls and between horizontal and vertical elements.
The research was motivated by the lack of guidelines or indications in the scientific literature on how to account for these interactions in numerical models, without the need for modelling the entire aggregate or considering only the isolated structure.

A preliminary step of the study has been a **sensitivity analysis** for evaluating the influence of the main interaction factors on the global seismic performance of prototype aggregates, defined on the basis of the features of the typical aggregates of the suburbs of Florence (Chapter 4). Several modelling configurations have been generated from the combination of basic S.U.s of defined characteristics and the investigated factors have been, in detail: the aggregate typology, the number of S.U.s, the position of the S.U. in the aggregate, the floors typology, the presence of material heterogeneities and of differences in height. Nonlinear static (pushover) analyses have been performed. The variability of the seismic performance has been evaluated in terms of seismic capacity, by means of the maximum base shear V_{bu} and the equivalent stiffness k^*, by considering 3 levels of analysis: global– (V_{bu} and k^* of the global model), S.U.– (V_{bu} and k^* of the S.U. in the global model) and wall– level (V_{bu} and k^* of the wall in the global model).
Two main typologies have been analysed, row and L aggregates, as they are very common configurations. Their different behaviours have been highlighted: while for the row aggregate the capacity in the transversal direction generally doubles that in the longitudinal one, for the L aggregate this is comparable in the two directions of analysis.
Since the seismic performance of a S.U. is also influenced by its position in the aggregate, 3 different conditions have been analysed: external S.U., internal S.U. and corner S.U; the external position is generally the most sensitive to the interaction factors, while the corner one is the least influenced. The number of S.U.s is the most influential factor at global– level, especially for the row aggregate, with increments of around 70% in terms of V_{bu} and 100% in terms of k^*; on the contrary, it is the least determining at S.U.– level, since the influence of the other buildings on the target S.U. decreases with distance. Indeed, it has

been shown that the seismic capacity of the S.U. is unvaried if it is placed within an aggregate of 5, 7 or 9 S.U.s., regardless of its position and the aggregate typology. Consequently, the study of the row aggregate and the L aggregate composed of 5 S.U.s. has been deepened.

The presence of material heterogeneities significantly influences the seismic performance; indeed, the capacity of the aggregate increases as the number of more rigid S.U.s grows. For example, when the 3 internal S.U.s are the most rigid, the increments are major than 80% in terms of V_{bu} and 90% in terms of k^*. These increases are also evident at S.U.– level, especially for the most rigid S.U.s, for which they are major than 200%; on the contrary, the behaviour of the buildings not subject to material changes is not influenced.

Moreover, the presence of taller S.U.s generally produces a reduction of the seismic capacity, especially in terms of stiffness with values of around 40%, because of more fragile walls.

Finally, the floors typology is generally less relevant compared to the other factors.

Hence, the new **"target structural unit approach"** procedure has been presented and applied on the prototype aggregates (Chapter 5), for providing general schemes in function of the analysed case, and validated on two case studies (Chapter 6): a L aggregate in Faro (Portugal) and a row aggregate in Castelnuovo (L'Aquila).

The general framework of the proposed *"target structural unit approach"* is shown in Figure 7-1.

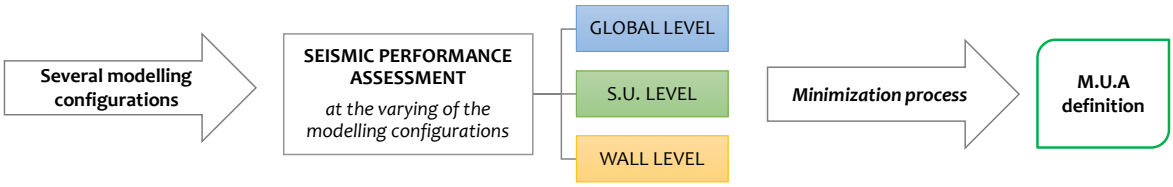

Figure 7-1: Framework of the proposed "target structural unit approach".

The procedure consists of different phases and is characterized by two main features. The first aspect is the definition of several boundary conditions for the target S.U., in addition to the complete aggregate configuration. The isolated condition is not considered because is an excessive simplification, that neglects the effects of interaction. The second feature is the performing of the seismic assessment by means of nonlinear static analyses at 3 levels of detail: global- level (analysis of the global modelling configurations of the aggregate, models M_i), S.U.- level (analysis of the target S.U. in each configuration, models M^*_i) and wall- level (analysis of the boundary walls of the target S.U. in each configuration).

The *S.U.– level* is introduced as a fundamental verification level to understand the variability of the seismic response of the case study building in function of different boundary conditions and to identify the MUA. For this reason, the procedure is referred to as *"target structural unit approach"*.

The M.U.A. corresponds to the global configuration (model M_i), for which the target S.U. (model M^*_i) presents the closest seismic response to that of the reference configuration, that is the complete aggregate condition. For this reason, the application of the procedure is meaningful only if the aggregate is exhaustively investigated and the global models M_i are reliable.

When the complete aggregate condition is affected by uncertainties, the reference configuration for the target S.U. can be unknow. In this case, the procedure can allow identifying the variation range of the M.U.A., excluding the extreme conditions.

Theoretical M.U.A. have been provided in function of the interaction factors, for the row and L aggregates (Chapter 5). Moreover, with the aim to generalize the outcomes, the **conventional strength** C, calculated as the ratio between the shear resistance value and the weight, has been evaluated for each S.U. and its distribution in the aggregate has been considered in function of the analysed cases.

Analysing an **internal S.U.** of a **row aggregate**, in absence of heterogeneities or when this is between S.U.s of the same height (having same C value), the M.U.A. should generally include the immediately adjacent S.U. on each side.

In presence of material heterogeneities, if some more rigid S.U.s are present in the aggregate, they influence considerably the target S.U. For example, if the target and the immediately adjacent ones are the most rigid in the aggregate (with change of C value with respect to the average value of the aggregate greater than 50%), the M.U.A. should also include the next less resistant S.U.s on each side, otherwise its seismic capacity would be too much increased compared to the reference configuration. Moreover, if the internal S.U. is adjacent to more resistant structures on one side (having greater C value), the M.U.A. should also incorporate the next more resistant one, in addition to the immediately adjacent S.U.s. On the contrary, if these S.U.s are taller (having inferior C value), the next one of the same height should also be included in the M.U.A.

For an **external S.U.**, if the target S.U. is adjacent to more resistant S.U.s or is one of the tallest in the aggregate (having inferior C value), the M.U.A. generally includes 2 S.U.s. For the other cases, models with 2 or 3 adjacent S.U.s have provided similar results.

In the case of a **L aggregate**, the M.U.A. results to be the same for all the cases, suggesting that its complex plan configuration is more influential than the investigated factors. Analysing a **corner S.U.**, two different M.U.A have been defined in function of the analysis direction, excluding the external S.U. in the transversal row, respectively.

For an **external S.U.**, the M.U.A is the configuration that excludes the opposite external S.U.

Finally, the theoretical M.U.A. obtained for the prototype aggregates have been applied to different S.U.s of the two real masonry aggregates (Chapter 6), by evaluating the distribution of the conventional strength, C, in the aggregate. The results have been therefore validated by applying the proposed procedure to the target S.U.s. and they are partially consistent, stressing the necessity to identify the M.U.A. by considering, in addition to the conventional strength C distribution, structural features that influence the seismic behaviour, but that often cannot be represented by numerical values, as for example the planimetric configuration of the S.U.s in the aggregate and the distribution of the resistant area.

The main achievements of this work are summarized below.

- The study of the prototype aggregates has allowed to evaluate the influence of the main interaction factors and to highlight the principal aspects of the seismic behaviour of row and L aggregates.

- The importance of the number of S.U.s in the aggregate has been deepened, showing that the influence of the adjacent S.U.s on the investigated one decreases in function of the distance. For this reason, in presence of wide-large aggregates, the analysis can concern just a portion composed of at most 5 S.U.s, reducing the uncertainties related to a knowledge process of too extended areas, that may be in part inaccessible.

- The proposed procedure improves the global seismic performance assessment of masonry buildings in aggregate with a view to define a unitary methodology for the analysis of these structures. Its main characteristic is the adaptability to aggregates of various configurations and to S.U.s in different position.

- General indications for identifying the M.U.A. have been provided in function of the interaction factors, especially for the row aggregates. Of course, they should be adapted to the analysed case study, since each aggregate is characterized by different structural features.

- The comparison of the values of the conventional strength C allows to evaluate the respective relationship of influence between the S.U.s in the aggregate and it can be a useful tool for the identification of M.U.A. In general, a S.U. characterized by a relevant value of C is influential in the aggregate and can affect the behaviour of the analysed structure, especially if placed at a distance of 2-3 S.U.s at most.

- Relevant errors in the evaluation of the seismic response can be made through a too simplified modelling of the investigated S.U. (as the isolated S.U. or modelled with the loads deriving from the immediately adjacent structures). Referring to both an internal and an external S.U. of a row aggregate, the isolated conditions generally present a reduction of the seismic capacity in the longitudinal direction (inferior to 30%) and an increment in the transversal one (major than 20%), suggesting that a simplified model can be in favour of safety in the first direction, but not in the second one.

Reminding that in the scientific literature extreme approximations have been usually applied for this type of study, the proposed *"target structural unit approach"* represents a useful tool for the seismic risk assessment of masonry buildings in aggregate. It provides opportunities for future researches, aiming at defining guidelines for this structural typology and supporting retrofitting strategies. To this end, the principal outlooks would concern the improvement of the proposed procedure and of the provided general schemes, both by increasing the number of the investigated aggregates and by deepening the analysis of more complex aggregate typologies.

References

AA.VV. Dirett. scientifico Borri, A. (2011). Manuale delle murature storiche. Roma: D.E.I. Tipografia del Genio Civile.

Amadio, C., Rinaldin, G., Puppin, A., & Camillo, M. (2011). Analisi semplificata della vulnerabilità sismica di un aggregato edilizio in muratura il complesso denominato Vaticano (Trieste). *XIV Convegno ANIDIS "L'Ingegneria Sismica in Italia"*. Bari.

ASCE/SEI 41-13. (2014). *Seismic evaluation and retrofit of existing buildings*. American Society of Civil Engineers, Reston.

Athanassiadou, C. J., Penelis, G., & Kappos, A. J. (1994). Seismic response of adjacent buildings with similar or different dynamic characteristics. *Earthquake Spectra, 10*(2).

Benedetti, D., & Petrini, V. (1984). Sulla vulnerabilità di edifici in muratura: Proposta di un metodo di valutazione. In *L'industira delle costruzioni, Vol. 149, No. 1* (p. 66-74).

Bernardini, A., Giovinazzi, S., Lagomarsino, S., & Parodi, S. (2007 A). Matrici di probabilità di danno implicite nella scala EMS-98. *XII Convegno ANIDIS "L'Ingegneria Sismica in Italia".* Pisa.

Bernardini, A., Giovinazzi, S., Lagomarsino, S., & Parodi, S. (2007 B). Vulnerabilità e previsione di danno a scala territoriale secondo una metodologia macrosismica coerente con la scala EMS-98. *XII Convegno ANIDIS "L'Ingegneria Sismica in Italia".* Pisa.

Bernardini, C., Boschi, S., Empelmann, M., & Vignoli, A. (2017). Sensitivity analysis of seismic behaviour of masonry aggregates. *XVII Convegno ANIDIS "L'Ingegneria Sismica in Italia".* Pistoia.

Bernardini, C., Maio, R., Boschi, S., Ferreira, T. M., Vicente, R., & Vignoli, A. (2018). The seismic vulnerability assessment of a stone masonry building enclosed in aggregate. *16th European Conference on Earthquake Engineering*. Thessaloniki.

Bernardini, C., Maio, R., Boschi, S., Ferreira, T. M., Vicente, R., & Vignoli, A. (2019). The seismic performance-based assessment of a masonry building enclosed in aggregate in Faro (Portugal) by means of a new target structural unit approach. *Engineering Structures*, (191) 386-400.

Betti, M., Borghini, A., Ciavattone, A., Boschi, S., Del Monte, E., & Vignoli, A. (2011). Assessment of the seismic risk of the museum of Casa Vasari in Arezzo (Italy). *International Journal of Masonry Research and Innovation*, (2) 107-133.

Borghini, A., Del Monte, E., Ortolani, B., & Vignoli, A. (2011). Studio degli effetti del sisma del 06/04/2009 sulla Frazione di Castelnuovo, Comune di San Pio delle Camere (AQ). Bari.

Borri, A., Corradi, M., Castori, G., & De Maria, A. (2015). A method for the analysis and classification of historic masonry. *Bullettin of Earthquake Engineering*, 13: 2647–2665.

Boschi, S. (2015). Seismic risk analysis of masonry buildings in aggregate. *Ph.D. Thesis*. Università di Firenze & Technical University Carolo-Wilhelmina Braunschweig.

Boschi, S., Borghini, A., Del Monte, E., Ortolani, B., & Vignoli, A. (2013). Methodology for ante and post-earthquake assessment of existing masonry buildings: a case study of an aggregate. *XV ANIDIS Conference "L'Ingegneria Sismica in Italia"*. Padova.

C.M. 617/2009. (2009). *Istruzioni per l'applicazione delle nuove norme tecniche per le costruzioni di cui al D.M. 14/01/2008*. Rome: Ministry of Infrastructure.

Calderoni, B., Cordasco, E., & Lenza, P. (2009). La modellazione degli edifici storici in muratura per la valutazione della vulnerabilità sismica. *XIII Convegno ANIDIS "L'Ingegneria Sismica in Italia"*. Bologna.

Calvi, G. (1999). A displacement-based approach for vulnerability evaluation of classes of buildings. *Journal of Earthquake Engineering*, Vol 3, No. 3, 411-438.

Calvi, G., Pinho, R., Magenes, G., Bommer, J., Restrepo-Vélez, L., & Crowley, H. (2006). Development of Seismic Vulnerability Assessment Methodologies Over the Past 30 Years. *Journal of Earthquake Technology*, Vol. 43, No. 3, 75-104.

Caniggia, G., & Maffei, G. (1979). *Lettura dell'edilizia di base*. Padova: Marsilio.

Carocci, C. (2001). Guidelines for the safety and preservation of histrical centres in seismic areas. In P. R. P.B. Lourenço, *Historical Constructions*. Guimarães.

Carocci, C. (2006). Classificazione degli aggregati. *ReLUIS 2005-2008 Research Project No. 1: Assessment and reduction of the vulnerability of masonry buildings*.

Carocci, C. (2006). Lettura critica degli aggregati. *ReLUIS 2005-2008 Research Project No. 1: Assessment and reduction of the vulnerability of masonry buildings*.

Carocci, C. (2012). Small centres damged by 2009 L'Aquila earthquake: on site analyses of historical masonry aggregates. *Bulletin of Earthquake Engineering*(10), 45–71.

Carocci, C., & Marino, M. (2009). Gli aggregati murari della città storica: conoscenza e interpretazione per la valutazione della vulnerabilità sismica. *XIII Convegno ANIDIS "L'Ingegneria Sismica in Italia"*. Bologna.

Carocci, C., & Tocci, C. (2007). Sicurezza sismica degli aggregati edilizi storici: alcuni casi di studio. *XII Convegno ANIDIS "L'Ingegneria Sismica in Italia"*. Pisa.

Cattari, S., Curti, E., Giovinazzi, S., Lagomarsino, S., Parodi, S., & Penna, A. (2004). Un modello meccanico per l'analisi di vulnerabilità del costruito in muratura a scala urbana. *XI Convegno ANIDIS "L'Ingegneria Sismica in Italia"*. Genova.

Cattari, S., Degli Abbati, S., Ferretti, D., Lagomarsino, S., Ottonelli, D., Rossi, M., & Tralli, A. (2012). The seismic behaviour of ancient masonry buildings after the earthquake in Emilia (Italy) on May 20th and 29th, 2012. *Ingegneria Sismica*, vol. 29, pp. 87–119.

Cattari, S., Lagomarsino, S., Bosiljkov, V., & D'Ayala, D. (2015). Sensitivity analysis for setting up the investigation protocol and defining proper confidence factors for masonry buildings. *Bullettin of Earthquake Engineering*, 13: 129–151.

Chiarandini, A. (1999). *Leggi di correlazione tra danno, intensità e vulnerabilità sismica sulla base dei dati di Venzone, Tarcento e San Daniele del Friuli*. Università di Udine.

Chopra, A., & Goel, R. (1999). Capacity-Demand-Diagram methods based on inelastic design spectrum. *Earthquake Spectra, 15*(4), 637-655.

CNR-DT 212. Guide for the probabilistic assessment of the seismic safety of existing buildings. (2014). Rome.

Corsanego, A., & Petrini, V. (1990). Seismic vulnerability of buildings. *SEISMED 3*. Trieste.

D'Ayala, D., & Paganoni, S. (2011). Assessment and analysis of damage in L'Aquila historic city centre after 6th April 2009. *Bullettin of Earthquake Engineering*, (9) 81-104.

Damoni, C., & Belletti, B. (2011). Valutazione del livello di rischio sismico di edifici storici tramite analisi globale e locale. *XIV Convegno ANIDIS "L'Ingegneria Sismica in Italia"*. Bari.

D'Ayala, D., & Speranza, E. (2002). An integrated procedure for the assessment of seismic vulnerability of historic buildings. *12th European Conference on Earthquake Engineering*. London.

De Felice, G., & Giannini, R. (2001). Out-of-plane seismic resistance of masonry walls. *Journal of Earthquake Engineering*, vol. 5, no. 2, pp. 253–271.

Dolce, M., & Moroni, C. (2004). La valutazione della vulnerabilità e del rischio sismico degli edifici pubblici mediante le procedure VC (vulnerabilità c.a.) e VM (vulnerabilità muratura). INGV/GNDT - Gruppo Nazionale per la Difesa dei Terremoti.

EN1996-1-1:2005. (2005). *CEN. Eurocode 6: Design of masonry structures - Part I: General rules for reinforced and unreinforced masonry structures*. Brussels.

EN1998-1:2004. (2004). *CEN. Eurocode 8: Design of structures for earthquake resistance - Part I: General rules, seismic action and rules for buildings*. Brussels.

EN1998-3:2004. (2004). *CEN. Eurocode 8: Design of structures for earthquake resistance - Part 3: assessment and retrofitting of buildings*. Brussels.

Fagundes, C., Bento, R., & S., C. (2017). On the seismic response of buildings in aggregate: Analysis of a typical masonry building from Azores. *Structures*, 10: 184–196.

Fajfar, P. (2000). A non linear analysis method for performance based seismica design. *Earthquake Spectra, 16*(3), 573-592.

FEMA 273. (1997). *NEHRP guidelines for the seismic rehabilitation of buildings*. Washington DC: Federal Emergency Management Agency.

FEMA 274. (1997). *NEHRP commentary on the guidelines for the seismic rehabilitation of buildings*. Washington DC: Federal Emergency Management Agency.

FEMA 440. (2005). *Improvement of Nonlinear Static Seismic Analysis Procedures*. Washington DC: Federal Emergency Management Agency.

Ferreira, T. M., Costa, A., & Costa, A. (2015). Analysis of the Out-Of-Plane Seismic Behavior of Unreinforced Masonry: A Literature Review. *International Journal of Architectural Heritage*, vol. 9, no. 8., pp. 949–972.

Ferreira, T. M., Vicente, R., & Varum, H. (2012). Vulnerability assessment of building aggregates: a macroseismic approach. *15 WCEE*. Lisboa.

Ferreira, T. M., Vicente, R., Mendes da Silva, J., Varum, H., & Costa, A. (2013). Seismic vulnerability assessment of historical urban centres: case study of the old city centre in Seixal, Portugal. *Bulletin of Earthquake Engineering*.

Ferreira, T. M., Vicente, R., Varum, H., Costa, A., & Mendes da Silva, J. (2012). Seismic vulnerability assessment of the old city centre of Seixal, Portugal. *15 WCEE*. Lisboa.

Ferrito, T., Milosevic, J., & Bento, R. (2016). Seismic vulnerability assessment of a mixed masonry–RC building aggregate by linear and nonlinear analyses. *Bulletin of Earthquake Engineering*, 14(8): 2299–2327.

Fonti, Formisano, & Mazzolani. (2011). L'edificato storico di Poggio Picenze (AQ): il caso studio di un aggregato su pendio. *XIV Convegno ANIDIS "L'Ingegneria Sismica in Italia"*. Bari.

Formisano, A. (2016). Theoretical and numerical seismic analysis of masonry building aggregates: case studies in San Pio Delle Camere (L'Aquila, Italy). *Journal of Earthquake Engineering*, 1–19.

Formisano, A., Florio, G., Landolfo, R., & Mazzolani, F. (2015). Numerical calibration of an easy method for seismic behaviour. *Advances in Engineering Software, 80*, 116-138.

Freeman, S. (1998). The Capacity Spectrum Method. *1th European Conference on Earthquake Engineering*. Paris.

Giovinazzi, S. (2005). The vulnerability assessment and the damage scenario in seismic rick. *Ph.D. Thesis*. University of Firenze and Technical University Carolo-Wilhelmina Braunschweig.

Giuffrè, A. (1990). Mechanics of historical masonry and strengthening criteria. *XV Regional Seminar on Earthquake Engineering*.

Giuffrè, A. (1993). *Sicurezza e conservazione dei centri storici: il caso Ortigia.* Bari: Laterza.

Giuffrè, A., & Carocci, C. (1999). *Codice di pratica per la sicurezza e la conservazione del centro storico di Palermo.* Roma: Laterza.

GNDT. (1993). *Rilevamento della vulnerabilità sismica degli edifici in muratura - Istruzioni per la compilazione della scheda di 2° livello.* Roma, Consiglio Nazionale delle Ricerche - Gruppo Nazionale per la Difesa dei Terremoti.

GNDT. (1993). *Rischio sismico di edifici pubblici - Parte I - Aspetti metodologici.* Roma, Consiglio Nazionale delle Ricerche - Gruppo Nazionale per la Difesa dei Terremoti.

Grimaz, S., Meroni, F., Petrini, V., Tomasoni, R., & Zonno, G. (1996). Il ruolo dei dati di danneggiamento del terremoto del Friuli nello studio di modelli di vulnerabilità sismica degli edifici in muratura. *La scienza e i terremoti – Analisi e prospettiva dall'esperienza del Friuli – 1976/1996.*

Grünthal. (1998). Vol. 15 - European Macroseismic Scale 1998. In *Cahiers du Centre Européen de Géodynamique et de Séismologie*. Luxembourg.

Guagenti, E., & Petrini, V. (1989). Il caso delle vecchie costruzioni: verso una nuova legge danni intensità. *4th Italian Conference on Earthquake Engineering*, (p. Vol. I, pp. 145-153). Milano.

HAZUS. (1999). *Earthquake Loss Estimation Methodology - Technical and User Manuals.* Federal Emergency Management Agency. Washington, D.C.

http://www.ingv.it/it. (s.d.).

Indelicato, D. (2010). Valutazione e riduzione della vulnerabilità sismica degli aggregati edilizi nei centri storici. *PhD Thesis*. Catania.

Lagomarsino, S., Cattari, S., Degli Abbati, S., & Ottonelli, D. (2014). Seismic assessment of complex monumental buildings in aggregate: the case study of Palazzo del Podestà in Mantua (Italy). *9th SAHC Conference.* Mexico City, Mexico.

Lagomarsino, S., Penna, A., Galasco, A., & Cattari, S. (2013). TREMURI program: An equivalent frame model for the nonlinear seismic analysis of masonry buildings. *Engineering Structures*, 56: 1787–1799.

Lang, K. (2002). Seismic vulnerability of existing buildings. *Ph.D. Thesis*. Zurich.

Maio, R., Vicente, R., Formisano, A., & Varum, H. (2015). Seismic vulnerability of building aggregates through hybrid and indirect assessment techniques. *Bulletin of Earthquake Engineering*(13), 2995–3014.

Margottini, C., Molin, D., & Serva, L. (1992). Intensity versus ground motion: A new approach using Italian data. *Engineering Geology*, 45-58.

Milutinovic, Z. V., & Trendafiloski, G. S. (2003). WP4: Vulnerability of current buildings. *Risk-UE Project: An advanced approach to earthquake risk scenarios with applications. http://www.risk-ue.net*.

Neves, F., Costa, A., Vicente, R., Oliveira, C. S., & Varum, H. (2012). Seismic vulnerability assessment and characterisation of the buildings on Faial Island, Azores. *Bulletin of Earthquake Engineering*(10), 27–44.

NTC. (2008). *D.M. 14/01/2008: Norme tecniche per le costruzioni (Official Bullettin n. 29 of 04/02/2008)*. Rome: Ministry of Infrastructure.

O.P.C.M. n. 3431 del 03/05/2005. (2005). *Ulteriori modifiche ed integrazioni all'Ordinanza del Presidente del Consiglio dei Ministri n. 3274*. Ministry of Infrastructure.

Penna, A., Lagomarsino, S., & Galasco, A. (2014). A nonlinear macro-element model for the seismic analysis of masonry buildings. *Earthquake Engineering & Structural Dynamics*, 43:159–179.

Pujades, L., Barbat, A., González-Drigo, R., Avila, J., & Lagomarsino, S. (2012). Seismic performance of a block of buildings representative of the typical construction in the Eixample district in Barcelona (Spain). *Bulletin of Earthquake Engineering*, 10: 331–349.

Regione Toscana - Settore Sismica. (2016). Delibera del 12/12/2016, n.1271 . *Aggiornamento del Documento conoscitivo del rischio sismico 2016 (L.R. 58/2009 art. 4 comma 1)*.

Regione Umbria. (1998). Deliberazione Giunta Regionale del 14 settembre 1998, n. 5180. *Modalità e procedure per la concessione dei contributi previsti dall'art. 4 della l. n. 61/1998*.

Regione Umbria. (2002). Legge Regionale del 23/12/2002, n.18 . *Norme in materia di prevenzione sismica del patrimonio edilizio*.

ReLUIS. (2010). *Linee guida per il rilievo, l'analisi ed il progetto di interventi di riparazione e consolidamento sismico di edifici in muratura in aggregato*.

Rota, M., Penna, A., & Magenes, G. (2010). Methodology for deriving analytical fragility curves for masonry buildings. *Engineering Structures*(32), 1312-1323.

Rota, M., Penna, A., Strobbia, C., & Magenes, G. (2011). Typological seismic risk maps for Italy. *Earthquake Spectra*, Vol 27, No. 3 (p. 907-926).

Sandi, H. (1986). EAEE Working Group on Vulnerability and risk analysis for individual structures and systems. *8th European Conference on Earthquake Engeneering*. Lisbon.

STADATA. (2017). 3Muri program: seismic analyser of 3D masonry buildings. *Technical Report Release 11.0.0.8.*

Turnšek, V., & Cačovic, F. (1971). Some experimental results on the strength of brick masonry walls. *2nd International Brick Masonry Conference*, (p. 149-156). Stoke-on-Trent.

Ulrich, T., Negulescu, C., & Ducellier, A. (2015). Using the discrete element method to assess the seismic vulnerability of aggregated masonry buildings. *Bulletin of Earthquake Engineering* , 13(10): 3135–3150.

Vailati, M., & Monti, G. (2009). Procedura di analisi non lineare statica per la valutazione sismica degli edifici in aggregato. *XIII Convegno ANIDIS "L'Ingegneria Sismica in Italia"*. Bologna.

Vailati, M., & Monti, G. (2011). L'analisi di aggregati edilizi con solai rigidi e flessibili. *XIV Convegno ANIDIS "L'Ingegneria Sismica in Italia".* Bari.

Valluzzi, M., Munari, M., Modena, C., Cardani, G., & Binda, L. (2007). Analisi di vulnerabilità sismica degli aggregati storici: il caso di Castelluccio di Norcia. *XII Convegno ANIDIS "L'Ingegneria Sismica in Italia".* Pisa.

Valotto, C., Taffarel, S., Marson, C., Munari, M., Da Porto, F., & Modena, C. (2016). Seismic vulnerability assessment of corner buildings in the historical centre of Timisoara. *IB2MAC - 16° International Brick and Block Masonry Conference.* Padova.

Vicente, R. (2008). Estratégias e metodologias para intervenções de reabilitação urbana. *Ph.D. Thesis*. Universidade de Aveiro.

Vicente, R., D'Ayala, D., Ferreira, T. M., Varum, H., Costa, A., Mendes da Silva, J., & Lagomarsino, S. (2014). Seismic Vulnerability and Risk Assessment of Historic Masonry Buildings. In A. C. al., *Structural Rehabilitation of Old Buildings, Volume 2 of the series Building Pathology and Rehabilitation* (p. 307-348). Springer.

Vicente, R., Ferreira, T., Maio, R., Costa, A., Oliveira, C., Varum, H., & Estevão, J. (2016). URBSIS – Avalição da vulnerabilidade e gestão do risco sísmico à escala urbana. Aveiro, Portugal: Tipografia Lusitania.

Vicente, R., Parodi, S., Lagomarsino, S., Varum, H., & Mendes Silva, J. (2011). Seismic vulnerability and risk assessment: case study of the historic city centre of Coimbra, Portugal. *Bullettin of Earthquake Engineering, 9*, 1067–1096.

Vidic, T., Fajfar, P., & Fishinger, M. (1994). Consistent inelastic design spectra: strenght and displacement. *Earthquake Engineering and Structural Dynamics*, (23) 502-521.

Vignoli, A. (2012). *Ricostruire dopo il terremoto: il caso Castelnuovo (AQ).* Firenze: Alinea Editrice.

Whitman, R. (1973). *Damage probability Matrices for Prototype Buildings.* R73-57, Cambridge, Massachussets.

Withman, R., Reed, J., & Hong, S. T. (1974). Earthquake Damage Probability Matrices. *5 WCEE.* Roma.

Zuccaro, G. (2004). Inventory and vulnerability for residential buildings at National territorial level, risk maps and socio-economic losses. *SAVE, INGV/GNDT Project*. Napoli.

Annex A.
Results of the prototype aggregates

For the prototype aggregates, the results obtained for all cases are resumed in the following tables.

A1. Row aggregate – Different floors typology

Internal S.U.

Table A 1: Row aggregate – internal S.U.: F floors.

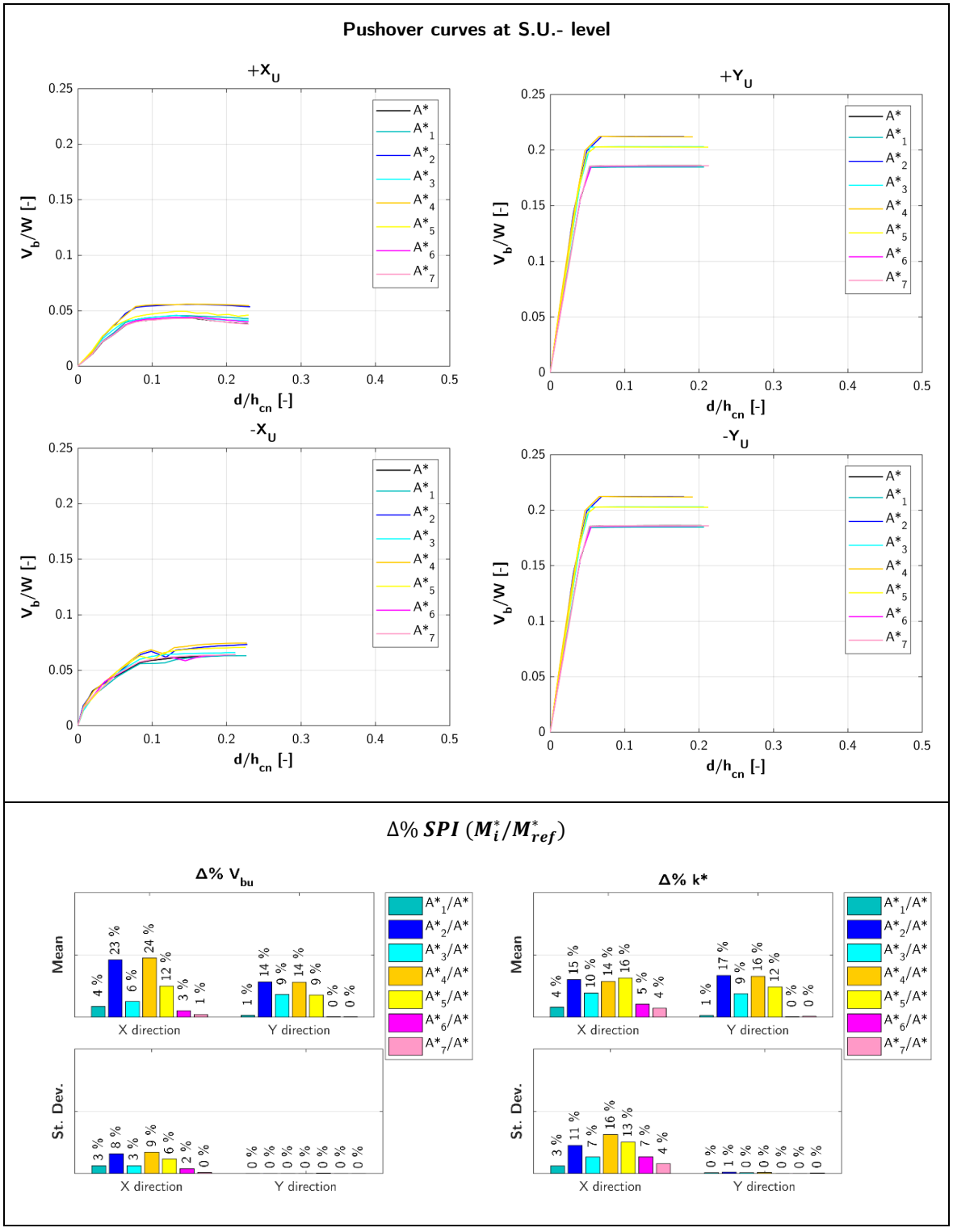

Table A 2: Row aggregate – internal S.U.: RRFFF floors.

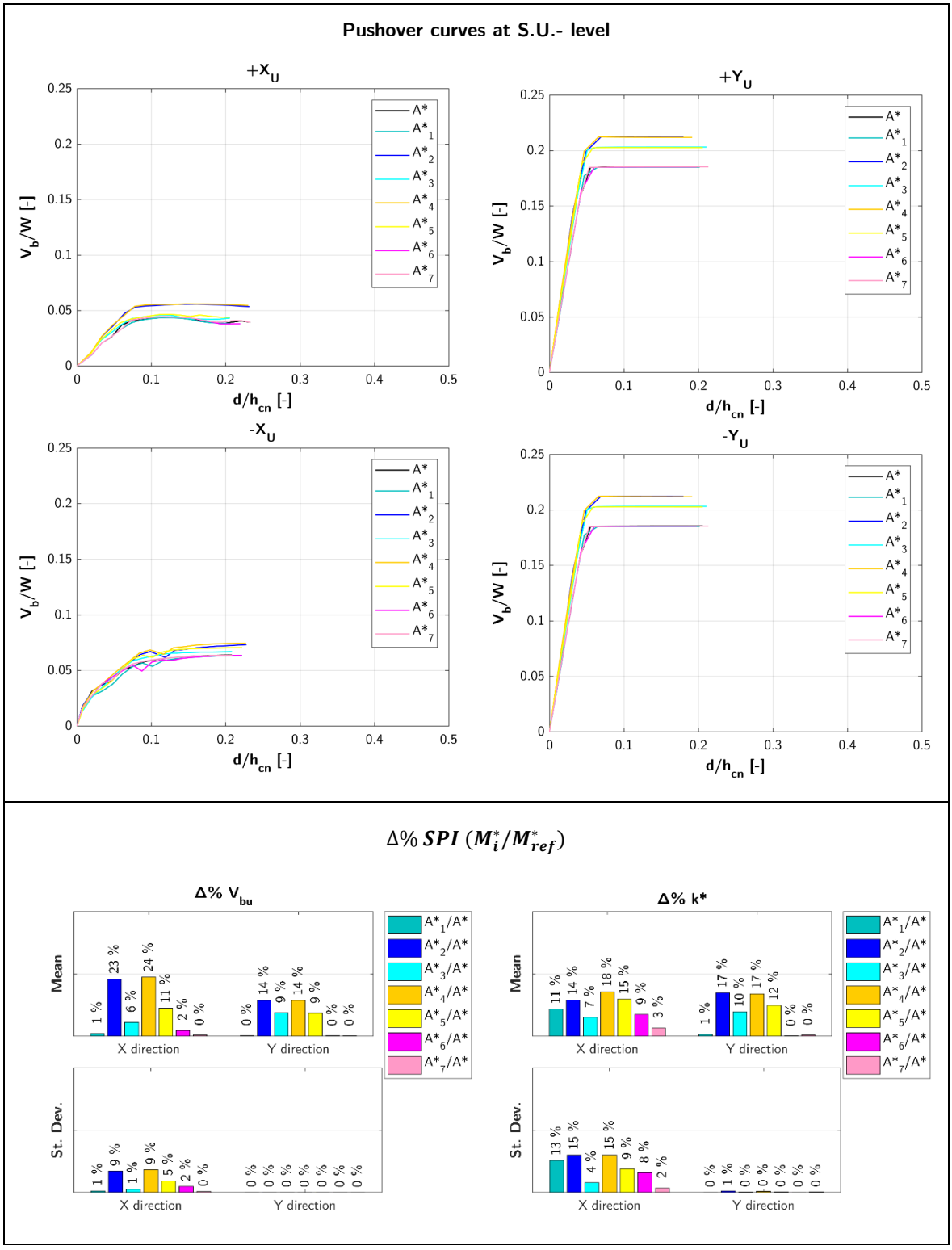

Table A 3: Row aggregate – internal S.U.: FFRFF floors.

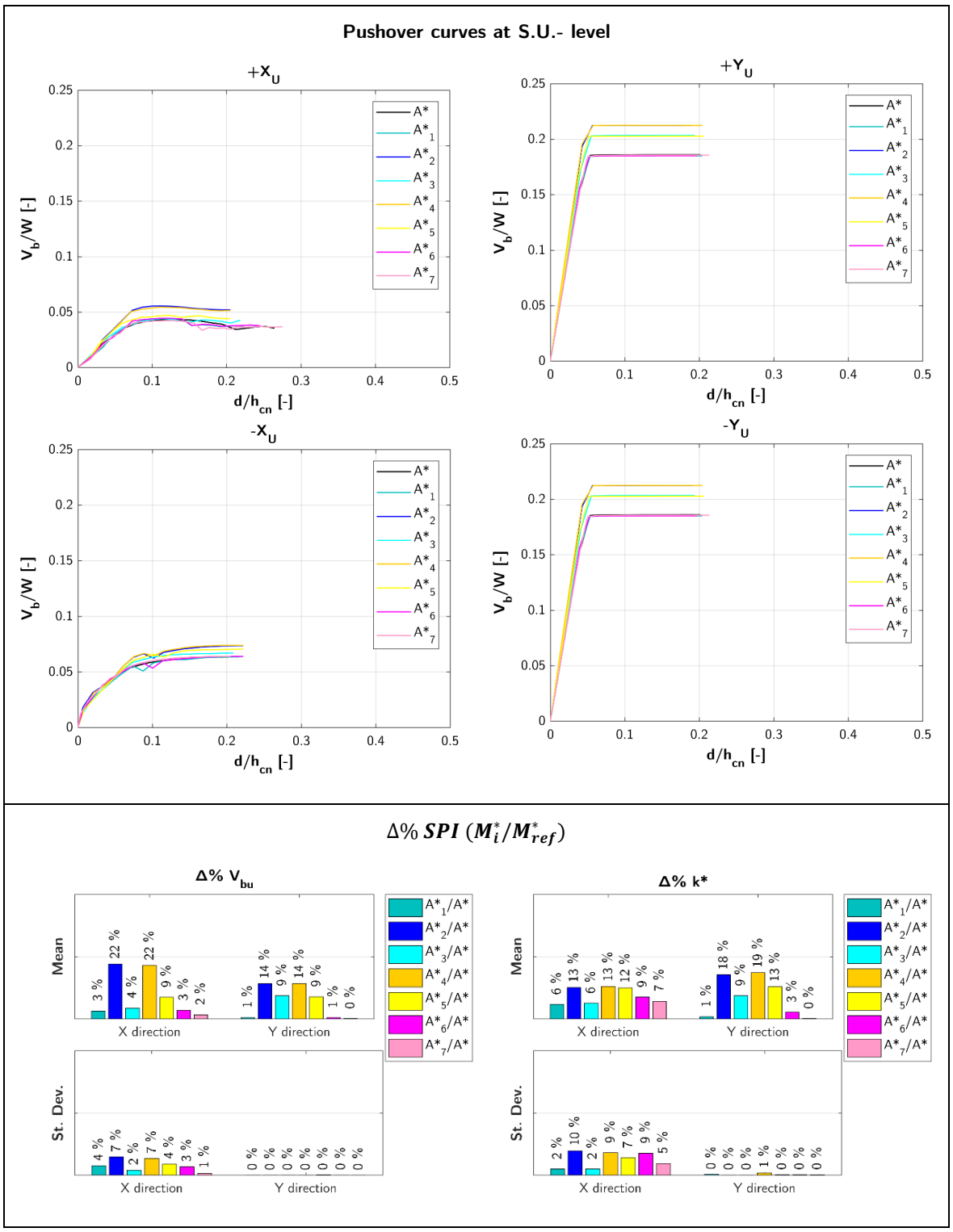

Table A 4: Row aggregate – internal S.U.: FRRRF floors.

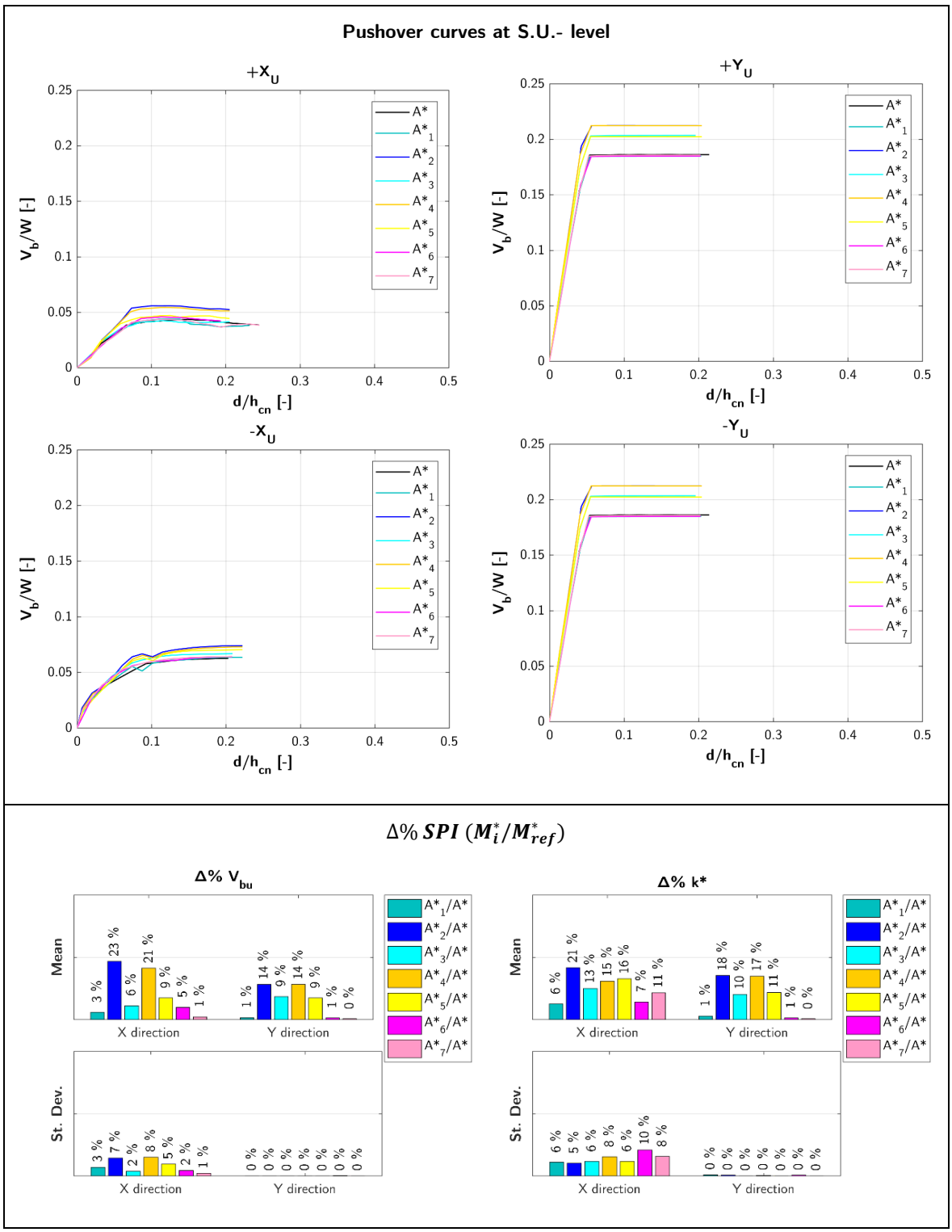

External S.U.

Table A 5: Row aggregate – external S.U.: R floors.

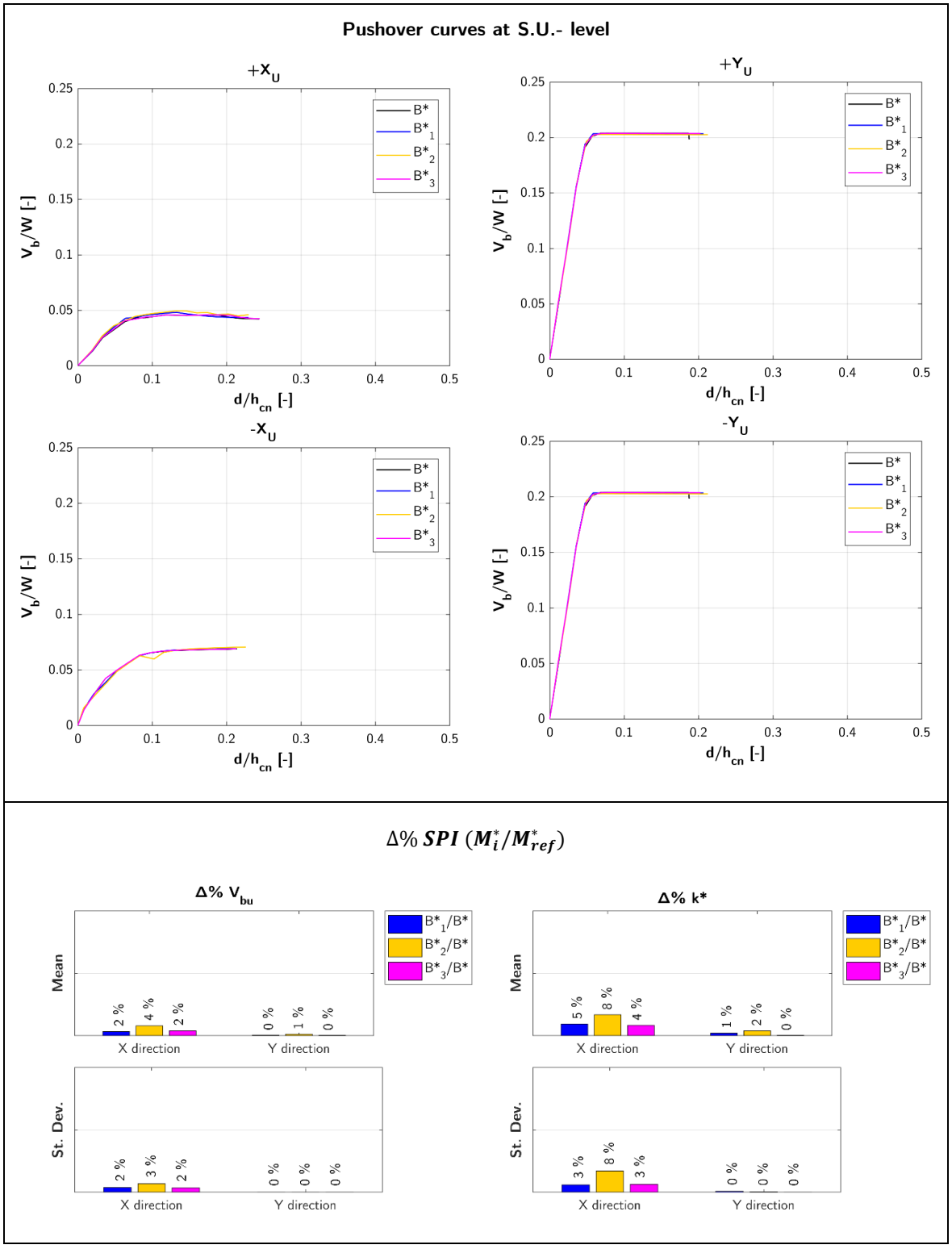

Table A 6: Row aggregate – external S.U.: F floors.

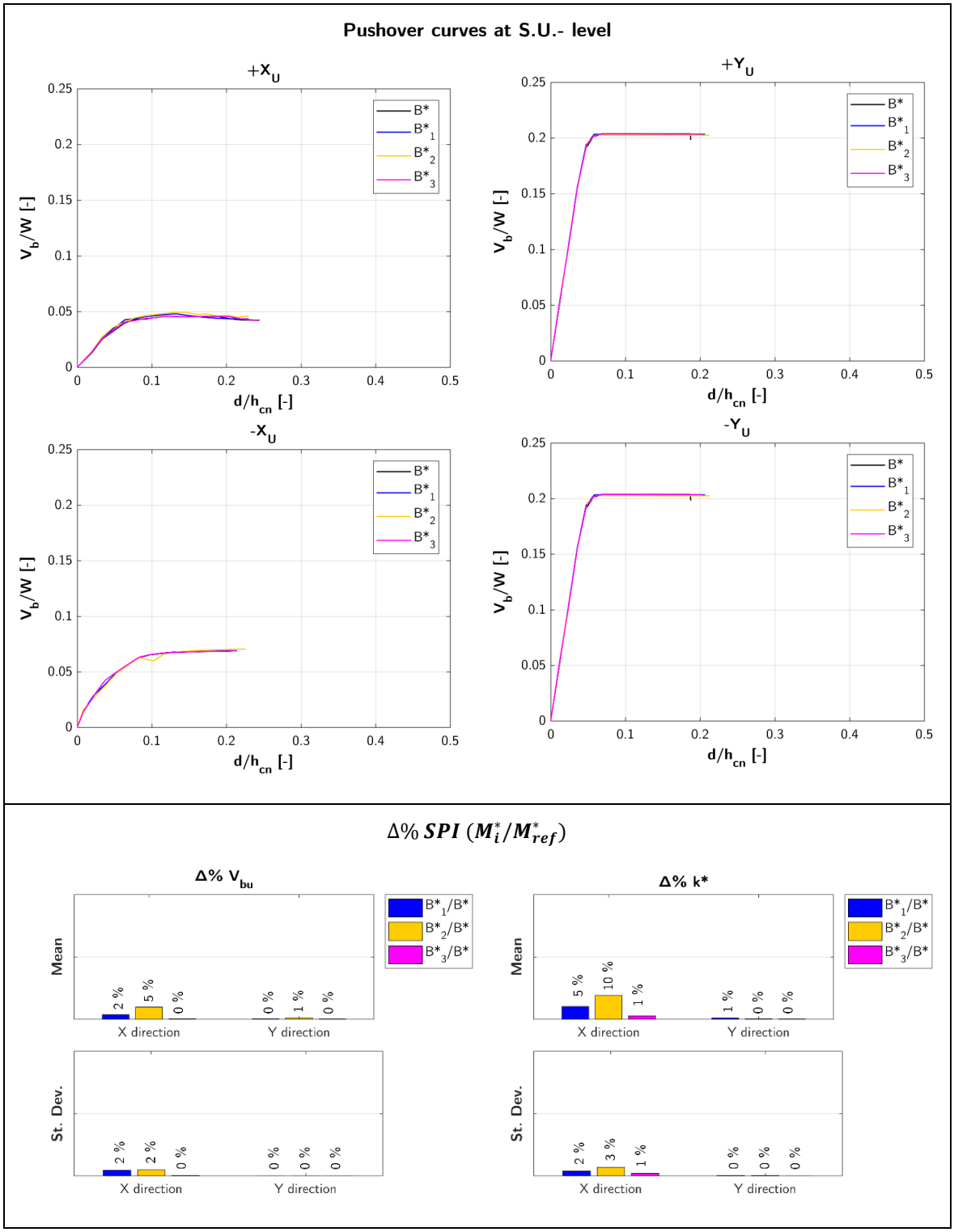

Table A 7: Row aggregate – external S.U.: RRFFF floors.

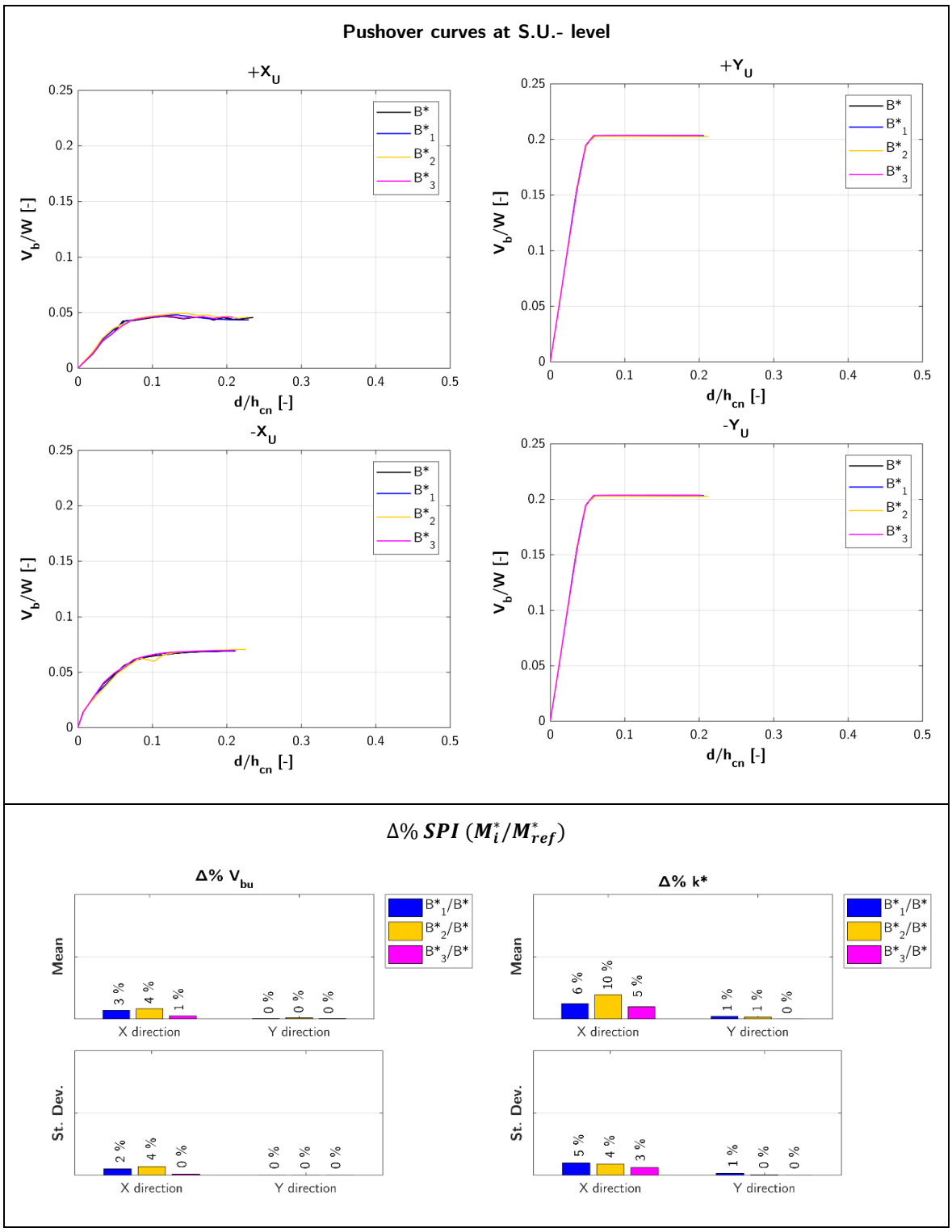

Table A 8: Row aggregate – external S.U.: FFRFF floors.

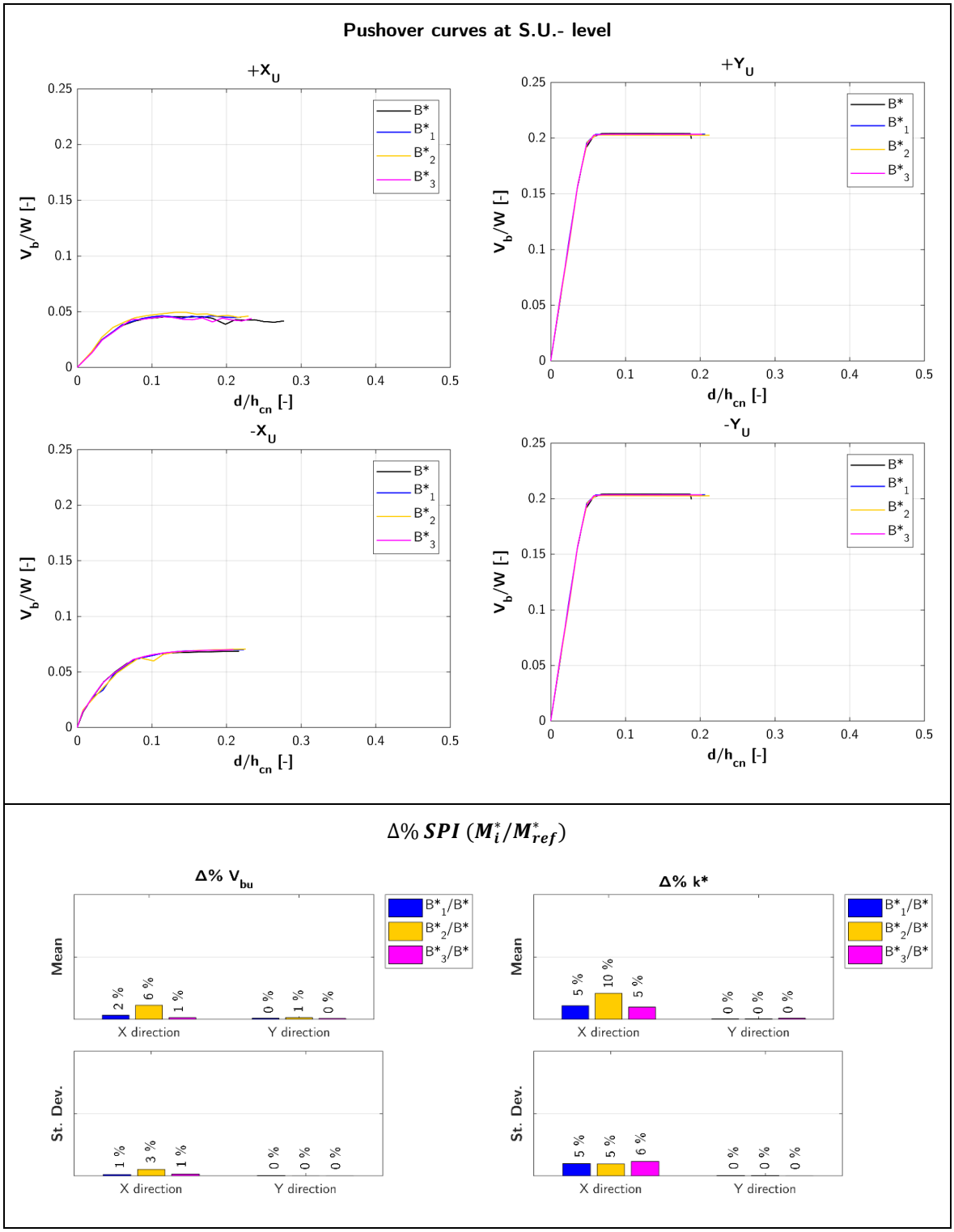

Table A 9: Row aggregate – external S.U.: FRRRF floors.

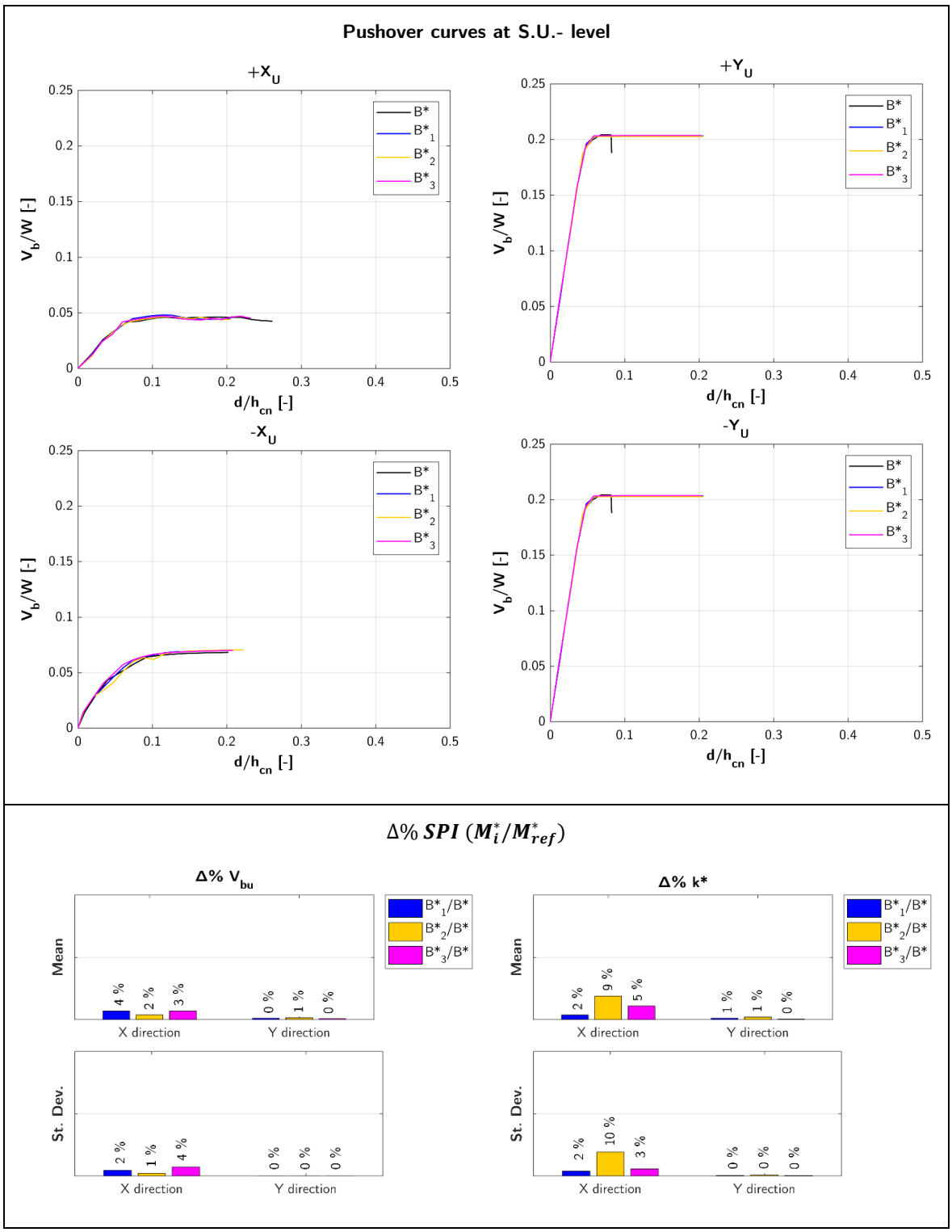

A2. L AGGREGATE – DIFFERENT FLOORS TYPOLOGY

Corner S.U.

Table A 10: L aggregate – corner S.U.: R floors.

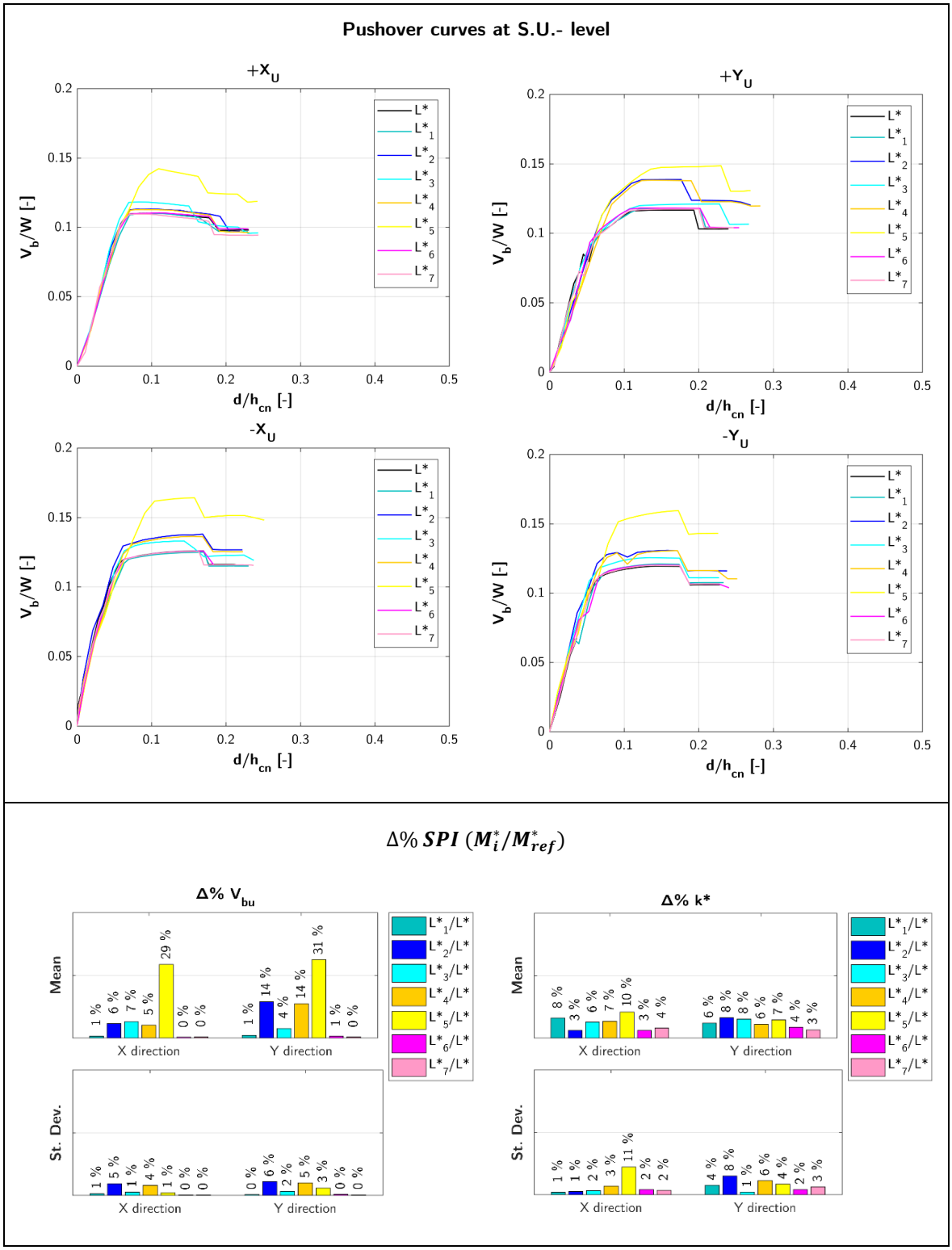

Table A 11: L aggregate – corner S.U.: F floors.

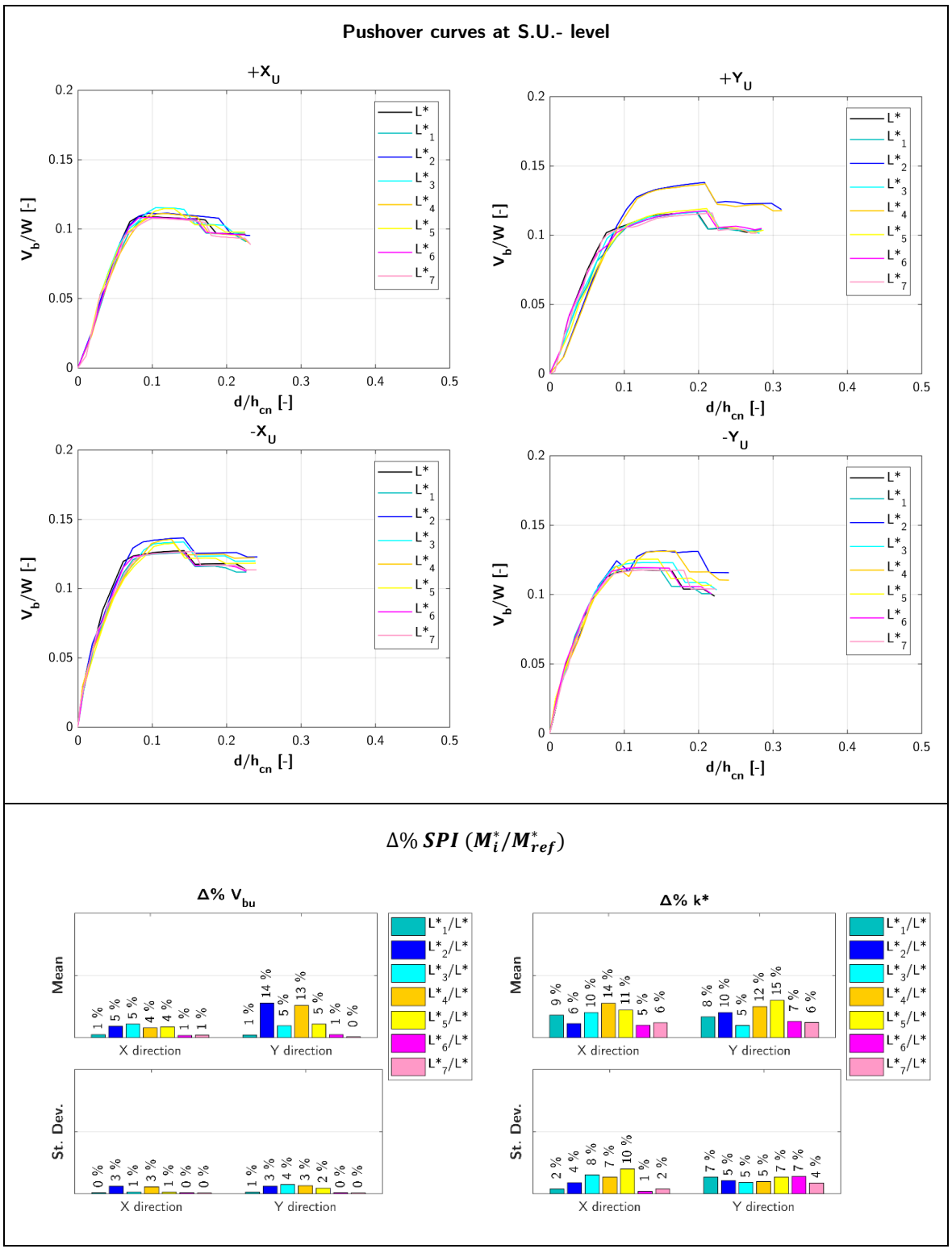

Table A 12: L aggregate – corner S.U.: RFF floors.

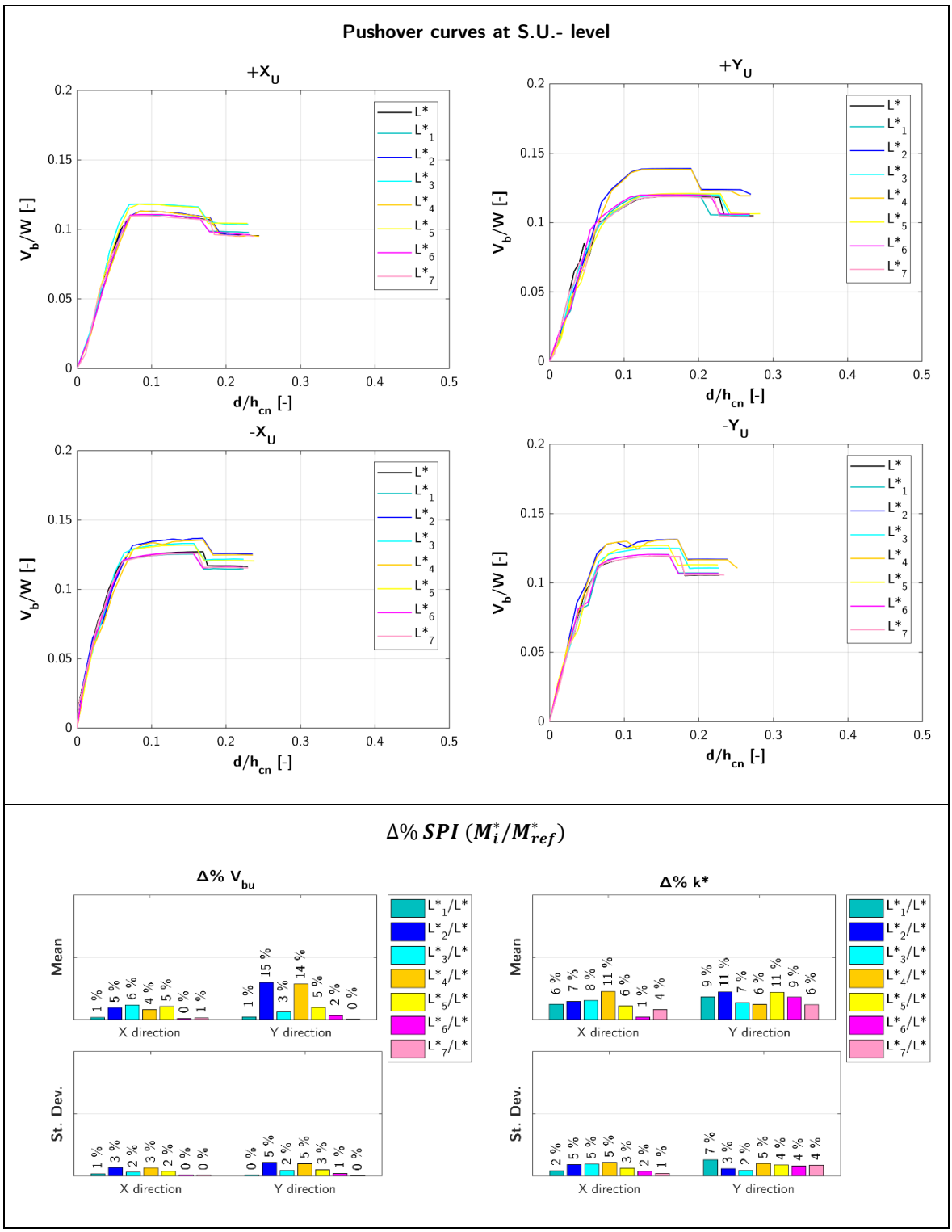

Table A 13: L aggregate – corner S.U.: FRR floors.

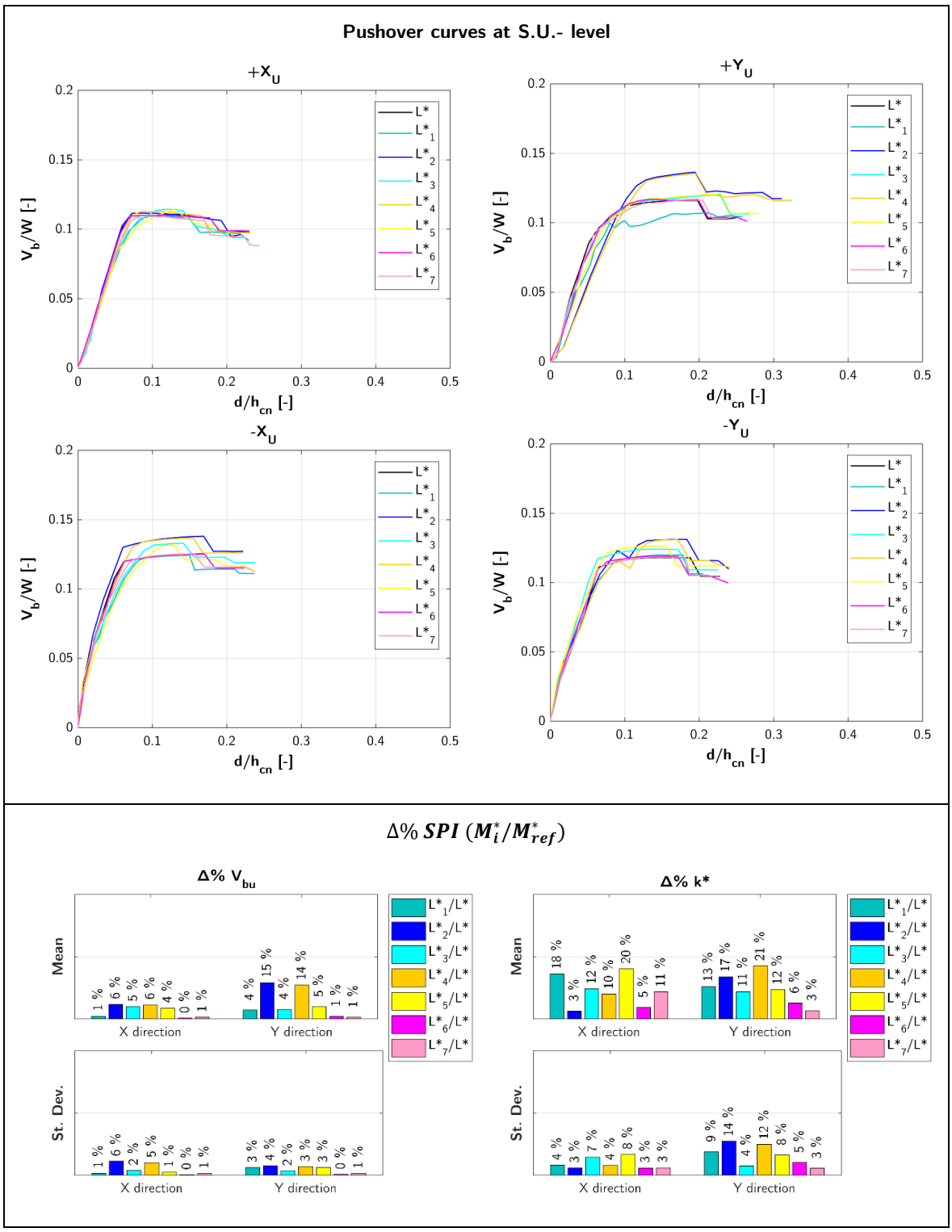

External S.U.

Table A 14: L aggregate – external S.U.: R floors.

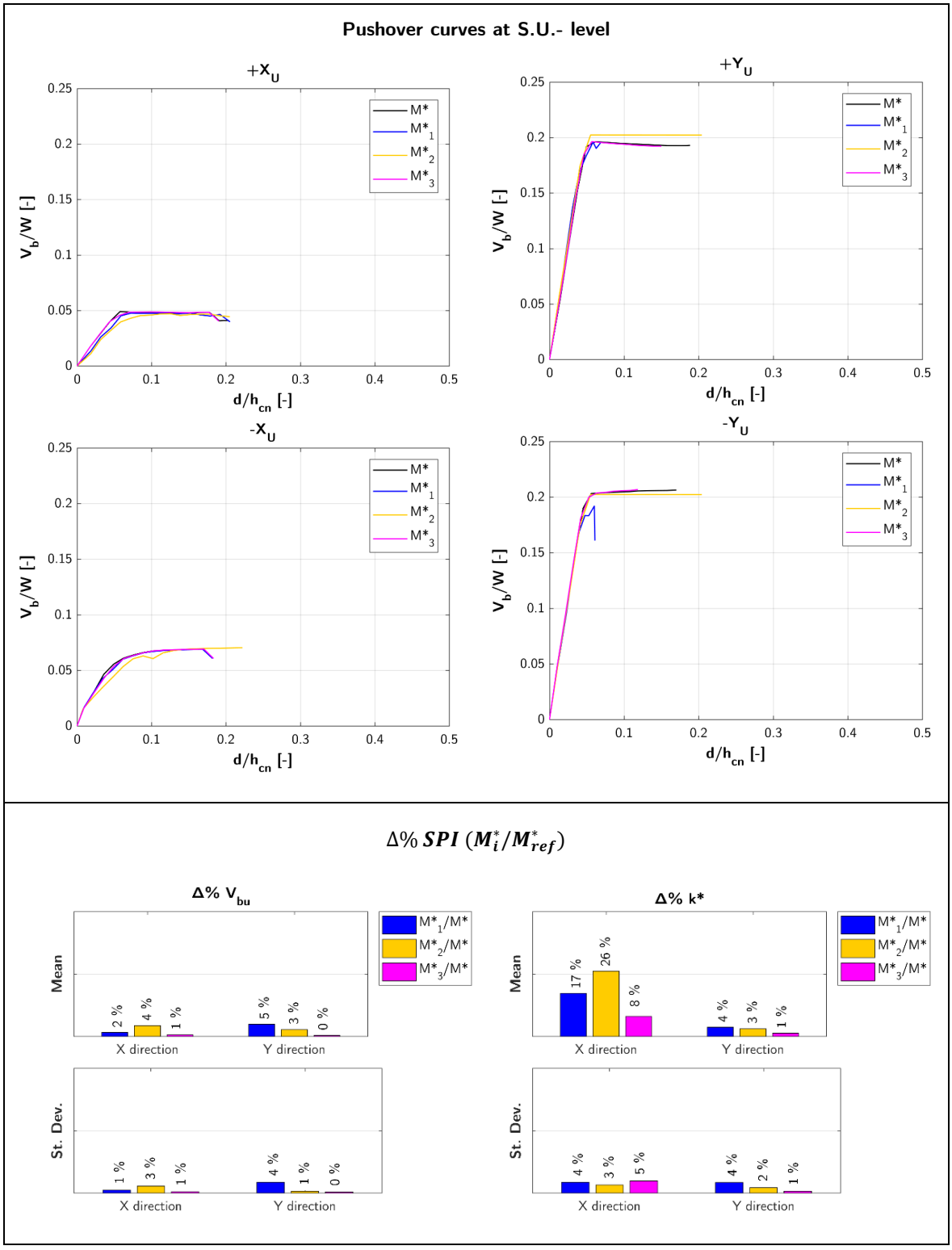

Table A 15: L aggregate – external S.U.: F floors.

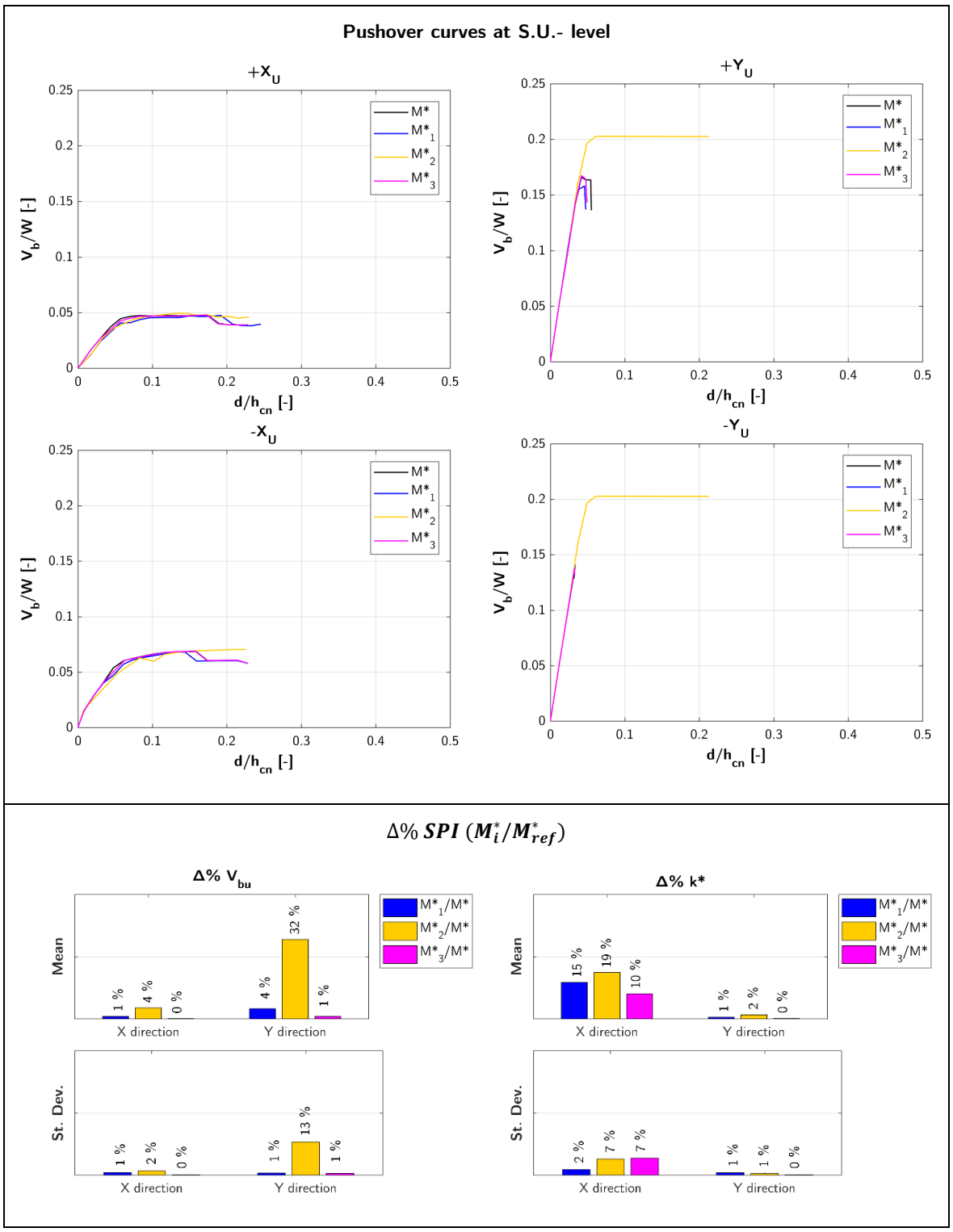

Table A 16: L aggregate – external S.U.: RFF floors.

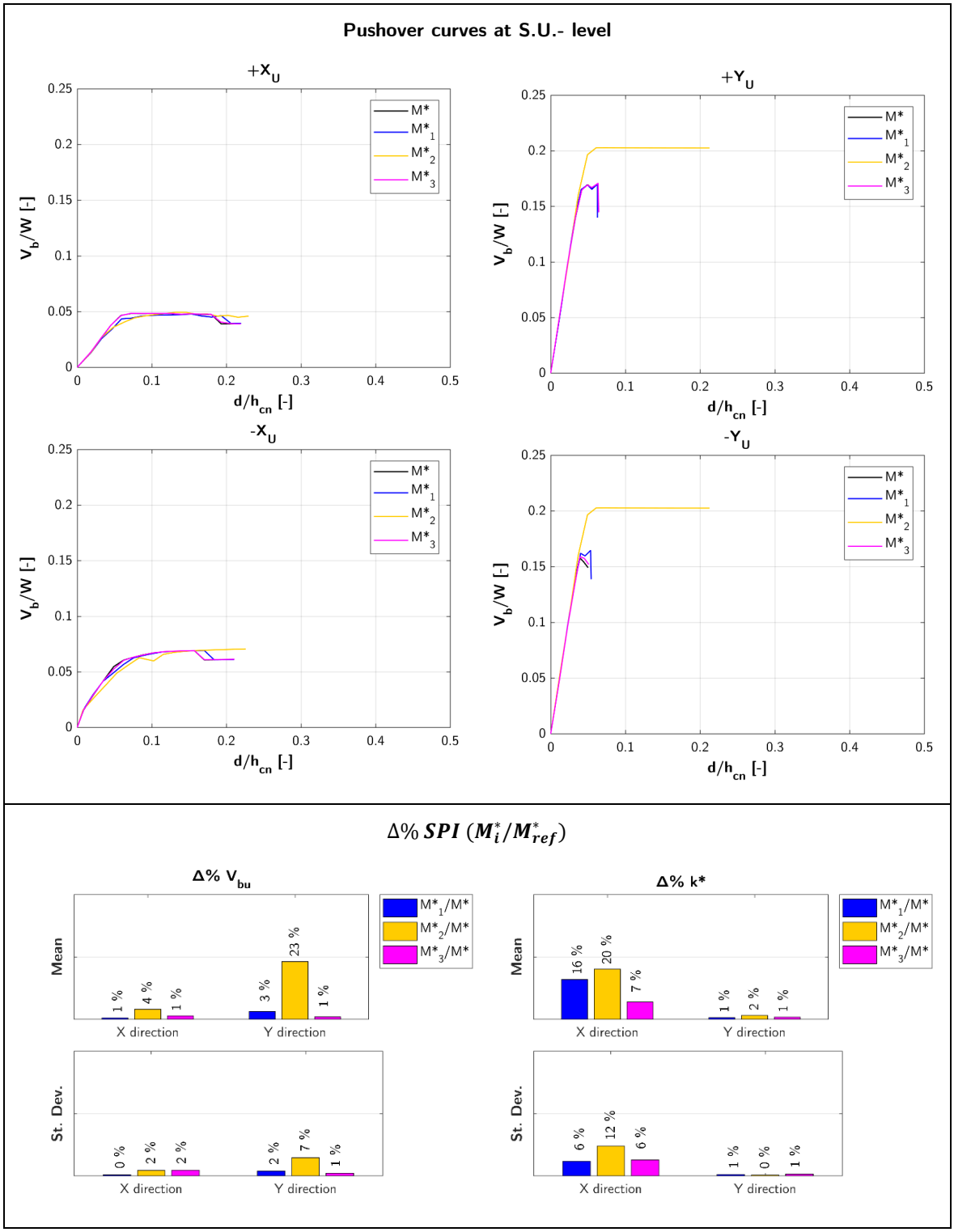

Table A 17: L aggregate – external S.U.: FRR floors.

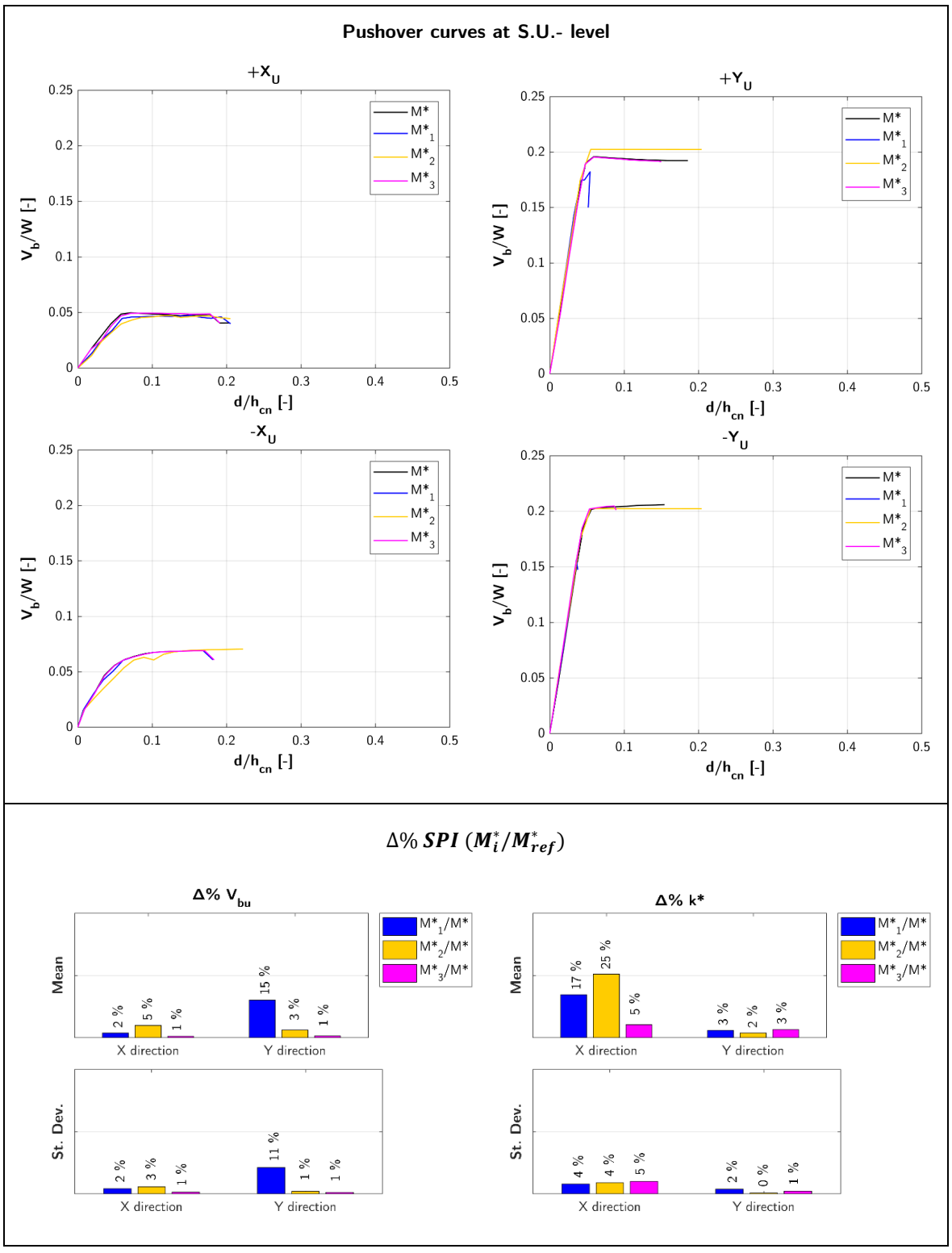

A3. Row aggregate – Material heterogeneities

Internal S.U.

Table A 18: Row aggregate – internal S.U.: murB - R floors.

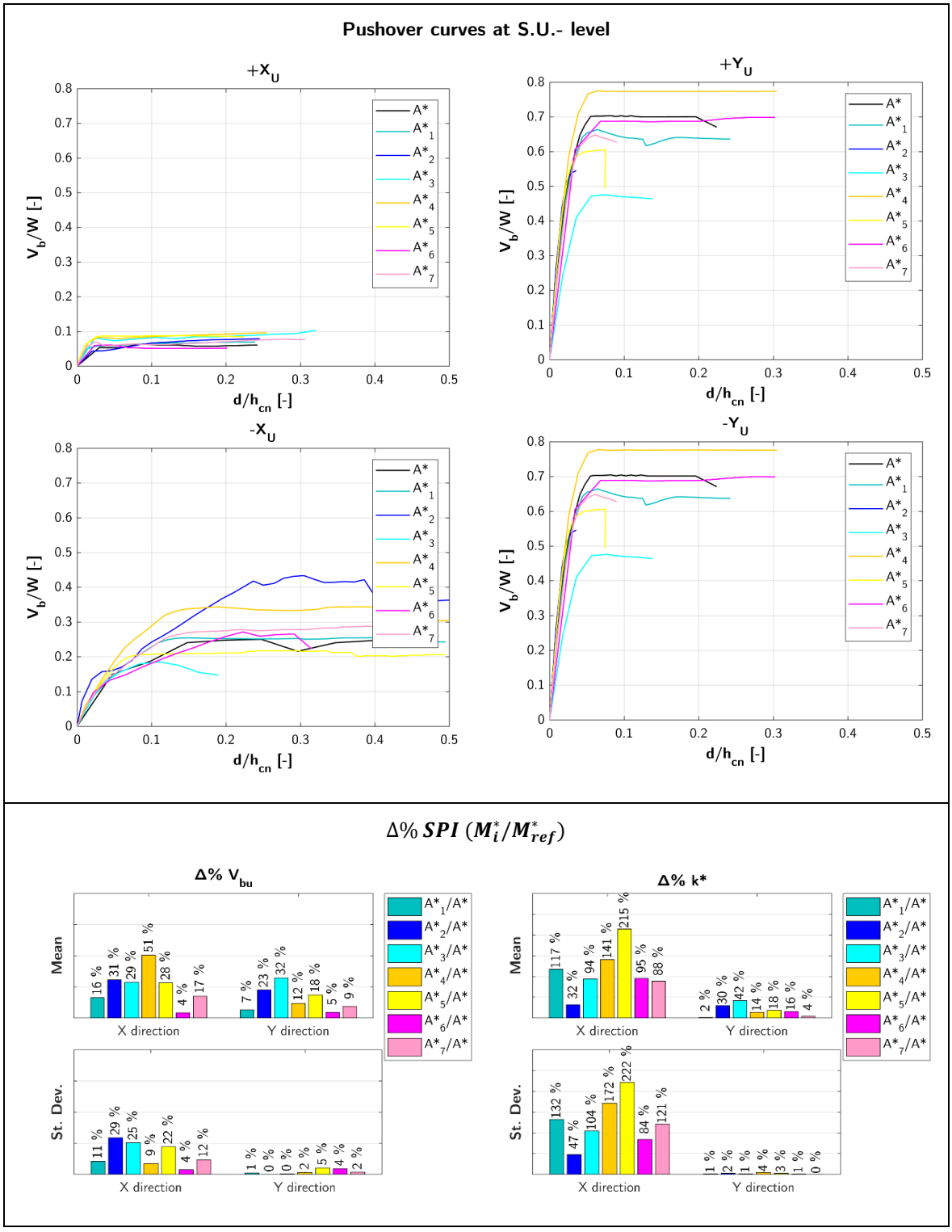

Table A 19: Row aggregate – internal S.U.: murB - F floors.

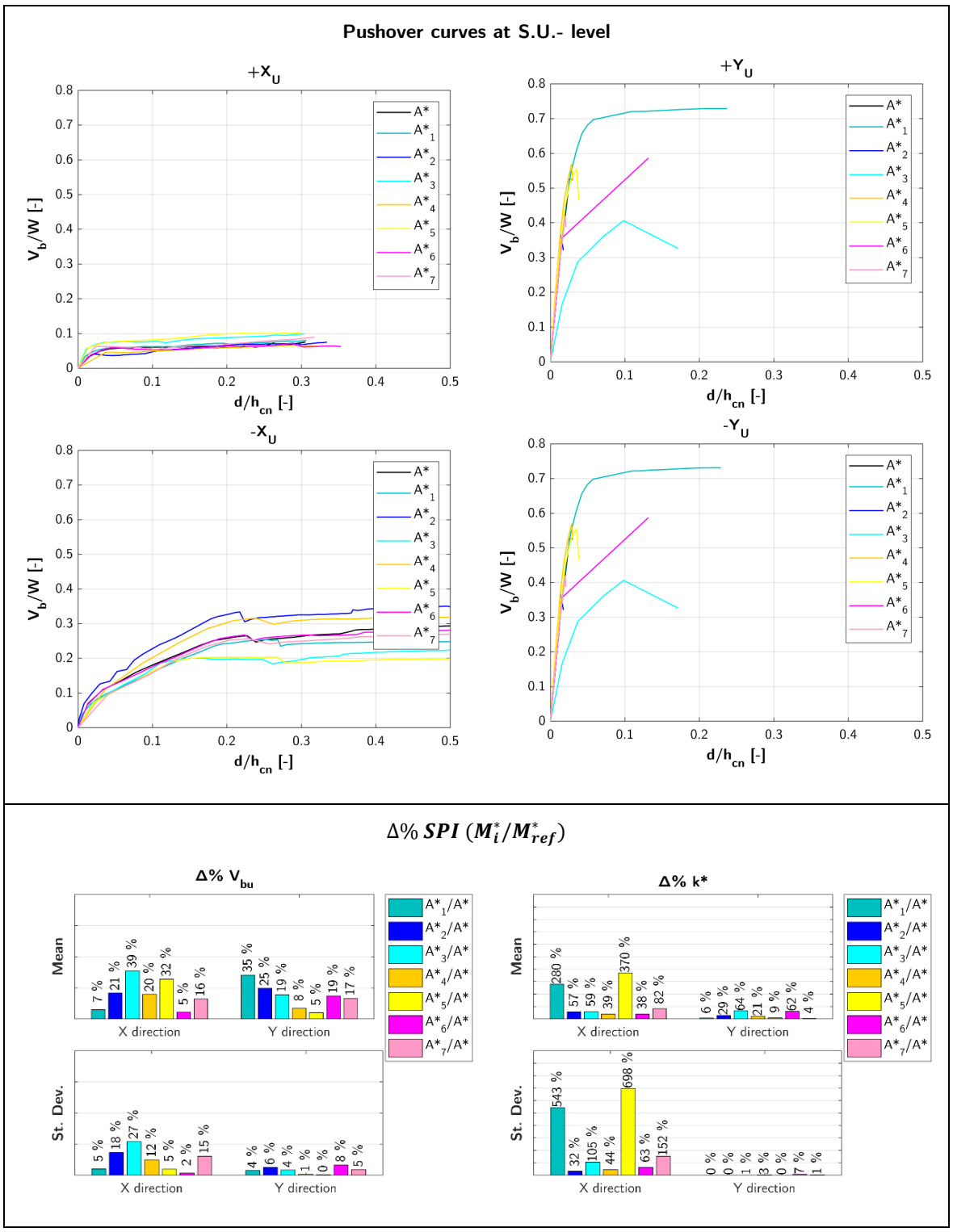

Table A 20: Row aggregate – internal S.U.: murC - R floors.

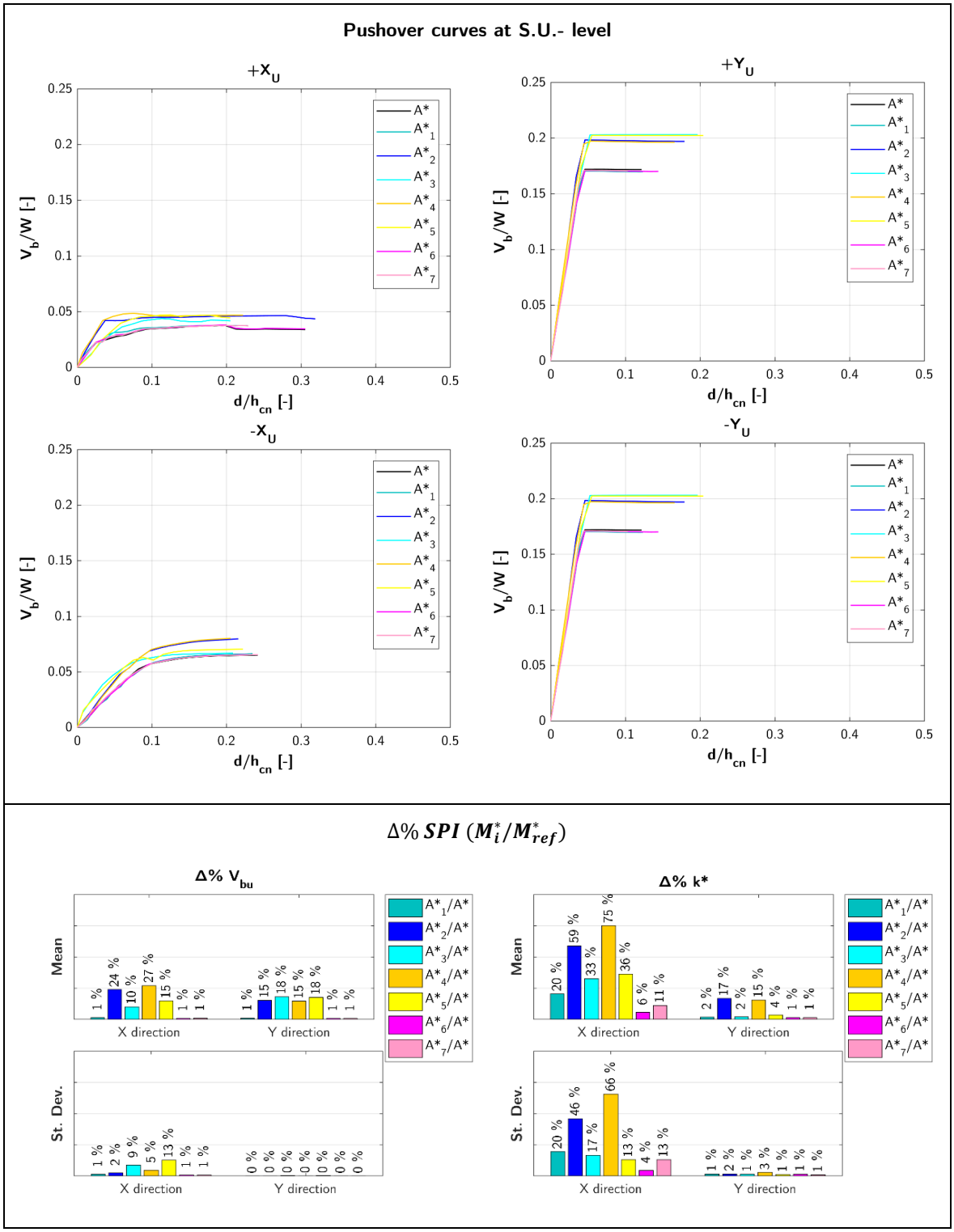

Table A 21: Row aggregate – internal S.U.: murC - F floors.

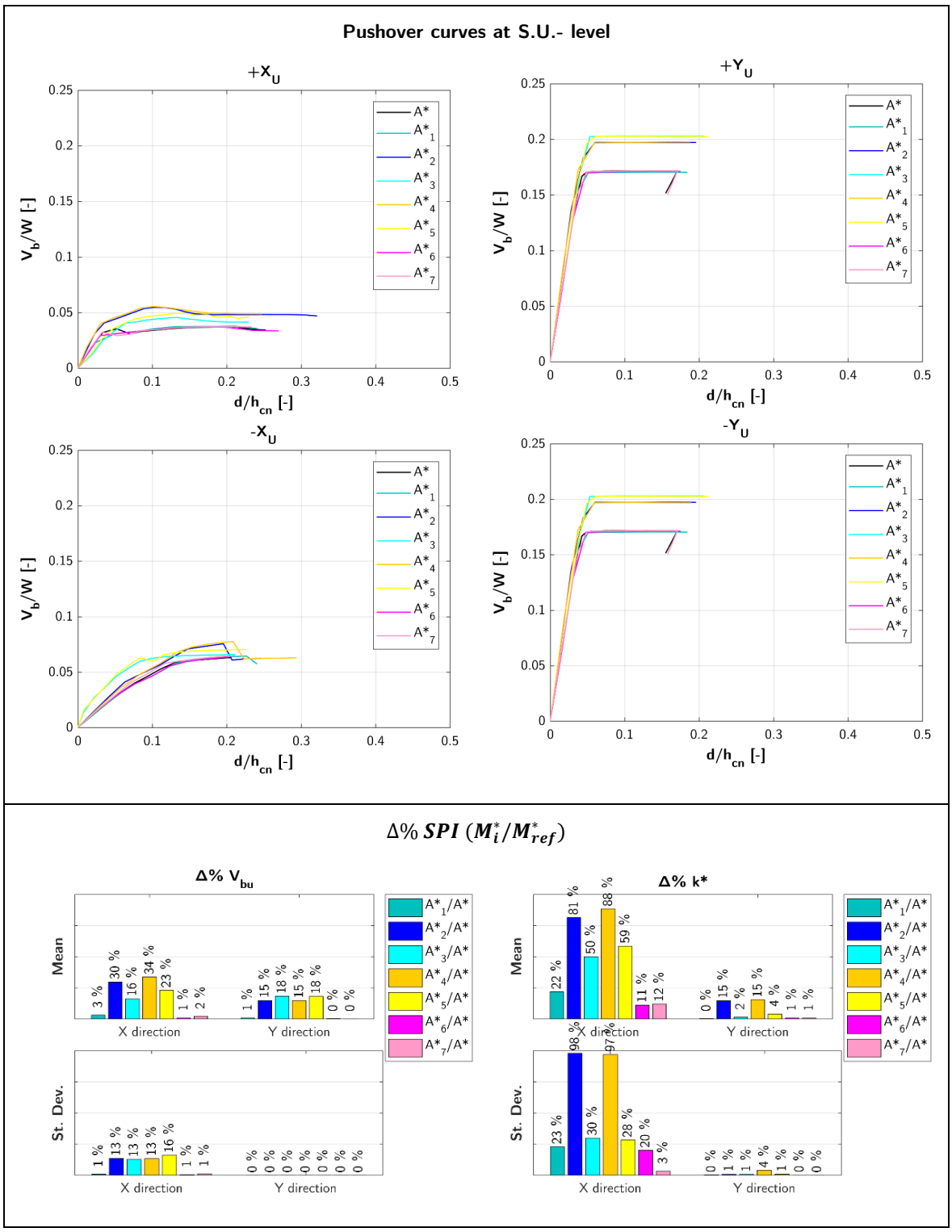

External S.U.

Table A 22: Row aggregate – external S.U.: murB - R floors.

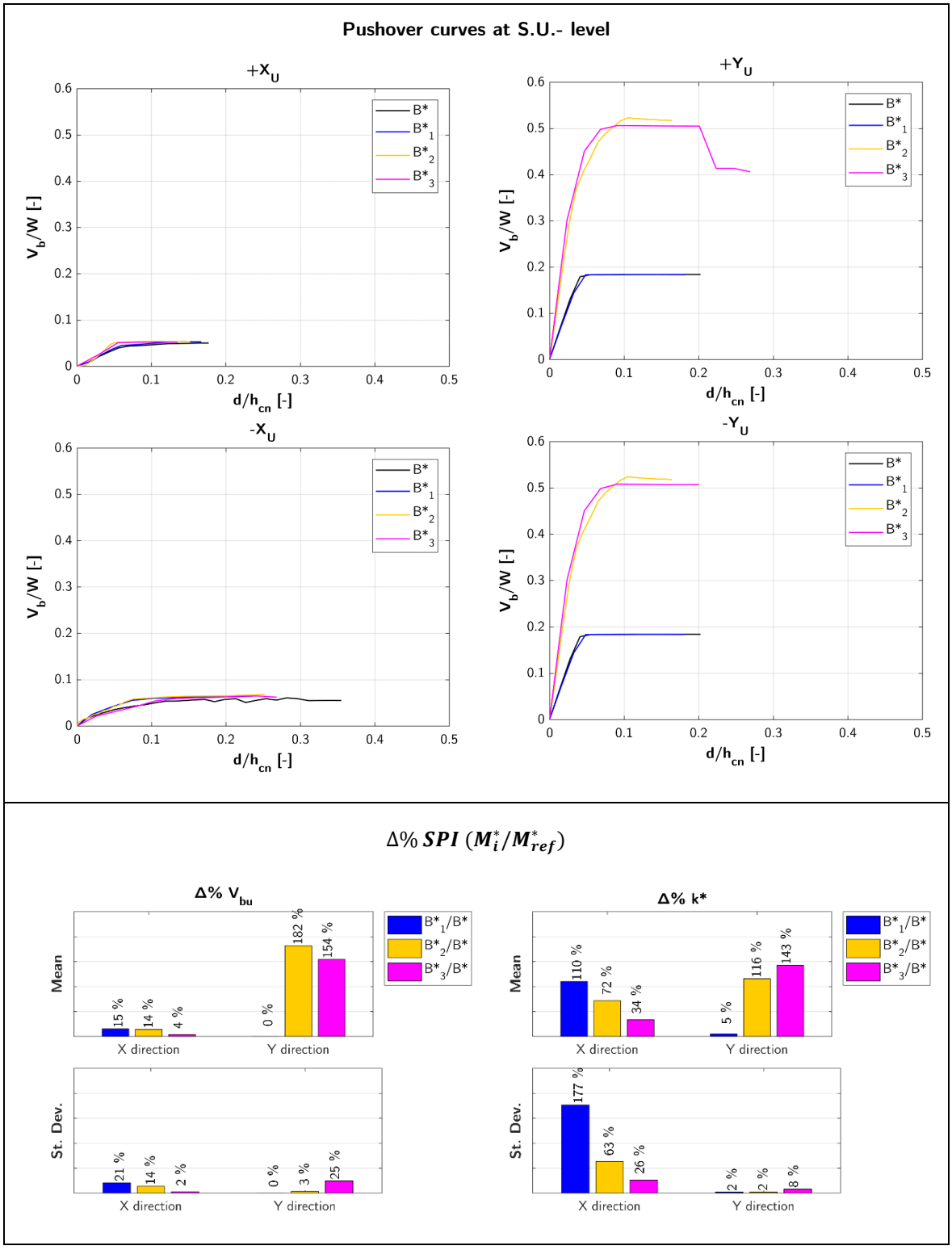

Table A 23: Row aggregate – external S.U.: murB - F floors.

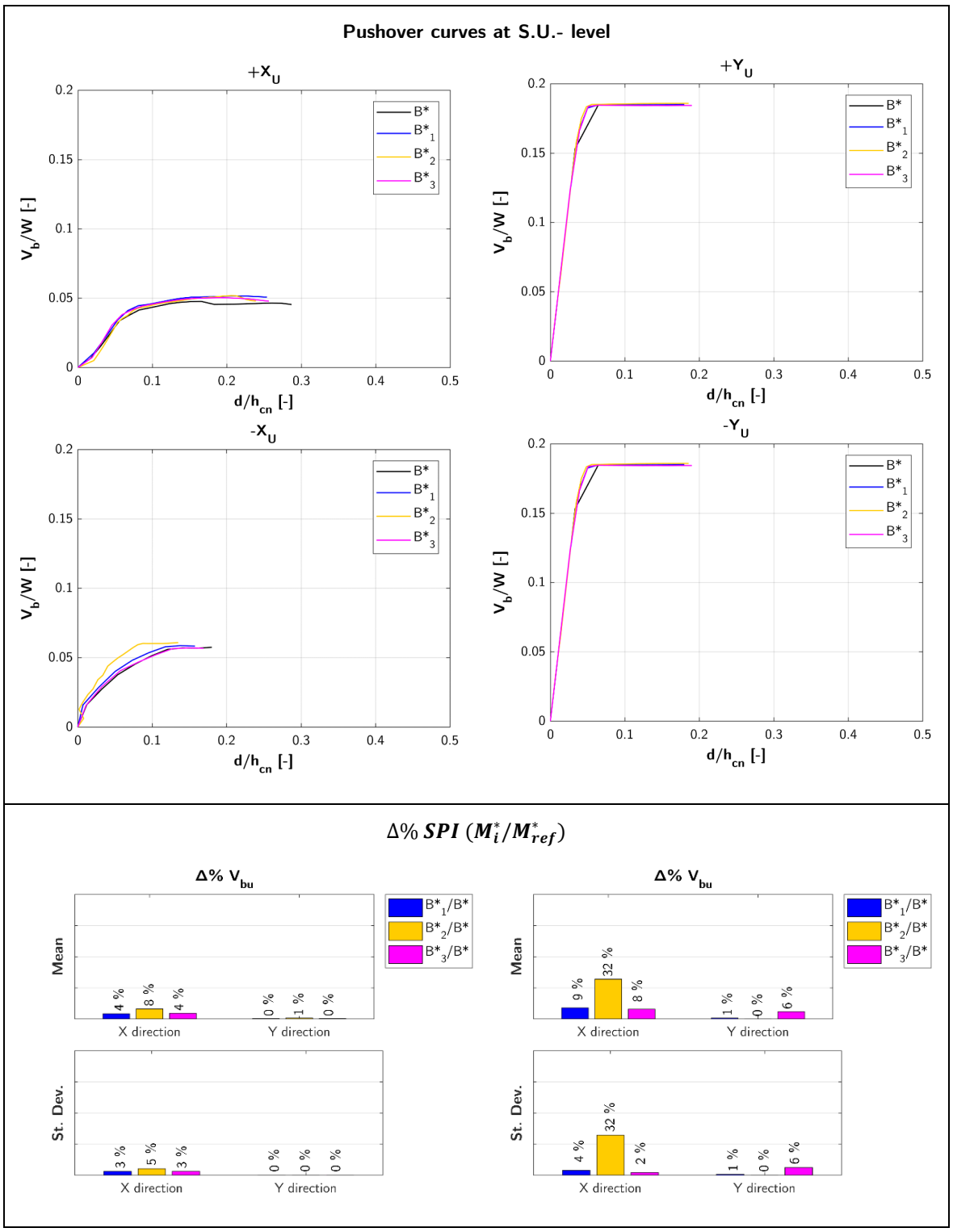

Table A 24: Row aggregate – external S.U.: murC - R floors.

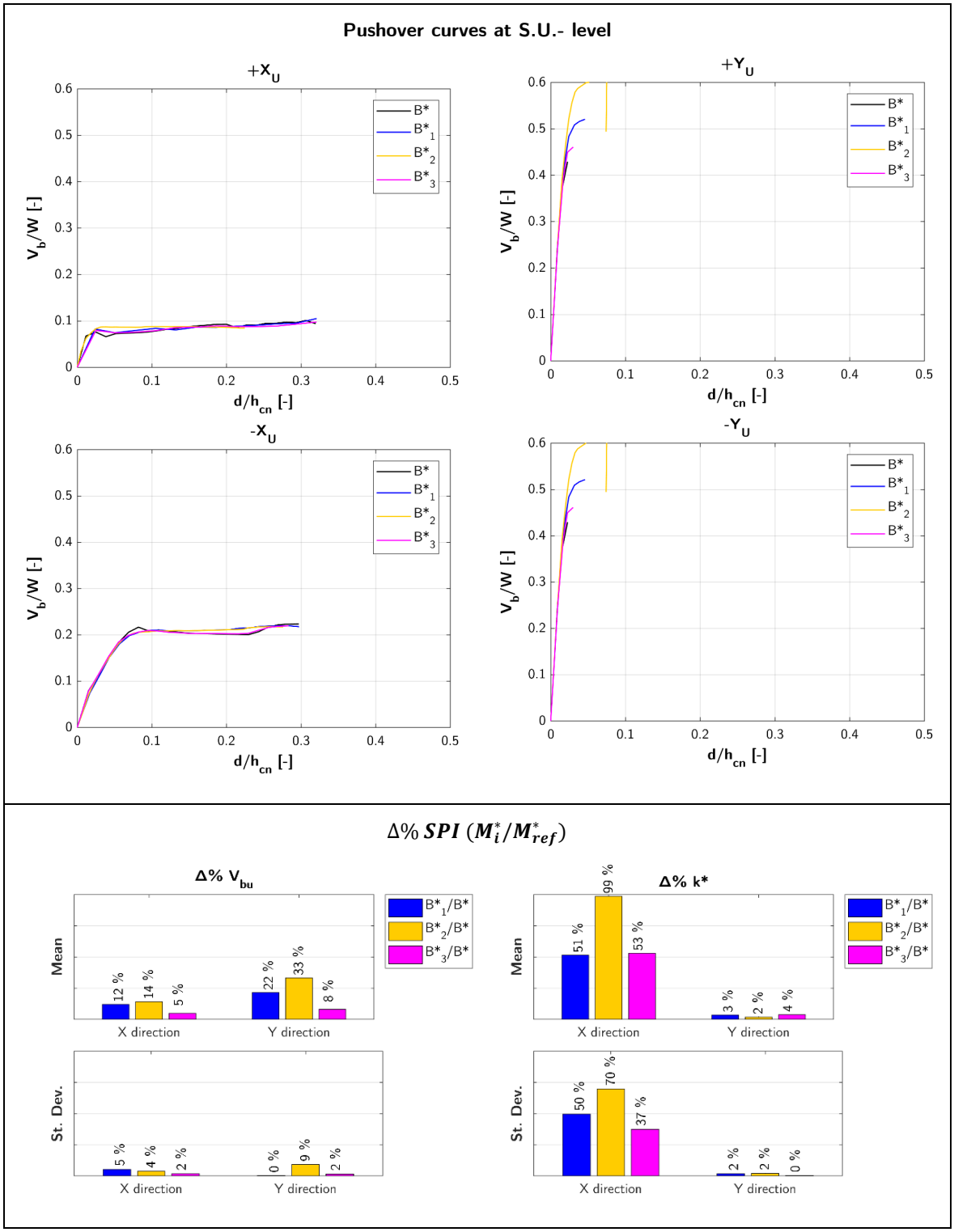

Table A 25: Row aggregate – external S.U.: murC - F floors.

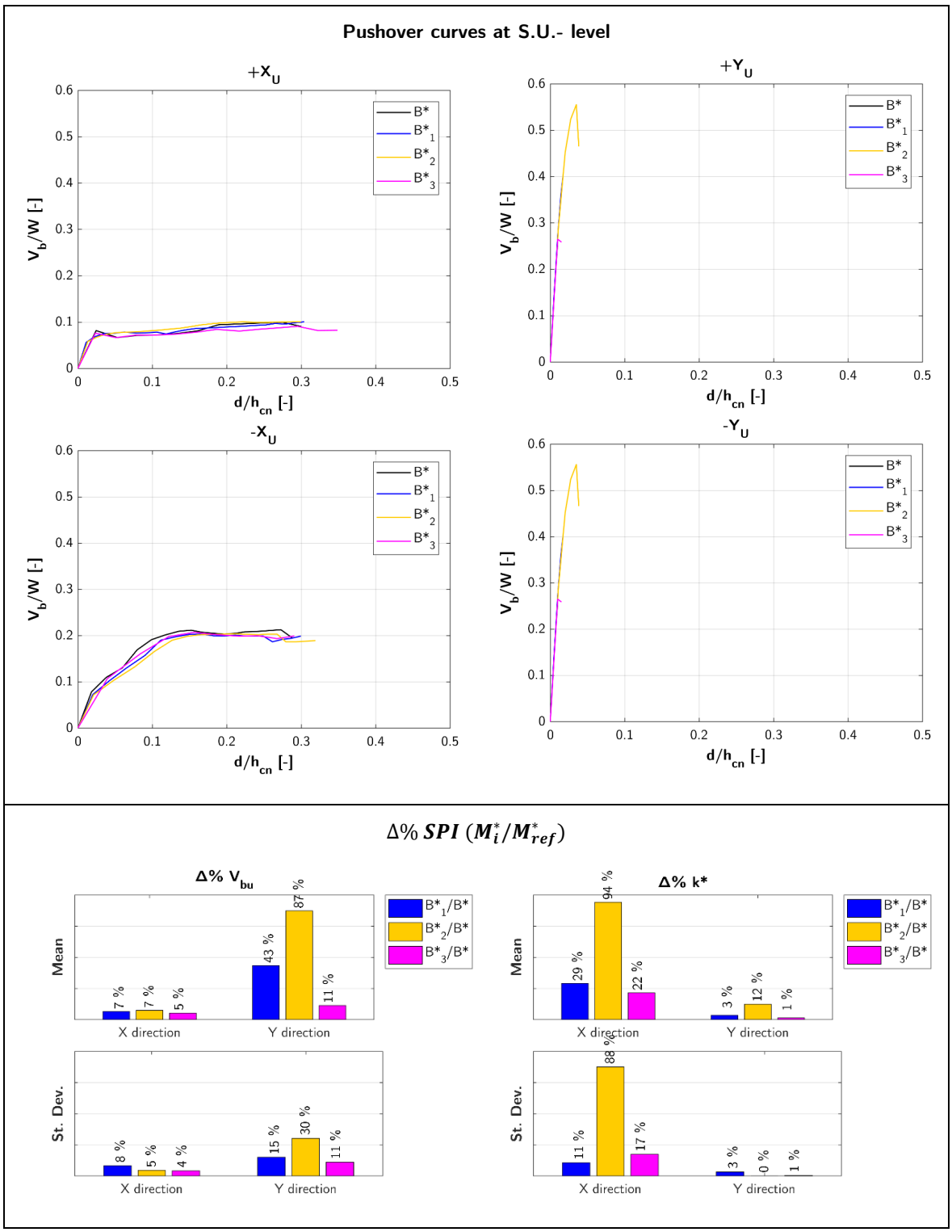

A4. L AGGREGATE – MATERIAL HETEROGENEITIES

Corner S.U.

Table A 26: L aggregate – corner S.U.: murB - R floors.

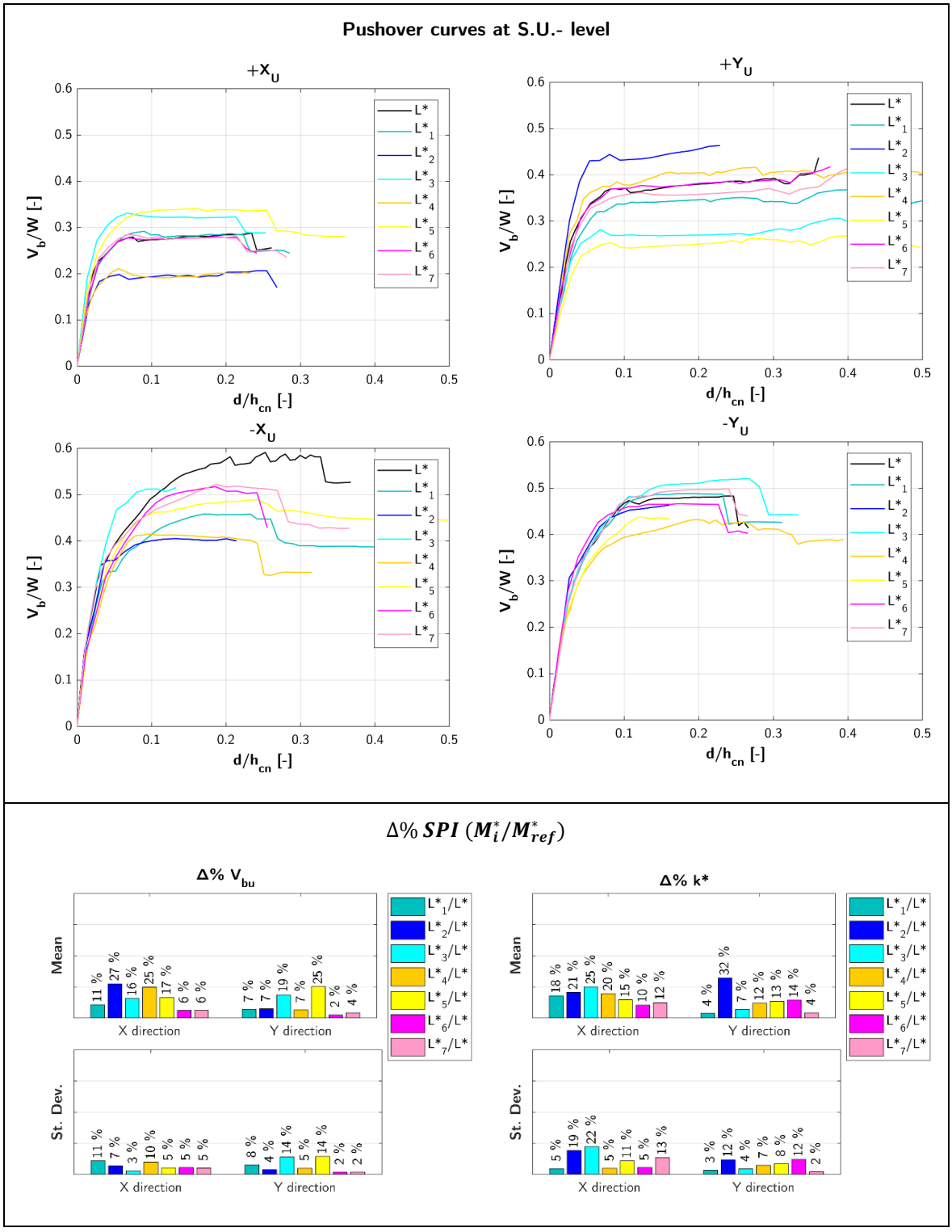

Table A 27: L aggregate – corner S.U.: murB - F floors.

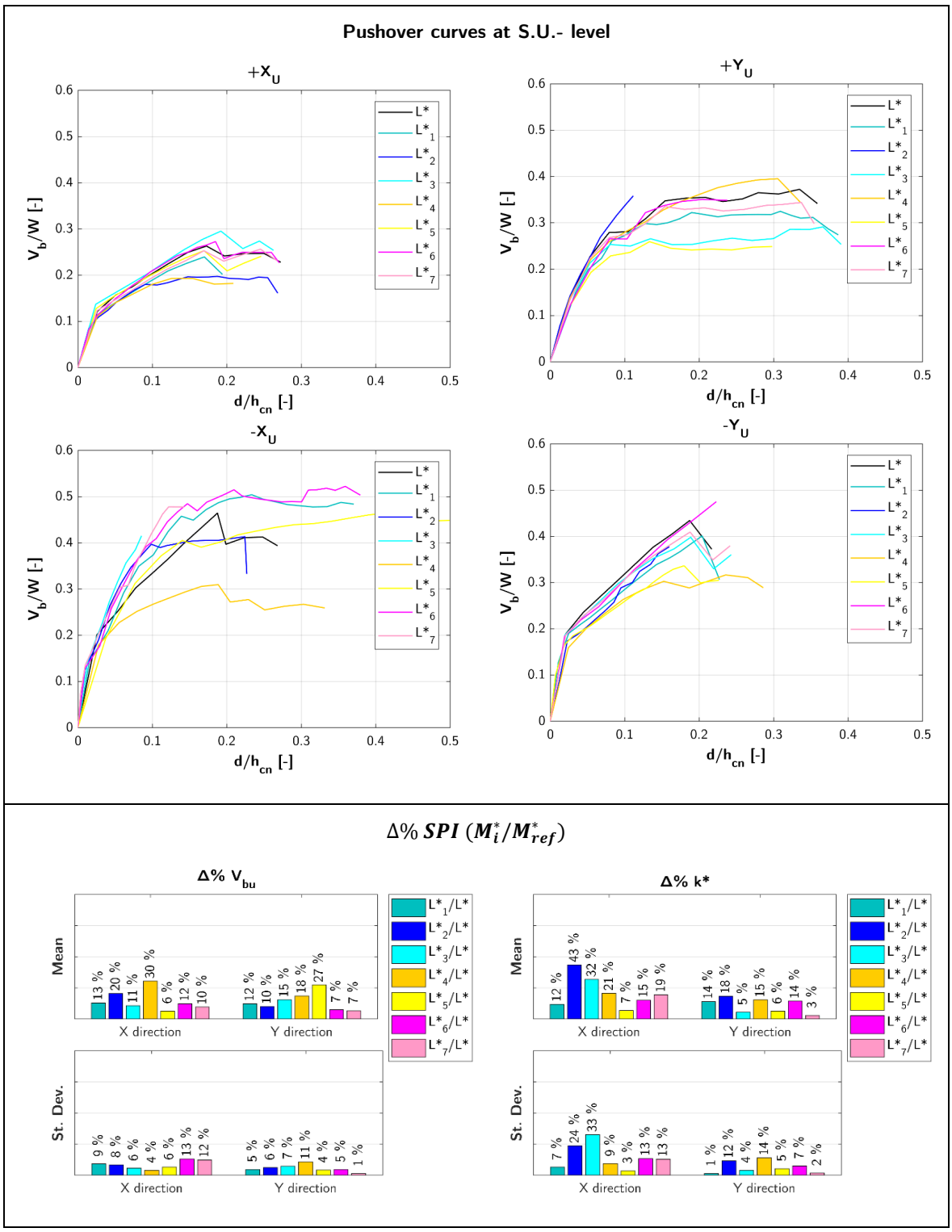

Table A 28: L aggregate – corner S.U.: murC - R floors.

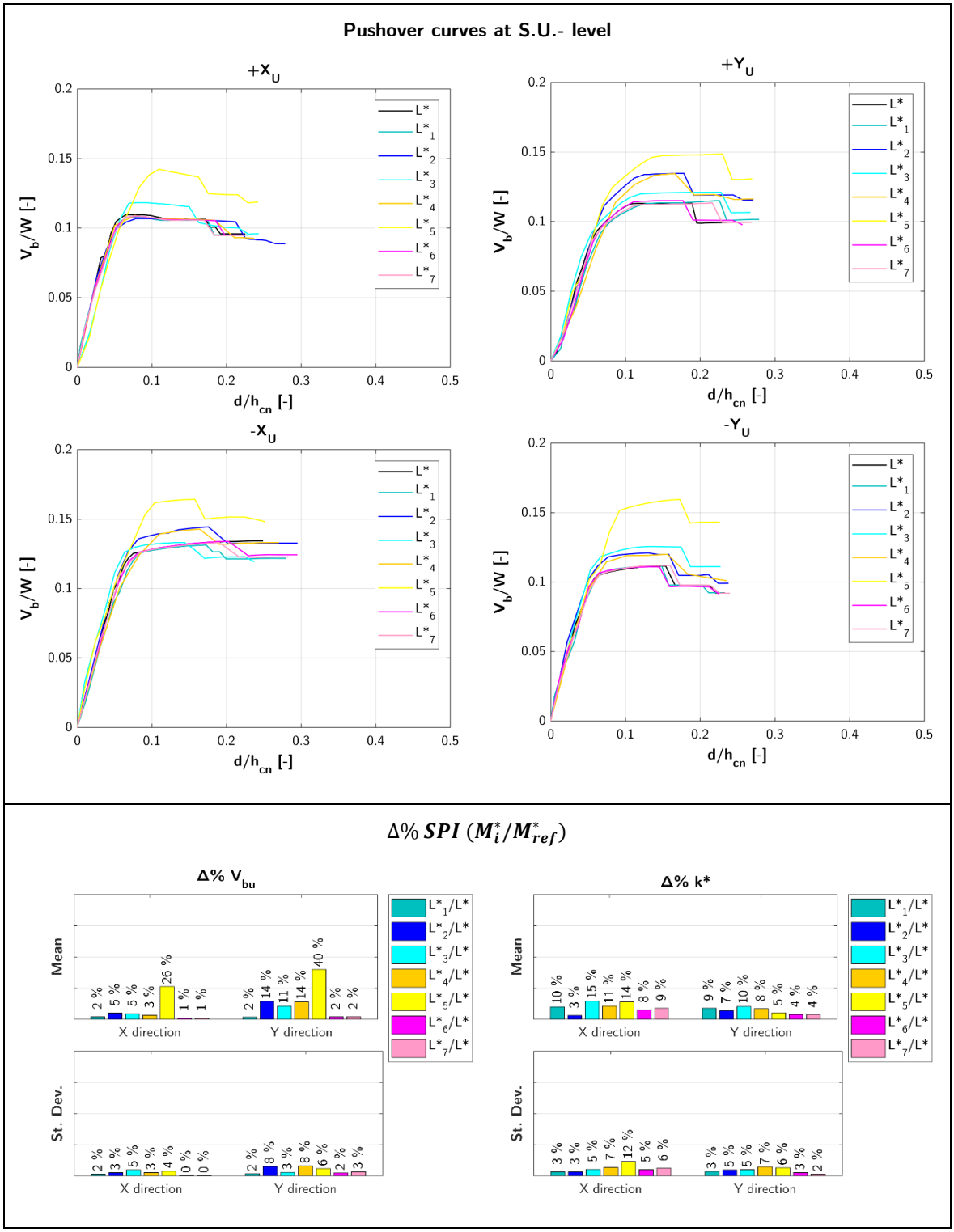

Table A 29: L aggregate – corner S.U.: murC - F floors.

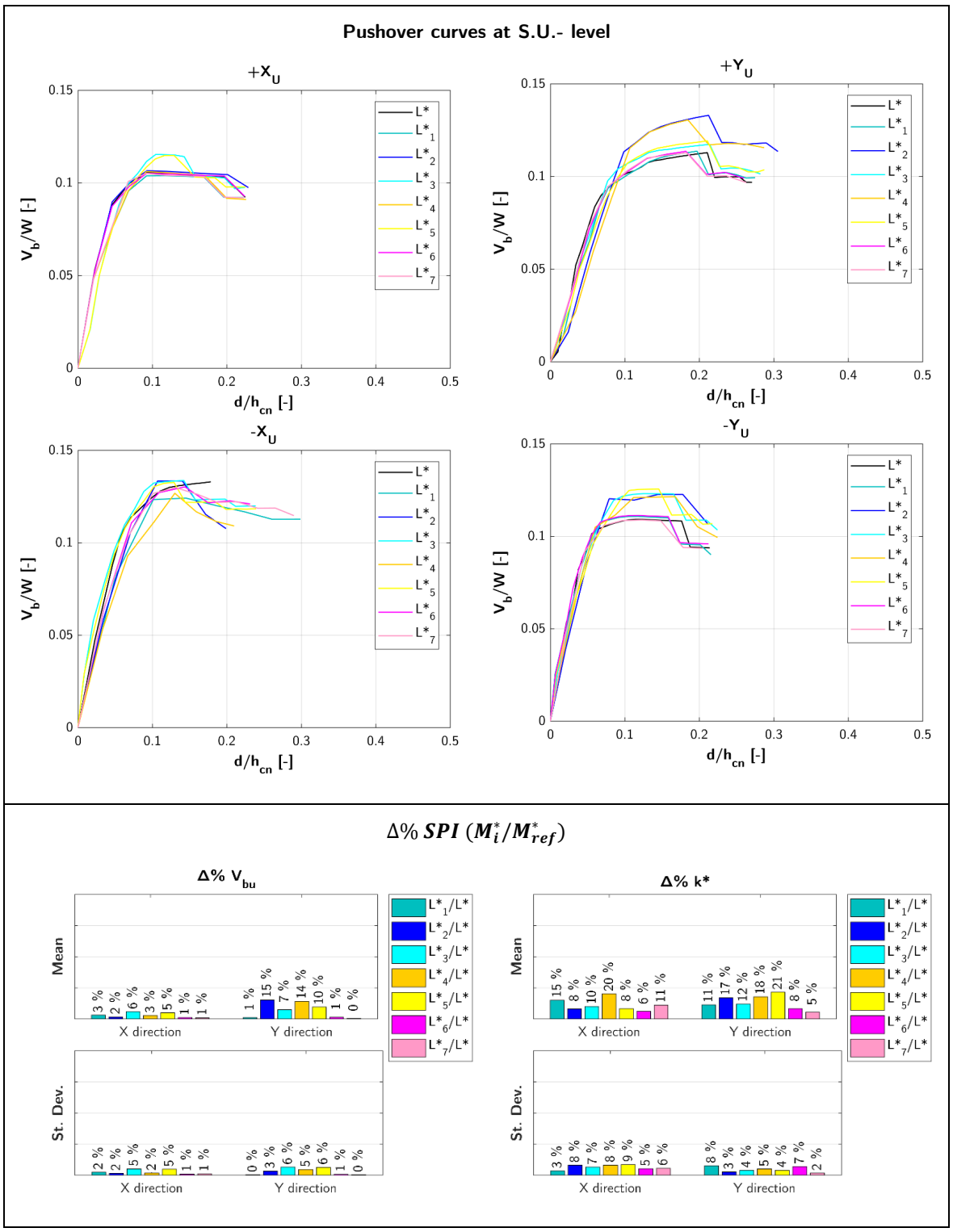

External S.U.

Table A 30: L aggregate – external S.U.: murB - R floors.

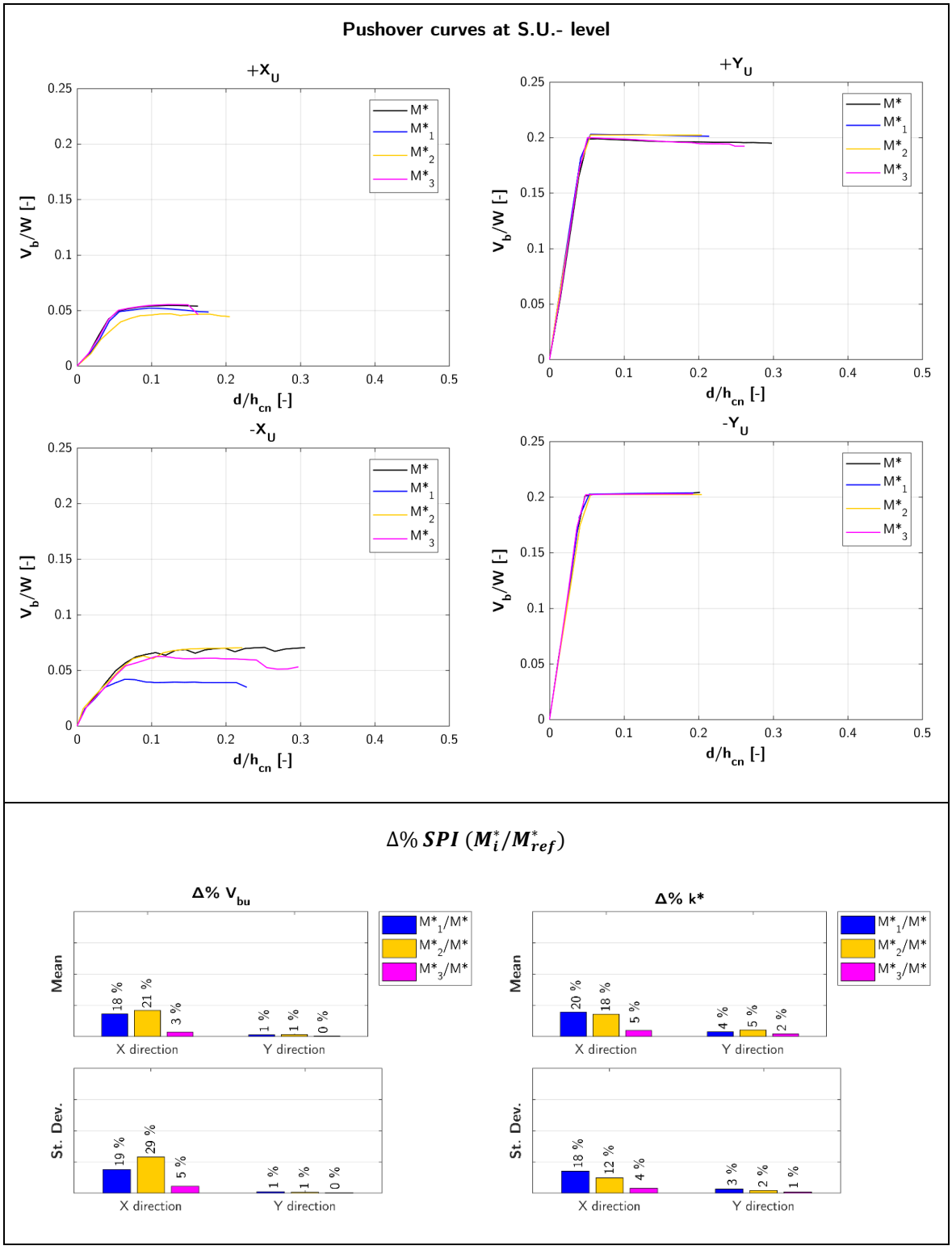

Table A 31: L aggregate – external S.U.: murB - F floors.

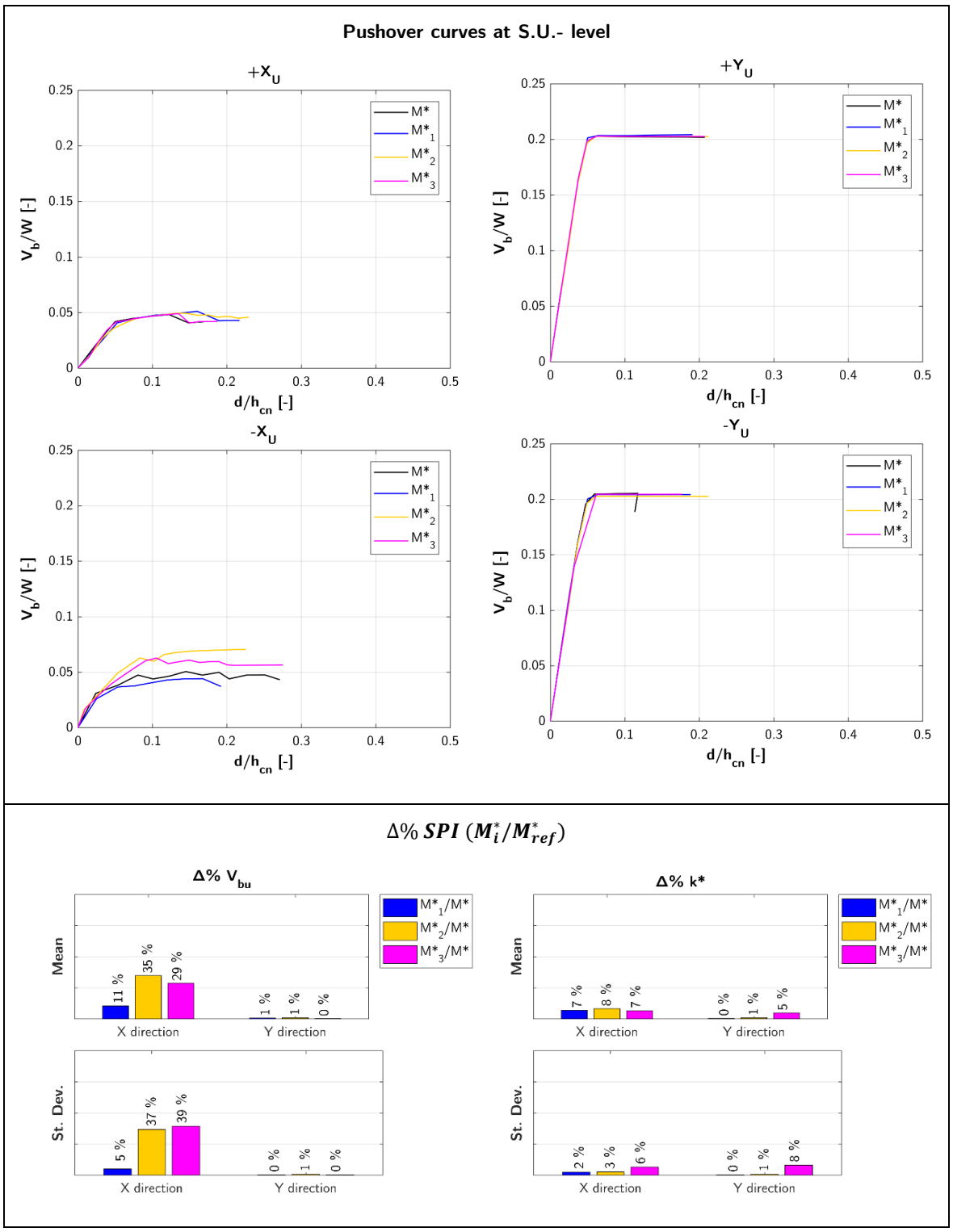

Table A 32: L aggregate – external S.U.: murC - R floors.

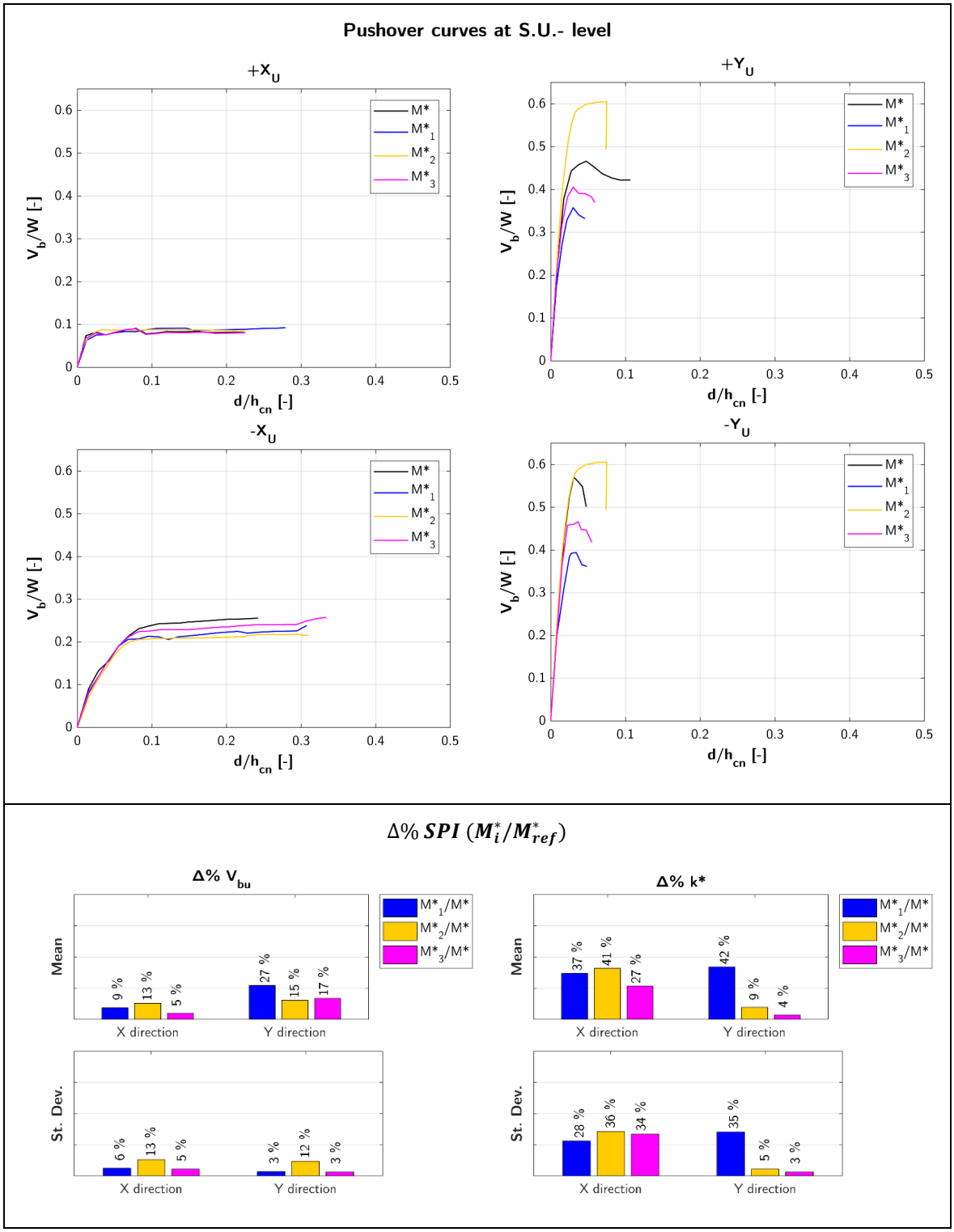

Table A 33: L aggregate – external S.U.: murC - F floors.

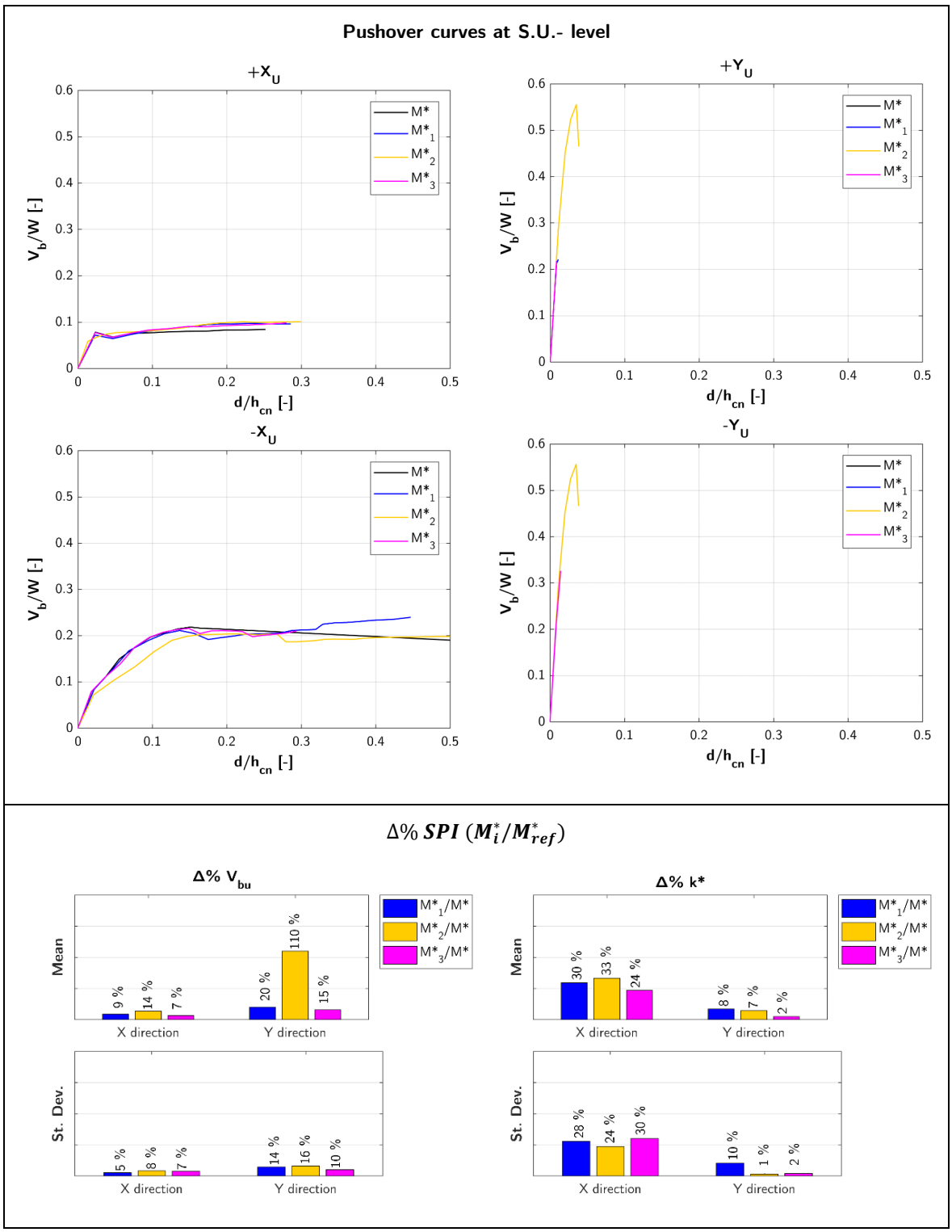

A5. ROW AGGREGATE – DIFFERENCES IN HEIGHT

Internal S.U.

Table A 34: Row aggregate – internal S.U.: hB - R floors.

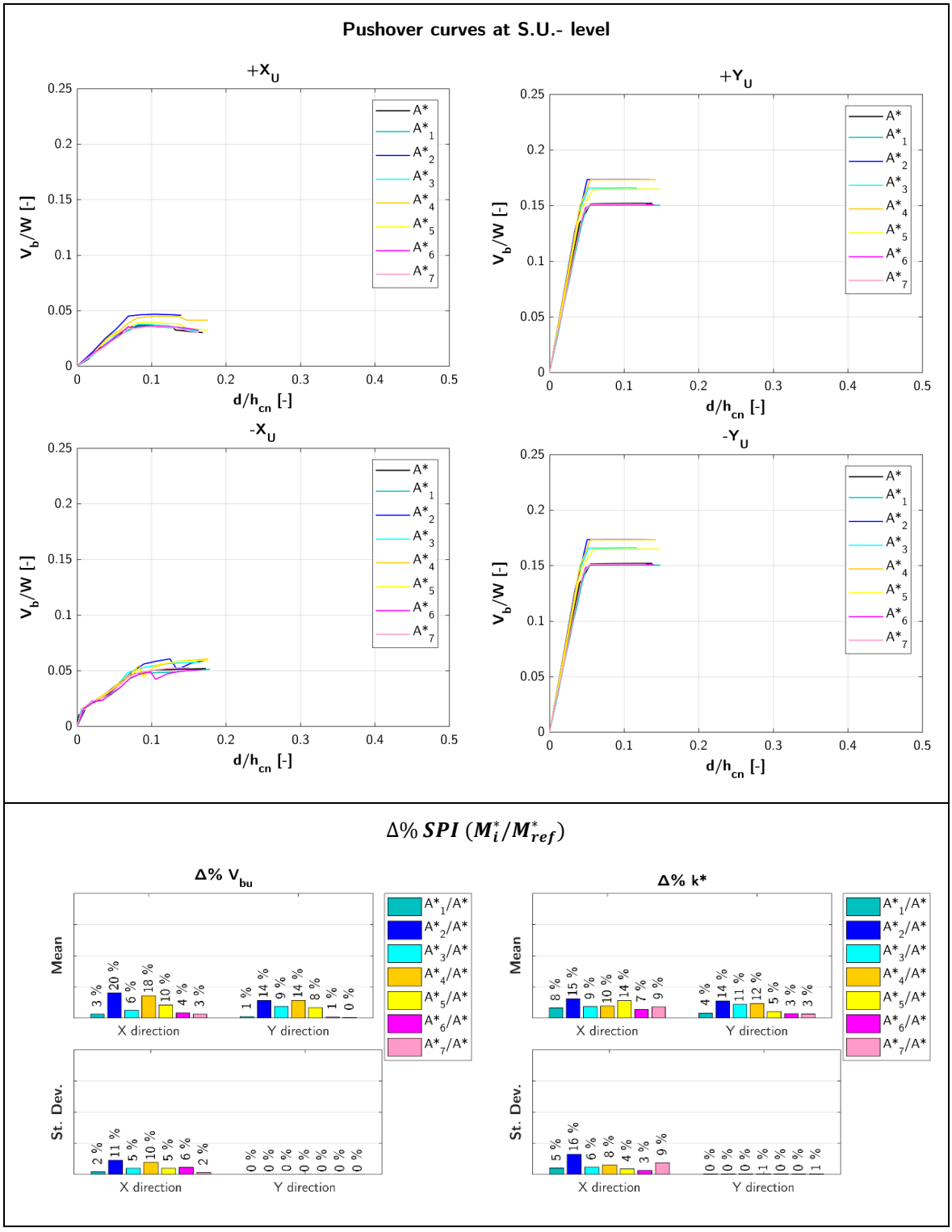

Table A 35: Row aggregate – internal S.U.: hB - F floors.

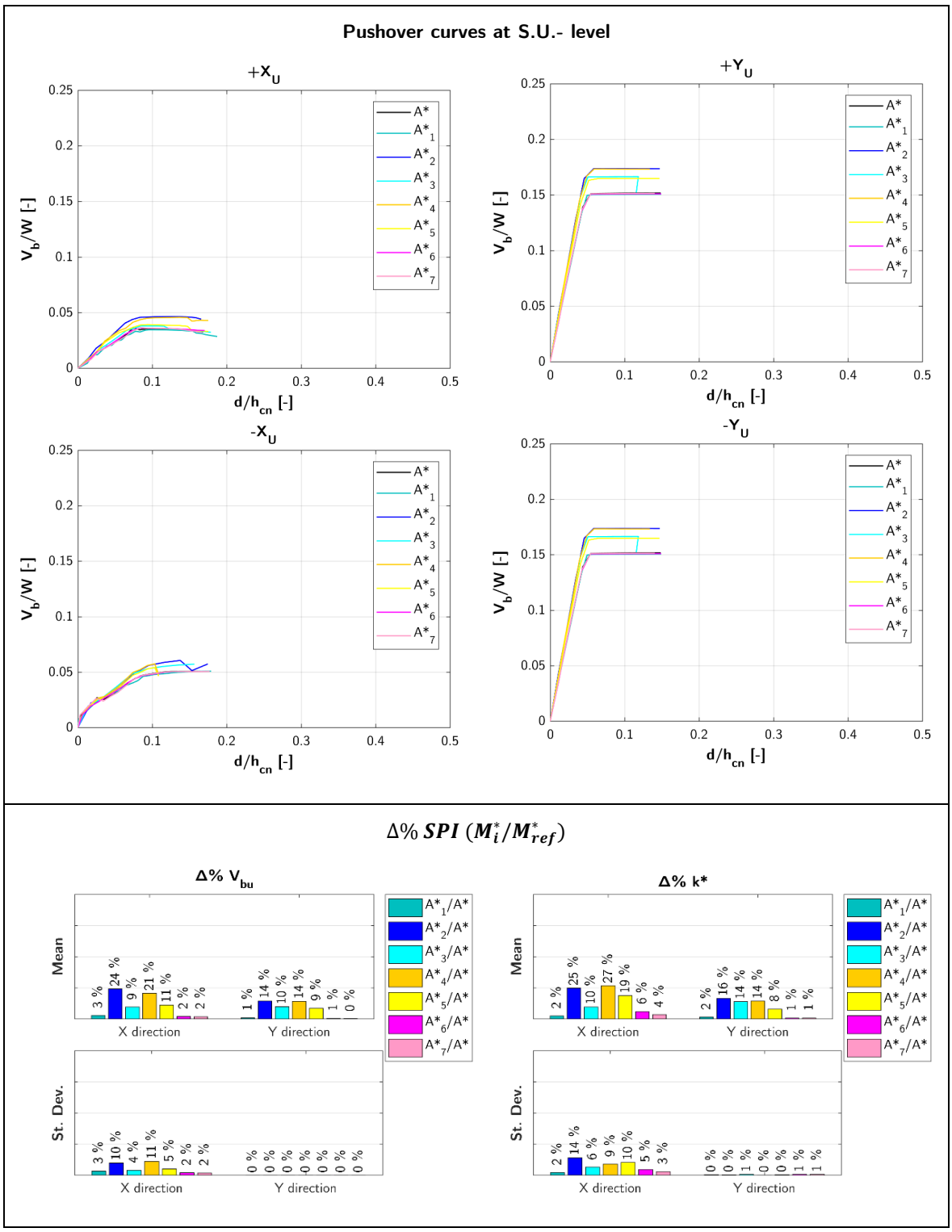

Table A 36: Row aggregate – internal S.U.: hC - R floors.

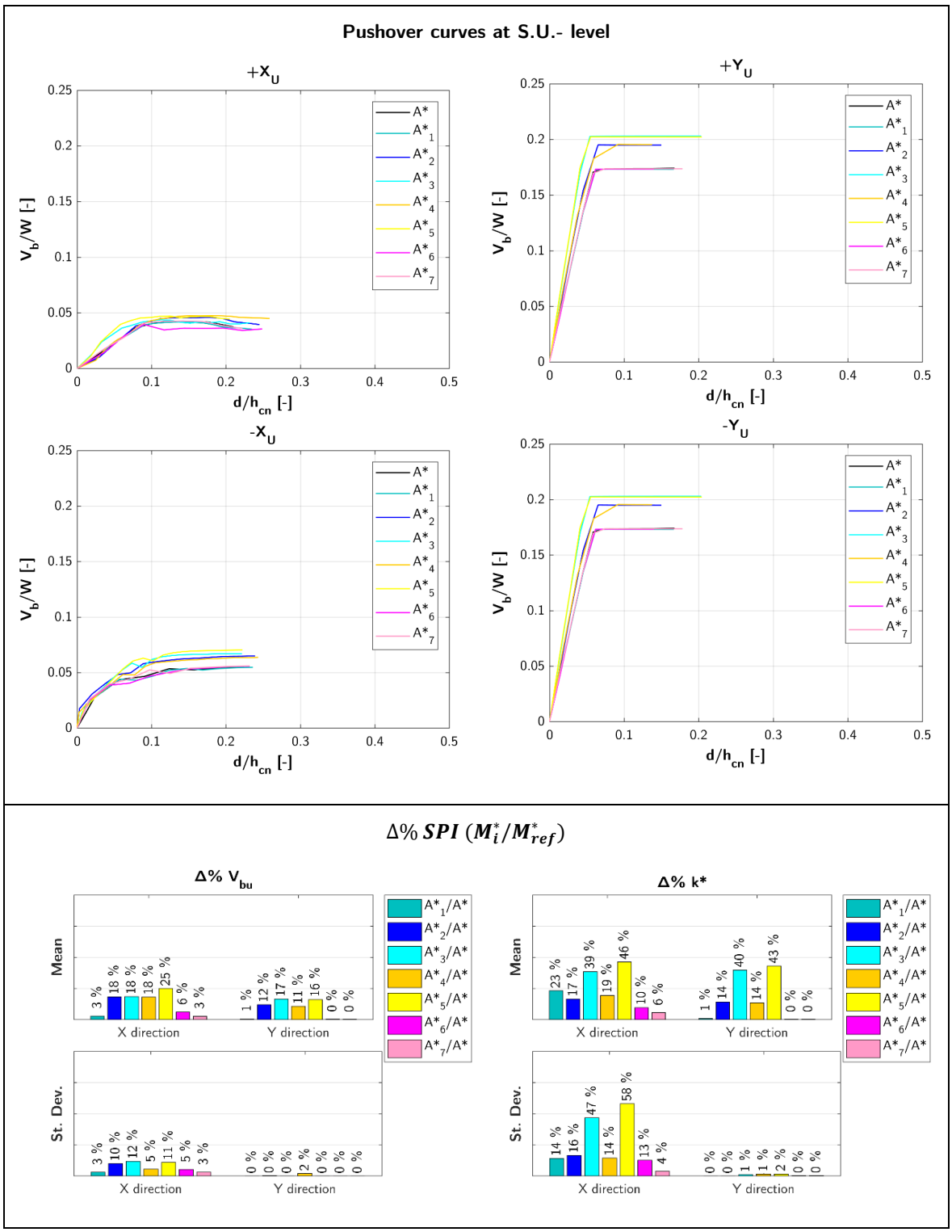

Table A 37: Row aggregate – internal S.U.: hC - F floors.

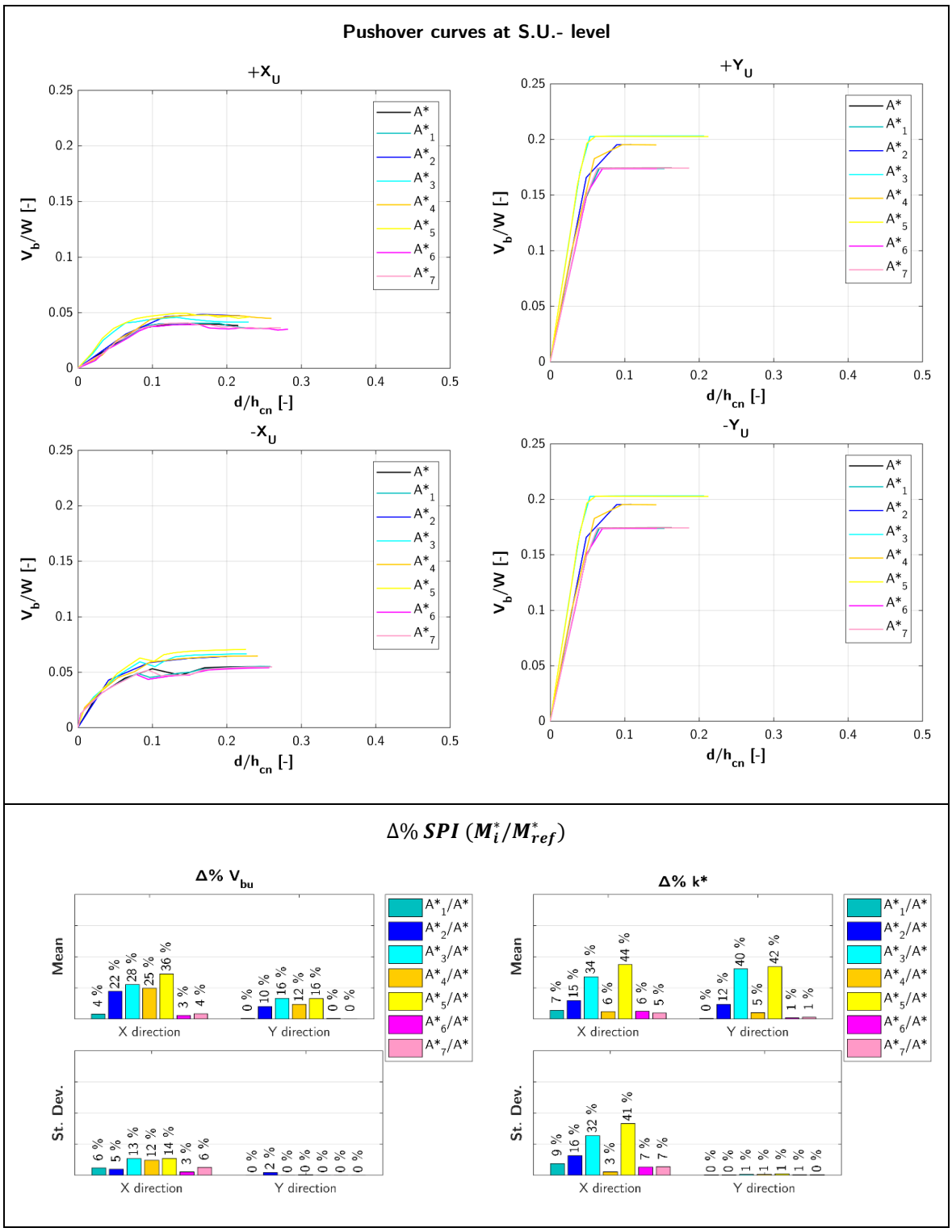

External S.U.

Table A 38: Row aggregate – external S.U.: hB - R floors.

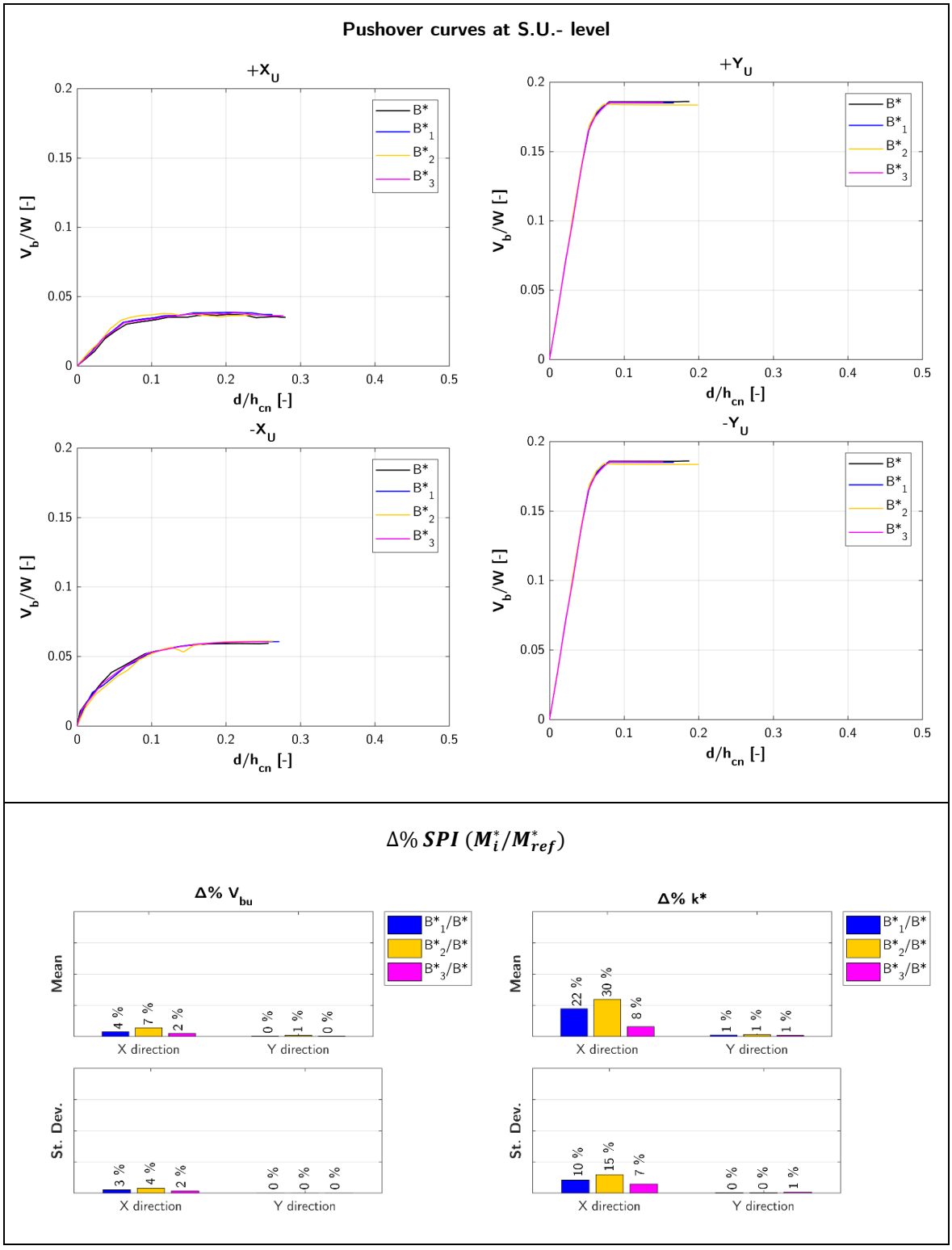

Table A 39: Row aggregate – external S.U.: hB - F floors.

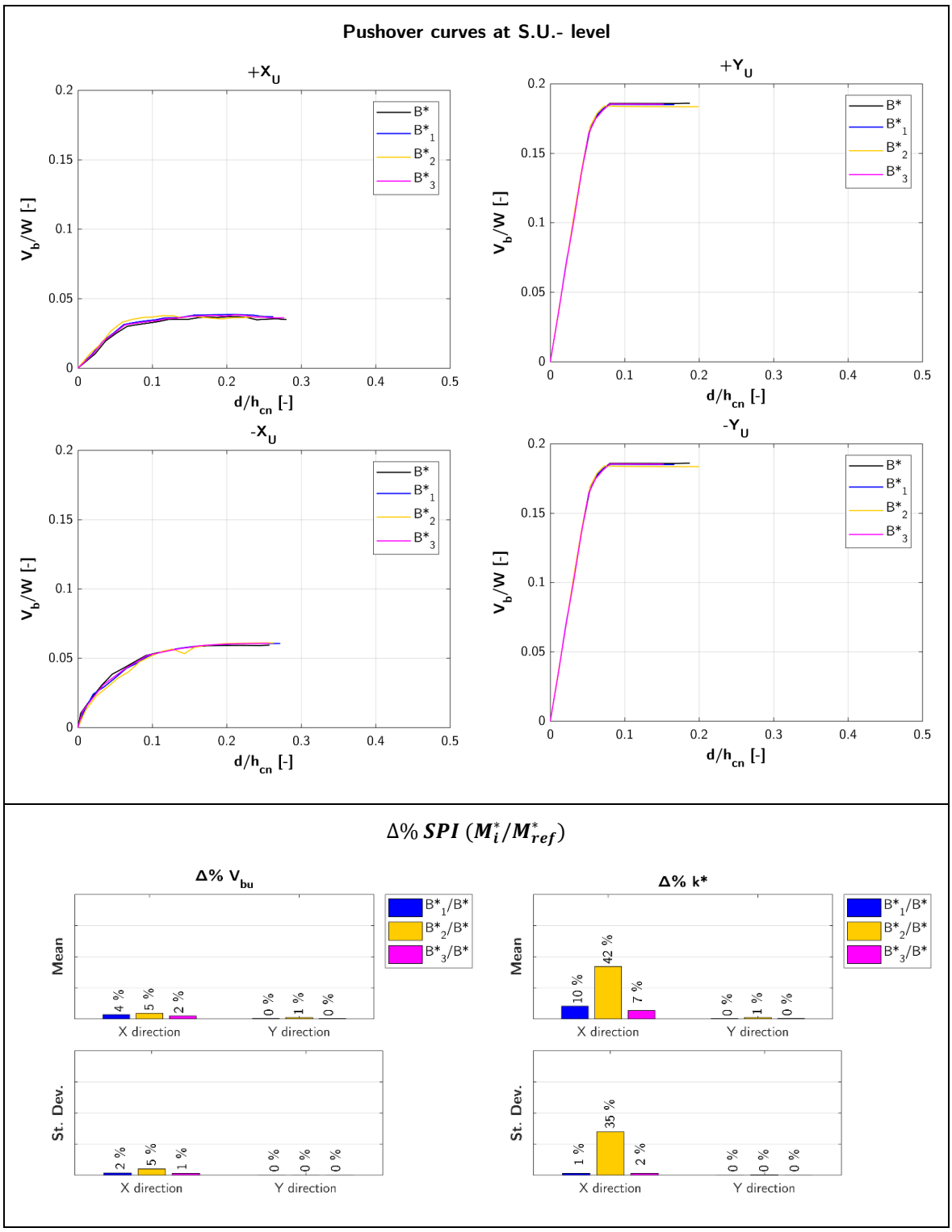

Table A 40: Row aggregate – external S.U.: hC - R floors.

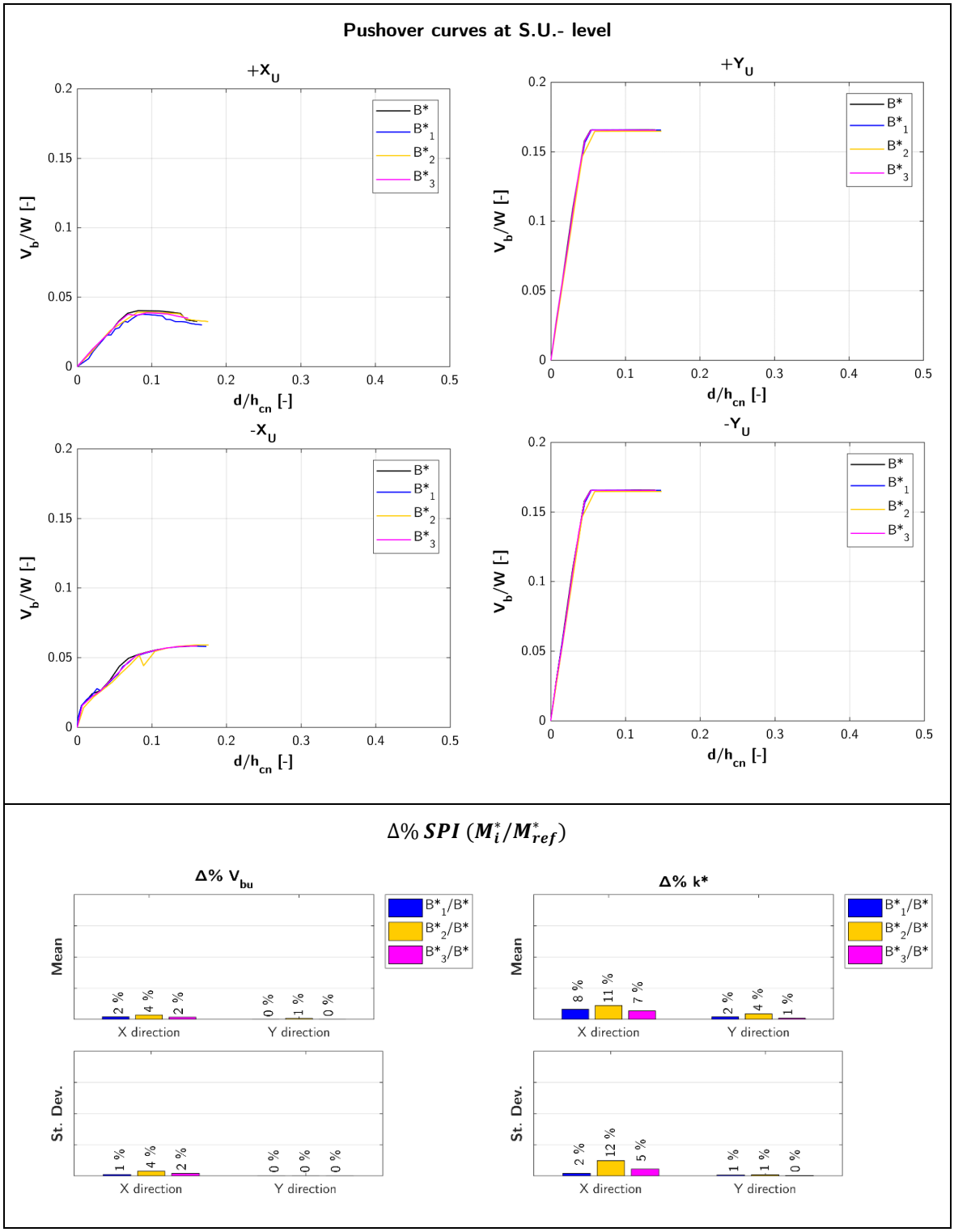

Table A 41: Row aggregate – external S.U.: hC - F floors.

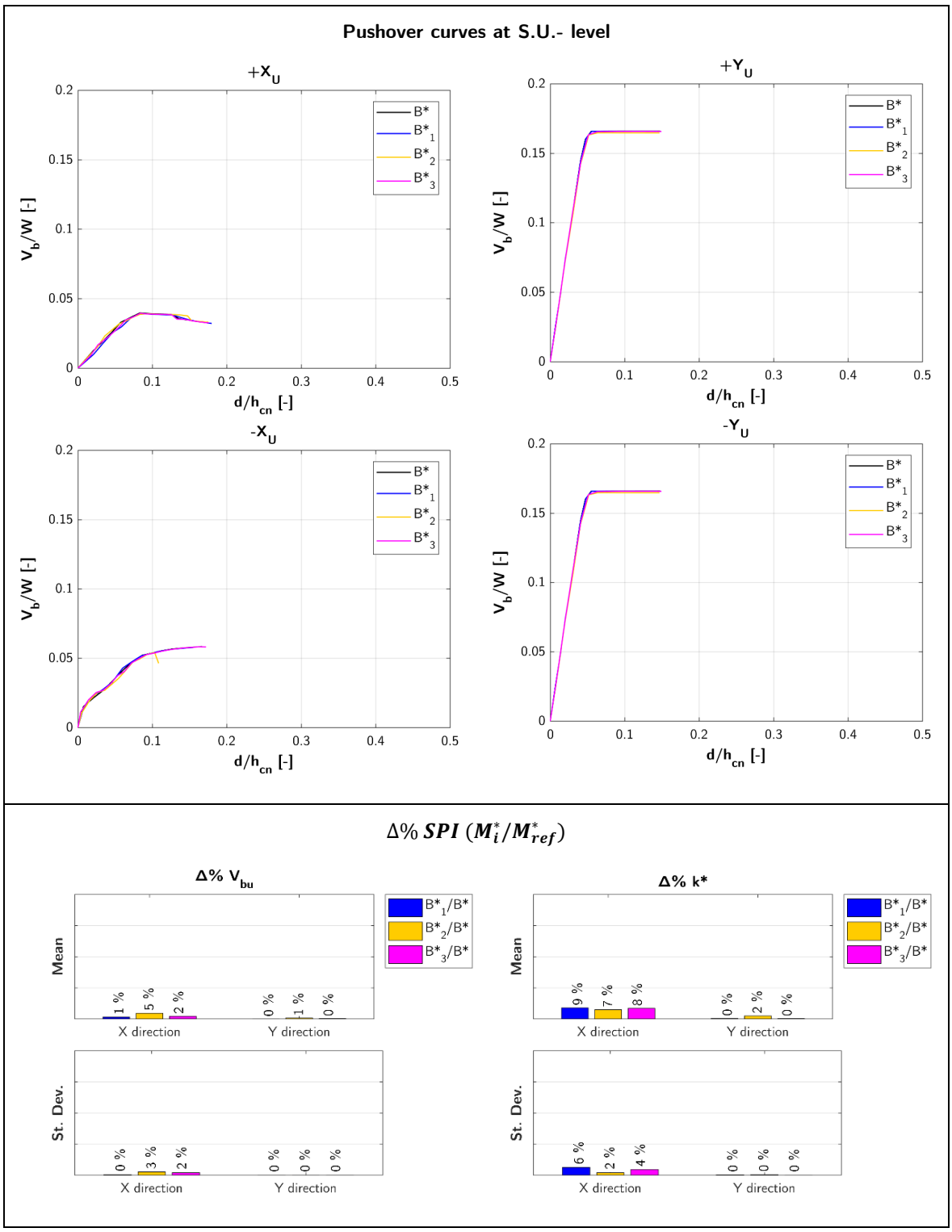

A6. L AGGREGATE – DIFFERENCES IN HEIGHT

Corner S.U.

Table A 42: L aggregate – corner S.U.: hB - R floors.

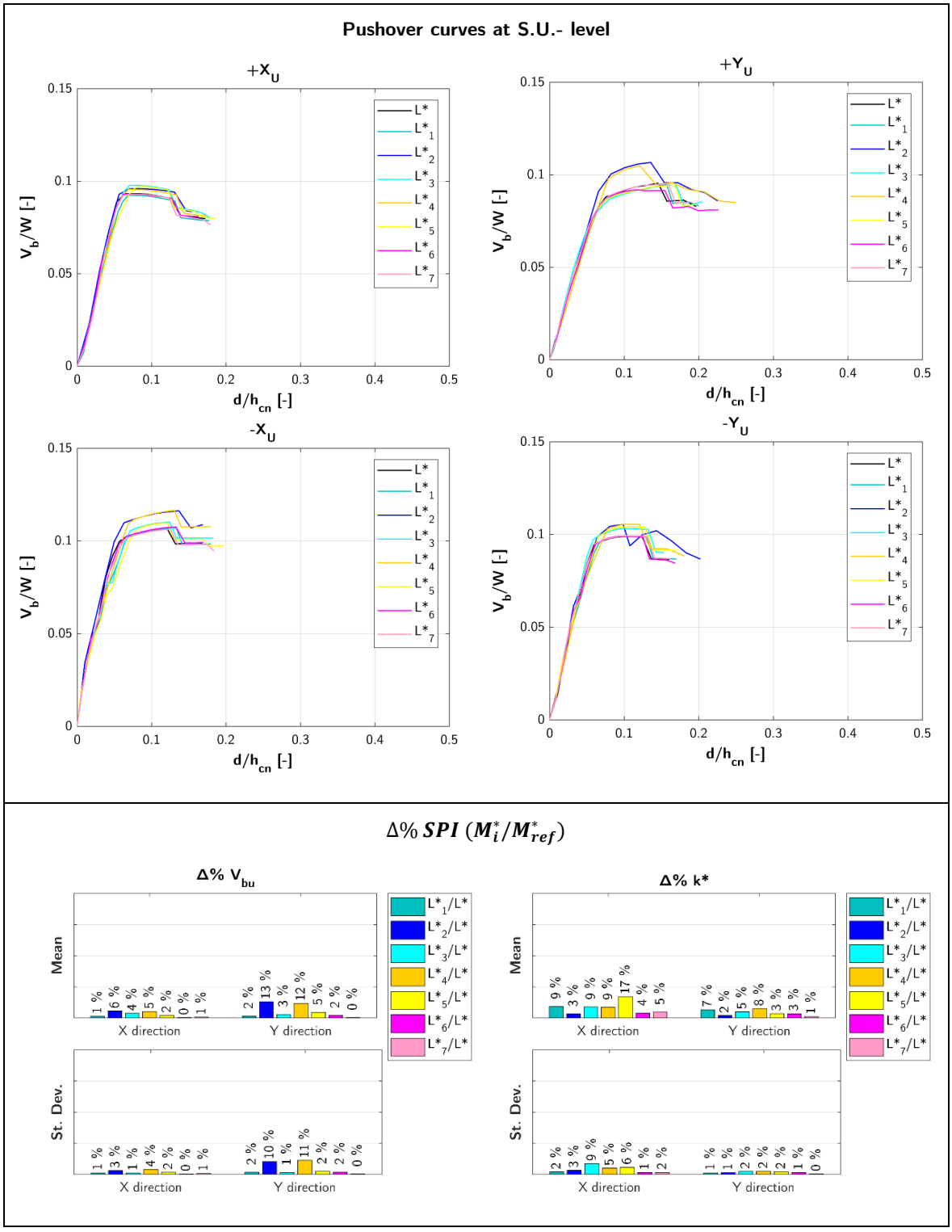

Table A 43: L aggregate – corner S.U.: hB - F floors.

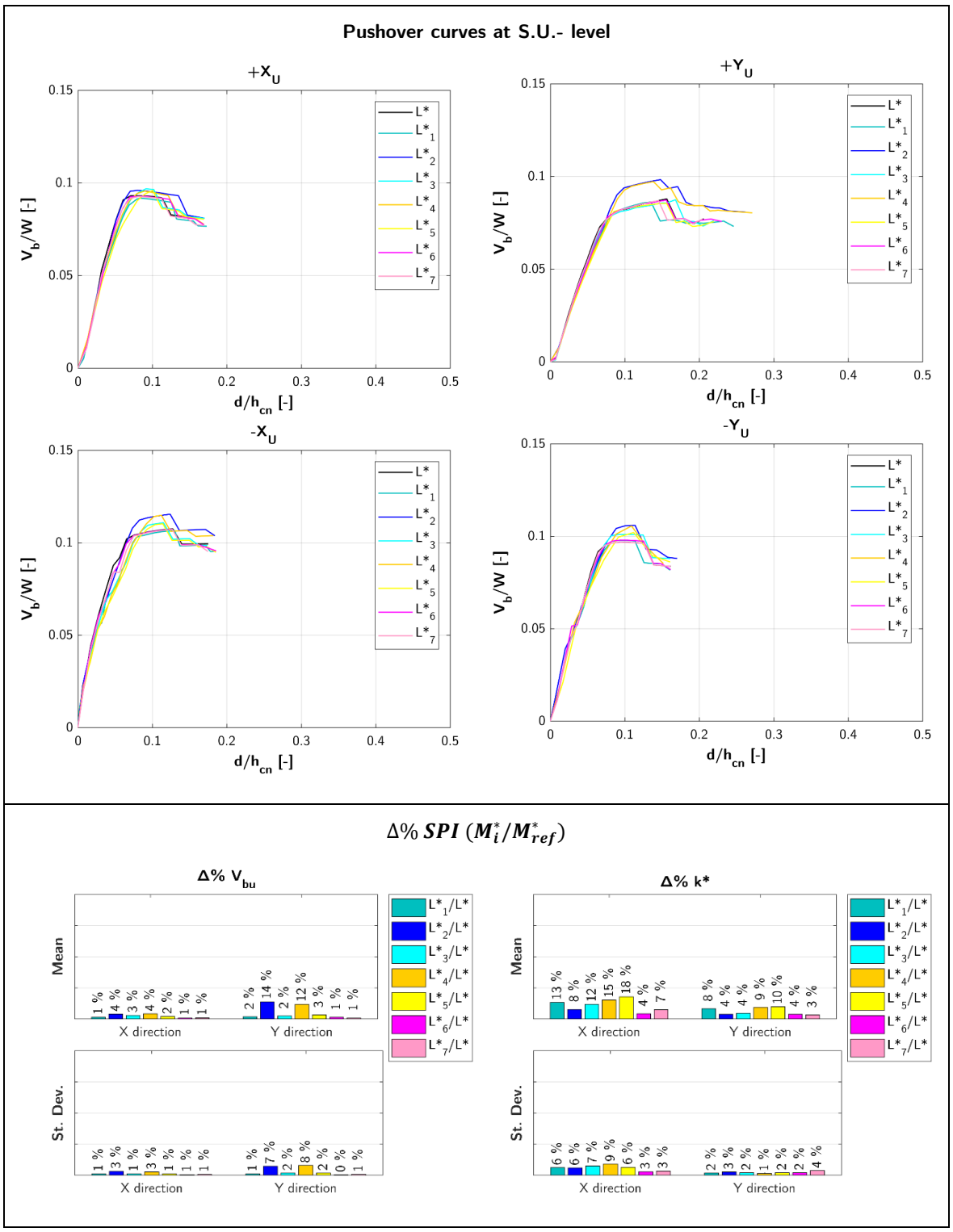

Table A 44: L aggregate – corner S.U.: hC - R floors.

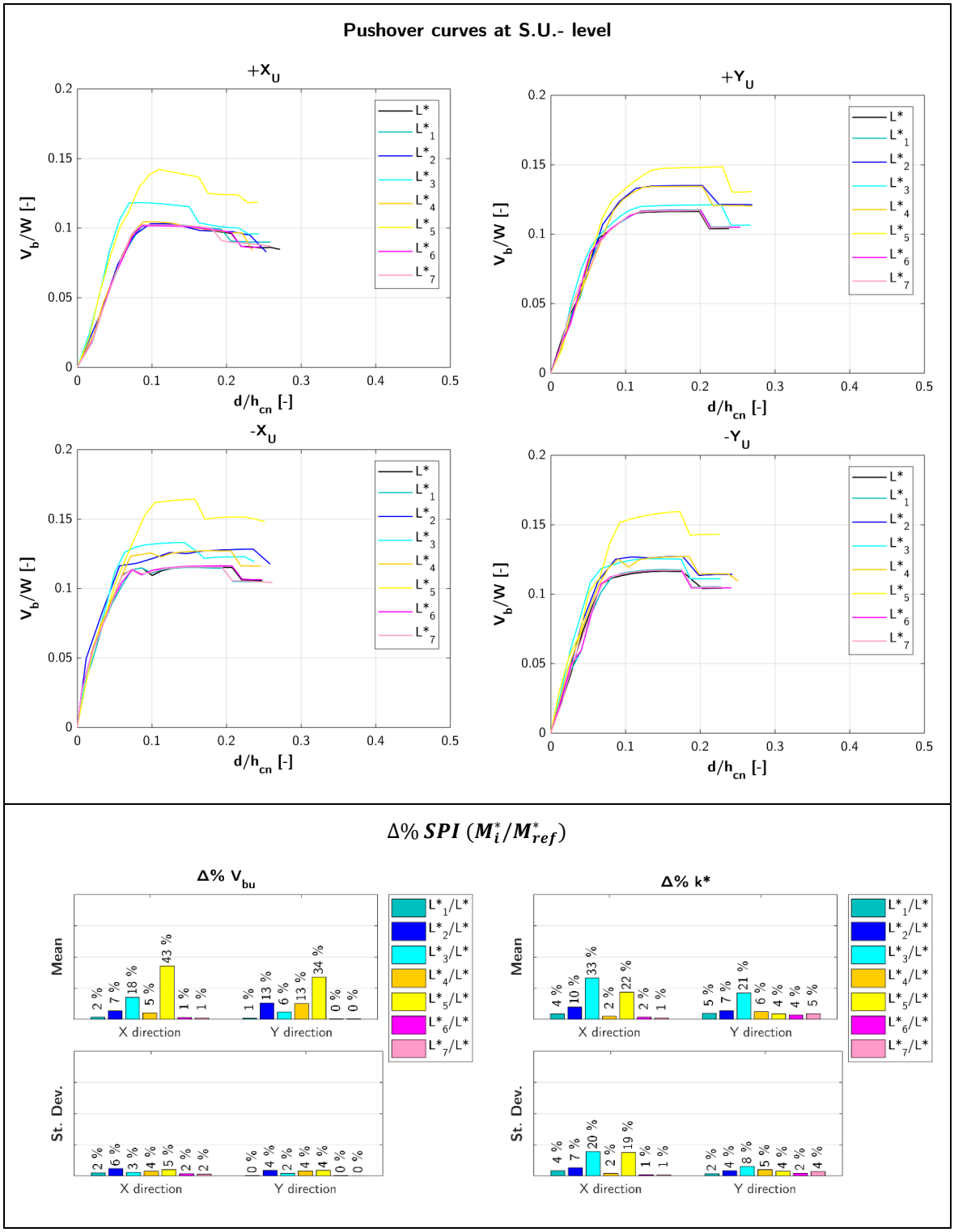

Table A 45: L aggregate – corner S.U.: hC - F floors.

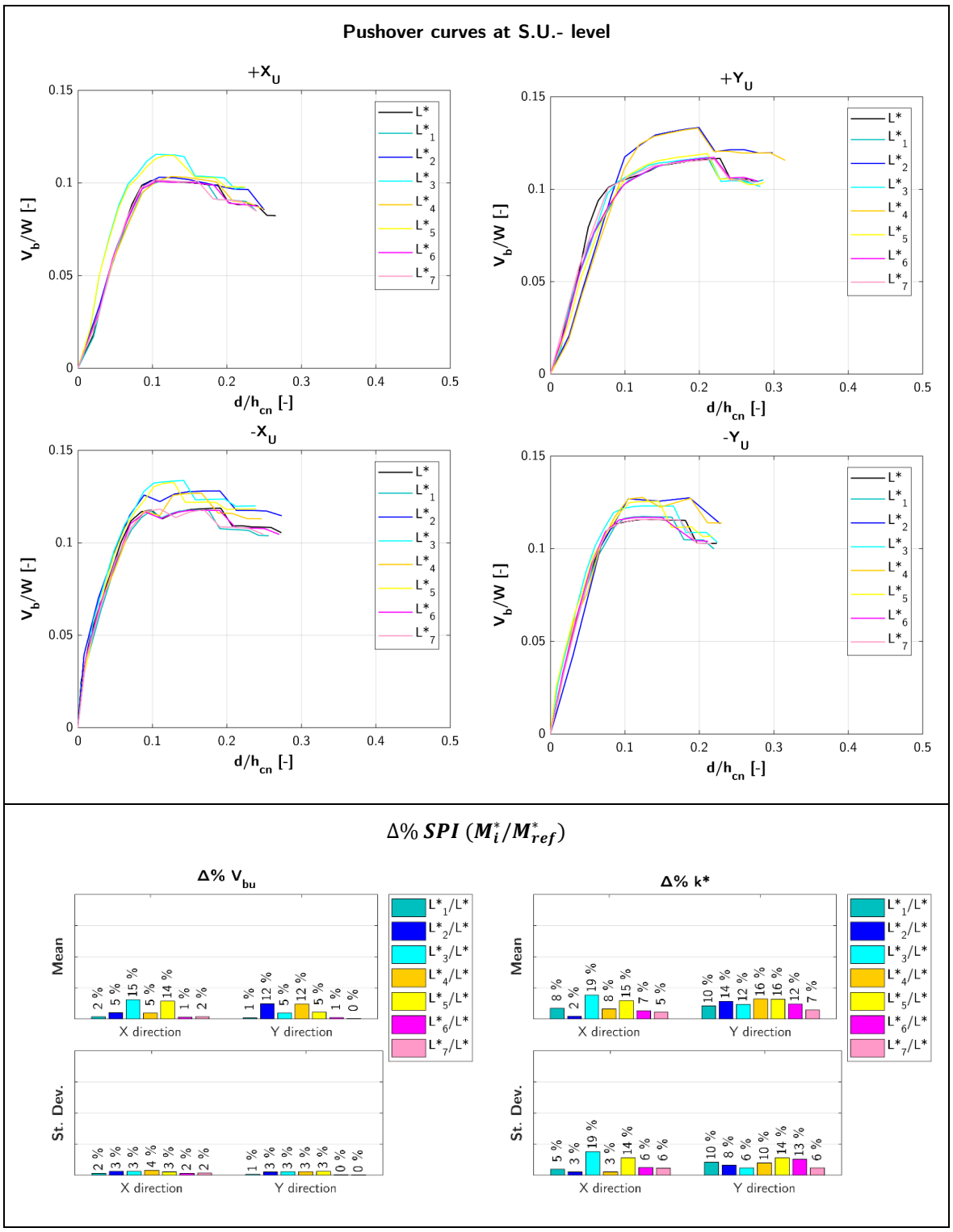

External S.U.

Table A 46: L aggregate – external S.U.: hB - R floors.

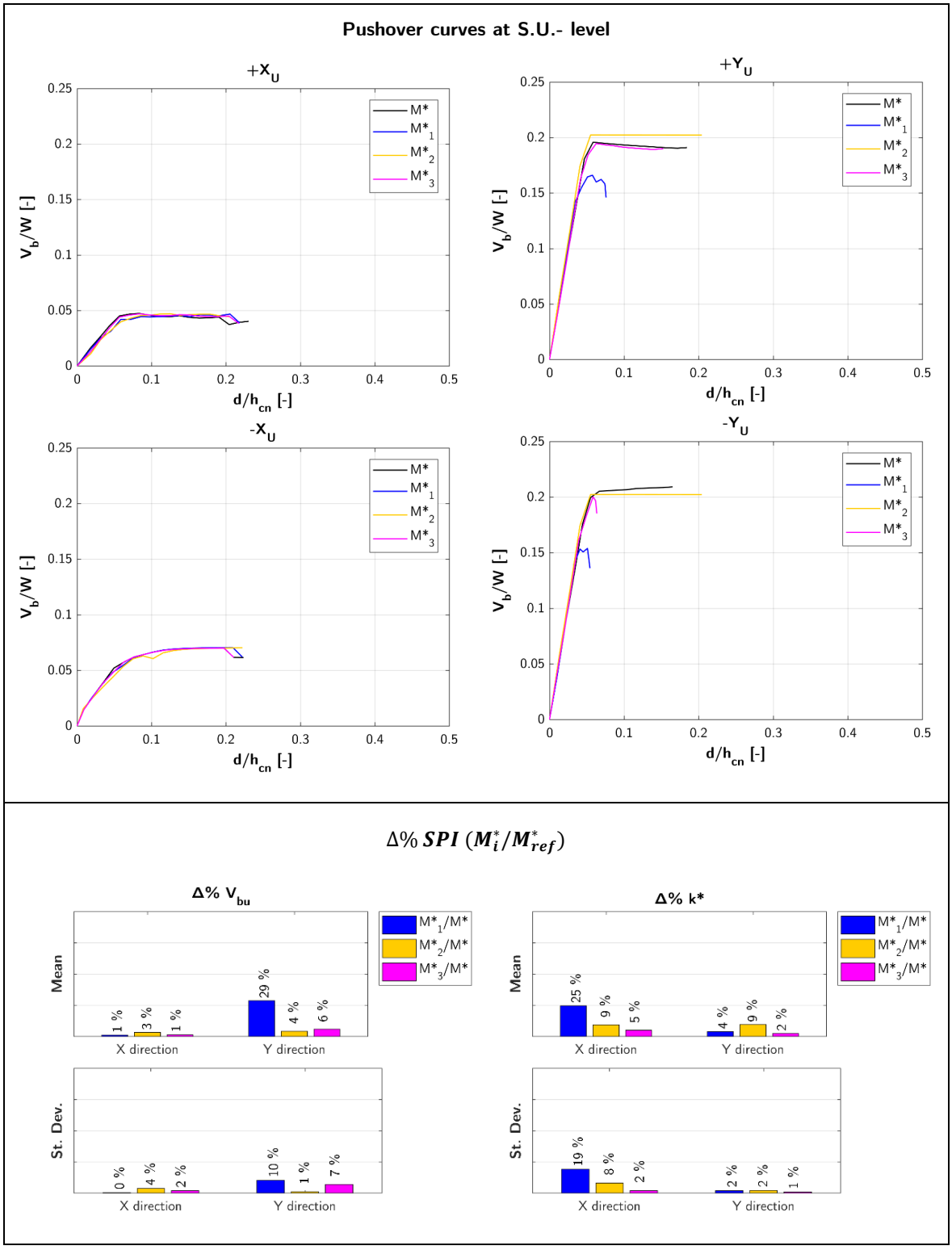

Table A 47: L aggregate – external S.U.: hB - F floors.

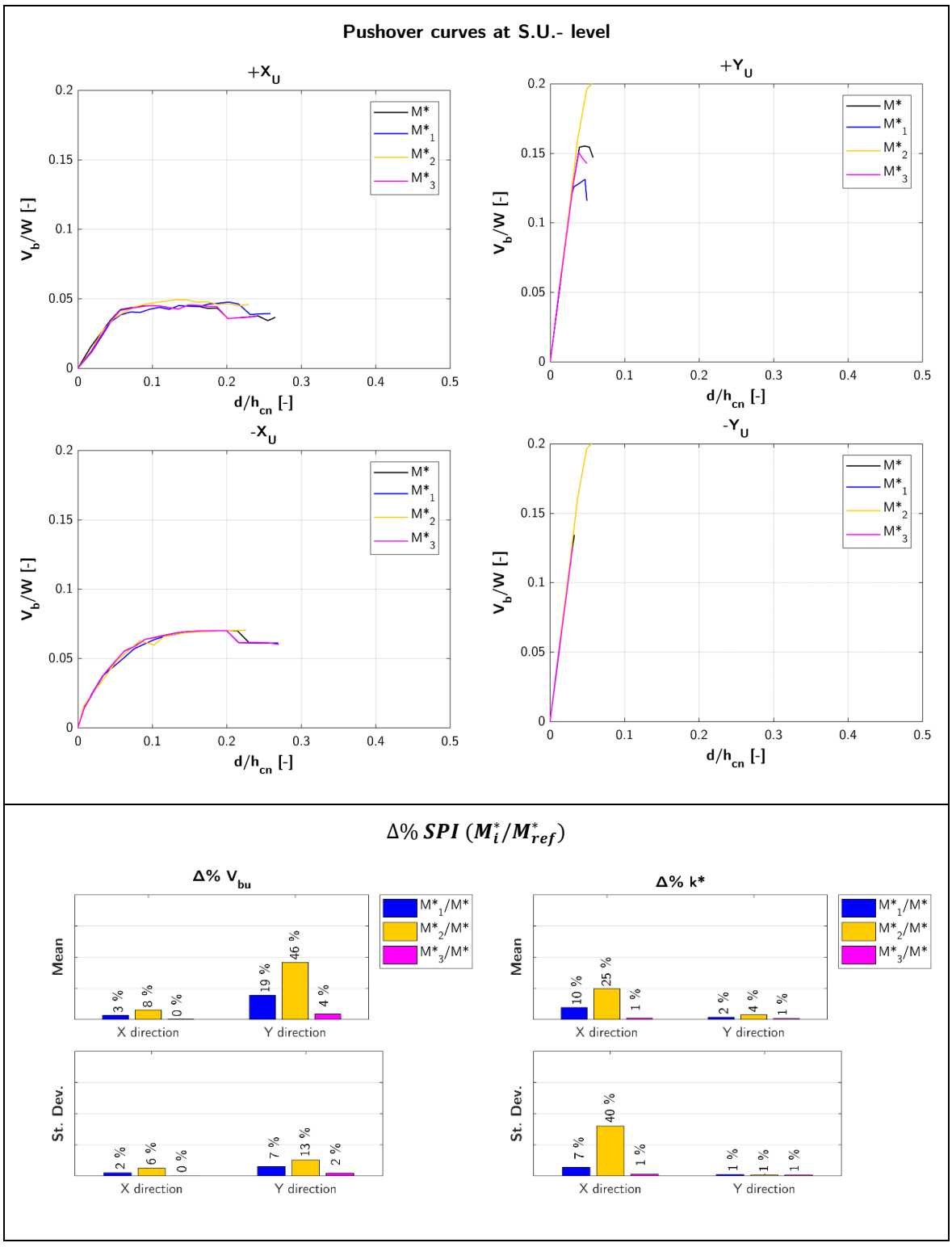

Table A 48: L aggregate – external S.U.: hC - R floors.

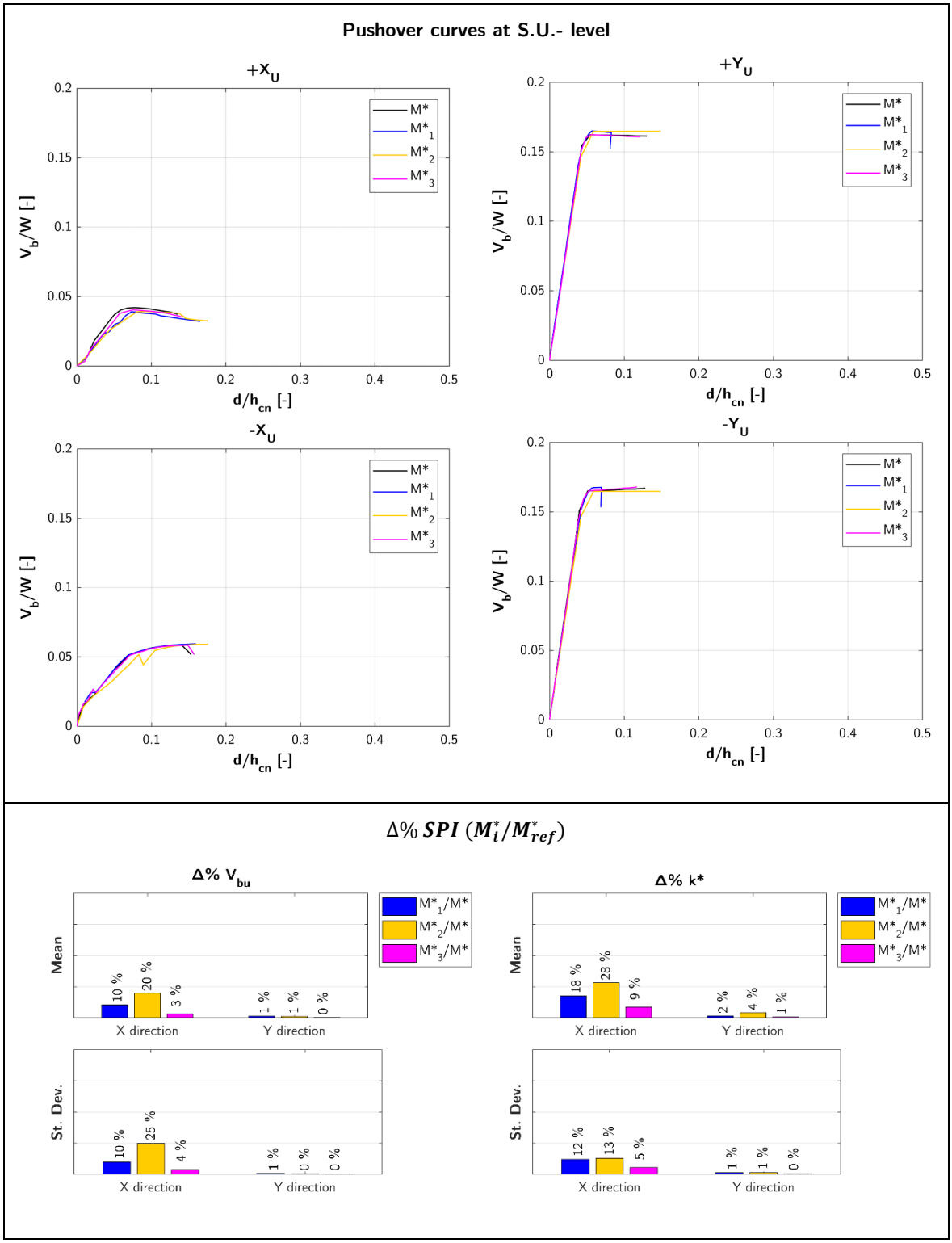

Table A 49: L aggregate – external S.U.: hC - F floors.

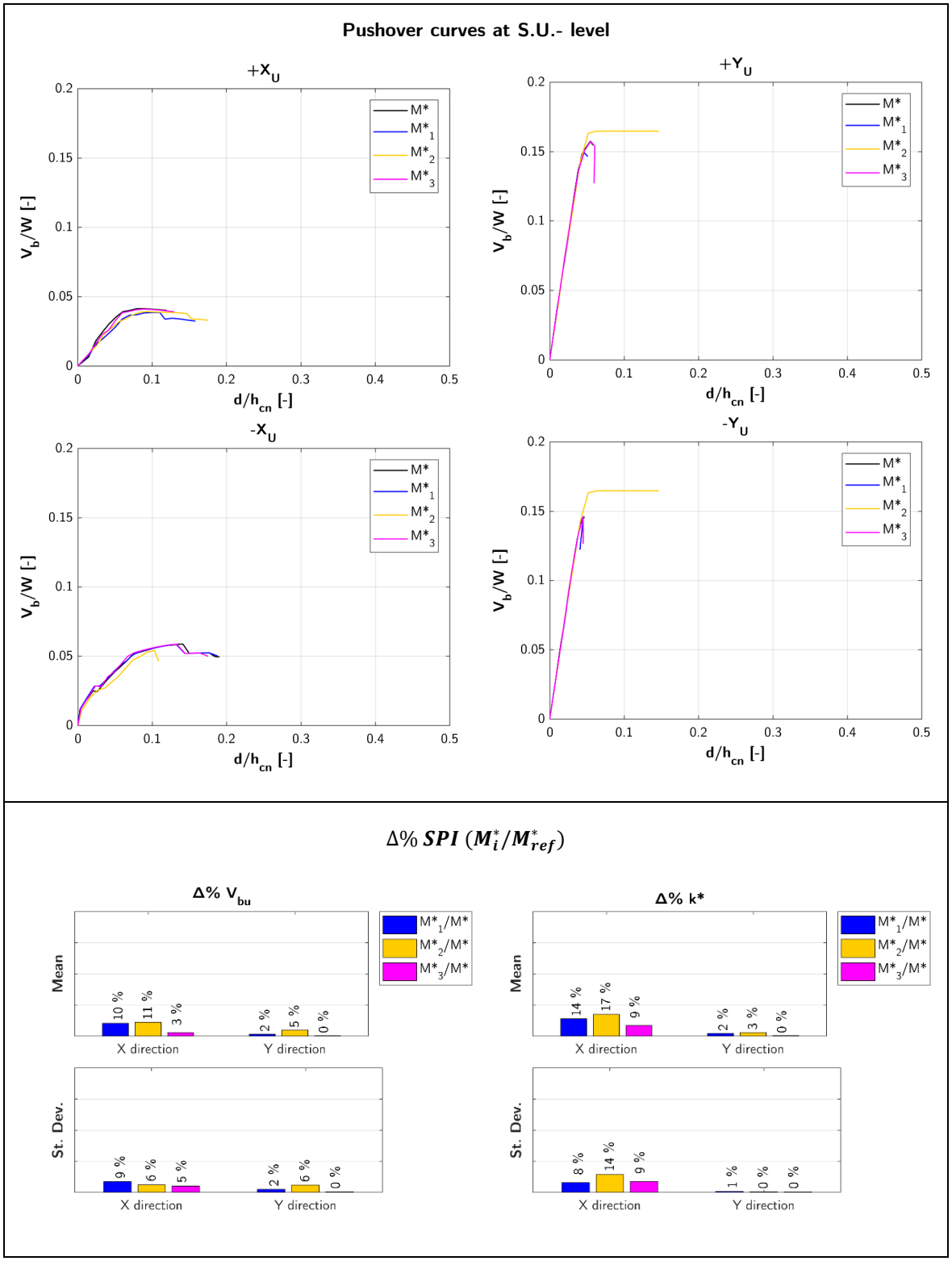

Annex B.
Results of the real masonry aggregates

For the real masonry aggregates, the pushover curves obtained at global- and wall- level are shown in the following tables.

B1. L AGGREGATE IN FARO (PORTUGAL)

Table B 1: Faro aggregate – external S.U. A.

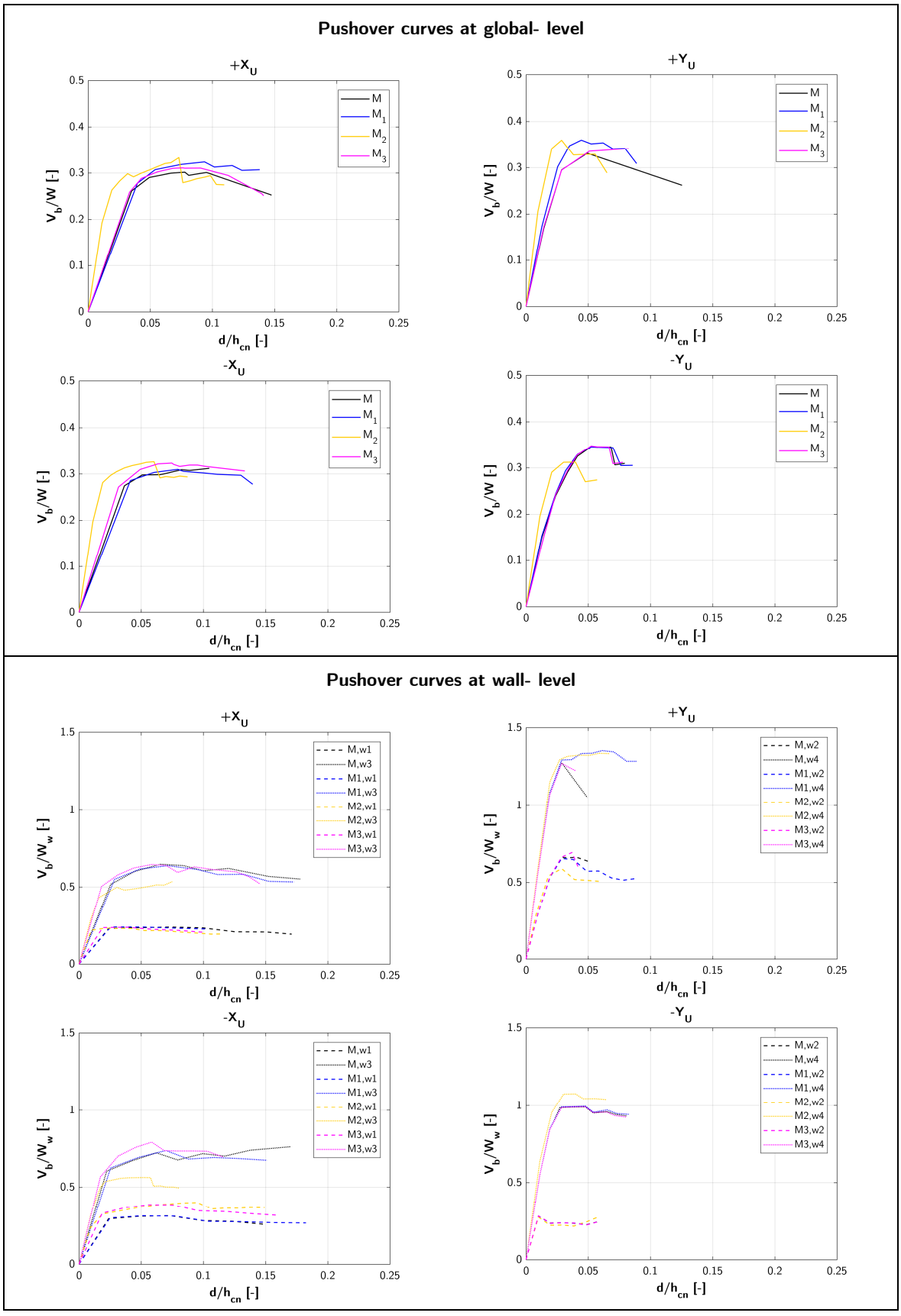

B2. ROW AGGREGATE IN CASTELNUOVO (AQ)

Table B 2: Castelnuovo aggregate – internal S.U. 6.

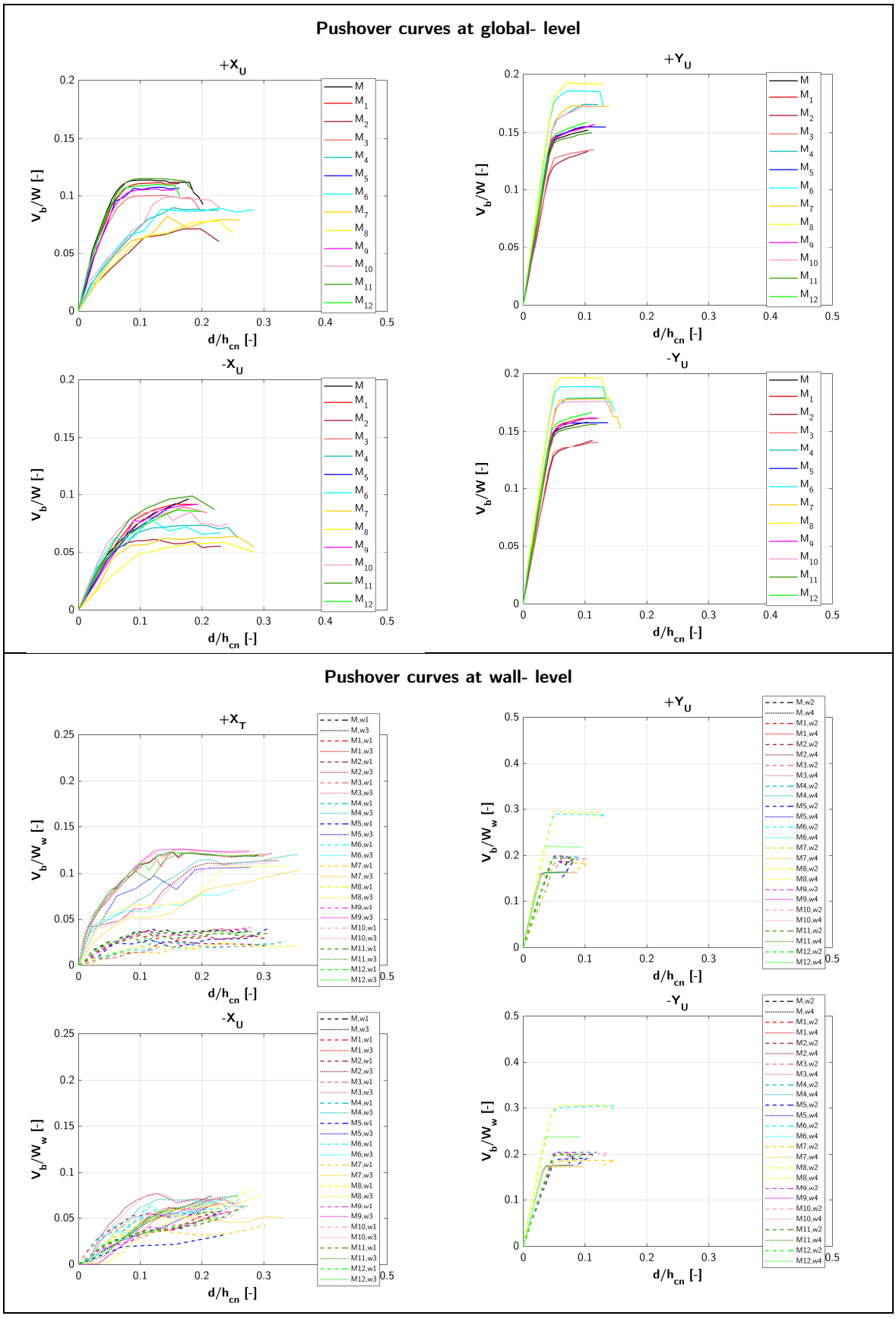

Table B 3: Castelnuovo aggregate – internal S.U. 9.